technische universität
dortmund

Organotin-Containing Crown Ethers-Substituted Ferrocene/Ferrocenophanes for Simultaneous Complexation of Cations and Anions

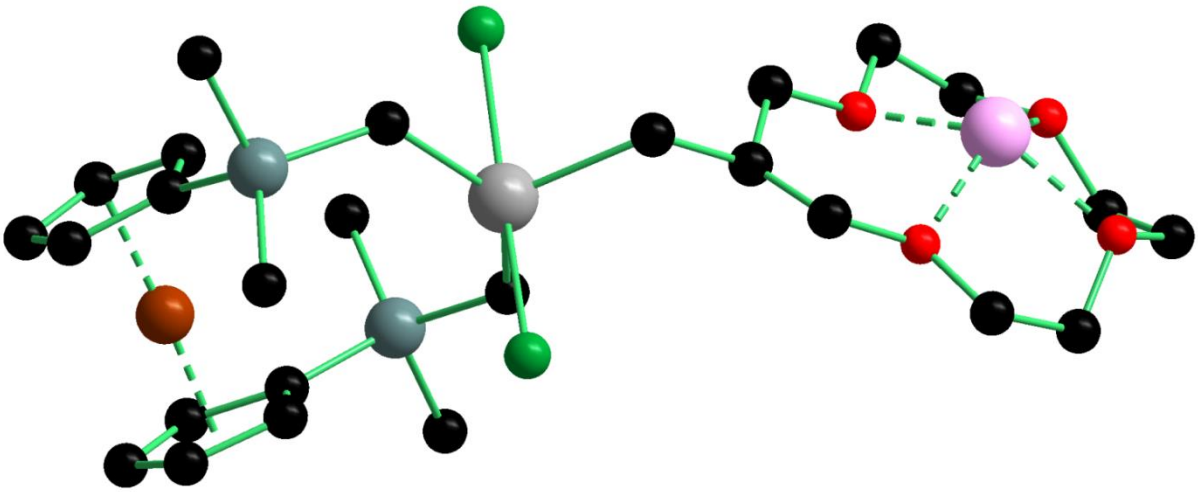

by

Anicet Siakam Wendji

Master of sciences

Thesis presented for obtaining the degree of

DOKTOR DER NATURWISSENSCHAFTEN

(Doctor rer. nat.)

First Reviewer: Prof. Dr. K. Jurkschat

Second Reviewer: Prof. Dr. V. Jouikov

This thesis is dedicated to my parents Wendji Tchouamo Paul and Siakam Djomassi Bernadette who encouraged and helped me at every stage of personal and academic life, and longed to see this achievement come true.

The present work was carried out from October 2009 until October 2012 at the Lehrstuhl für Anorganische Chemie II of the Technische Universität Dortmund

Under the supervision of

Prof. Dr. K. Jurkschat

Whom I express my sincere gratitude for the continuous support during the course of my Ph.D, for his patience, motivation, enthusiasm, and immense knowledge. His guidance helped me in all the time of research and writing of this thesis. I could not have imagined having a better supervisor for my Ph.D study.

Prof. Dr. V. Jouikov

Whom I thank for writing the second reviewer report and for recording the cyclic voltammetry data, the grafting analysis and the DFT calculations.

I would like to show my gratitude to the German academic exchange services (DAAD) for the financial support. I thank also Prof. Dr. R. Pöttgen for recording the ^{119}Sn Mössbauer spectroscopy. I am also grateful to the staff of the analytical laboratories of the Faculty of Chemistry of the Universität Dortmund for recording elemental analysis, electrospray mass spectra and NMR spectra.

I am also indebted to all the group members of Prof. Dr. K. Jurkschat with whom I have interacted during the course of my graduate studies. Particularly, I would like to acknowledge Christina Dietz, Michael Lutter, Thomas Zöller, Dr. Ljuba Iovkova-Berends and Dr. Dieter. Schollmeyer for the great number of X-ray diffraction analysis. I would like to thank all the staff of the Inorganic Chemistry of the University of Yaoundé I (UYI) for the formation during my stay at the UYI.

I very much grateful to my dear friend Dr. A. Tagne for his help in my first experiments in the lab and for his fruitful discussions and ideas throughout the course of this research.

My deepest gratitude goes to my brothers and sisters P. Wendji, H. Tchouameni, R. Tchamou, H. Botchack, L. Moukam, C. Deumeni, Mr. and Mrs. Tadié, Mr. and Mrs. Njiné for their unflagging love and support. My gratitude goes to my family and my parents-in-law for their encouragement. I owe sincere thankfulness to the Family Djialeu-Tchuani, Mr. and Mrs. Theumoubé, A. Djilankoue and M. Djonkam for encouraging and supporting me during the days in the graduate school.

I am also thankful to my close friend Dr. G. Kamgang for his permanent support during the course of this work. I am also grateful to the following friends for their various forms of support during my graduate study: R. Fodjeu, C. Maamdem, V. Tchieda, E.Tatchouala, N. Djoko, G. Tabue, M. Tessouop, L. Meka, A. Mantho, F.Talontsi.

I owe my loving thanks to my wife Odile Flora Siakam Wendji, my son Daniel Akim Siakam Wendji for their love and encouragement throughout this entire journey. Without their understanding, I would have struggled to find the inspiration and motivation needed to complete this dissertation.

Contents

List of Abbreviations

General abbreviations			
Ar	Aryl	*i*	Ipso-position in aromatic
t-Bu	tert-butyl	*m*	Meta-position in aromatic
Calcd	calculated	Me	Methyl
Cp	Cyclopentadienyl	mp	Melting point
E°	Standard electrode potential	*o*	Ortho-position in aromatic
$E_{1/2}$	half-wave potential	*p*	Para-position in aromatic
EDA	Electron donor atom	Ph	Pheny
EIS	Electrochemical impedance spectroscopy	R	Organic group
eq	equation	THF	Tetrahydrofuran
Fc	Monosubstituted Ferrocene	X	Halide
fc	1,1'-disubstituted ferrocene	GC	Glassy carbon

Spectroscopy/Spectrometry			
bs	broad signal	$\nu_{1/2}$	Line width
δ	Chemical shift in ppm	m	multiplet
d	doublet	MS	Mass spectrometry
dd	Doublet of doublet	*m/z*	Mass per charge
NMR	Nuclear magnetic resonance	Hz	hertz
ESI-MS	Electrospray-mass spectrometry	ppm	part per million
^{n}J	Coupling constant through n-bonds	s	singulet
IR	infrared	t	triplet
q	quartet		

Molecular Structure Determination			
a, b, c	Unit cell dimensions	ρ_{calcd}	Calculated density
F(000)	Number of electrons in the unit cell	μ	Absorption coefficient
α,β,γ	angles	R	Rest value
V	Volume of the unit cell	F	Structure Factor
Z	Number of the molecules in the unit cell	Å	Angström
σ	Standart deviation	wR	Weigthed rest value

1. General introduction

Since the discovery of crown ethers[1] in 1967 by *Pedersen*, a large number of acyclic and macrocyclic compounds have been synthesized as molecular receptors for cation recognition.[2-4] These hosts are divided into several classes. The first category are crown ethers (Figure 1, **I**). These are able to encapsulate cations of different radii through donor atoms such as oxygen or nitrogen. The second category are the cryptands reported by *Jean Marie Lehn* et al. in 1969 that exhibit a spheroidal cavity for the binding of cations (Figure 1, **II**).[5] The last category are spherands, designed by *Cram* and coworkers in 1981 (Figure 1, **III**), which are preorganized during the formation of the complex.[6] In 1987, the Nobel Prize for Chemistry had been awarded to *Lehn*, *Cram* and *Pedersen* for the discovery of these three classes of receptors and their unexpected complexation properties.

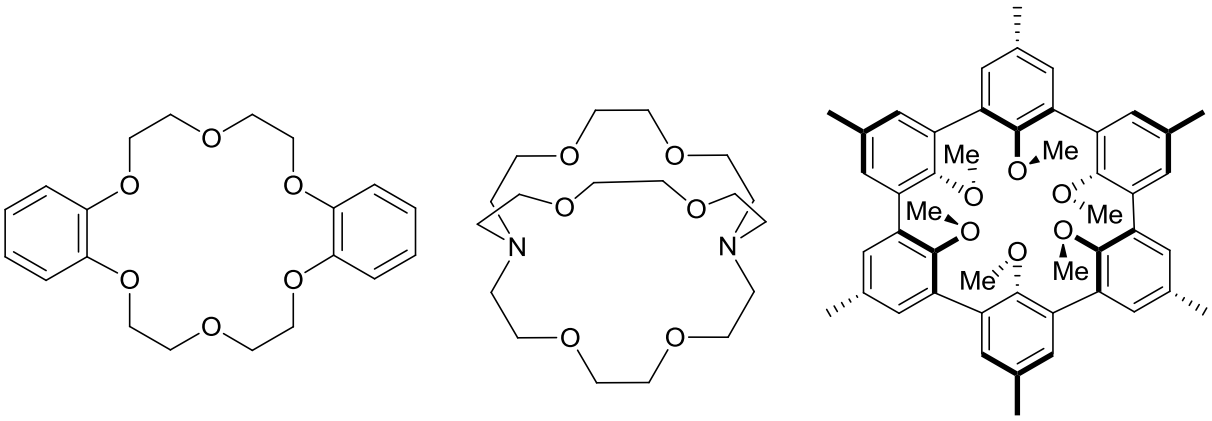

Figure 1. Crown Ether Dibenzo-18-crown-6 (I), Cryptand (II) and Spherand (III).

Another important class of host molecules are the macrocyles formed by cyclooligomerization of phenol and formaldehyde and which are called Calixarenes. They were synthesized by *Gutsche* in 1978 (Figure 2, **IV**)[7] and are able to complex cations, anions, and neutral molecules. Their multifunctional properties have made them a standard among supramolecular host molecules.[8]

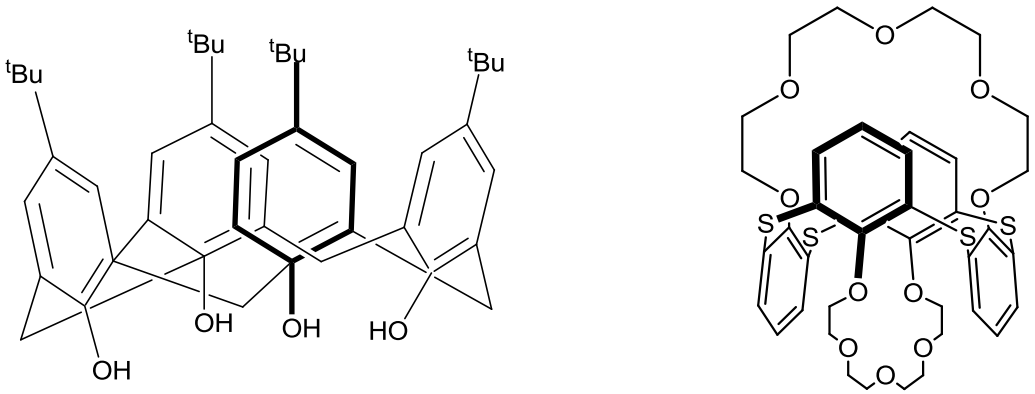

IV **V**

Figure 2. Calixarene(**IV**) and Calixcrown(**V**).

Calixcrowns are a family of cation receptors in which calixarenes are combined to crown ethers (Figure 2, **V**).[9] Calixcrowns have been applied in the study of hydrogen-bonding and electrostatic interactions as well as cation–π interactions that occur when ions are complexed by these hosts.[8] They have been generally used for ion recognition.[10-14] Furthermore, crown ether-based calixarenes have been described to be useful for ionophores in ion-selective electrodes (ISE) for various cations,[15-19] transition metals,[14,20] heavy metals,[21-24] lanthanides,[25,26] and alkylammonium ions.[27,28]

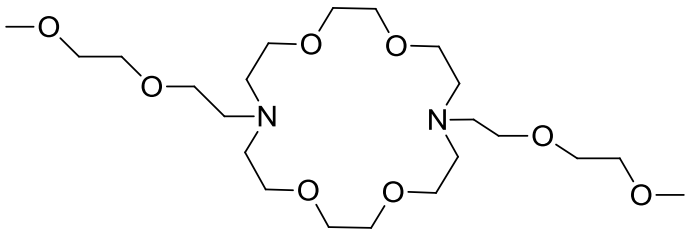

VI

Figure 3. Lariat ether.

Another class of cation receptors resulting from crowns ethers and cryptands are lariat ethers (Figure 3, **VI**). According to *Gokel*, lariat ethers are a blend of crowns and cryptands.[29] They were described to have the three dimensionality of cryptands while retaining the faster complexation dynamics of crown ethers.[30] Lariat ethers are intermediate between these two species in that they are generally better binders[31] than simple crowns but poorer binders than cryptands. In most cases, lariat ether

sidearms are attached to the macroring at the nitrogen atom, which permits the sidearm maximum flexibility.[8] In continuation of the work on the macrocyclic compounds based on the principles of shape, size complementary and preorganization mentioned above, numerous receptors for cations and neutral guests have been reported.[32-44] Beside these kinds of responsive systems, many molecular sensor systems for cationic guest species were designed that involve (i) crown ether dyes in which the complexation of the cation is manifested by a color change of the chromophore. For example, the 15-crown-5 derivative **VII** (Figure 4) [45,46] turns from orange to red when bound to K^+ or Rb^+; (ii) fluorophore groups whereby fluorescence is quenched by a partial charge, typically the free lone pair of electrons on a nitrogen atom.[8] In 1986, *De Silva* and co-workers designed the first molecule of this type (Figure 4, **VIII**).[47] In this system, potassium demonstrated an excellent `off–on´ fluorescence signal and the binding constant of the cation with the fluorescent macrocycle was nearly similar to that with the free macrocycle.[47]

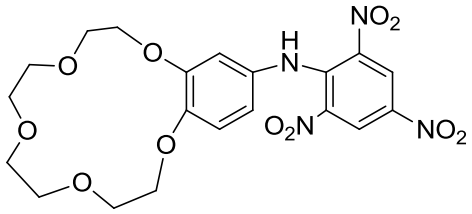

VII

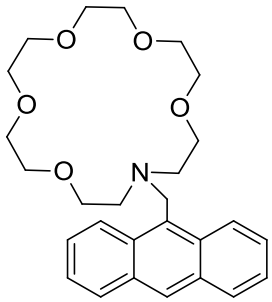

VIII

Figure 4. Crown-based dyes for spectrophotometric detection (**VII**) and *De Silva´s* anthracenylmethyl lariat ether for fluorescence signaling (**VIII**).

iii) redox-active groups in which the binding of a cation causes an anodic shift in the redox potential of the redox active group. The majority of the redox-active cation receptor use ferrocene as a redox reporter group. The pioneer of this work is *Saji* who conjugated ferrocene to crown ether (Figure 5, **IX**).[48,49] These compounds are sensors for Group I cations. Many research groups are focusing their work on the combination of ferrocene with a variety of macrocycles and numerous redox active cation receptors have been reported.[50-68]

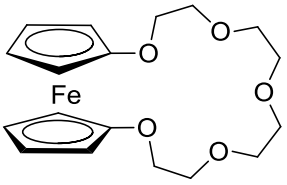

IX

Figure 5. Ferrocene crown ether conjugates.

Over the years, anion complexation by synthetic host molecules has become an important area of supramolecular chemistry and many reviews of the subject have been reported.[69-80] The interest on this topic stems from their potential application in biological, chemical, environmental and health processes. The complexation of anions by a host is more difficult to achieve than the binding of cations. This is due to the diffuse nature of anions. Indeed, and in contrast to cations which differ one from another only by the spherical radii, anions exist in a wide variety of geometries and are more likely to be polyatomic. They can exist as linear, trigonal-planar, tetrahedral, square-planar or octahedral geometry. Moreover, anions are larger than isoelectronic cations and have smaller charge to radius ratios.

In 1968, *Park* and *Simmons* designed the first anion receptor (Figure 6, **X**).[81] The latter was called Kapitanate and showed the ability to bind bromide and chloride through hydrogen bonding and electrostatic interactions.

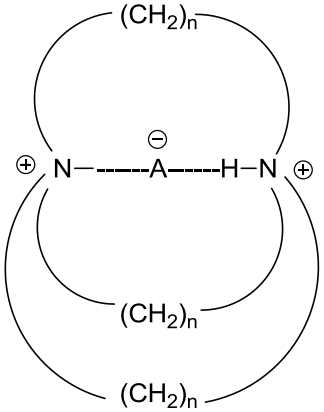

n =7-10, A = Cl, Br

X

Figure 6. Kapitanate.

Numerous research groups have followed this strategy to synthesize novel receptor for anion. *Kondo*, *Unno* and coworkers have shown the ability of compound **XI**

(Figure 7) to use four OH groups for the complexation of a chloride anion in CD_3CN.[82] The same anion has been complexed by the compound **XII** (Figure 7) through C–H hydrogen bonds in CD_2Cl_2.[83]

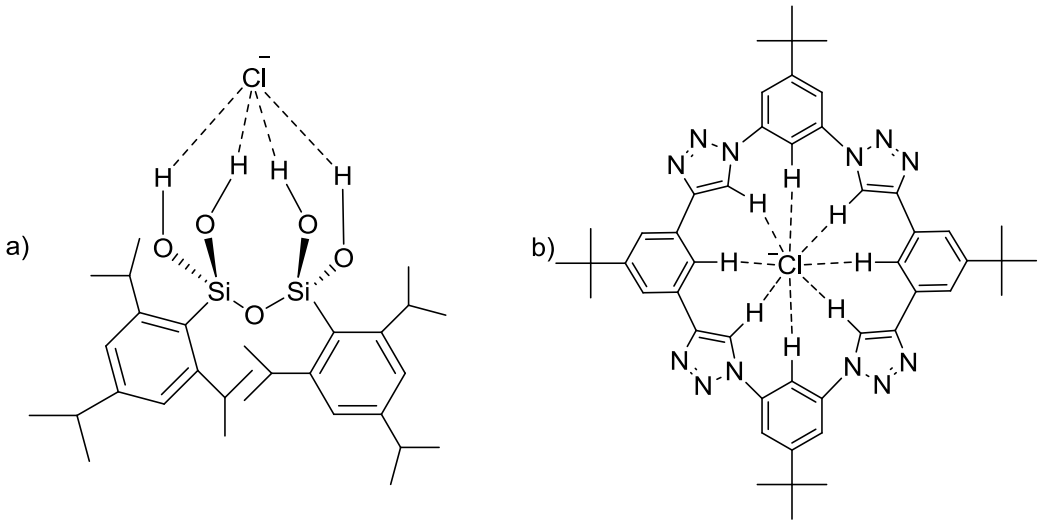

XI **XII**

Figure 7. Receptor for anion recognition using a) hydroxyl group (**XI**), b) C–H hydrogen bond (**XII**).

Only recently, *Gale* and co-workers have reported the synthesis of receptor **XIII**[84] that has shown a high potential to complex oxo-anions. Interestingly, in the latter complex the hydrogen phosphate interacts with all six hydrogen bonds.

Due to its key role in the development and preservation of life on this planet,[85] water is of particular importance. Its very low cost and ability to interact intermolecularly via strong hydrogen bonds have motivated chemists to involve water in anion recognition processes. Representative examples are compounds **XIV** and **XV** (Figure 8) [86,87] that were found to be able to interact with anions such as Cl^-, I^-, NO_3^-, ClO_4^-, AcO^-, $H_2PO_4^-$, SO_4^{2-}, and SeO_4^{2-} in aqueous solution.

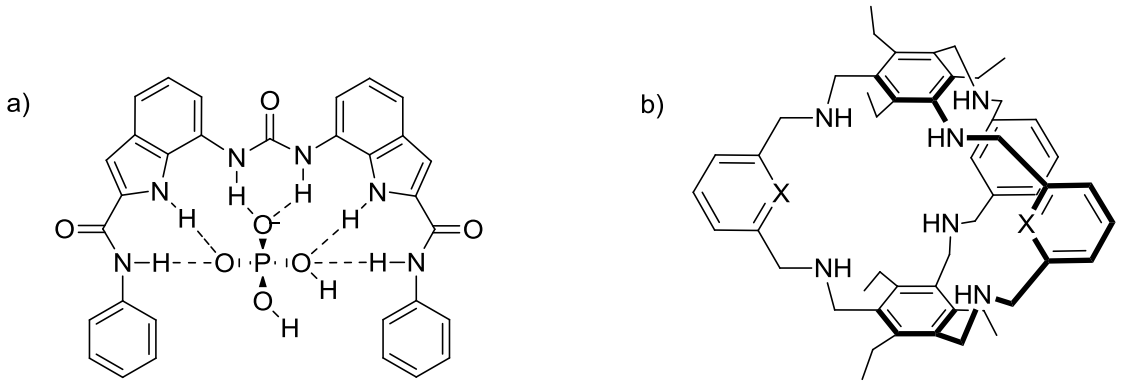

XIII

XIV, X = CH
XV, X = N

Figure 8. Receptor for a) oxoanion (**XIII**) and b) anion recognition in water (**XIV** and **XV**).

Anion complexation can also be achieved by using Lewis acidic metal/element centers as receptors for anions. The first neutral receptors containing Lewis-acidic tin binding sites were the distannacyclo- and bicycloalkanes reported by *Newcomb* (Figure 9, **XVI**). These compounds are able to bind selectively chloride and bromide ions.[88-90]

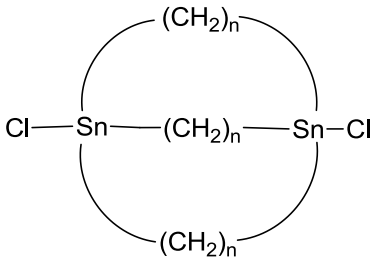

XVI

Figure 9. First anion receptor based on Lewis acidic groups (**XVI**).

During the last decades, numerous reports in this area have been published.[91-119] Most remarkable examples are (i) the cationic phosphonium boranes (Figure 10, **XVII**–**XX**)[120] reported by *Kim and Gabbaï*. The latter compounds have proven to be excellent receptors for fluoride anion in water; (ii) the bis(fluoro-di-n-octylstannyl)methane (Figure 10, **XXI**),[121] published in 2005 by *Chaniotakis*, *Jurkschat* and co-workers and in which the fluoride anion is chelated by the two tin atoms.

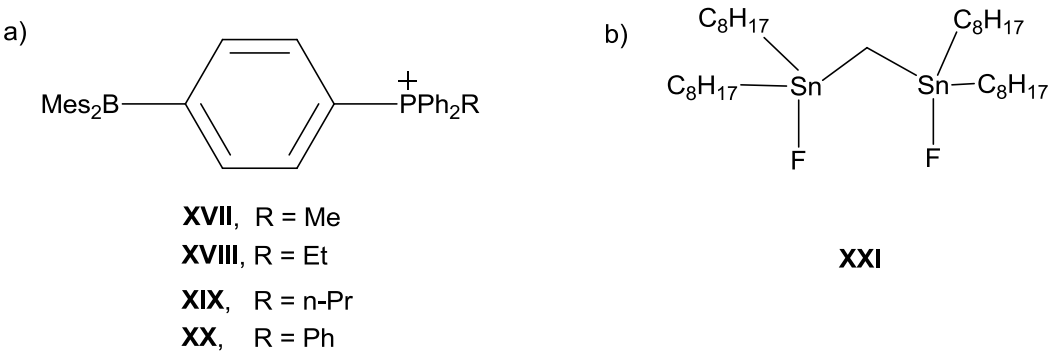

XVII, R = Me
XVIII, R = Et
XIX, R = n-Pr
XX, R = Ph

XXI

Figure 10. Lewis acidic anion receptors.

The combination of two or more different Lewis-acidic metal/elements in a system is an alternative to design receptors for the complexation of anions. Examples of such systems are generally based on B/In,[122] B/Ga,[122] B/Si,[123], Sn/Ga,[124] B/Hg.[125]
Many efforts have also been made in the design of anion transport. Amongst the report on this topic, compound **XXII** (Figure 11)[126] was described to be the "champion" with a transport half life of 26 seconds at the low transporter.

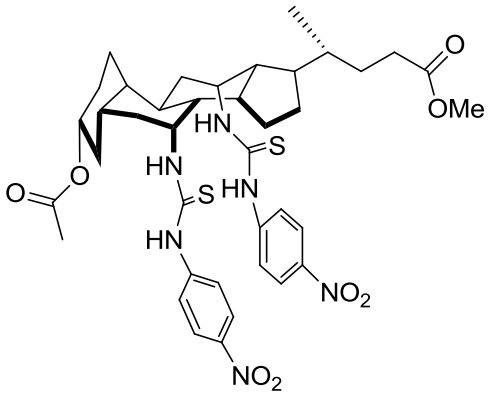

XXII

Figure 11. Receptor for anion transport.

Anions can be also recognized by redox sensing. The first redox active anion receptors studied was the cobalticinium macrocycle compound **XXIII** (Figure 12) reported by *Beer* and co-workers.[127] Electrochemistry studies revealed the receptor to be redox-responsive toward the bromide anion.[127]

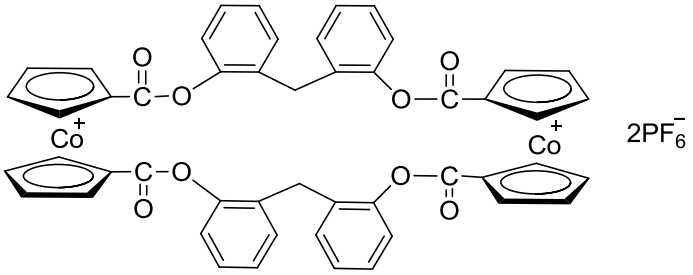

XXIII

Figure 12. First redox active anion receptor.

In the two last decades a number of compounds based on ferrocene anion sensors have been reported. In Figure 13, receptor **XXIV**,[128] possesses a secondary amide group for hydrogen-bonding interactions with anions. It showed cathodic shifts in the ferrocene/ferrocenium oxidation wave of 120 mv induced by $H_2PO_4^-$. Of particular relevance is the recognition of fluoride in aqueous media due to the strongly hydrated nature of the anion. *Shinkai* and coworkers reported the ferrocene–boronic acid (Figure 13, **XXV**), in which fluoride has been sensed electrochemically in water.[129]

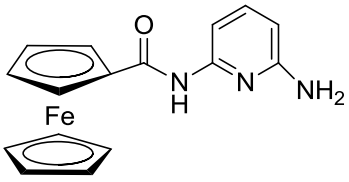

XXIV

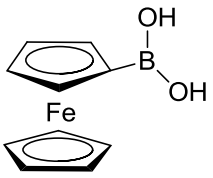

XXV

Figure 13. Redox active anion receptor.

In order to improve anion sensing, ferrocene can be combined with more than one organometallic unit. *Jurkschat* and coworkers used this strategy to synthesize the bimetallic anion sensor (Figure 14, **XXVI**).[130] The electrochemistry of this receptor showed that Cl^-, F^-, $H_2PO_4^-$ induced cathodic shifts in both the ferrocene/ferrocenium redox couple.

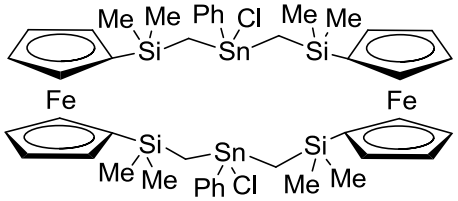

XXVI

Figure 14. Bimetallic anion sensor reported by *Jurkschat* and coworkers.

However, In the case of both anion and cation receptors, the binding of the individual cation or anion requires an energetic cost in order to separate each ion from its counterion. As a result of ion pairing effects, researchers have designed systems containing recognition sites for both the cation and anion. These systems are called heteroditopic receptors. *Smith* and coworkers demonstrated the advantage of heteroditopic over monotopic receptors. They showed that strongly ion-paired species can reduce the binding affinity of an ion by a monotopic receptor. For instance, the presence of alkali metal cations in [D_6]DMSO, inhibited the anion binding to the urea-based anion receptor (Figure 15, **XXVII**), with this effect being more pronounced with sodium ions, as a consequence of competing ion pairing outside the receptor.[131] This ion pairing effect can be overcome by incorporation of a crown ether into the receptor in order to design a receptor capable to complex both cations and anions simultaneously (Figure 15, **XXVIII**).

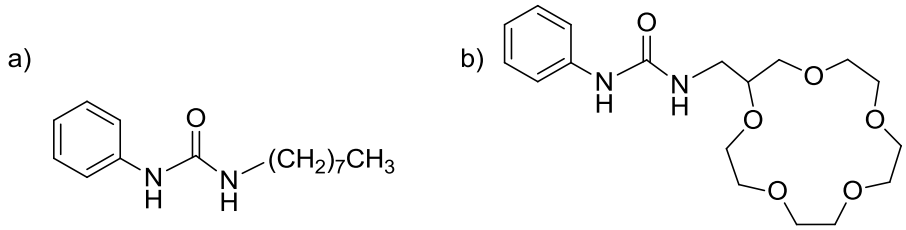

XXVII **XXVIII**

Figure 15. a) Anion receptor and b) ion-pair receptor reported by *Smith* and coworkers.

To achieve cation recognition, the majority of ion pair receptors take advantage of lone pair electron donor including crown ethers[8] and π-electron donors, such as functionalized calixarenes.[132,133]

In contrast, most ion pair receptors used hydrogen bonding donors (urea, amide, imidazolium, pyrrole, and hydroxyl group) to effect anion recognition.[69,74,134-139] Selected examples of this class of compounds are shown in Figure 16. Compound **XXIX** binds CsCl as a solvent-separated ion pair with a water molecule bridging the cation and anion, whereas compound **XXX**[140] complexes NaBr as contact ion pair. Interestingly, the presence of the ferrocene group in **XXX** allows electrochemical studies with the observation of a cathodic shift of the ferrocene redox couple and the increase of the magnitude of the shift in the presence of sodium cation.

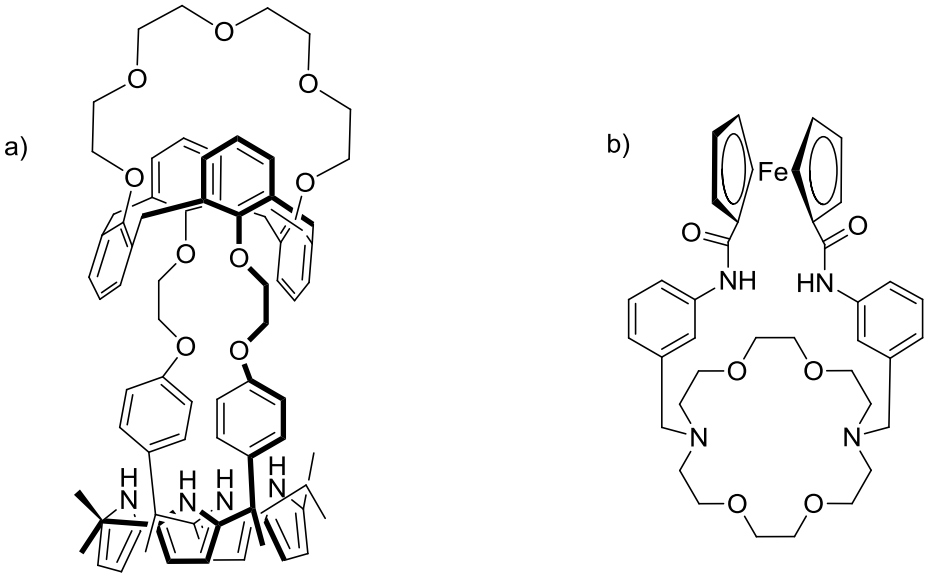

XXIX **XXX**

Figure 16. Ion pair receptors reported by a*) Sessler* and coworkers and b) *Tuntulani* and coworkers.

Examples of ion pair receptors based on positively charged components for anion recognition are rare. *Lockhart* and coworkers reported compound **XXXI**[141] and showed by means of NMR spectroscopy their ability to bind KCl. In 2003 , *De Silva* and coworkers synthesized the fluorogenic compound **XXXII**[142] containing benzo[15]crown-5 moiety and polyammonium group as Na^+ and $H_2PO_4^-$ binding sites, respectively, linked via an anthracene fluorophore. The authors showed that the fluorescence of compound **XXXII** was enhanced only when the simultaneous complexation of a Na^+ cation and an $H_2PO_4^-$ anion takes place.

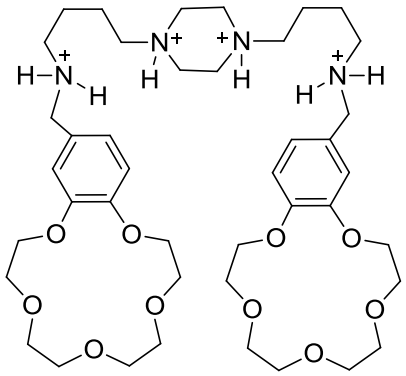

XXXI

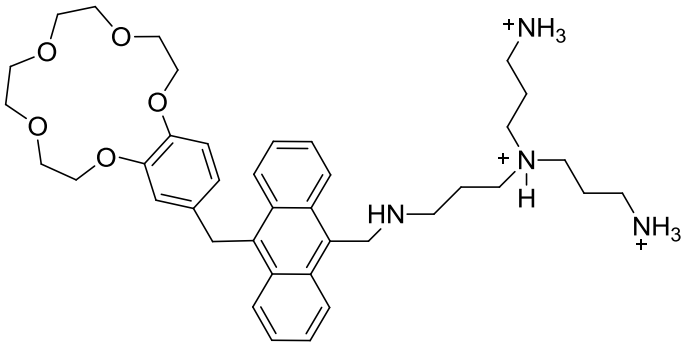

XXXII

Figure 17. Ion pair receptors based on positively charged components for anion recognition.

Ion pair receptors based on Lewis acidic groups is another strategy to achieve anion recognition. *Reetz* and coworkers were the first to highlight this category of receptor in 1991. Compound **XXXIII**[143] consists on a crown ether moiety coupled to a Lewis-acidic boron center for cation and anion recognition, respectively. The compound binds potassium fluoride both in solution and in the solid state, but is stable only under inert conditions. In 2003 *Rissanen* and coworkers reported an uranyl–salophen (Figure 18, **XXXIV**),[144] in which cesium chloride was bound to the receptor as contact ion pair. Related ion pair receptor based on Lewis acidic groups for anion recognition have been reported and were based on Zn,[145] Ru,[146] Re.[146]

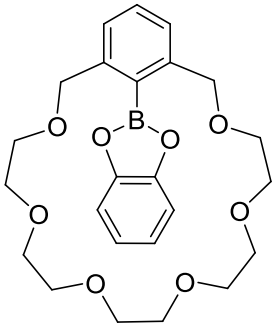

XXXIII

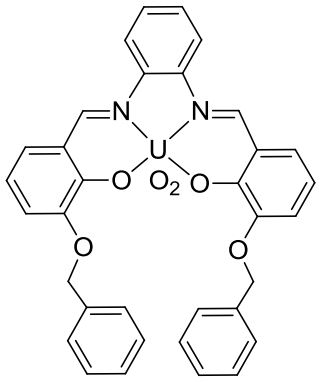

XXXIV

Figure 18. Ion pair receptors based on Lewis acidic groups.

In 2001, *Willem* and coworkers synthesized the ditopic receptor **XXXV** (Figure 19)[147] and showed its ability to complex sodium thiocyanate. Due to the kinetic lability of the Sn–O bond, the complex formed was unstable in solution.

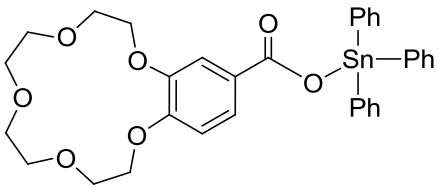

XXXV

Figure 19. Ion pair receptor reported by *Willem* and coworkers.

In the last ten years, *Jurkschat* and coworkers reported a series of receptors shown in Figure 20. Most remarkably, and in contrast to the *Whillem´s* receptor, the organotin fragment is bound to the crown ether ring through a kinetically inert tin-carbon (Sn–C) bond. Compounds of type **XXXVI** [148] are able to bind sodium rodhanide in a heterotopic fashion and receptor of type **XXXVII**[149-151] complexes ditopically alkalimetal thiocyanate. The increase of the Lewis acidity of **XXXVII** by adding a second organotin moiety linked via a methylene bridge to the first tin atom and by functionalization of the tin atoms with electron withdrawing atoms affords compounds of type **XXXVIII**[151,152] and **XXXIX**[149,151,153], respectively. The former is able to overcome the high lattice energy of sodium and potassium fluoride in acetonitrile and in methanol, respectively, and to complex the corresponding salt as solvent- and host-separated ion pair in the solid state, respectively. The latter shows affinities for alkali metal chlorides and ditopic complexation were observed both in solution and in the solid state. Only recently, *Jurkschat* and coworkers followed this strategy to synthesize the receptor of type **XXXX** (Figure 20).[154] The authors showed that the latter bind alkali metal halides in solvents including water. Interestingly, all these compounds are able to extract salts from an aqueous phase and to transport them through an organic membrane.

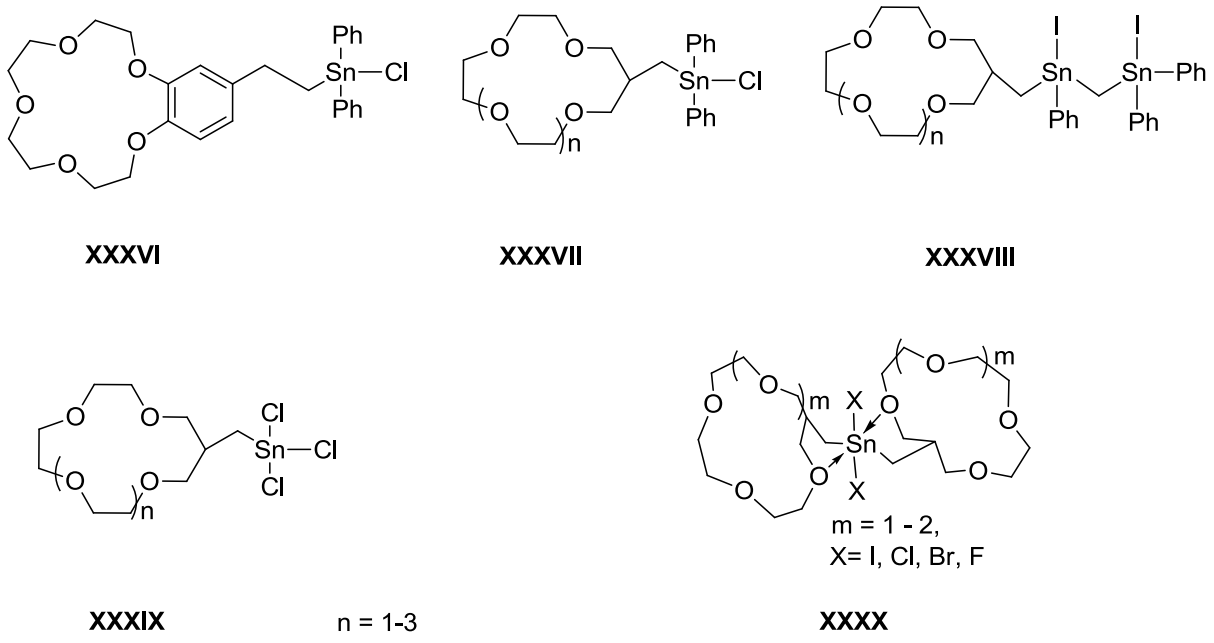

Figure 20. Ion pair receptor reported by *Jurkschat* and coworkers.

The goal of this work were the syntheses of new ditopic receptors based on tin-containing crown ether-substituted ferrocene and ferrocenophanes, respectively, (Figure 21) and the study of their complexation behavior and electrochemical properties toward inorganic salts.

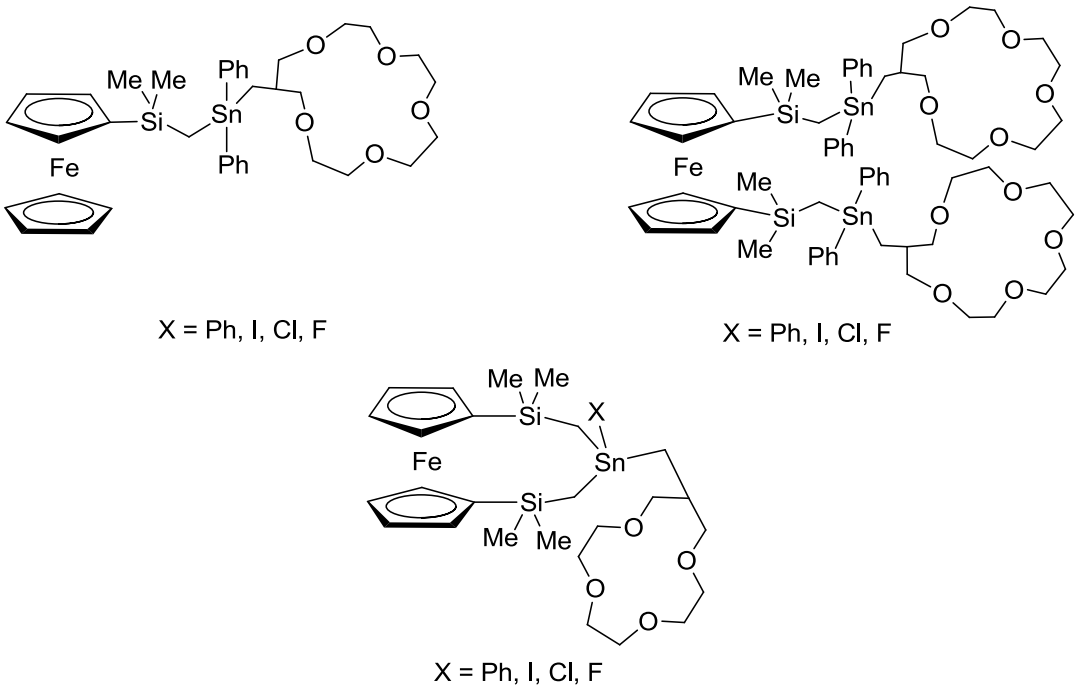

Figure 21. Open-chain ferrocene- and ferrocenophane-based organotin(IV) substituted crown ethers.

The first chapter of this work deals with the syntheses of open-chain ferrocene- and ferrocenophane-containing organotin(IV) compounds (Figure 21). Additionally to the studies of the complexation behaviour of the latter compounds, their ability to act as redox active sensors was investigated. It will be demonstrated the affinity of these receptors to bind alkali metal salts in ditopic fashion. Cyclic voltammetry will be also used to confirm the formation of the complexes. Moreover, it is also shown that these compounds may be involved in surface modification. Indeed, covalent grafting of these molecules, via the formation of C-Sn bond, occurs allowing one to immobilize Fc moiety at such surfaces.

The second chapter is related to the reactivity of the monoorganotin(IV) cation **XXXXI** (Figure 22) with thio- and alkohol groups as well as with fluorinating agents. Interestingly, a rare example of the monomeric monoorganotin(IV) trifluoride, the trifluoridomonoorganotin(IV)-substituted-crown-5 ether (**XXXXII)**, in the solid state, will be presented. Its complexation behaviour towards $Et_4NF{\cdot}2H_2O$, NaF and D_2O will be investigated.

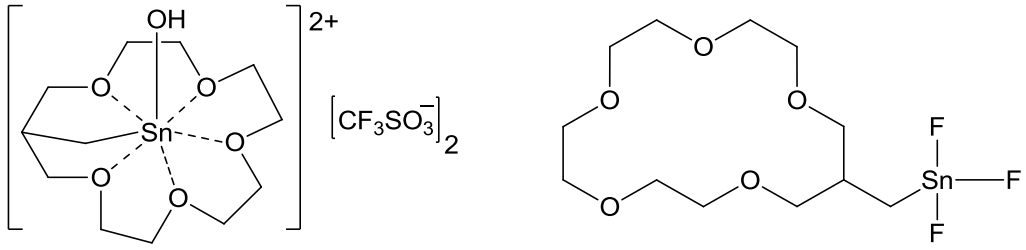

XXXXI **XXXXII**

Figure 22. Monoorganotin(IV) dications (**XXXXI**) and monoorganotin(IV) trifluoride (**XXXXII**).

Novel tetraorgaonodistannoxanes (Figure 23) containing three different organic groups at the Sn_2O_2 four-membered ring will be highlighted in the third chapter. It will be shown that according to the crown ether ring size at the *endo*-cyclic tin atoms, the intramolecular O→H interactions can take place.

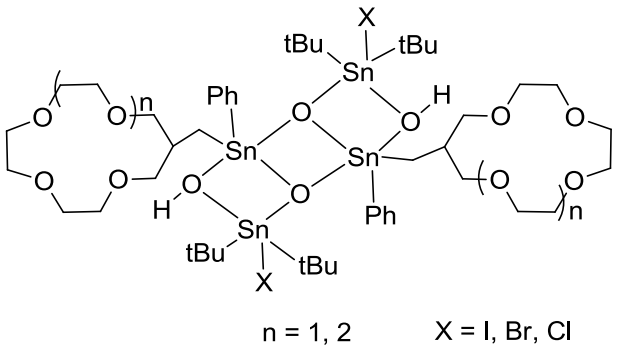

Figure 23. Tetraorganodistannoxanes.

2. Organotin Containing Crown Ether-substituted Ferrocene as Ditopic Receptor for Alkali Metal Salts.

2.1. Introduction

For many decades, numerous macrocyclic receptors have been designed, synthesized and their ability to bind anions or cations has been intensively investigated. However, during the complexation process, the counter ion always remains bound to the targeted ion through electrostatic interactions, which can hinder the single-ion recognition process.[131,155,156] An alternative to overcome this problem is to design a system that is able to complex simultaneously both cation and anion. Such compounds are called ditopic receptors and are defined as multifunctional ligands having two or more binding sites in their frameworks and being able to complex both ions of a salt (Figure 24).

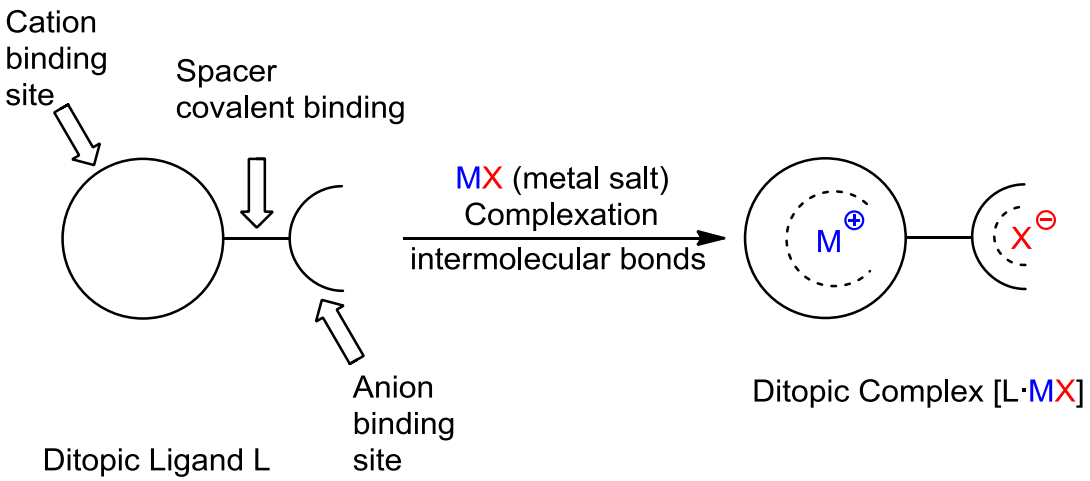

Figure 24. Ditopic receptor.

Ion pair recognition can be classified according to the three different binding modes illustrated in Figure 25. In Figure 25a, the cation and the anion are bound inside the host molecule as contact ion pairs, wherein the cation and the anion are in close proximity. In the second design, the salt is complexed as a solvent-separated ion pair with one or more solvent molecules being bridged between the anion and the cation (Figure 25b). The third coordination mode involves a host-separated ion pair, wherein the distance between the anion and the cation are relatively far from one another.

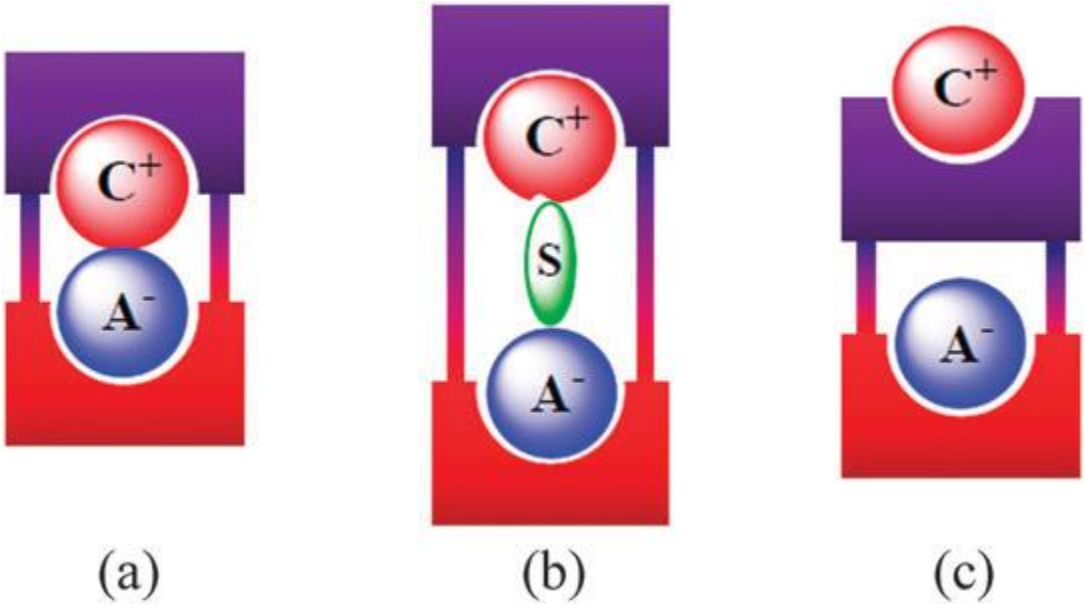

Figure 25.[157] Common design of ditopic receptors: a) contact ion pair, b) solvent-bridged ion pair, and c) host-separated ion pair. A^- is referred to anion, the cation is represented as C^+, and the solvent is shown as S.

Ditopic receptors are of great interest regarding their potential application in many areas such as:

–Salt extraction agents that are related to the removal or the separation of species from mixture (Figure 26).

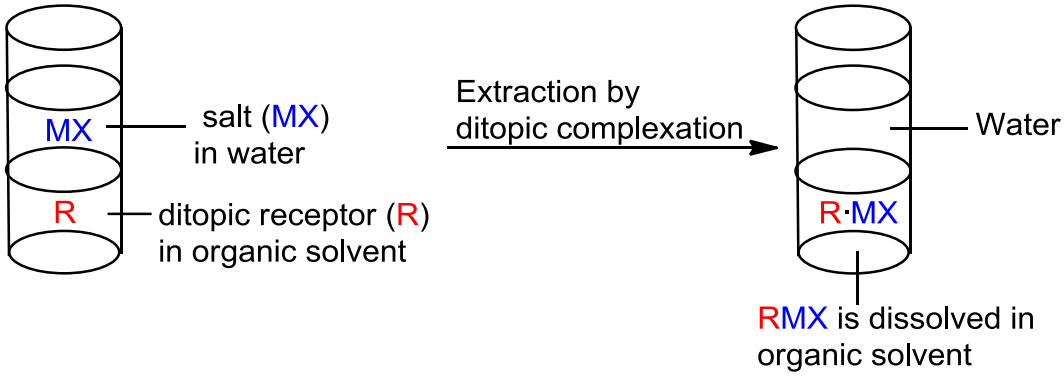

Figure 26. Salt extraction.

One solution to environmental problems can be the design of receptors for extraction and removal of radioactive ions or pollutants. A straightforward example is a salen receptor reported by *Tasker* and coworkers. They showed the ability of compound **XXXXIII** (Figure 27)[158] to extract $CuSO_4$ from aqueous solution into chloroform.

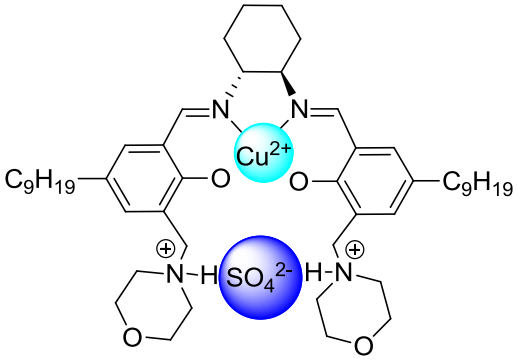

XXXXIII

Figure 27. Salen receptor for extracting $CuSO_4$ as reported by *Tasker* and coworkers.

–Salt solubization agents, in which the solubility of a hydrophilic salt is enhanced in organic solvent (Figure 28).

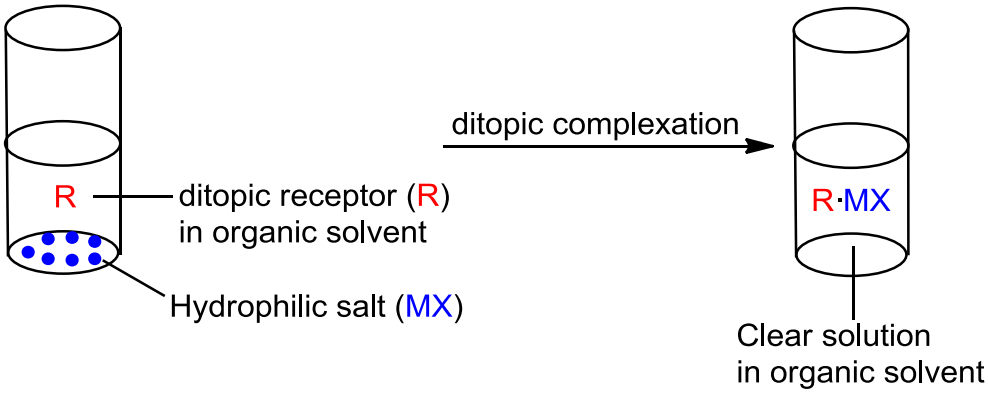

Figure 28. Salt solubilization.

For example the calix[4]semitube based receptor **XXXXIV** (Figure 29)[159] was described as solubilization agent for alkali-metal halides.

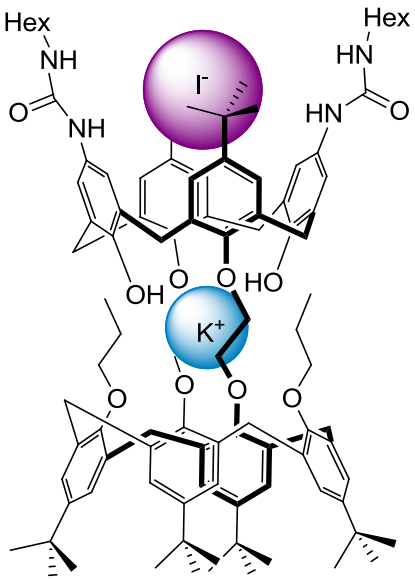

XXXXIV

Figure 29. Calix[4]semitube for the solubilization of alkali-metal halide salts as reported by *Beer* and coworkers.

–Membrane transport agents which are related to salt solubilization and salt extraction. It consists in the removal of hydrophilic salts from aqueous phase and to transport them through an organic membrane to another aqueous phase (Figure 30).

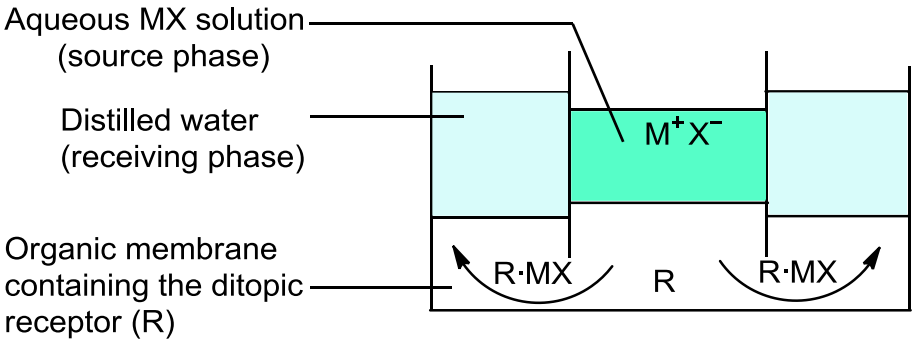

Figure 30. Salt transport.

A straightforward example for membrane transport agents is the system **XXXXV** (Figure 31) developed by *Reinhoudt* (Figure 31)[160] and that has proved to be suitable for the transport of KCl.

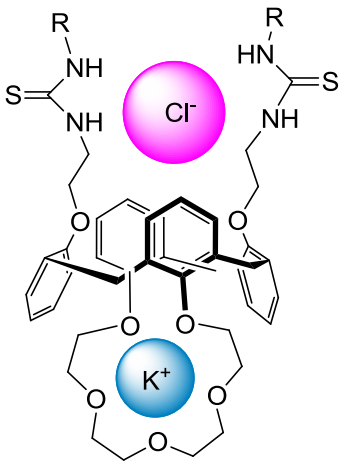

R = 2-ethylhexyl

XXXXV

Figure 31. Heteroditopic receptor for studying menbrane transport of KCl as reported by *Reinhoudt* and coworkers.

–Sensors in which the targeted ion pair is simultaneously detected by a suitable electrochemical reporter group incorporated into the receptor design (Figure 32).

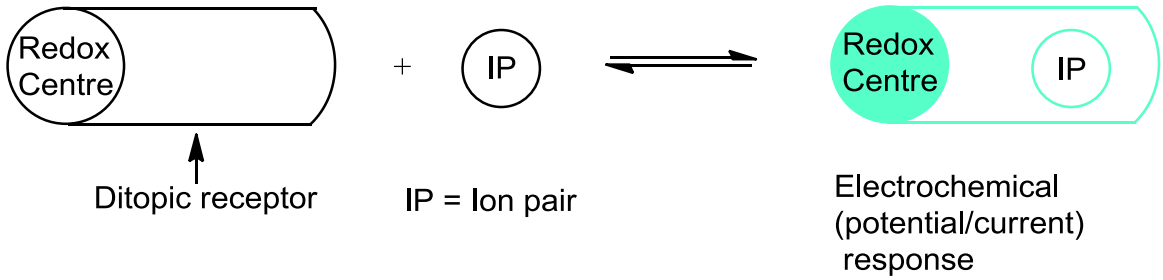

Figure 32. Sensors for ion pair.

This application is important for the detection of biologically and environmentally relevant ion pairs.[161] In order that the sensing of ion-pair binding takes place, the receptor design must be incorporated into a suitable optical or electrochemical reporter group. However, and due to the competitiveness of the ion pairing outside the receptor and the precipitation of the ion pair, there are only few examples of ditopic receptors that make use of an electrochemical sensor for sensing ion pair binding. A rare example of such system is the ferrocene-based receptor **XXXXVI** shown in Figure 33[162] which displays cathodic shifts of the ferrocene/ferrocenium redox couple upon addition of hydrogen sulfate to the receptor in the presence of

barium and anodic shifts upon addition of barium to the receptor in the presence of hydrogen sulfate.

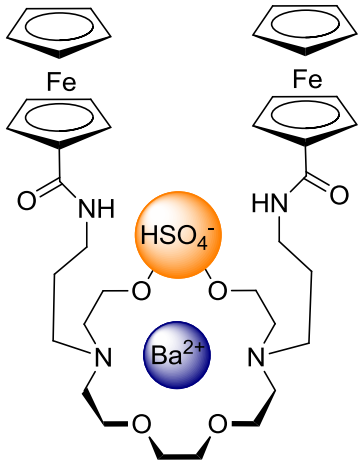

XXXXVI

Figure 33. Ferrocene ion pair receptor as sensors reported by *Beer* and coworkers.

To the best of our knowledge, there is no report based on ditopic receptors using an electrochemical reporter group coupled to the Lewis acidity of organometallic moieties for sensing of ion-pair. We present here the first examples of this class of compounds and their complexation behaviour as well as their electrochemical studies toward inorganic salts. Cathodic grafting of ferrocenyl moieties onto glassy carbon surface is also discussed.

2.2. Syntheses, Structures and Complexation Behaviour of the Organotin-Containing Crown Ether-substituted Ferrocene.

2.2.1. Synthesis and Structures in Solution of the Tetraorganotin-substituted Crown Ethers.

The reaction of the Grignard reagent $FcSi(Me_2)CH_2MgCl$[130] and $fc(Si(Me_2)CH_2MgCl)_2$[130] with one and two molar equivalent of Iodo(1,4,7,10,13-pentaoxacyclohexadec-15-ylmethyl)diphenylstannane[150] gave the tetraorganotin-substituted crown ethers **1** and **2**, as viscous red oils, in 64 % and 69 % yield, respectively (eq. 1 and 2).

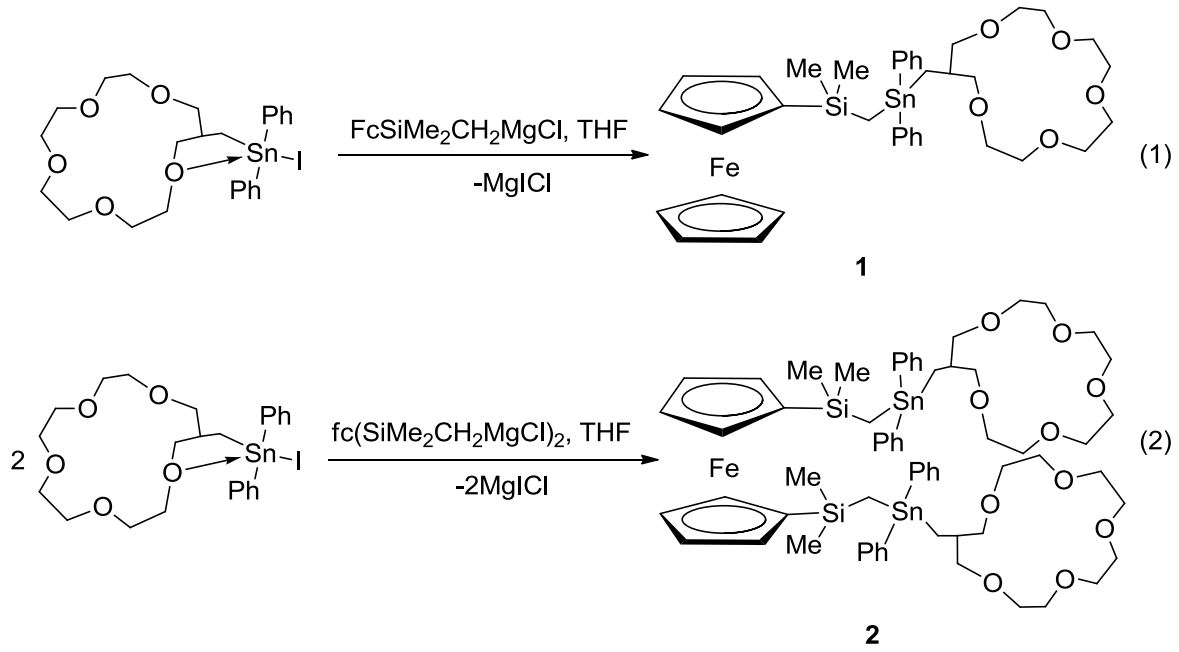

The ^{119}Sn NMR spectra in $CDCl_3$ of compounds **1** and **2** show resonances at δ – 66 which are comparable to that measured for the analogous $(Me_3SiCH_2)Ph_2SnCH_2$-[19]-crown-6 (δ –64)[163]. These chemical shifts are close to δ –60 and –68 reported for Ph_2SnMe_2,[164] and Ph_2MeSnI,[165]respectively, and correspond to tetracoordinated tin atoms.

2.2.2. Synthesis of the Triorganotin Halide-substituted Crown Ethers.

The nature of the substituents at the tin atom determines the Lewis acidity of organotin compounds. Tetraorganotin compounds are generally known to have a weak acidity and the tin atom is not electrophilic enough to undergo strong interactions with electron-donating atoms (EDA). The increase of the Lewis acidity of

the tin atom is a strategy to allow such interactions. The functionalization of the tin atom with electron withdrawing substituents such as halogen atoms is a method to achieve this goal. Reaction in CH_2Cl_2 under ice-cooling of the tetraorganostannane **1** and **2** with one and two molar equivalent of iodine gave the corresponding iodidotrioganotin-substituted crown ethers **3** and **4**, respectively, in almost quantitative yield (eq. 3 and 4).

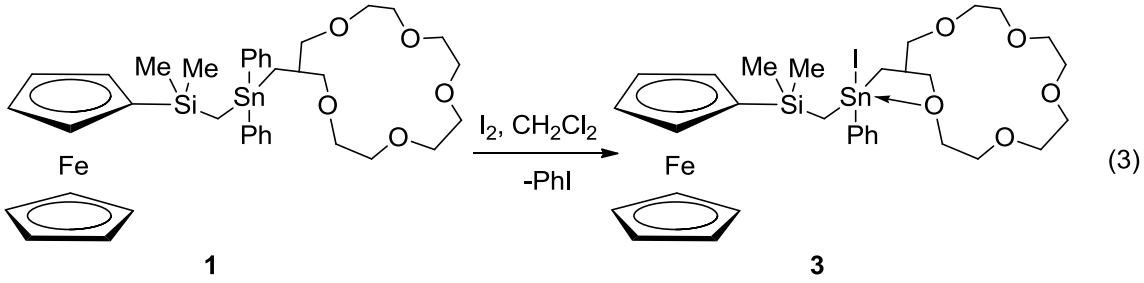

1 **3** (3)

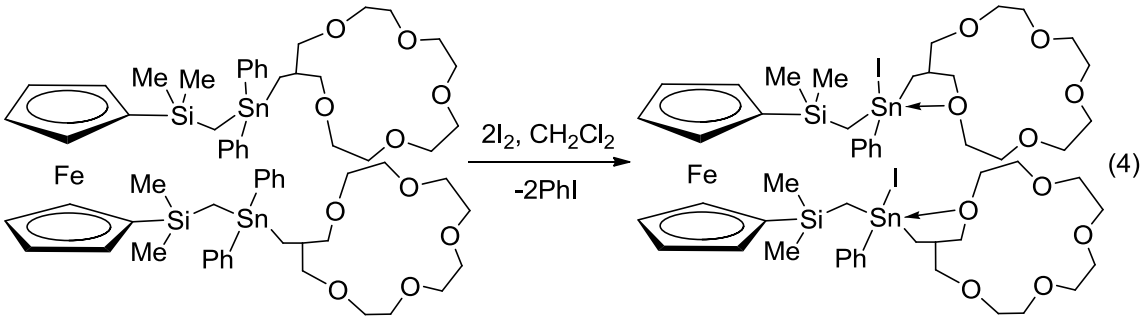

2 **4** (4)

Treatment of **3** and **4** with an excess of AgCl in acetonitrile over a period of 14 days afforded the triorganotin chlorides **5** and **6**, respectively (eq. 5 and 6).

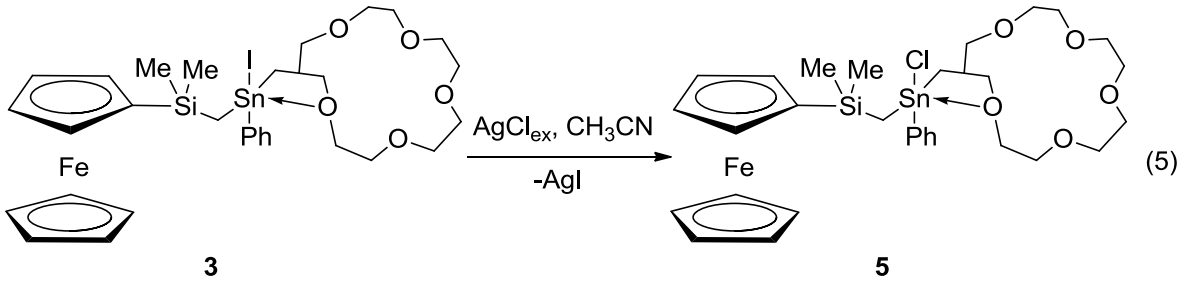

3 **5** (5)

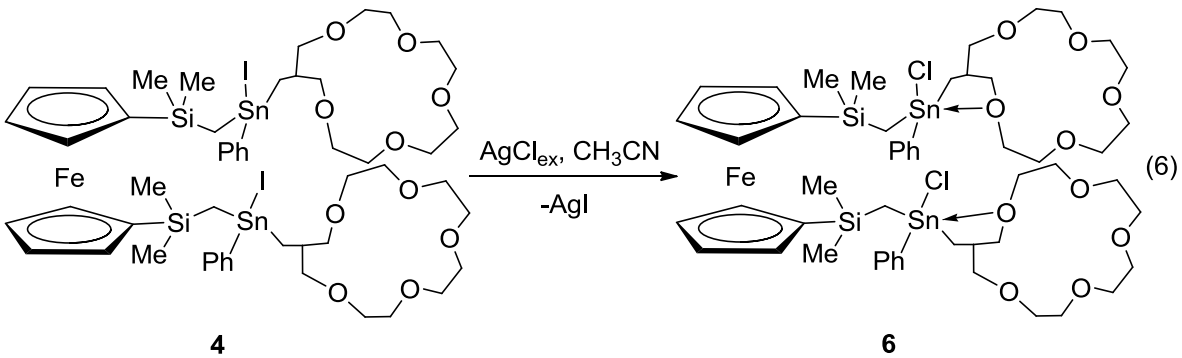

4 **6** (6)

In a similar manner, compounds **3** and **4** were converted into the corresponding triorganotin fluoride **7** and **8**, respectively, by the reaction with an excess of potassium fluoride, KF, in the biphasic mixture CH_2Cl_2/H_2O for two days (eq. 7 and 8).

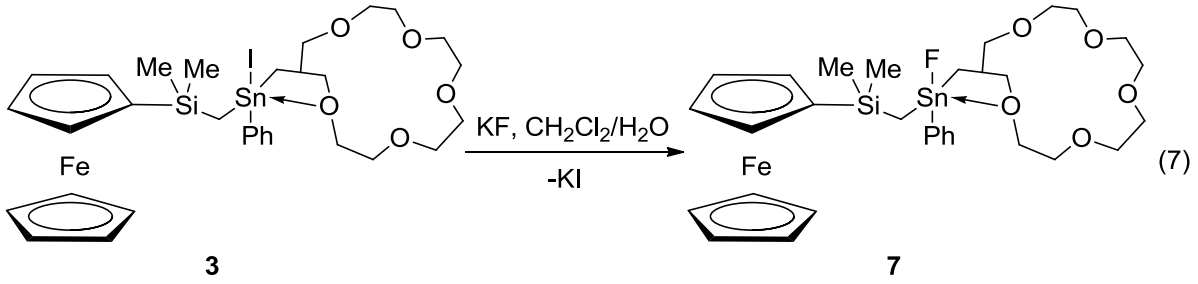

3 **7**

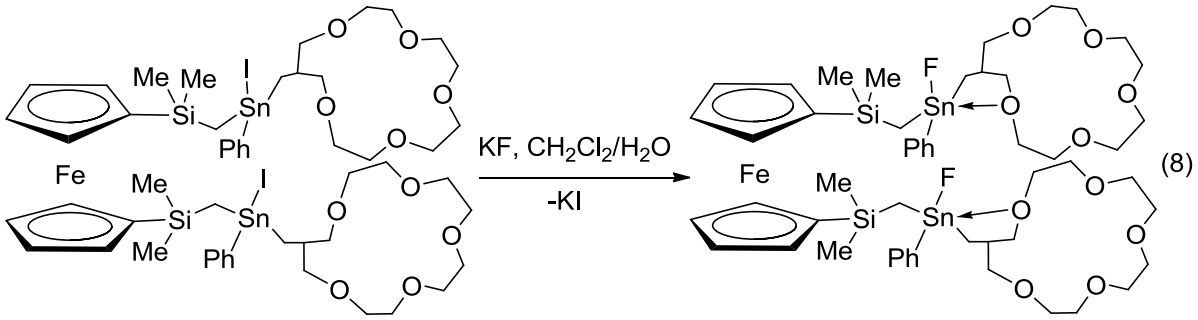

4 **8**

All these compounds are air stable materials and were isolated as viscous oils that are soluble in common organic solvents such as dichloromethane, chloroform, acetone, THF and acetonitrile.

Attempts at synthesizing the triorganotin bromides **9** and **10** by treatment of compounds **1** and **2** with one and two molar equivalent of bromine, Br_2, respectively, failed (eq. 9 and 10).

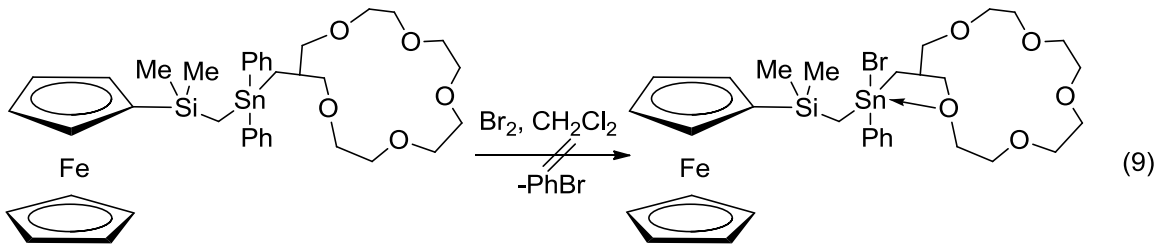

1 **9**

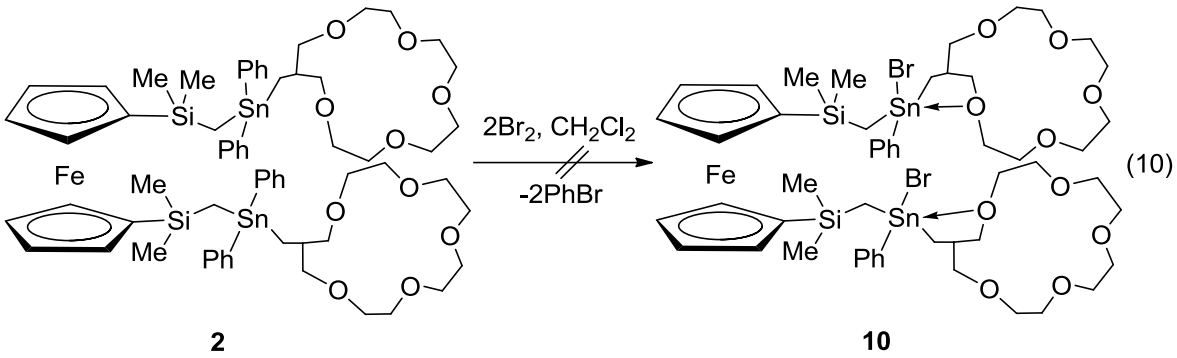

2 **10**

The ^{119}Sn NMR spectra in $CDCl_3$ at room temperature of a mixture of **1** or **2** with Br_2 showed single signal at δ – 29, respectively, whereas the ^{29}Si NMR spectra showed no resonance. The ^{1}H NMR spectra of these solutions displayed broad resonances indicating exchange processes being fast at room temperature. After few days, the color of the solution turns from red to green, indicating the oxidation of ferrocene to ferrocenium. The paramagnetic solution obtained is likely due to a redox reaction involving bromine and the ferrocene unit.

2.2.3. Structures of the Triorganotin Halide-substituted Crown Ethers in Solution.

The ^{119}Sn- and ^{19}F-NMR chemical shifts of the triorganotin halides **3**–**8** in $CDCl_3$ (**3**, **7**, **8**) and CH_3CN (**5**, **6**) are summarized in Table 1.

Table 1: Chemical shifts of the triorganotin halides **3**–**8**.

Compounds	^{119}Sn-NMR ppm	$^{1}J(^{119}Sn–^{19}F)$ Hz	^{19}F-NMR ppm	$^{1}J(^{19}F–^{119}Sn)$ Hz
3	s, –72			
4	s, –72			
5	s, –17			
6	s, –18			
7	d, –22	2184	184	2182
8	d, –23	2181	184	2182

They are high-field shifted in comparison to the ^{119}Sn chemical shifts of nonsubstituted iodidotriorganotin compounds such as $\{(Me_3SiCH_2)_2SnI\}_2CH_2$ (δ 45),[166] , $Ph_2EtSnCl$ (δ 17),[167] $(PhCMe_2CH_2)_3SnF$ (δ 139),[168] $(Me_3SiCH_2)Ph_2SnF$ (δ

25, $^{1}J(^{119}Sn–^{19}F)$ 2380).[110] This observation indicates for these compounds the presence of the intramolecular O→Sn coordination (see eq. 3-8). The ^{119}Sn NMR spectra of the triorganotin iodides **3** and **4** and of the triorganotin fluorides **7** and **8** are close to those found for $Ph(Me_2SiCH_2)ISnCH_2$-[19]-crown-6 (δ –70),[163] and of $Ph(Me_2SiCH_2)FSnCH_2$-[19]-crown-6 (δ –16, $^{1}J(^{119}Sn–^{19}F$ = 2182 Hz).[163] As expected, on the ^{13}C NMR time scale, compounds **3–6** display, at ambient temperature, symmetric structures in solution, as evidenced by the ^{13}C NMR spectra showing for each compound pairs of equivalent carbon atoms C6/C8, C5/C9, C3/C11, C2/C12, and C14/C16 (according to the atom numbering shown in scheme 18). Suchs findings were also observed for [Ph_2XSn-CH_2-[16]-crown-5 (X = Cl, I, Br)],[150] wherein more detailed reasoning for this statement has been given. However, in contrast to compounds **3–6**, the triorganotin trifluorides **7** and **8** show each 11 resonances for the crown ether carbon atoms, which indicate an unsymmetrical structure in solution (Figure 34).

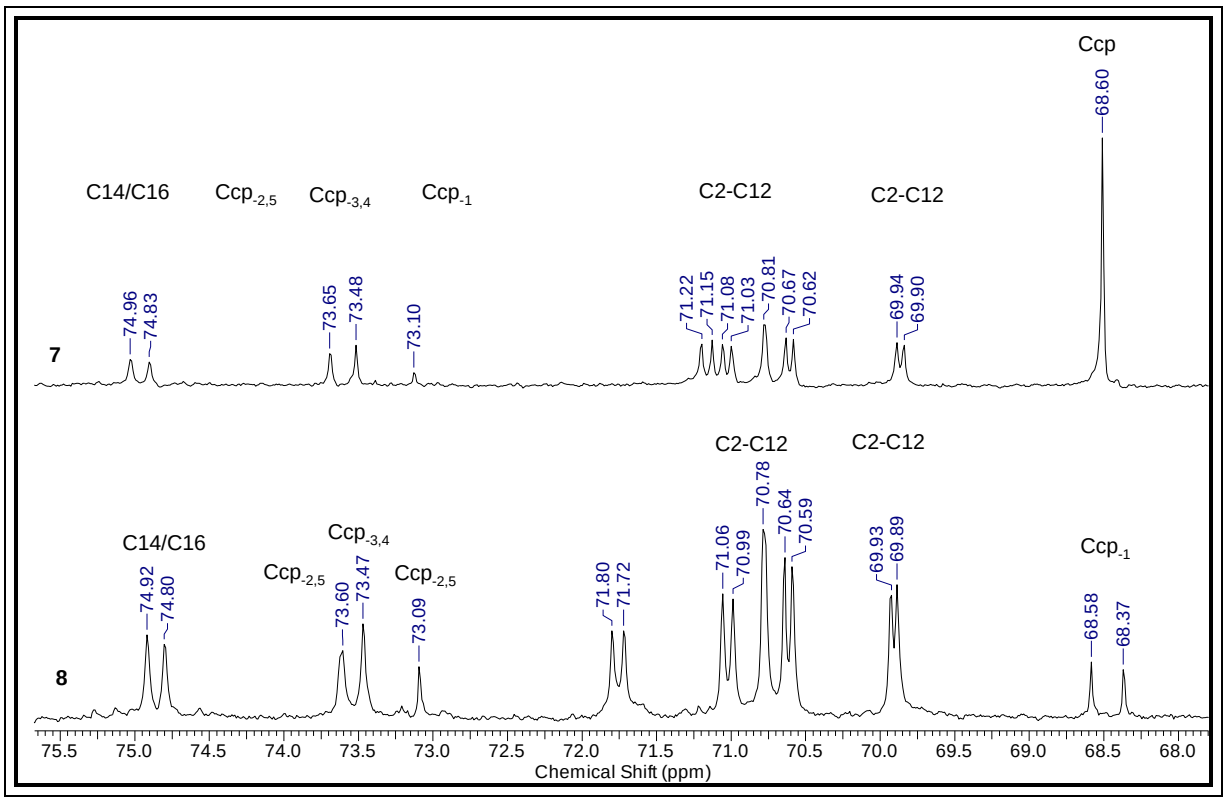

Figure 34. ^{13}C-NMR spectra of **7** and **8** in $CDCl_3$ showing the resonances for the crown ether carbon atoms C2-C12 and C14/C16 and for the cyclopentadiene carbons.

Moreover, the ^{13}C NMR spectra in $CDCl_3$ of the two latter compounds display for each compound two resonances for the methyl carbon atoms at *δ* 0.32 and 0.54 (**7**) and *δ* 0.85 and 1.04 (**8**), four resonances for the methylene carbon atoms at *δ* 2.35, 2.48, 15.36 and 15. 50 (**7**) and *δ* 2.89, 3.01, 15.84 and 15.96 (**8**), five and six resonances for the cyclopentadiene carbon atoms, respectively, at *δ* 68.12, 70.33, 72.62, 72.99, 73.17 (**7**) and *δ* 68.37, 68.58, 70.78, 73.09, 74.47, 73.60 (**8**), and two resonances for the *ipso*-carbon atoms of the phenyl groups at *δ* 143.20 and 143.33 (**7**) and 143.66 and 143.77 (**8**) ppm.

Furthermore, compounds **3**–**8** exhibit, at ambient temperature and on the ^{1}H NMR time scale, as a result of their diastereotopism, ABX-type resonances for the $SiCH_2Sn$ and $SnCH_2$ protons. As a representative example of the trioganotin compounds **3**–**8**, the ^{1}H NMR spectrum (400,13 MHz) of the triorganotin fluoride **8** is presented in Figure 35. It shows ABX-type resonances for the $SiCH_2Sn$ and $SnCH_2$ protons at *δ* 0.80/0.93 ($^{2}J(^{1}H–^{1}H)$ = 12.0Hz, $^{4}J(^{1}H–^{1}H)$ = 12.0Hz, $^{2}J(^{1}H–^{117}Sn)$ = 80.0 Hz, $^{2}J(^{1}H–^{119}Sn)$ = 104.0 Hz) and *δ* 1.33/1.52 ($^{2}J(^{1}H–^{1}H)$ = 8.0Hz, $^{3}J(^{1}H–^{1}H)$ = 12.0Hz, $^{2}J(^{1}H–^{117}Sn)$ = 56.0 Hz, $^{2}J(^{1}H–^{119}Sn)$ = 80.0 Hz), respectively, which indicate the stability on the ^{1}H NMR time scale of the tin atom in compound **8**.

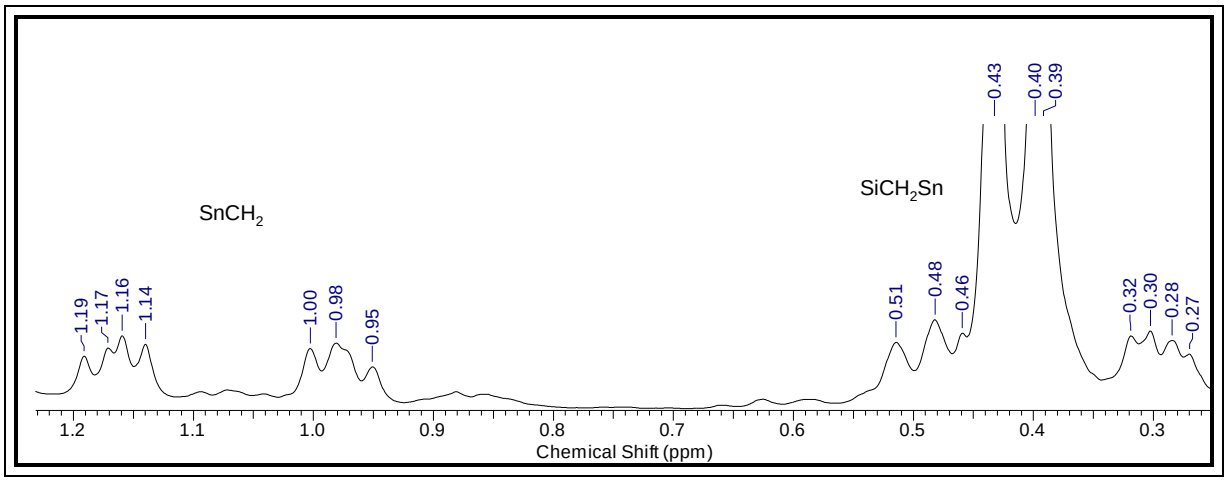

Figure 35. ^{1}H-NMR spectrum showing the resonances for the $SnCH_2$ and $SiCH_2Sn$ protons of **8** in $CDCl_3$.

The ESI-MS spectra in the negative mode of compounds **5** and **6** showed mass clusters centered at m/z 771.1 and 1321.4 that are assigned to {FcSi$(Me_2)CH_2SnClPhCH_2$-[16]-crown-5·Cl}$^{-}$ and {fc(Si$(Me_2)CH_2SnPhClCH_2$-[16]-crown-$5)_2$·Cl}$^{-}$, respectively. In the ESI-MS spectra (positive mode) of **5** and **6**, there are mass clusters centered at m/z 736.2 and 1249.3 that are assigned to FcSi

$(Me_2)CH_2Sn(OH)PhCH_2$-[16]-crown-5·$H_2O\}^+$ and {fc(Si$(Me_2)CH_2SnPhCH_2$-[16]-crown-5)$_2$·OH·$H_2O\}^+$, respectively. In addition, for **5** there is a mass cluster centered at m/z 759.2 that is assigned to {FcSi$(Me_2)CH_2Sn(OH)PhCH_2$-[16]-crown-5·$CH_3CN\}^+$. In the ESI-MS spectrum (positive mode) of **4**, there is a mass cluster centered at *m/z* 1231.4 that is assigned to [FcSi$(Me_2)CH_2SnPhCH_2$-[16]-crown-5)$_2$·$OH]^+$. In the negative mode, a mass cluster centered at *m/z* 729.1 was observed that is assigned to [fc(Si$(Me_2)CH_2SnPhICH_2$-[16]-crown-5)$_2$·$OH]^-$. The ESI-MS spectrum in the positive mode of compounds **7** showed a mass cluster centered at m/z 701.2 that is assigned to {FcSi$(Me_2)CH_2SnPhCH_2$-[16]-crown-5$\}^+$. The ESI-MS spectra in the positive mode of compounds **8** showed mass clusters centered at m/z 1233.4 and 1252.4 that are assigned to {fc(Si$(Me_2)CH_2SnPhCH_2$-[16]-crown-5)(Si$(Me_2)CH_2SnFPhCH_2$-[16]-crown-5)·F$\}^+$ and to {fcSi$(Me_2)CH_2SnFPhCH_2$-[16]-crown-5)$_2$·$\}^+$

2.2.4. Complexation Studies of the Triorganotin Halides and Bis(trihalogenidoorganostannyl)-substituted Crown Ether.

2.2.4.1. Complexation behavior of the Triorganotin Chlorides 5 and 6 toward Chloride salts.

The ^{119}Sn NMR spectrum of a solution of the triorganotin chloride **6** in acetonitrile to which had been added two molar equiv of tetraphenylphosphonium chloride, Ph_4PCl, showed a resonance at δ –83 ($\nu_{1/2}$ = 1765 Hz) that is by 70 ppm high field shifted in comparison with the signal of pure **6** (δ –13). This observation is consistent with the formation of the bis(dichloroorganostannane) complex {fc($Me_2SiCH_2SnPhClCH_2$-[16]-crown-5)$_2$·2Cl$\}^-${2$Ph_4P\}^+$ (Scheme 1).

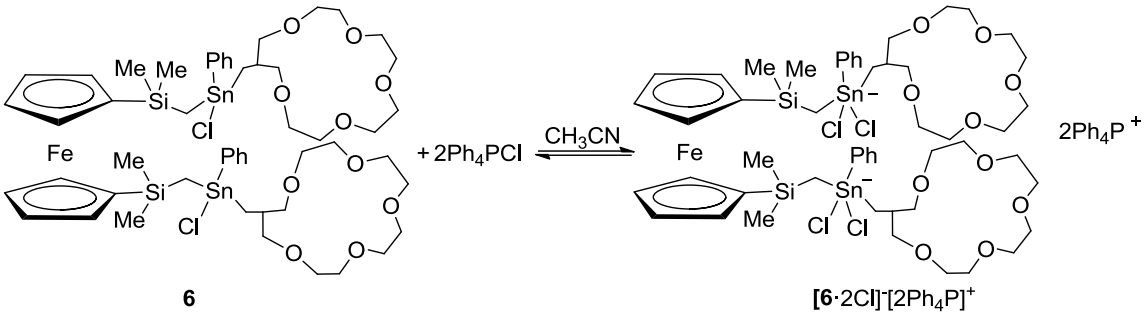

Scheme 1. Reaction of compound **6** with Ph_4PCl in CH_3CN.

After we had learned about the formation of the anionic complex $[\mathbf{6}\cdot 2Cl]^-[2Ph_4P]^+$, we investigated the ability of compound **6** to complex salts in a ditopic fashion. Thus, the lipophilic cation was replaced by lithium.

The ^{119}Sn NMR spectra at room temperature of solutions of compound **5** and **6** in CH_3CN to which had been added an excess of lithium chloride displayed single resonances at δ –126 (386 Hz) and –106 (811Hz), respectively, which are shifted by 89 and 105 ppm to high field, with respect to the parent compound **5** and **6**, respectively. The high displacement of the chemical shifts are assigned to the ditopic complexes [**5**·LiCl] and [**6**·2LiCl], respectively (Scheme 2 and 3).

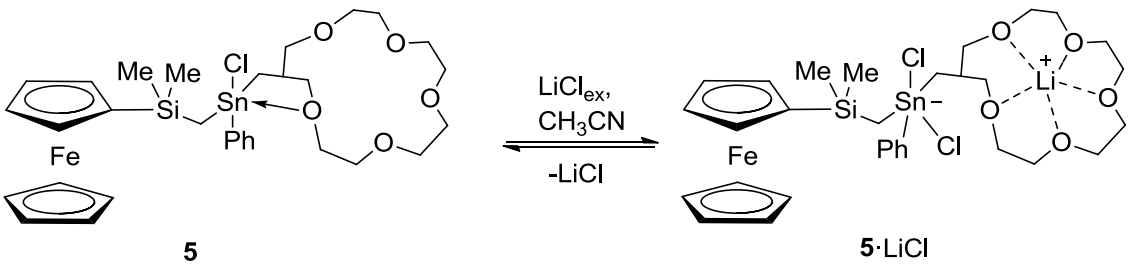

Scheme 2. Reaction of compound **5** with LiCl in CH_3CN.

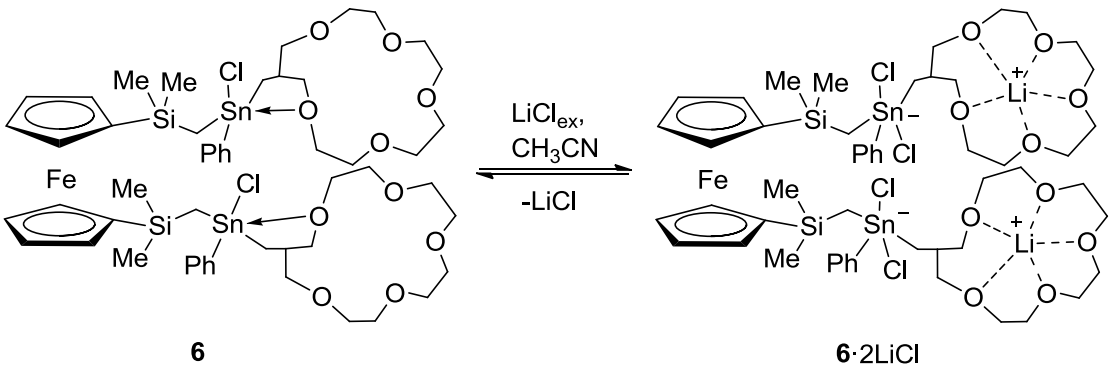

Scheme 3. Reaction of compound **6** with LiCl in CH_3CN.

The formation of [**5**·LiCl] and [**6**·2LiCl] is further supported by ^{1}H and ^{13}C NMR spectroscopy.

The ^{13}C NMR spectra of (**5** + $LiCl_{ex}$) and (**6** + $LiCl_{ex}$) in CH_3CN showed significant low field shifts for the $SiCH_2Sn$ ([**5**·LiCl], $\Delta\delta$ = 6.40; [**6**·2LiCl], $\Delta\delta$ = 7.30), $SnCH_2$ ([**5**·LiCl], $\Delta\delta$ = 6.30; [**6**·2LiCl], $\Delta\delta$ = 7.52) and C14/C16 carbon atoms ([**5**·2LiCl], $\Delta\delta$ = 6.13; [**6**·2LiCl], $\Delta\delta$ = 6.45) and high field shifts for the C15 carbon atoms ([**5**·LiCl], $\Delta\delta$ = 1.27; [**6**·2LiCl], $\Delta\delta$ = 1.05) in comparison with the chemical shifts of the host molecules **5** and **6**, respectively (Figure 36).

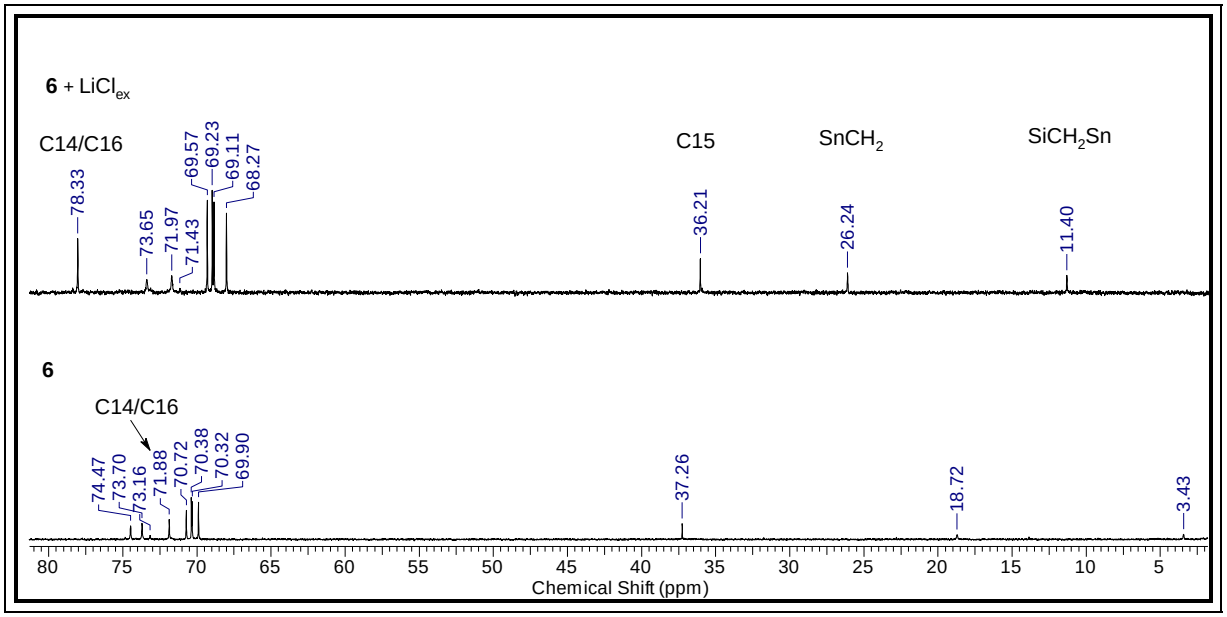

Figure 36. ^{13}C NMR spectrum showing the resonances for the C15, $SnCH_2$, $SiCH_2Sn$ and C14/C16 carbon atoms of pure **6** and of (**6** + $LiCl_{ex}$) in CD_3CN.

The ^{1}H NMR spectra of compounds **5** and **6** in acetonitrile displayed for the $SiCH_2Sn$ and $SnCH_2$ protons singlet and doublet resonances at δ 0.70 (s, $^{2}J(^{1}H–^{119/117}Sn)$ = 93.0Hz, 2H, $SnCH_2Si$), 1.31 (d, $^{3}J(^{1}H–^{1}H)$ = 9.0Hz, $^{2}J(^{1}H–^{117}Sn)$ = 69.0 Hz, $^{2}J(^{1}H–^{119}Sn)$ = 81.0 Hz, 2H, $SnCH_2$) (**5**) and δ = 0.81 (s, $^{2}J(^{1}H–^{119/117}Sn)$ = 96.0Hz) and δ = 1.32 (d, $^{3}J(^{1}H–^{1}H)$ = 8.0Hz, $^{2}J(^{1}H–^{117}Sn)$ = 68.0 Hz, $^{2}J(^{1}H–^{119}Sn)$ = 84.0 Hz) (**6**) respectively. They are characterized by the loss of diastereotopism of the methylene protons observed in the parent compound **6** (Figure 37).

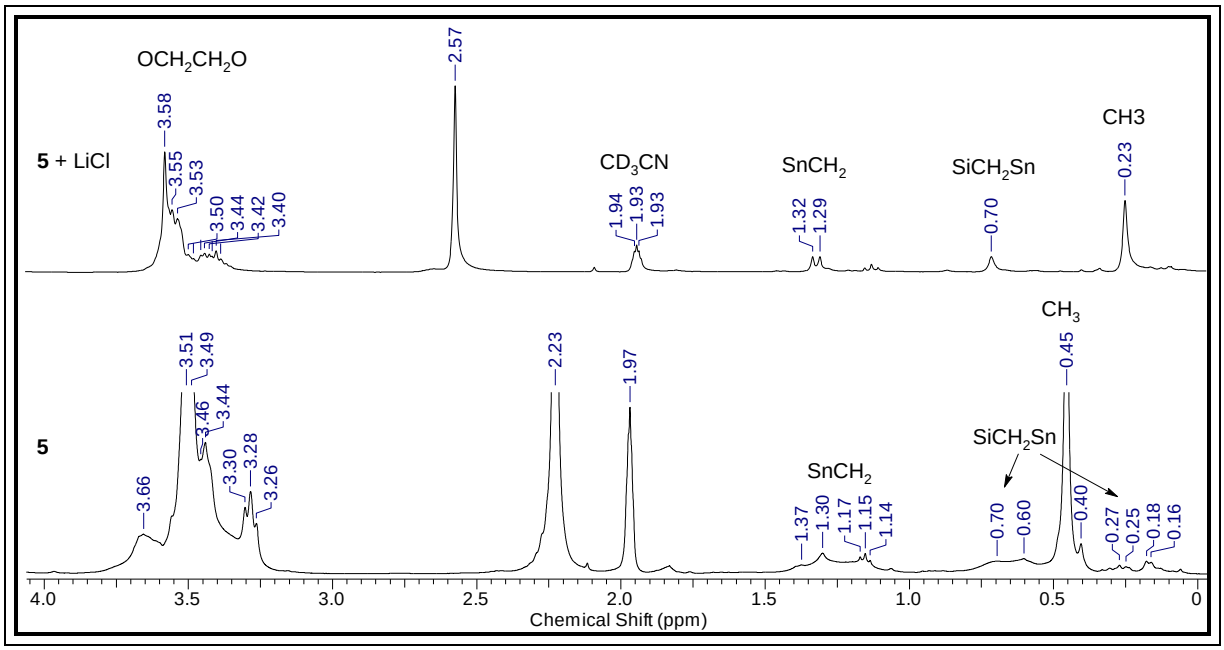

Figure 37. ^{1}H NMR spectrum showing the resonances for the $SnCH_2$, $SiCH_2Sn$, CH_3 and OCH_2 protons of pure **5** and (**5** + $LiCl_{ex}$) in CD_3CN.

Moreover, the complex patterns for the OCH_2 protons of [**5**·LiCl] and [**6**·2LiCl] observed at δ 3.45–3.67 and δ 3.40–3.58, respectively, are high field shifted and show narrower distribution than the parent compounds **5** and **6** (Figure 37).

An ESI-MS spectrum in the positive mode of a solution of (**5** + LiCl) showed mass clusters centered at 701.2, 743.2, 759.2 that are assigned to $[FcSi(Me)_2CH_2SnPhCH2\text{-}[16]\text{-}crown\text{-}5]^+$, $[FcSi(Me)_2CH_2SnPhCH_2\text{-}[16]\text{-}crown\text{-}5)_2\cdot CH_3CN\cdot H]^+$, $[FcSi(Me)_2CH_2SnPhCH_2\text{-}[16]\text{-}crown\text{-}5)_2\cdot CH_3CN\cdot OH]^+$, respectively. In the negative mode, there is a mass cluster centered at 771.1 that is assigned to $[FcSi(Me)_2CH_2SnClPhCH2\text{-}[16]\text{-}crown\text{-}5\cdot Cl]^-$. The ESI-MS spectrum in the positive mode of a solution of (**6** + LiCl) showed mass clusters centered at 1249.4, 1291.3 that are assigned to $[fc(Si(Me)_2CH_2SnPhCH_2\text{-}[16]\text{-}crown\text{-}5)_2\cdot H_2O\cdot OH]^+$ and $[fc(Si(Me)_2CH_2SnPhCH_2\text{-}[16]\text{-}crown\text{-}5)_2\cdot 2H_2O\cdot CH_3CN]^+$. The ESI-MS spectrum in the negative mode of a solution of (**6** + LiCl) showed a mass cluster centered at 1321.4 that is assigned to $[fcSi(Me)_2CH_2SnPhClCH_2\text{-}[16]\text{-}crown\text{-}5)_2\cdot Cl]^-$.

2.2.4.2. Complexation Behaviour of the Triorganotin Fluorides 7 and 8 toward Fluoride Salts.

The ^{119}Sn NMR spectrum in CD_3CN at room temperature of compound **8** to which had been added two molar equivalent of $Bu_4NF{\cdot}3H_2O$ showed a triplet resonance at δ –208 ($^1J(^{119}Sn - ^{19}F)$ = 1893 Hz) (Figure 38). The ^{19}F NMR spectrum of the same solution displayed a sharp singlet resonance flanked by satellites at δ –133 [($^{19}F–^{117}Sn$) = 1818 Hz, ($^1J(^{19}F–^{119}Sn)$ = 1895 Hz] (Figure 39).

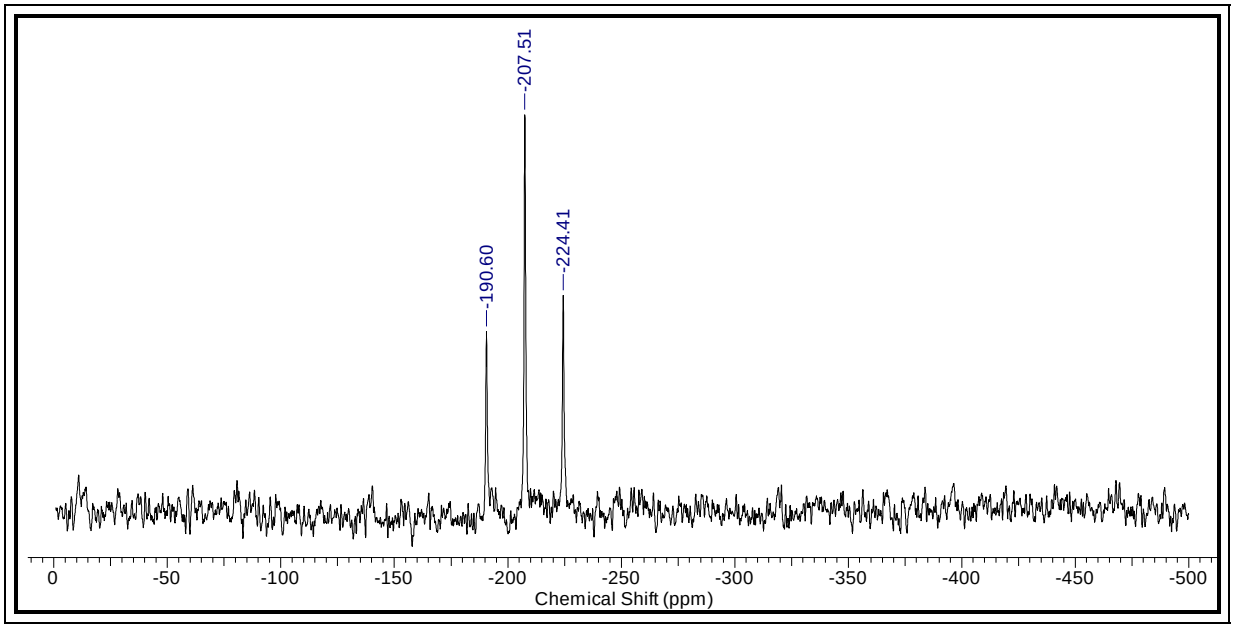

Figure 38. ^{119}Sn NMR spectrum of (**8** + Bu_4NF) in CD_3CN at 23° C.

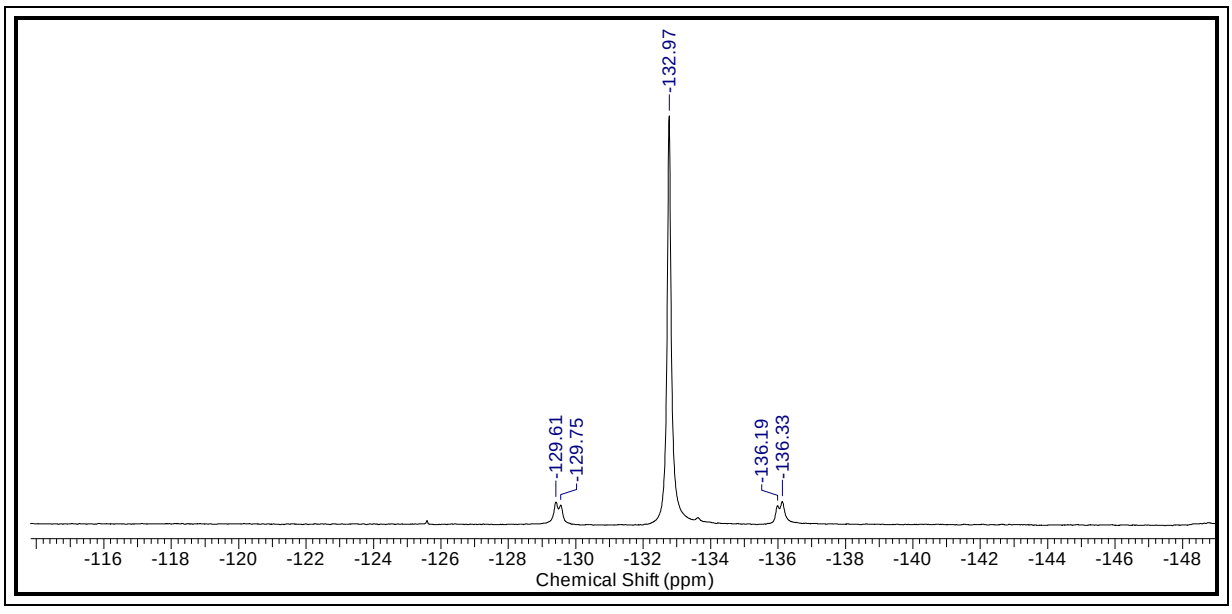

Figure 39. ^{19}F NMR spectrum of (**8** + Bu_4NF) CD_3CN at 23° C.

Both NMR spectra support the formation in situ of the dianionic species $\{Fc(Me_2SiCH_2SnFPhCH_2\text{-}[16]\text{-crown-}5)_2{\cdot}2F\}^{-}\{2Bu_4N\}^{+}$ (Scheme 4). Moreover, the ^{119}Sn and ^{19}F NMR spectra as well as the magnitudes of the couplings constant fall in the range of those obtained for the analogous anionic species $\{[Ph_2FSnCH_2\text{-}[19]\text{-crown-}6{\cdot}F]^{-}$, [$^{119}Sn$, t, δ –267 ($^1J(^{119}Sn–^{19}F)$ = 1867 Hz]; [^{19}F, s, δ –150 ($^1J(^{19}F–^{117/119}Sn)$ = 1809 Hz]$\}$[151].

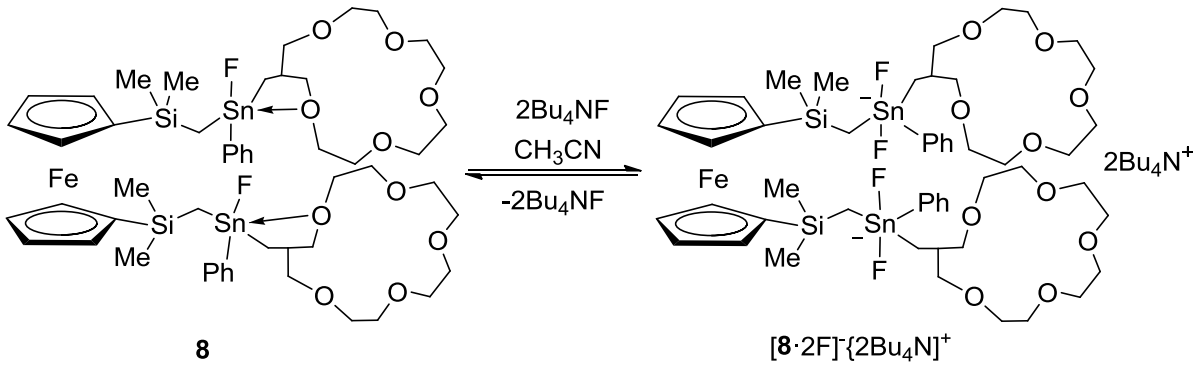

Scheme 4. Reaction of compound **8** with $Bu_4NF{\cdot}3H_2O$ in CH_3CN.

However, and in contrast to compound **8**, the ^{119}Sn NMR spectrum of compound **7** in $CDCl_3$ at room temperature, to which had been added one or two molar equivalents of $Bu_4NF{\cdot}3H_2O$ showed no signal and the ^{19}F NMR spectrum displays unresolved resonances in the area of 120 to 150 ppm. The ^{119}Sn and ^{19}F NMR spectra at – 40 °C are almost the same indicating exchange processes being fast even at low temperature. This lack of changes observed in ^{119}Sn and ^{19}F NMR spectra of a solution of **7** with $Bu_4NF{\cdot}3H_2O$ in $CDCl_3$ can be explained by the change of solvent. Indeed, as previously reported[148,149,151,152,163,169,170] the nature of the solvents strongly influences the complexation of a salt by a receptor.

In order to study the ability of **8** to form a heteroditopic complex, we replaced *n*-Bu_4N^{+} by Na^{+}. The ^{119}Sn NMR spectrum in CD_3CN at room temperature of a solution of **8** to which had been added two molar equivalent of NaF showed no change of the resonance. The non-formation of the corresponding fluoride complex is probably due to the high lattice energy (914 KJ/mol)[171] of sodium fluoride. Cesium fluoride has a lower lattice energy (748 kJ/mol)[171] than sodium fluoride. It has been demonstrated by *Ozutsumi* and coworkers that [12] crown-4 and Cs^{+} are able to form sandwich complexes[172] and only recently *Jurkschat* and coworkers reported sandwich

complexes formed between [13] crown-4 and CsF, with this complex being stabilized by a fluoride bridge.[149]

The ^{19}F NMR Spectrum at room temperature of a CD_3CN solution containing compound **8** and CsF in a molar ratio 1:1 showed broad resonances in the area of δ –130 to – 146, δ –147 to –183 and δ –183 to –213 and the ^{119}Sn NMR spectrum displayed no resonances. At –32° C the ^{119}Sn NMR spectrum showed a doublet of doublets resonance at δ –144.9 ($^1J(^{119}Sn–^{19}F_a)$ = 1936 Hz; $^1J(^{119}Sn–^{19}F_b)$ = 1316 Hz) (Figure 40) and the ^{19}F NMR spectrum at the same temperature displayed three signals at δ –117.9, δ –137.1 ($^1J(^{19}F_a–^{119}Sn$ = 1903 Hz), – δ 178.2 ($^1J(^{19}F–^{119}Sn$ = 2033 Hz) and unresolved resonances at δ –122.8, –127.7, –146.3, –151.3 and 153.15 for which the $^{117/119}Sn$ satellites could not be detected unambiguously (Figure 41).

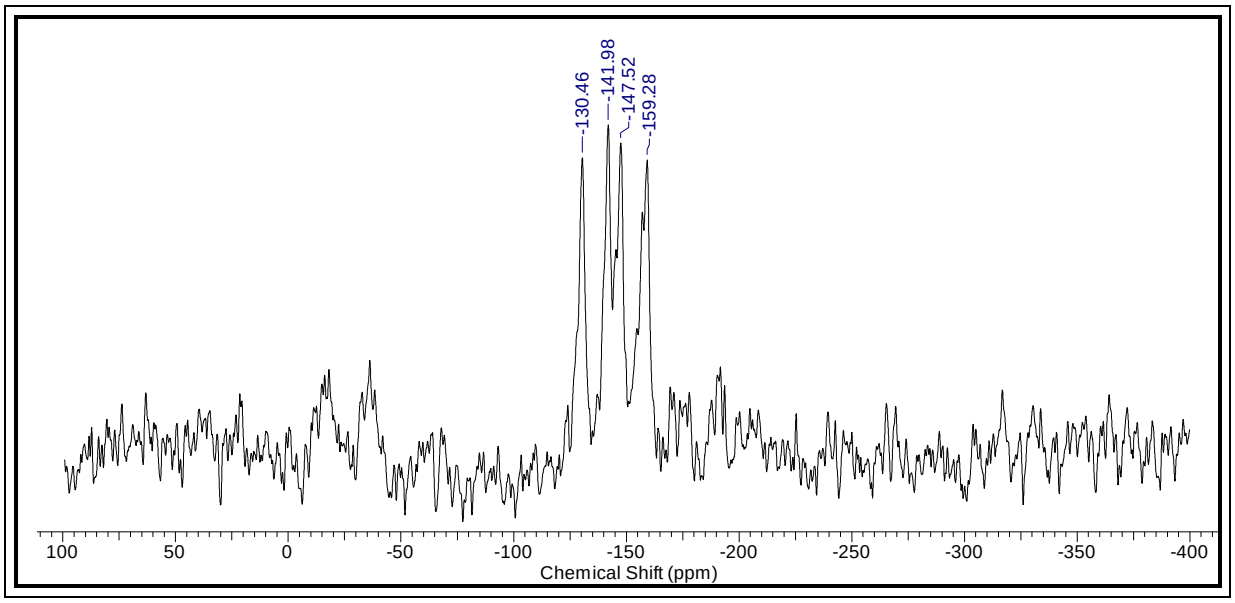

Figure 40. ^{119}Sn NMR spectrum of **8** + CsF in CD_3CN at –32° C.

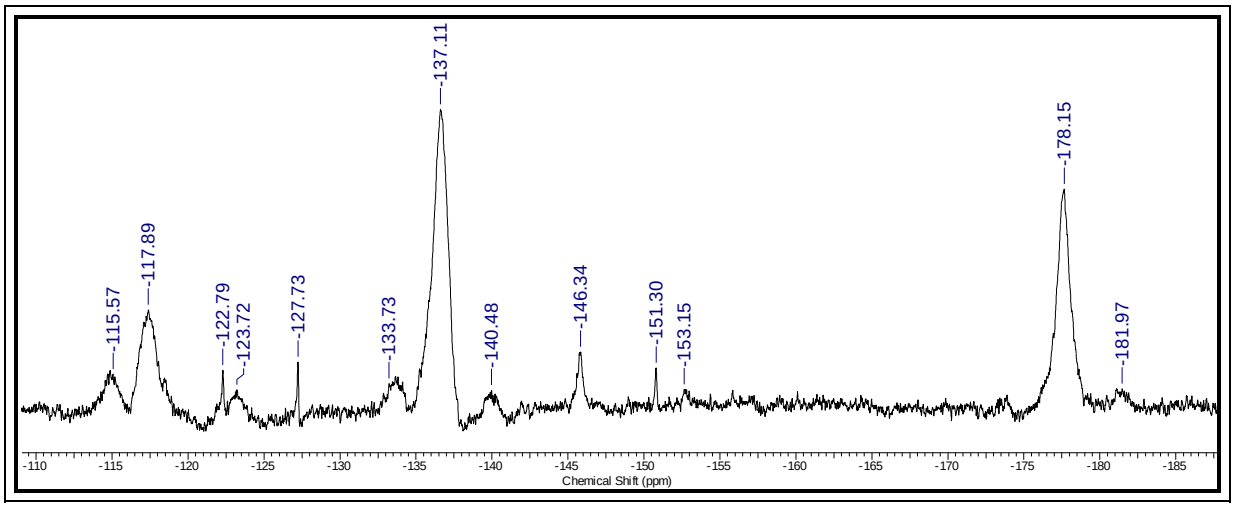

Figure 41. ^{19}F NMR spectrum of **8** + CsF in CD_3CN at –32° C.

The chemical shifts and the magnitudes of the $^{1}J(^{119}Sn–^{19}F)$ and $^{1}J(^{19}F–^{119}Sn)$ coupling constants are close to what was seen with {[fc($SiMe_2CH_2SnFPhCH_2SiMe_2$)$_2$fc·F]$^-$[$Bu_4N$]$^+$ [δ –128.1(dd), $^{1}J(^{119}Sn–^{19}F_a)$ = 1887 Hz, $^{1}J(^{119}Sn–^{19}F_b)$ = 1251 Hz, δ –109.8 (F_b), δ –152.7 (Fa)}[130] and {[*o*-$C_6H_4(SnF_3Me_2)$]$^-$[Et_4N]$^+$ [δ –126.8, $^{1}J(^{19}F_b–^{119}Sn)$ = 1172 Hz (F_a); δ –155.4, $^{1}J(^{19}F_a–^{119}Sn)$ = 1887 Hz (F_a)][173]. These findings are consistent with the formation in solution of the 1:1 ditopic complex [**8**·CsF] (Scheme 5), with the latter being kinetically labile on the ^{19}F and ^{119}Sn NMR times scales at room temperature and stabile at low temperature.

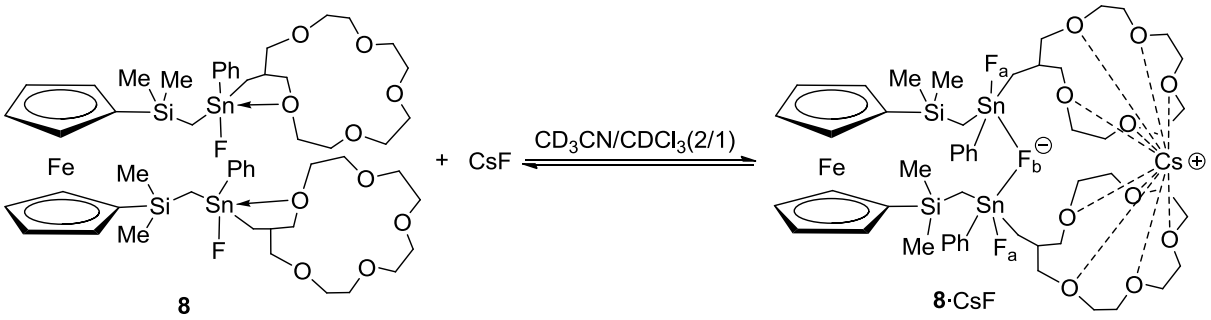

Scheme 5. Reaction of compound **8** with CsF in $CD_3CN/CDCl_3$.

Further support for the formation of a ditopic complex between receptor **8** and cesium fluoride came from the ^{1}H and ^{13}C NMR spectra.

In the ^{1}H NMR spectrum at room temperature of a $CD_3CN/CDCl_3$ (2/1) solution containing (**8** + CsF) in a molar ratio 1:1, the signals of the OCH_2 protons show

narrower distribution than the pure compound **8**. Moreover, the $SiCH_2Sn$ and $SnCH_2$ protons for (**8** + CsF) show, in contrast to the diastereotopism observed for the analogous protons in **8**, a singlet at δ –0.45 ($^2J(^1H\ -^{117/119}Sn)$ = 88.0 Hz) and a doublet at δ –1.06 ($^3J(^1H\ -^1H)$ = 8.0 Hz, $^2J(^1H-^{117}Sn)$ = 32.0 Hz, $^2J(^1H-^{117/119}Sn)$ = 40.0 Hz), respectively(Figure 42). Furthermore, only one signal for the methyl protons at δ 0.28 is observed in the ^1H NMR spectrum of **8** + CsF in comparison to two signals for pure **8**.

The changes are especially manifested in the ^{13}C NMR spectrum of (**8** + CsF) by a symmetric structure of the crown ether carbon atoms (C2/C12, C3/C11, C5/C9, C6/C8, C14/C16) rather than an unsymmetrical structure observed for the parent compound **8** (Figure 43).

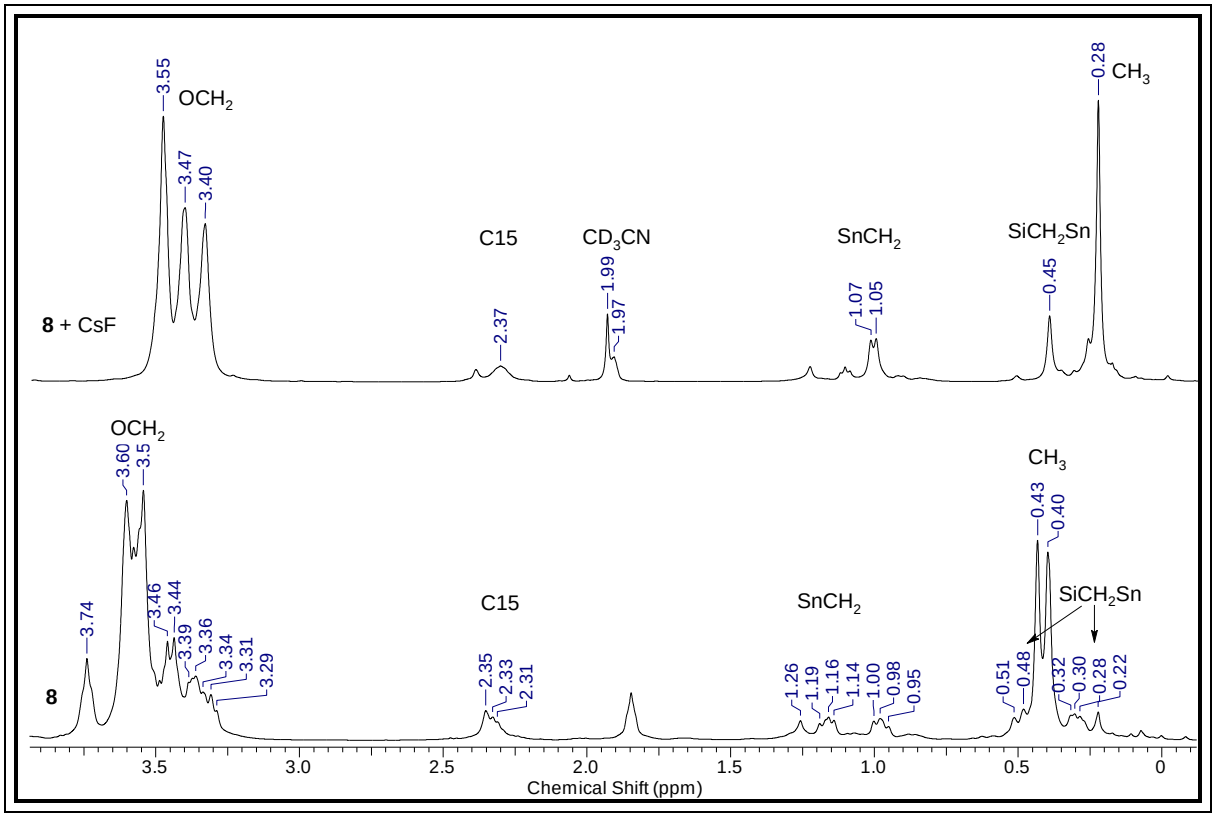

Figure 42. ^1H NMR spectra of compounds **8** and (**8** + CsF) showing the resonances for the CH_3, $SiCH_2Sn$, $SnCH_2$, C15, OCH_2 protons.

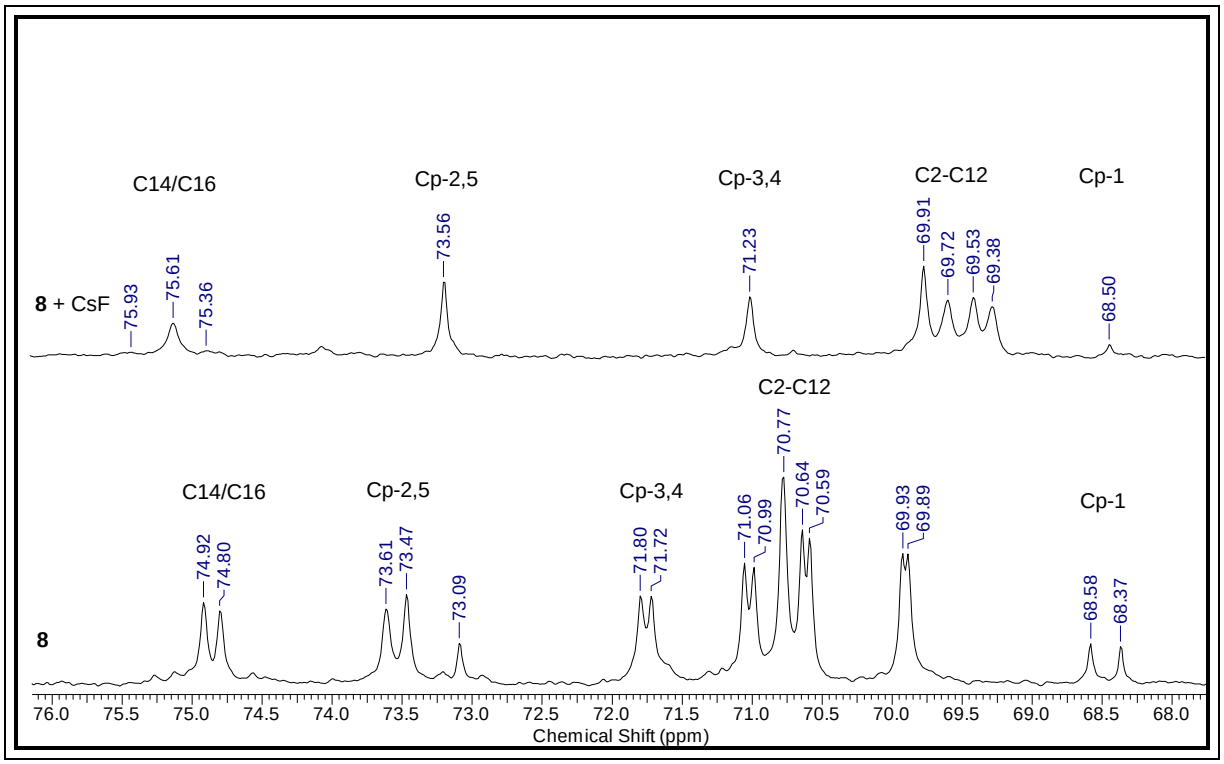

Figure 43. ^{13}C NMR spectra of compounds **8** and (**8** + CsF) showing the resonances for the OCH_2 and cyclopentadienyl carbon atoms.

2.2.5. Synthesis of the Diorganotin(IV) Dihalides substituted Crown Ethers.

The reaction of the tetraorganotin-substituted crown ethers **1** and **2**, with two and four molar equivalents of iodine afforded the diiodidodiorganotin-substituted crown ethers **11** and **12,** respectively, in almost quantitative yield (eq. 11 and 12).

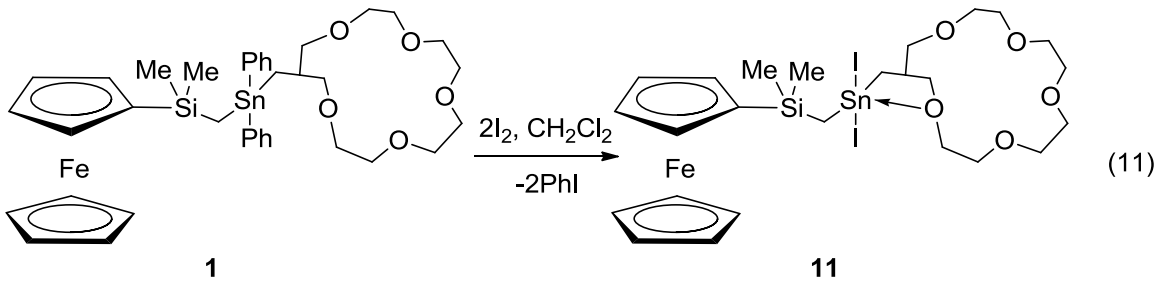

1 **11**

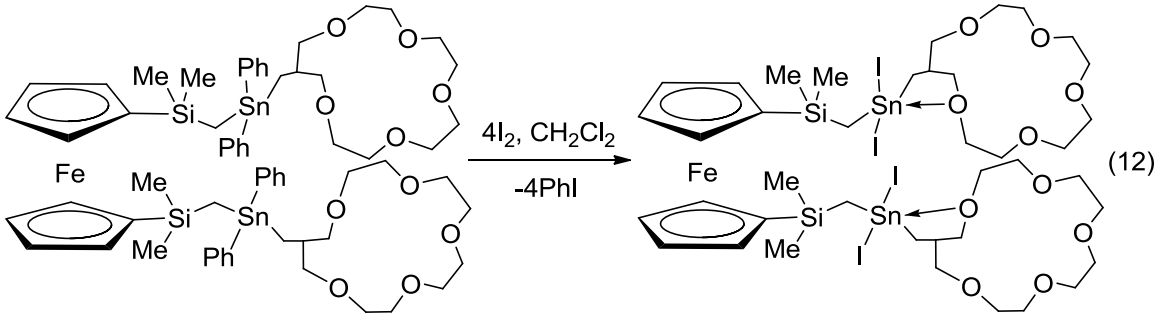

2 **12**

The treatment of the diorganotin diiodide **11** and the bis(diorganotin diiodide) **12** with an excess of AgCl in acetonitrile over a period of 14 days provided the corresponding chlorido-substituted derivatives dichloridodiorganotin **13** and **14**, respectively, (eq. 13 and 14).

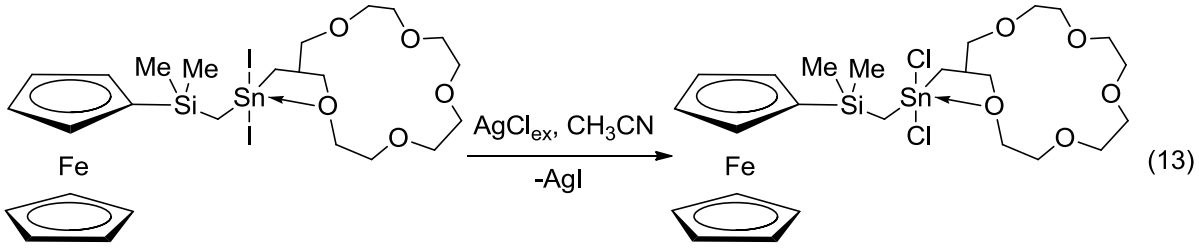

11 **13**

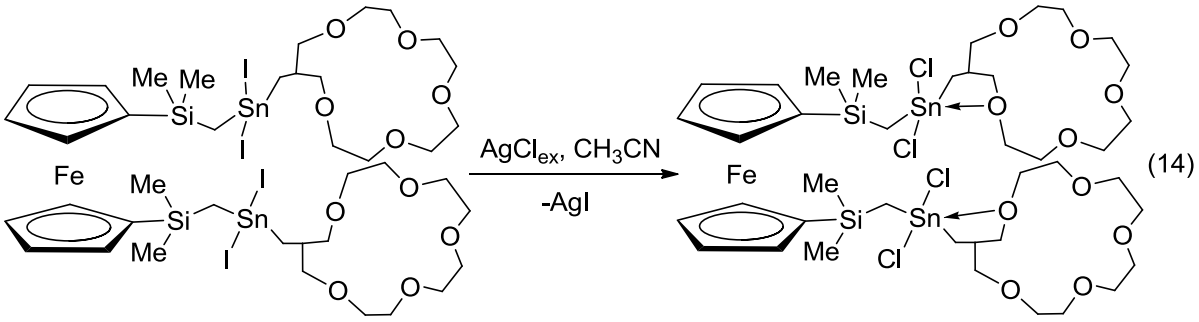

12 **14**

Compounds **12–14** were isolated as orange crystalline solids, whereas the diorganotin diiodide **11** is a viscous red oil. They are all well soluble in organic solvents such as CH_3OH, CH_3CN and CH_2Cl_2.

Attempts at synthesizing the diorganotin bromide **15** and the bis(diorganotin bromide) **16** by reaction of compounds **1** and **2** with two and four molar equivalents of elemental bromine, respectively, failed (eq.15 and 16).

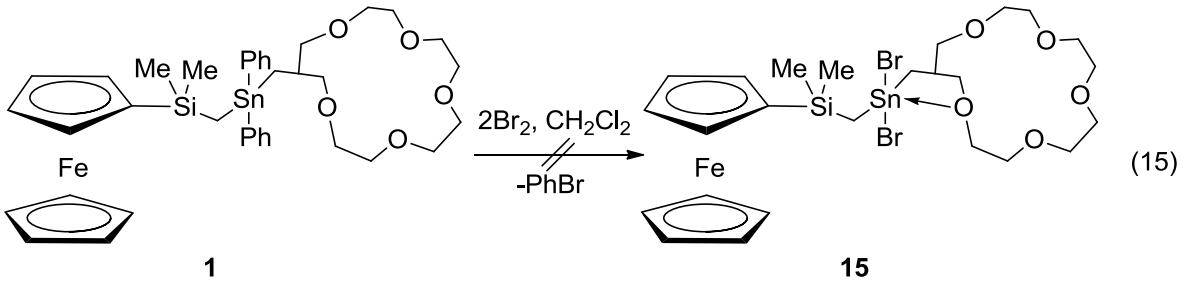

1 **15**

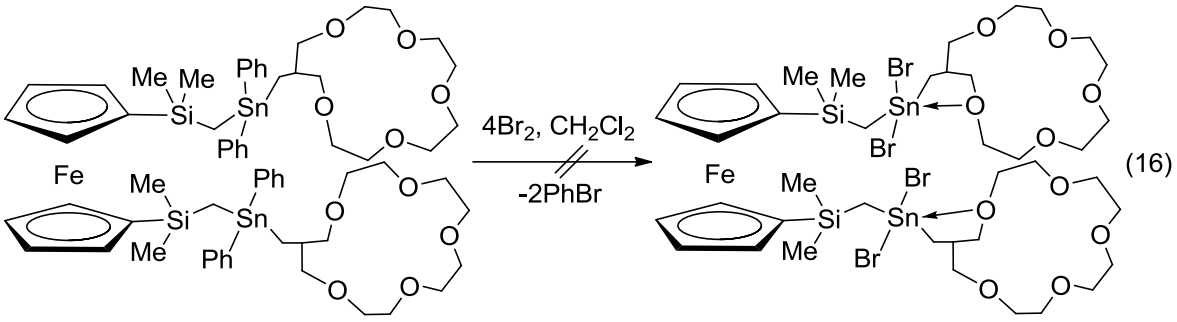

2 **16**

The reasons of the non-formation of the dibromidodiorganotin **15** and the bis(dibromidodiorganotin) **16** are given in paragraph **2.2.2.** Moreover, attempts at synthesizing the difluoridodiorganotin derivative **17** and the bis(difluoridodiorganotin) derivative **18** by treatment of the diorganotin diiodide **11** and the bis(diorganotin diiodide) **12** with two and four equivalents of AgF, respectively, failed (eq.17 and 18).

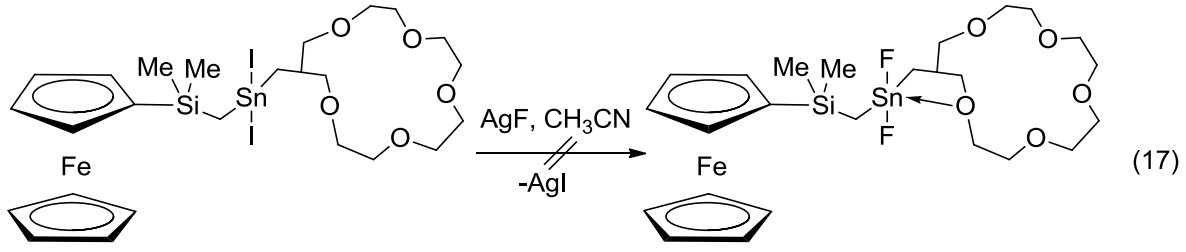

11 **17**

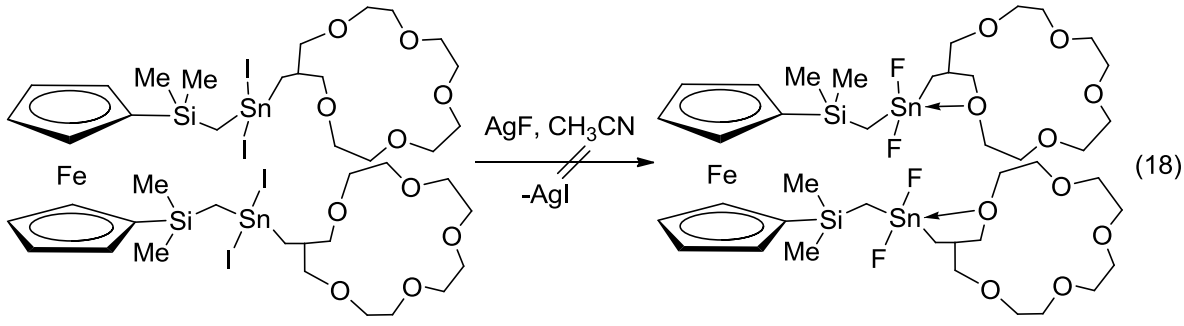

12 **18**

2.2.6. Molecular Structures of the Bis(diorganotin diiodide) 12, the Diorganotin dichloride 13 and the Bis(diorganotin dichloride) 14.

Single crystals suitable for X-ray diffraction analysis were obtained by cooling a solution of **12**, **13** and **14** in ethanol at –5 °C, respectively. Compounds **13** and **14** crystallized in the triclinic space group *P-1* with two and one molecules per unit cell, respectively. Compound **12** crystallized in the monoclinic space group *P2(1)/n* with two molecules per unit cell. The molecular structures of compounds **12**–**14** are shown in Figures 44–46. Selected bond distances and bond angles are collected in Tables 2 and 3.

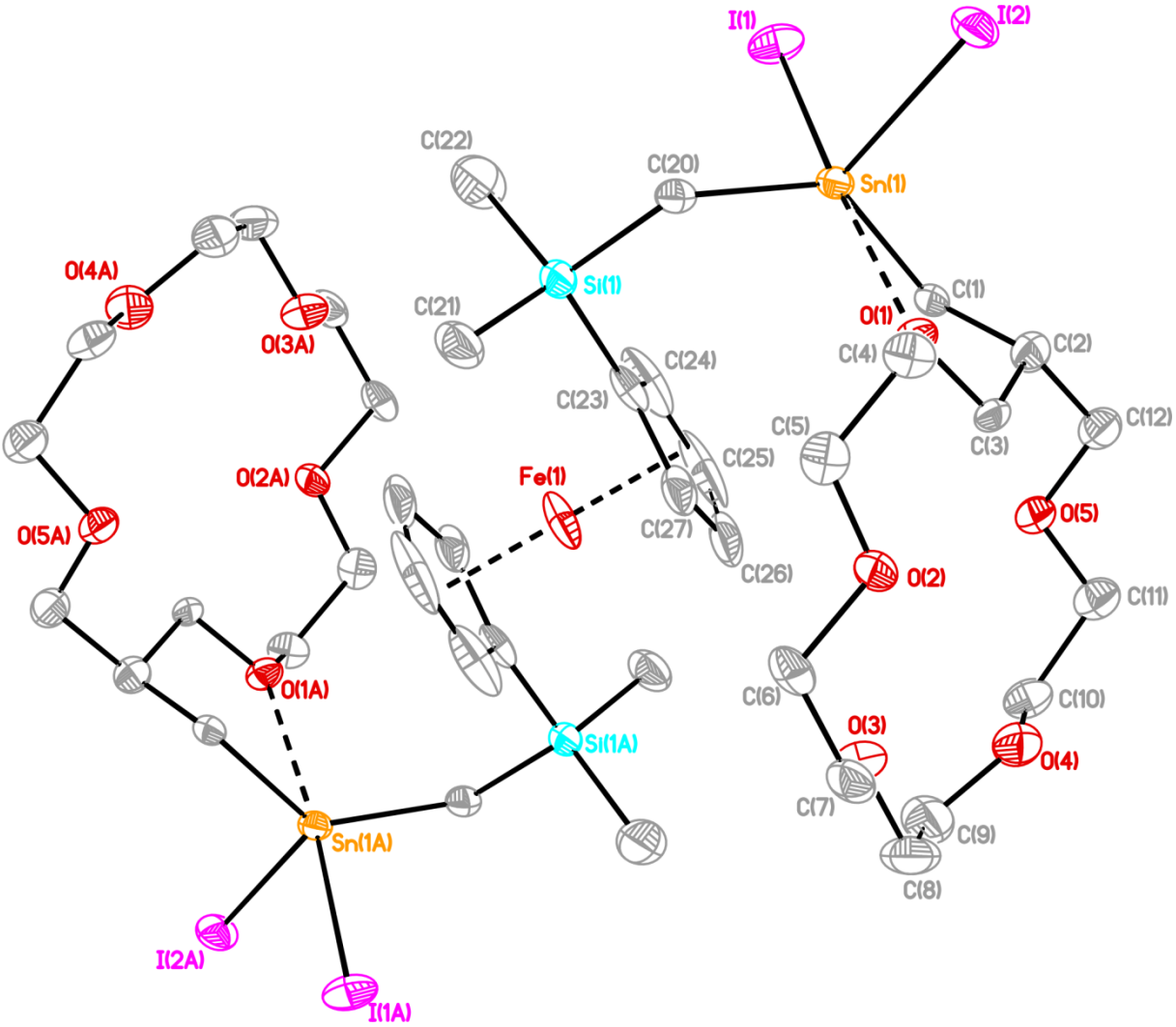

Figure 44. General view (SHELXTL) of a molecule of **12** showing 30% probability displacement ellipsoids and the crystallographic numbering scheme.

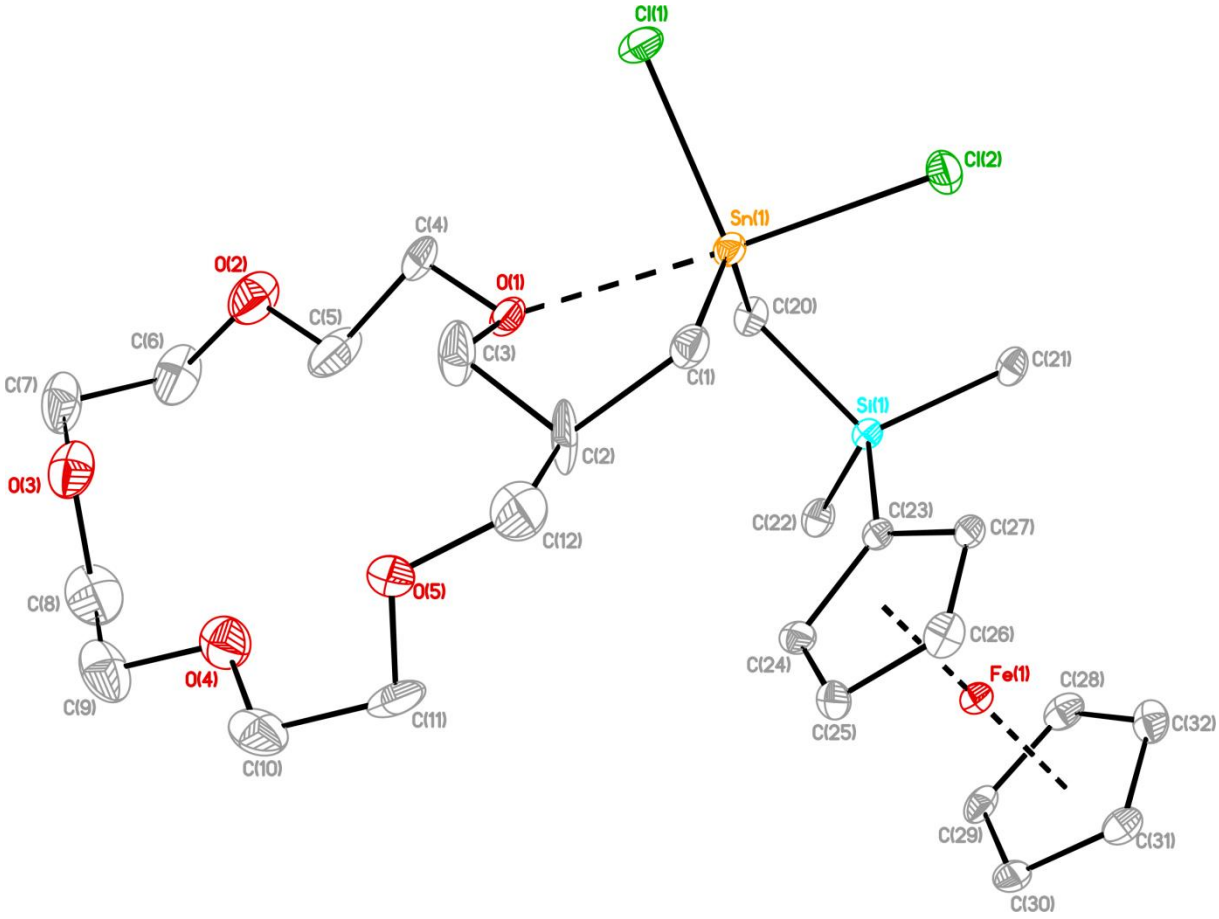

Figure 45. General view (SHELXTL) of a molecule of **13** showing 30% probability displacement ellipsoids and the crystallographic numbering scheme.

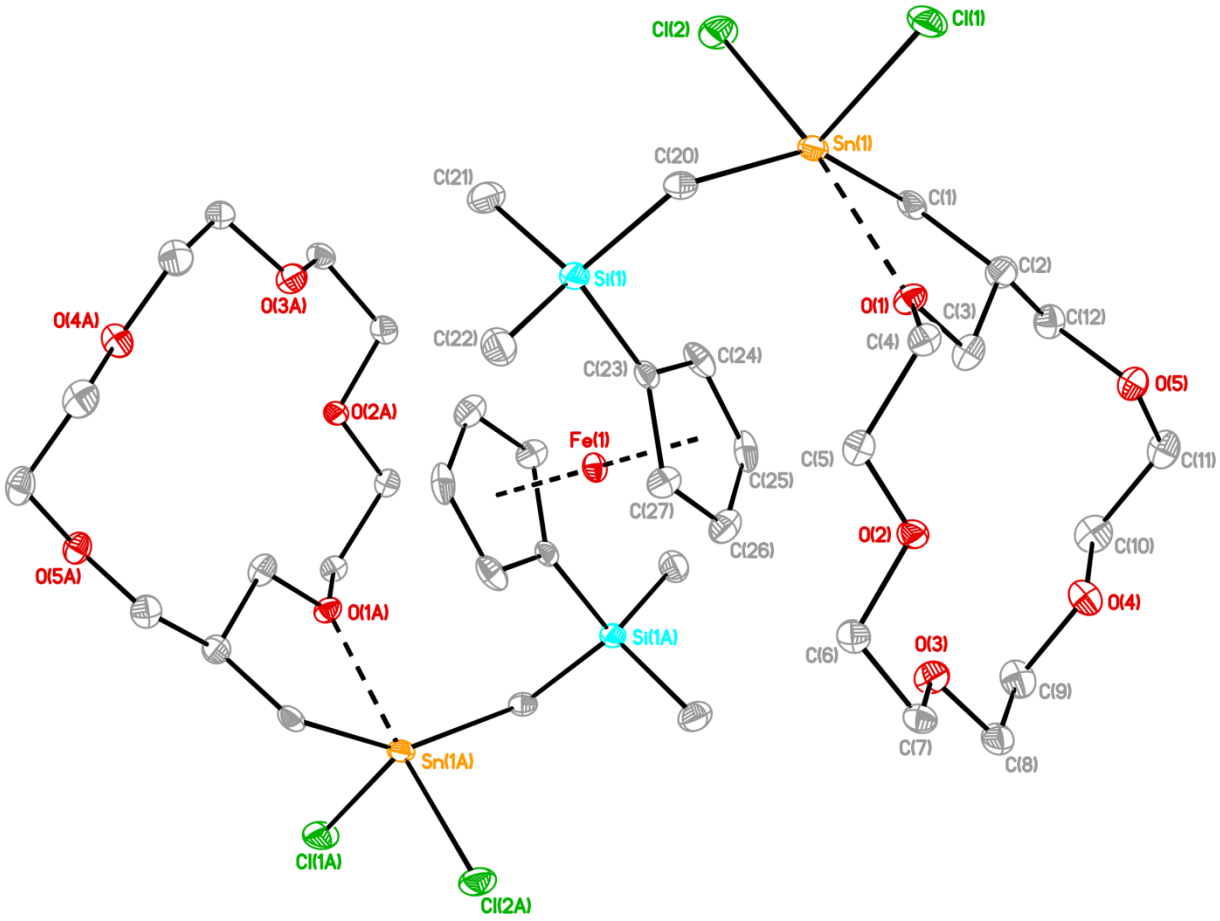

Figure 46. General view (SHELXTL) of a molecule of **14** showing 30% probability displacement ellipsoids and the crystallographic numbering scheme.

Table 2. Selected interatomic distances (Å) for compounds **12**, **13**, and **14**.

	12	**13**	**14**
	X(1) = I	X(1) = Cl	X(1) = Cl
	X(2) = I	X(2) = Cl	X(2) = Cl
Sn(1)–C(1)	2.125(5)	2.108(4)	2.117(3)
Sn(1)–C(20)	2.102(4)	2.117(4)	2.109(3)
Sn(1)–X(1)	2.7774(5)	2.3605(13)	2.3672(8)
Sn(1)–X(2)	2.7017(5)	2.4058(13)	2.4374(9)
Sn(1)–O(1)	2.552(3)	2.480(3)	2.480(3)

Table 3. Selected Bond Angles (deg) for compounds **12**, **13**, and **14**.

	12	**13**	**14**
	X(1) = I	X(1) = Cl	X(1) = Cl
	X(2) = I	X(2) = Cl	X(2) = Cl
C(1)–Sn(1)–X(1)	99.04(12)	113.89(13)	103.44(8)
C(1)–Sn(1)–X(2)	111.92(12)	98.39(14)	95.70(9)
C(1)–Sn(1)–O(1)	71.88(14)	75.86(15)	75.15(9)
C(20)–Sn(1)–C(1)	133.18(19)	131.82(17)	145.64(11)
C(20)–Sn(1)–O(1)	86.18(16)	86.48(15)	87.12(10)
C(20)–Sn(1)–X(1)	101.38(14)	107.69(13)	105.43(7)
C(20)–Sn(1)–X(2)	106.05(13)	101.52(13)	96.27(9)
O(1)–Sn(1)–X(2)	84.11(7)	172.01(9)	167.42(5)
O(1)–Sn(1)–X(1)	170.83(7)	82.89(8)	88.94(5)
X(2)–Sn(1)–X(1)	98.571(17)	94.62(5)	101.74(3)
C(2)–C(1)–Sn(1)	113.3(3)	111.3(3)	113.22(19)
C(3)–O(1)–Sn(1)	110.2(2)	106.0(3)	110.42(17)
C(4)–O(1)–Sn(1)	132.3(3)	127.2(3)	132.24(16)
Si(1)–C(20)–Sn(1)	118.1(2)	115.1(2)	117.56(13)

The tin atoms in compounds **12**–**14** are pentacoordinated, and each exhibits a distorted trigonal-bipyramidal environment (geometrical goodness[174] $\Delta\Sigma(\theta)$ 17.1(**12**), 58.9(**13**), 60.8(**14**) with C(1), I(2), C(20) (**12**), C(1), Cl(1), C(20) (**13**), C(1), Cl(1), C(20) (**14**) occupying the equatorial and O(1) and I(1) (**12**), O(1) and Cl(2) (**13**), O(1) and Cl(2) (**14**) occupying the axial positions. The distortion from the ideal geometry is especially manifested by the O(1)–Sn(1)–I(1) (**12**), O(1)–Sn(1)–Cl(2) (**13**) and O(1)–Sn(1)–Cl(2) (**14**) angles of 170.83(7)°(**12**), 172.01(9)°(**13**) and 167.42(5)°(**14**) instead of 180° and by the increase of the I(1)–Sn(1)–I(2) (**12**), Cl(1)–Sn(1)–Cl(2) (**13**) and Cl(1)–Sn(1)–Cl(2) (**14**) angles from 90° to 98.571(17)°(**12**), 94.62(5)°(**13**) and 101.74(74)°(**14**). Moreover, the C(1)–Sn–C(20) angles of 133.18(19) (**12**), 131.82(17) (**13**) and 145.64(11) (**14**) deviate from the ideal value of 180° and are close to that found in the corresponding dichloridodiorganotin compound [$Cl_2Sn(-CH_2$-[16]-crown-$5)_2$ (142.7)(1)].[154] They are smaller than those observed for [PhX_2Sn-CH_2-[16]-crown-

5 (X = I, Cl), 151.000(6) and 150.00(18)°][150]. The Sn(1) atom is displaced by 0.3802(4) (**12**), 0.3203(4) (**13**), and 0.2720(2) (**14**) Å from the corresponding trigonal plane in the direction of I(1), Cl(2), Cl(2), respectively. As result of the inversion center at the Fe(1) atom, the crown ether moiety in compounds **12** and **14** are in trans position to the ferrocene unit. As expected, the silicon atoms in **12**–**14** are tetracoordinated and the Sn–C, Si–C, and Fe–C bond lengths (Table 2–4) as well as the bond angles at silicon are close to those found in the literature[130,175-180].

The intramolecular Sn(1)–O(1) distances of 2.552(3) Å (**12**), 2.480(3) Å (**13**) and 2.436(3) Å (**14**) are shorter than the corresponding Sn–O distances found in [Cl_2Sn(-CH_2-[16]-crown-5)$_2$ (2.560)(2) Å][154] and [PhX_2Sn-CH_2-[16]-crown-5 (X = Cl, (2.522(1), (2.4793)(9) Å][150] and longer that in [PhI_2Sn-CH_2-[16]-crown-5 (2.482(2) Å][150], Most remarkably, the tin atoms in compounds **12**–**14** are intramolecularly coordinated by *one* oxygen atom of the crown ether ring and contrasts well with that observed for the analogous dihalogenidodiorganotin substituted crown ethers [PhX_2Sn-CH_2-[16]-crown-5 (X = Cl, I],[150] [Cl_2Sn(-CH_2-[16]-crown-5)$_2$].[154] Indeed, the tin atoms in the two latter compounds show a distorted octahedral configuration with each tin atom being intramolecularly coordinated by *two* oxygen atoms of the crown ether ring. This situation resembles that observes for PhX_2Sn-CH_2-[13]-crown-4 (X = Cl, I)[149] and I_3Sn-CH_2-[13]-crown-4,[149] indicating for the two latter compounds the higher rigidity of the [13]-crown-4 than the [16]-crown-5. The coordination of only one oxygen atom from the crown ether ring to the tin atom in **12**–**14** is the result of the steric hindrance of ferrocene which stabilizes the compound being avoid the coordination of the O(5) oxygen atom to the tin atom. As observed for the analogous PhX_2Sn-CH_2-[13]-crown-4 (X = Cl, I), [149] the Sn–X distance depends on the position of the halogen atom to the O(1) oxygen atom with the Sn–X distance being lengthened when it is located in trans position to the oxygen atom. Thus, the Sn(1)–I(1) distance of 2.7774(5) Å in **12** is lengthened as compared with the Sn(1)–I(2) bond length (2.7017(5) Å and exceeds the sum of the covalent radii of Sn and I (2.77 Å).[181] The diorganotin dichloride **13** and the bis(diorganotin chloride) **14** show the same effect. The Sn(1)–Cl(2) distances of 2.4058(13) Å (**13**) and 2.4374(9) Å (**14**) are longer than the Sn(1)–Cl(1) distances of 2.3605(13) Å (**13**) and (2.3672(9) Å (**14**) and are by 0.0158 Å and 0.0474 Å above the sum of the covalent radii of Sn and Cl (2.39 Å).[181]

2.2.7. Structures of the Diorganotin Halides and the Bis(dihalogenidoorganostannyl)-substituted Crown Ethers in Solution.

The ^{119}Sn NMR spectra in $CDCl_3$ of compounds **11**–**14** showed resonances at *δ* –204 (**11**), *δ* –207 (**12**), *δ* –8 (**13**), *δ* –10 (**14**), which are low-frequency shifted with respect to the ^{119}Sn chemicals shifts of the non-substituted compounds having similar substituent patterns about the tin atoms such as Me_2SnX_2 [*δ* –159 (X = I); 99 (X = Cl)],[182,183] $(PhI_2SnCH_2)_2$ (*δ* –169).[167] These results indicate that the tin atoms in compounds **11**–**14** are hypercoordinated. As a consequence, the intramolecular O→Sn coordination found in the solid state is retained in solution. In contrast to the triorganotin halides **3**–**8**, the ^{1}H NMR spectrum of compounds **11**-**14** in $CDCl_3$ show singlets for the $SiCH_2Sn$ [**11**: *δ* 1.40 $^2J(^1H–^{119/117}Sn)$ = 36.0Hz; **12**: 1.46 *δ* $^2J(^1H–^{119/117}Sn)$ = 100.0Hz; **13**: *δ* 0.90 $^2J(^1H–^{119/117}Sn)$ = 111.0Hz; **14**: *δ* 0.94 $^2J(^1H–^{119/117}Sn)$ = 108.0Hz] and doublets for the $SnCH_2$ [**11**: *δ* 1.63 $^3J(^1H–^1H)$ = 9.0Hz, $^2J(^1H–^{117}Sn)$ = 63 Hz, $^2J(^1H–^{119}Sn)$ = 81.0 Hz; **12**: *δ* 1.71 $^3J(^1H–^1H)$ = 8.0Hz, $^2J(^1H–^{117}Sn)$ = 64.0 Hz, $^2J(^1H–^{119}Sn)$ = 80.0 Hz; **13**: *δ* 1.30 (d, $^3J(^1H–^1H)$ = 9.0Hz, $^2J(^1H–^{117}Sn)$ = 75.0 Hz, $^2J(^1H–^{119}Sn)$ = 93.0 Hz; **14**: *δ* 1.34 ($^1H–^1H$) = 8.0 Hz, $^2J(^1H–^{117}Sn)$ = 80.0 Hz, $^2J(^1H–^{119}Sn)$ = 96.0 Hz] protons, respectively. These results are consistent with the loss of the diastereotopism observed for compounds **3**–**8**. The ^{13}C NMR sprectra of compounds **11**–**14** in $CDCl_3$ showed for each compound six resonances for the crown ether carbon atoms (C15, C14/C16, C2/C12, C3/C11, C5/C9, C6/C8), indicating, and in contrast to their non-symmetric structure in the solid state (**12**-**14**), symmetric structures in solution. Moreover, and as expected the ^{13}C NMR spectra of compounds **11**–**14** in $CDCl_3$ at room temperature display each a single sharp resonance for the methyl carbon atoms [**11**: *δ* -1.0; **12**: *δ* 16.2; **13**: *δ* 0.2 ($^3J(^1H–^{117/119}Sn)$ = 28.7 Hz, **14**: *δ* 1.1], for the methylene carbon atoms [**11**: *δ* 16.4 (C17), *δ* 29.7 ($SnCH_2Si$); **12**: *δ* 16.2 (C17), 29.8 ($SiCH_2Sn$); **13**: *δ* 14.5 (C17), 26.6 ($SiCH_2Sn$); **14**: *δ* 14.3 (C17), 26.6 ($SiCH_2Sn$)] and 3 sharp signals for the cyclopentadienyl carbon atoms [**11**: *δ* 71.7, 73.5, and 74.1; **12**: *δ* 72.3, 73.5, and 74.1 ; **13**: *δ* 71.6, 73.5, and 73.8 ; **14**: *δ* 71.3, 71.8, and 73.4].

The ESI-MS spectrum in the positive mode of compound **11** showed mass clusters centered at *m/z* 641.1 and 901.0 that are assigned to $[FcSiMe_2Sn(OH)CH_2$-[16]-crown-5$]^+$ and $[FcSiMe_2SnI_2CH_2$-[16]-crown-5·Na$]^+$, respectively. The ESI-MS

spectrum in the positive mode of compound **12** showed mass clusters centered at *m/z* 1093.3, 1639.4, and 1814.7 that are assigned to [fc($Me_2SiCH_2SnOHCH_2$-[16]-crown-5)($Me_2SiCH_2SnOCH_2$-[16]-crown-5)]$^+$, [fc($Me_2SiCH_2SnI_2CH_2$-[16]-crown-5)$_2$·CHOH·Na·OH]$^+$, [fc($Me_2SiCH_2SnI_2CH_2$-[16]-crown-5)$_2$·I·CH_2Cl_2·$2H_2O$]$^+$. In the ESI-MS spectrum (negative mode) of **12**, there is a mass cluster centered at *m/z* 1694.2 that is assigned to [fc($Me_2SiCH_2SnI_2CH_2$-[16]-crown-5)$_2$·I]$^-$. For compound **13**, the ESI-MS spectrum in the positive mode showed a mass cluster centered at *m/z* 681.1 that is assigned to [Fc$Me_2SiCH_2Sn(OH)_2CH_2$-[16]-crown-5·Na]$^+$. In the negative mode, a mass cluster centered at *m/z* 729.1 was observed that is assigned to [Fc$Me_2SiCH_2SnCl_2CH_2$-[16]-crown-5·Cl]$^-$. The ESI-MS spectrum in the positive mode of compound **14** showed a mass cluster at *m/z* 1093.3 that is assigned to [fc($Me_2SiCH_2SnOHCH_2$-[16]-crown-5)$_2$]$^{2+}$. In the negative mode, there is a mass cluster centered at *m/z* 1237.2 that is assigned to [fc($Me_2SiCH_2SnCl_2CH_2$-[16]-crown-5)$_2$·Cl]$^-$.

2.2.8. Complexation Studies of the Diorganotin Halides and the Bis(dihalogenidoorganostannyl)-substituted Crown Ethers.

2.2.8.1. Complexation Behavior of the Diorganotin Diiodides 11 and the Bis(diiodidodiorganotin)-substituted Crown Ether 12 Toward Iodide Salts.

The ^{119}Sn NMR Spectrum at room temperature of a solution of the diorganotin diiodide **11** in $CDCl_3$ to which had been added one molar equiv of *n*-Bu_4NI, displayed a resonance at δ –202 ($\nu_{1/2}$ = 122 Hz), which is close to the chemical shift of the pure compound in the same solvent (δ –204). Addition of a second molar equiv of iodide ion to **11** caused no change in the ^{119}Sn NMR Spectrum. The non-formation of the iodidostannate complex is due to the weak acidity of the tin atom in **11**, which is not able to interact with the Lewis base I^- by breaking the intramolecular coordination between the oxygen atom of the crown ether ring and the tin atom. The same effect was observed for the analogous diorganotin diiodide PhI_2SnCH_2-[19]-crown-6,[163] [I_2Sn(-CH_2-[16]-crown-5)$_2$][154] and bis(diorganotin diiodide) **12**.

The ^{119}Sn NMR Spectrum at room temperature of a solution of the diorganotin diiodide **12** in $CDCl_3$ to which had been added two molar equiv of NaI showed a

resonance at δ –146 ($\nu_{1/2}$ = 238 Hz), which is displaced by 61 ppm to low field with respect to the chemical shift of the parent compound **12** (δ –207). This indicates that the anion I^- is not coordinated to the tin atom and probably resides in the vicinity of the cation Na^+ (Scheme 6). This latter complexation mode is similar to what was reported in the literature[154,184] and the compound formed is assigned to be a homotopic complex [**12**·2NaI].

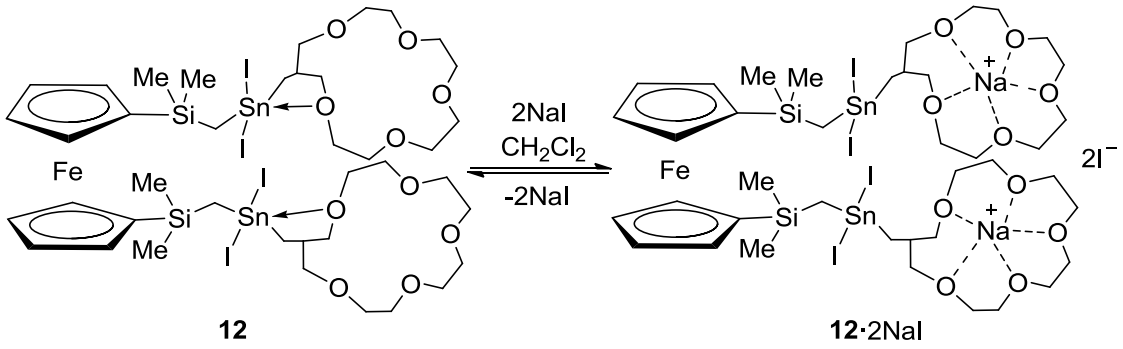

Scheme 6. Reaction of compound **12** with NaI in CH_3CN.

This interpretation is supported by the ^{13}C and ^{1}H NMR spectra. In the ^{13}C NMR spectrum of (**12** + 2 NaI) in $CDCl_3$, the signal of the C14/C16 carbon atoms is, with respect to the ^{13}C NMR chemical shift of pure **12** in $CDCl_3$, low field displaced by 5.81 ppm, while those of the C2–C12 crown ether carbon atoms moved by 0.9 ppm to high field (Figure 47). The ^{1}H NMR spectrum of (**12** + 2 NaI) in $CDCl_3$ showed for the crown ether protons narrower distribution than the pure **12**, whereas the methylene H_{C17} and the H_{C15} proton atoms are displaced by 0.09 and 0.18 ppm to high and low field, respectively (Figure 48).

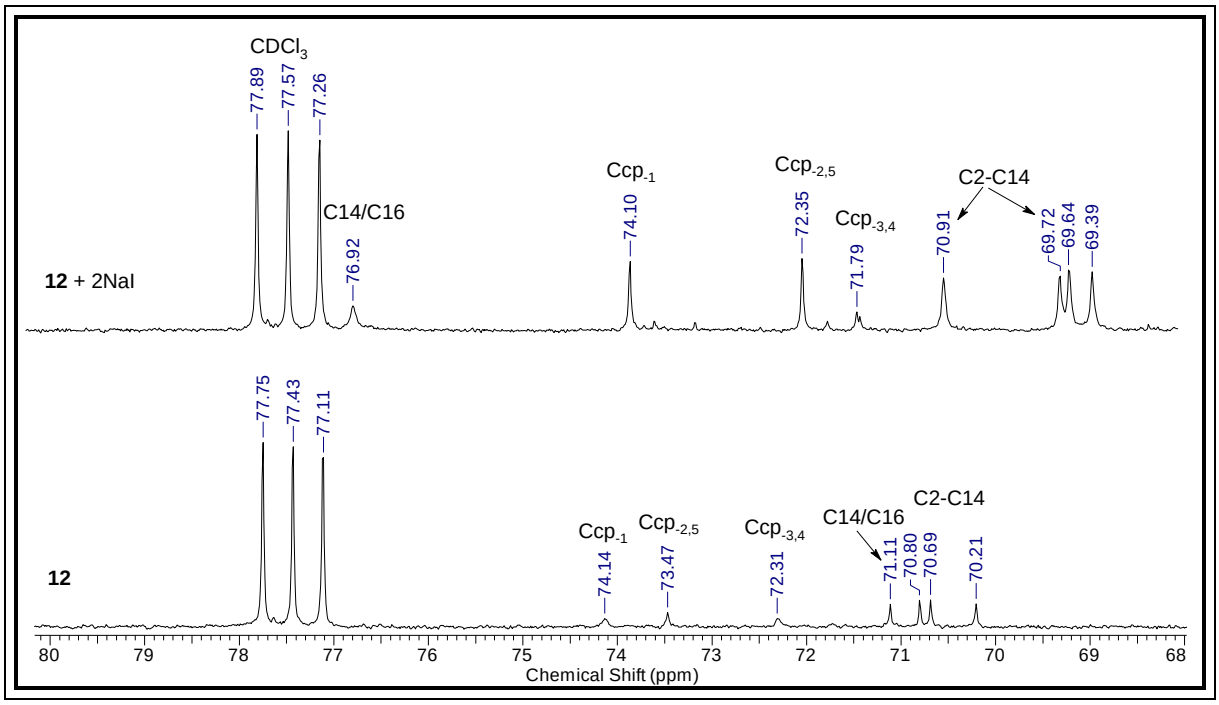

Figur 47. ^{13}C-NMR spectra showing the resonances for the C14/C16, C2-C12, Ccp-1, Ccp-2,5, Ccp-3,4 carbon atoms of pure **12** and of (**12** + 2 NaI) in $CDCl_3$.

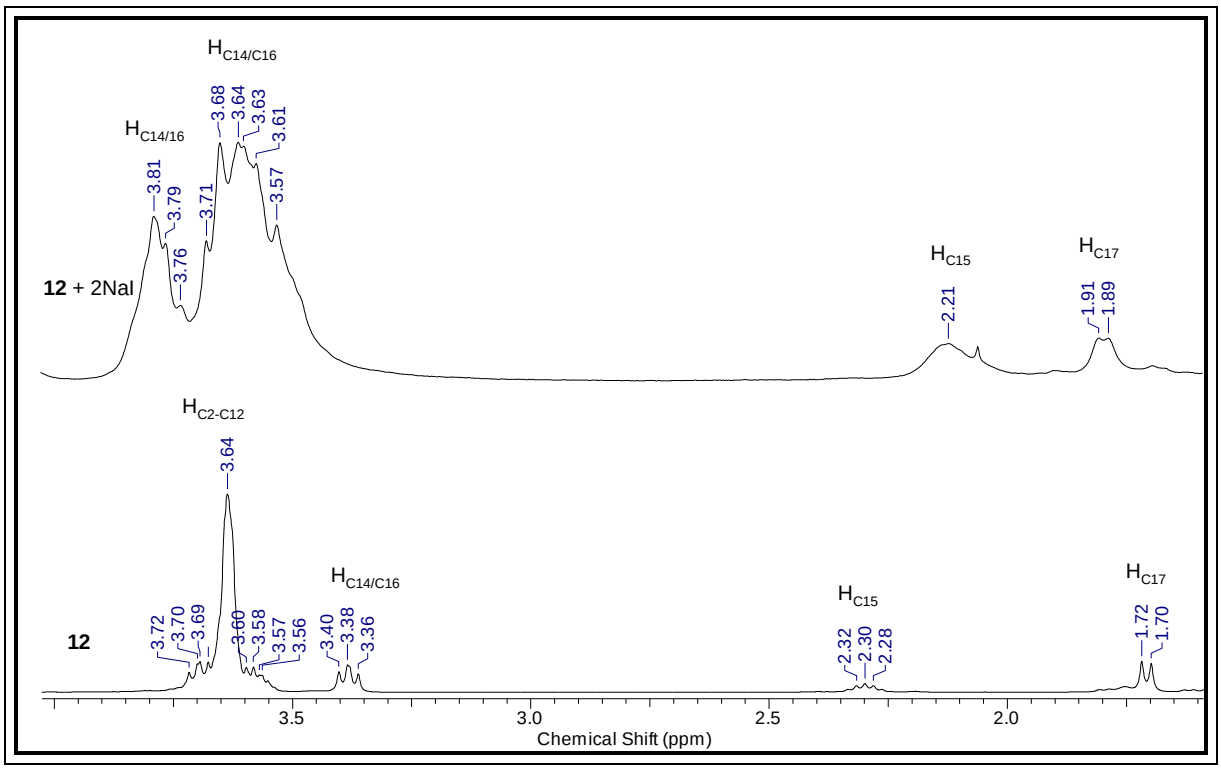

Figure 48. ^{1}H-NMR spectra showing the resonances for the H_{C2-C12}, $H_{C14/C16}$, H_{C15}, H_{C17} protons of pure **12** and of (**12** + 2 NaI) in $CDCl_3$.

Attempts to complex CsF by the ditopic receptor **12** and formation of a Sn–F–Sn bridge failed (Scheme 7).

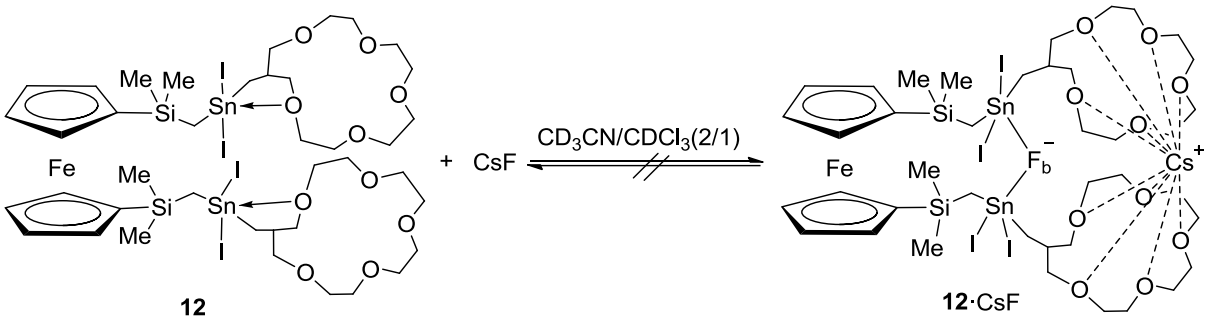

Scheme 7. Reaction of compound **12** with CsF in $CH_3CN/CDCl_3$.

2.2.8.2. Complexation Behavior of the Diorganotin Dichlorides 13 and the Bis(dichloridoorganotin)-substituted Crown Ether 14 toward Chlorides Salts.

The ^{119}Sn NMR chemical shifts of the organotin chlorides **13** and **14** in CD_3CN, to which had been added one respectively two equivalents of Ph_4PCl, $[(Ph_3P)_2N]Cl$, Bu_4PCl are shown in Table 4.

Table 4. ^{119}Sn NMR Chemical shifts in CD_3CN of compounds 1**3** and **14** upon addition of chloride salts.

Compounds	Salts	Equivalent(s)	δ ^{119}Sn(ppm)
13	Ph_4PCl	1	–51
14	Ph_4PCl	2	–186
13	$[(Ph_3P)_2N]Cl$	1	–48
13	Bu_4PCl	1	–119
14	Bu_4PCl	2	–199

They are all high field shifted in comparison with the chemical shift of the receptor **13** (δ –30) and **14** (δ –28) in CD_3CN, with the displacement being more pronounced with the receptor **14**. These observations are consistent with the formation of the diorganotrichloridostannate complexes and can be interpreted in terms of the

equilibrium shown in Schemes 8 and 9. The equilibrium is shifted to the right for the complexes [**13**·Cl]$^-$[Bu_4P]$^+$, [**14**·2Cl]$^-$[$2Ph_4P$]$^{2+}$ and [**14**·2Cl]$^-$[$2Bu_4P$]$^{2+}$ as the great difference between the ^{119}Sn chemical shifts of the complexes and the non-complexed compound is observed.

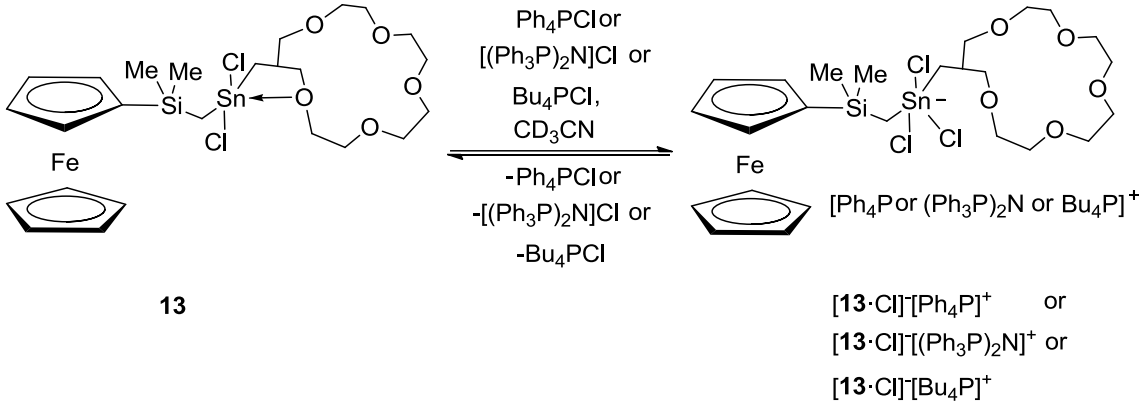

13

[**13**·Cl]$^-$[Ph_4P]$^+$ or
[**13**·Cl]$^-$[$(Ph_3P)_2N$]$^+$ or
[**13**·Cl]$^-$[Bu_4P]$^+$

Scheme 8. Reaction of compound **13** with chloride salts in CD_3CN.

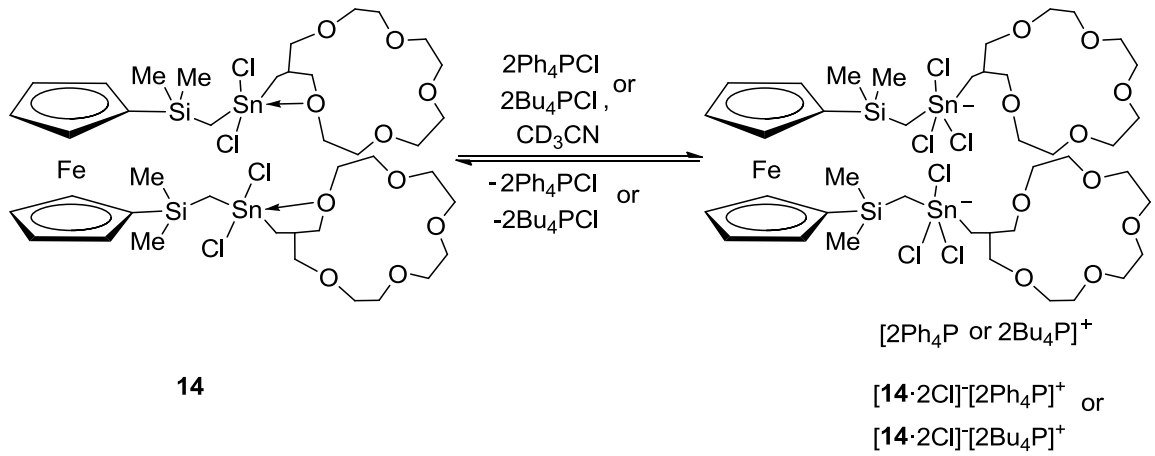

14

[**14**·2Cl]$^-$[$2Ph_4P$]$^+$ or
[**14**·2Cl]$^-$[$2Bu_4P$]$^+$

Scheme 9. Reaction of compound **14** with chloride salts in CD_3CN.

The trichloridostannate complex [**13**·Cl]$^-$[Bu_4P]$^+$ is used as a representative example of the anionic complexes [**13**·Cl]$^-$ and [**14**·2Cl]$^-$. The ESI-MS spectrum in the negative mode of a sample containing **13** and $Bu_4P^+Cl^-$ showed mass clusters centered at *m/z* 711.1 and 729.1 that are assigned to [$FcMe_2SiCH_2SnCl_2CH_2$-[16]-crown-5·OH]$^-$ and [$FcMe_2SiCH_2SnCl_2CH_2$-[16]-crown-5·Cl]$^-$, respectively. Analytical pure [**13**·Cl]$^-$[Bu_4P]$^+$ was isolated as orange crystalline material and characterized by X-ray diffraction analysis. The molecular structure of the complex [**13**·Cl]$^-$[Bu_4P]$^+$ is described in paragraph **2.2.10.**

In course of our attempts to grow single crystals of [**14**·2Cl]$^{-}$[Ph_4P]$^{+}$, we isolated instead a crystalline material that was identified to be the polymeric diaqua complex **14**·2H_2O. Its molecular structure is described in paragraph **2.2.11.**

The ^{119}Sn NMR spectra of a solution of **13** and **14** in CD_3CN at room temperature to which had been added excess lithium chloride, LiCl showed a single resonance at δ –124 and δ –129 that is by $\Delta\delta$ 95 ppm and $\Delta\delta$ 101 ppm high field shifted with respect to the parent compounds **13** and **14**, respectively, (Figure 49 and 50).

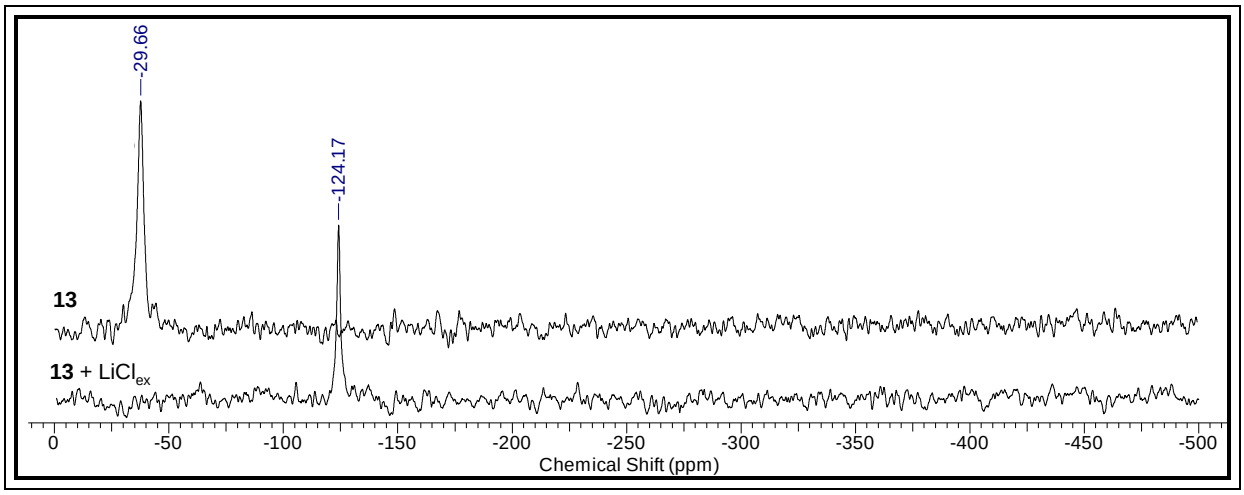

Figure 49. ^{119}Sn of pure **13** and of (**13** + $LiCl_{ex}$) in CD_3CN.

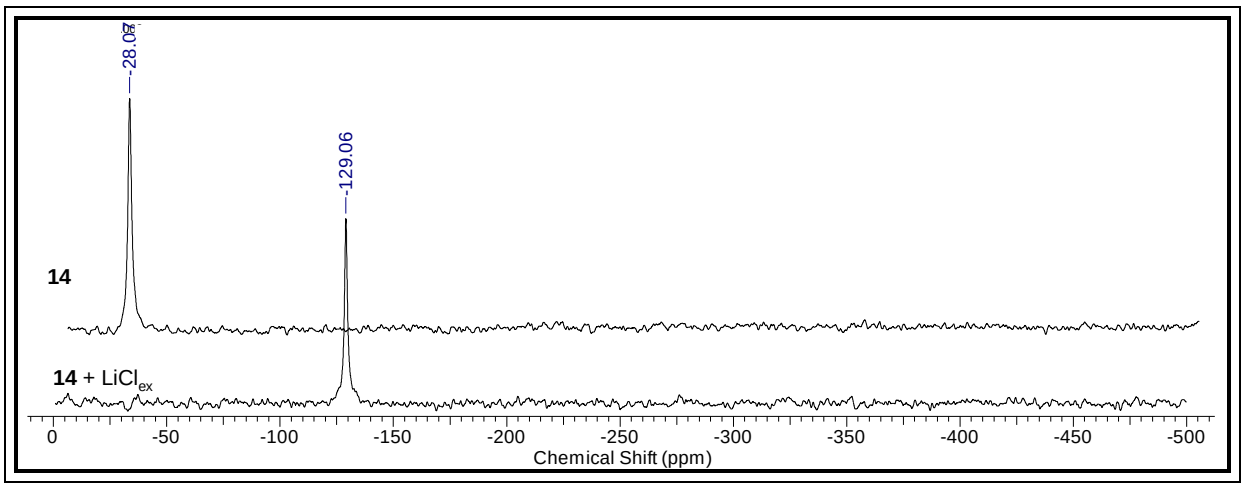

Figure 50. ^{119}Sn of pure **14** and of (**14** + $LiCl_{ex}$) in CD_3CN.

Such findings are consistent with receptors **13** and **14** coordinating the Li^{+} cation through the crown ether moiety and the Cl^{-} being bound to the Sn atom, respectively (Scheme 10 and 11).

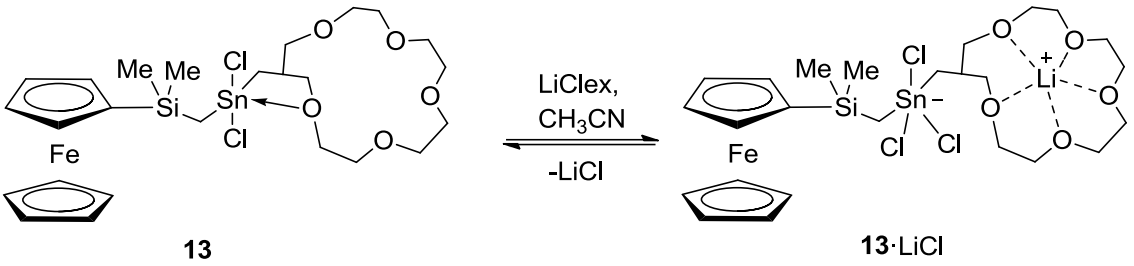

Scheme 10. Reaction of compound **13** with $LiCl_{ex}$ in CH_3CN.

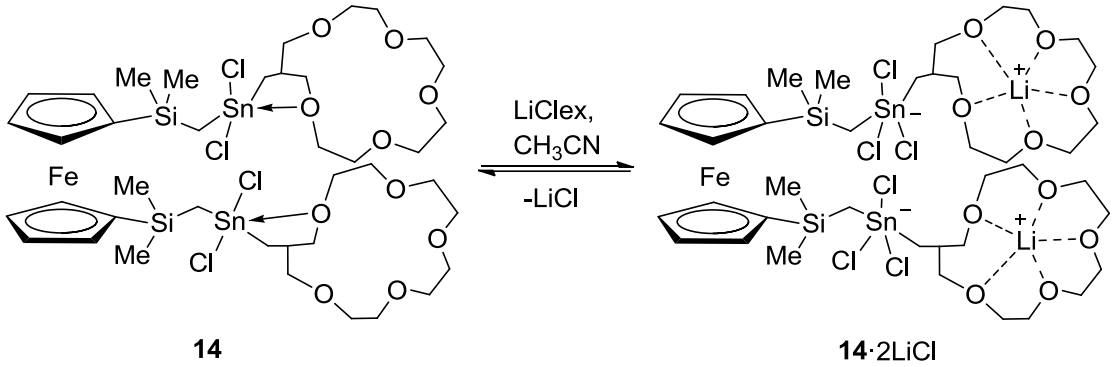

Scheme 11. Reaction of compound **14** with $LiCl_{ex}$ in CH_3CN.

For further proofs of the formation of LiCl-containing ditopic complexes, the ^{1}H NMR and ^{13}C NMR spectroscopy as well as ESI-MS spectrometry of samples containing **13** or **14** and an excess of LiCl were recorded. In the following, compound **14** was used as a representative example of the two latter compounds. In the ^{13}C NMR spectrum of a solution of (**14** + $LiCl_{ex}$) in CD_3CN, the signals of the C17, $SiCH_2Sn$ and C14/C16 carbon atoms are, with respect to the ^{13}C NMR chemical shifts of pure **14** in CD_3CN, significantly low field shifted by 8.0, 7.1 and 3.78 ppm, respectively, while the signals of C15 and C2-C12 crown ether carbon atoms moved by 0.39 and 1.91 ppm to high field (Figure 51).

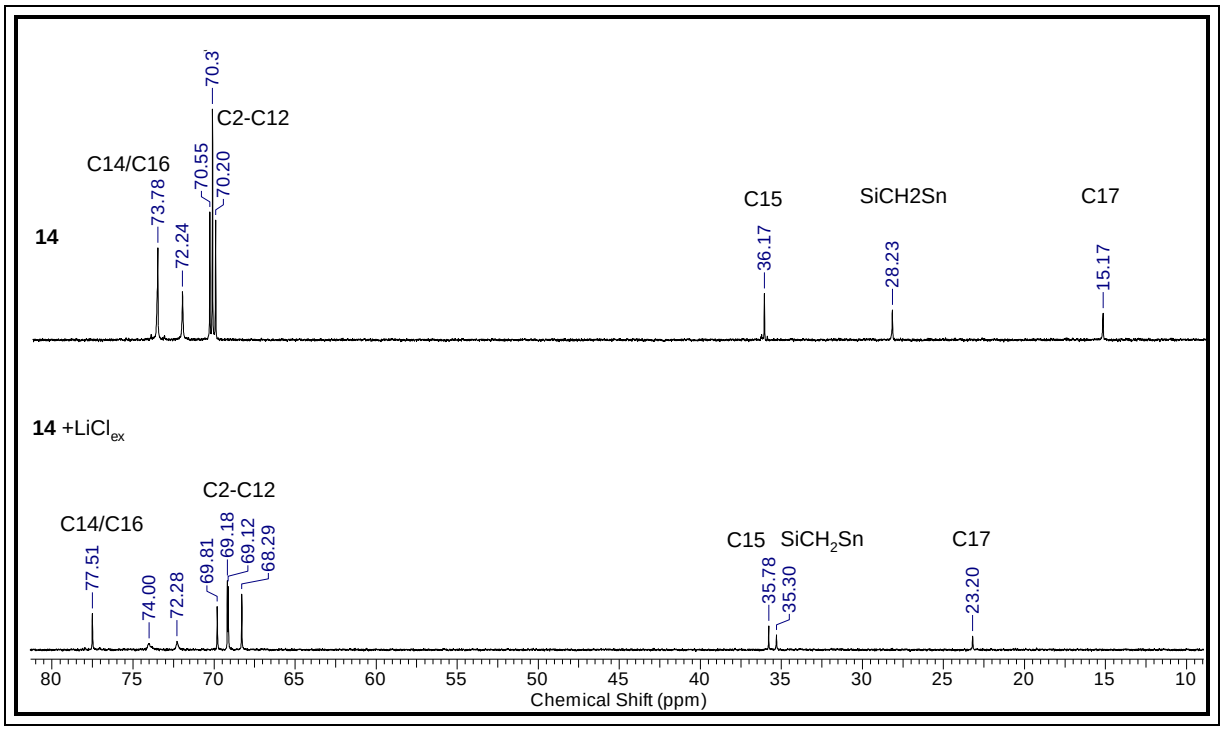

Figure 51. ^{13}C NMR spectrum of **14** showing the resonances for the C14/C16, C2-C12, C15, $SiCH_2Sn$, C17 carbon atoms of pure **14** and of **14** + $LiCl_{ex}$ in CD_3CN.

The ^1H NMR spectrum of (**14** + $LiCl_{ex}$) showed also changes for the $H_{C14/C16}$, H_{C2-C14} and H_{C15} hydrogen atoms, which are downfield shifted by 0.32, 0.04 and 0.51 ppm, respectively, in comparison with the ^1H NMR chemical shifts of pure **14** in CD_3CN (Figure 52). The ESI-MS spectrum in the positive mode of compound **13** showed an intense mass cluster centered at *m/z* 701.1 that is assigned to $\{FcMe_2SiCH_2SnCl_2CH_2\text{-}[16]\text{-crown-}5\cdot Li\}^+$. In the negative mode there is a mass cluster centered at *m/z* 729.0 that is assigned to $\{FcMe_2SiCH_2SnCl_2CH_2\text{-}[16]\text{-crown-}5\cdot Cl\}^-$. A less intense signal was observed at *m/z* 736.1 that is tentatively assigned to $\{FcMe_2SiCH_2SnCl_2CH_2\text{-}[16]\text{-crown-}5\cdot LiCl\}^-$. ESI-MS analysis of compound **14** showed a mass cluster at *m/z* 1237.2 that is assigned to $\{fc(Me_2SiCH_2SnCH_2\text{-}[16]\text{-crown-}5)_2\cdot(CH_2Cl_2)_2\cdot Li\}^{2+}$. In the negative mode there is a mass cluster centered at *m/z* 1257.2 that is assigned to $\{fc(Me_2SiCH_2SnCl_2CH_2\text{-}[16]\text{-crown-}5)_2\cdot Cl\cdot H_2O\cdot H_2\}^-$.

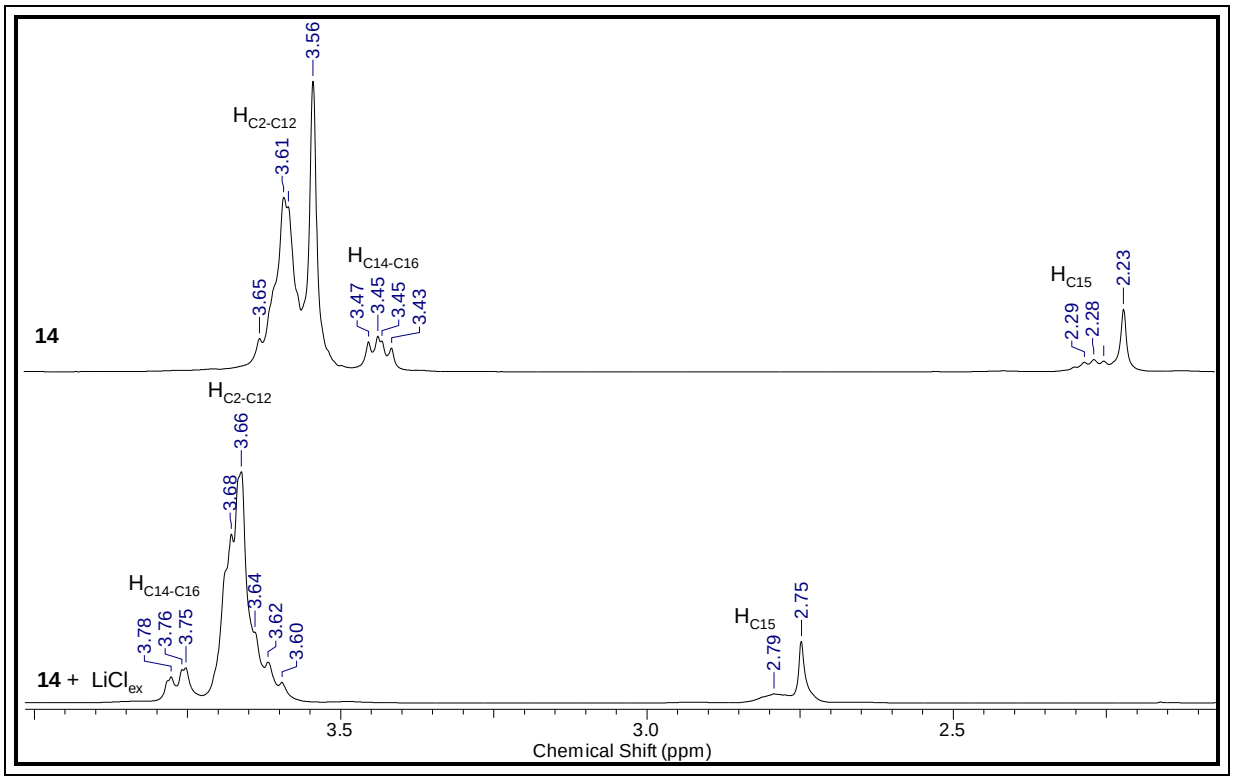

Figure 52. ^{1}H NMR spectrum of **14** showing the resonances for the $H_{C2\text{-}C12}$, $H_{C14/C16}$, H_{C15} protons of pure **14** and of (**14** + $LiCl_{ex}$) in CD_3CN.

Further evidence that receptors **13** and **14** can ditopically complex lithium chloride came from the electrochemical studies of these receptors.

2.2.9. Electrochemistry of substituted ferrocenes **1**, **2**, **5**–**8**, **12**–**14**.

Electrochemical studies were done by Prof. Dr. Viatcheslav Jouikov of the University of Rennes in France. Voltammetry of substituted ferrocenes **1**, **2**, **5**–**8**, **12**–**14** has been carried out in CH_3CN/0.1 M Bu_4NPF_6 solutions at a 3 mm glassy carbon (GC) disk electrode. Bu_4NPF_6 supporting electrolyte has been chosen because of its poorly coordinating PF_6^- anion. With Bu_4NClO_4 in place of Bu_4NPF_6, the measured E^o potentials had practically the same values; the difference, if any, does not exceed the experimental error of measurements under these conditions (± 2 mV). Since ClO_4^- anion does not show any specific interactions with the compounds studied, $LiClO_4$ and $NaClO_4$ have been used as sources of Li^+ and Na^+ cations, respectively. $(C_{16}H_{33})(C_6H_{13})Me_2NCl$ or $PhCH_2(Et)_3NCl$ were used for the addition of Cl^- anion to the solution. The F^- anion was added in form of 1 M solution of Bu_4NF in THF.

2.2.9.1. Anodic voltammetry

Upon oxidation under these conditions, all compounds of this reaction series show a distinct well-shaped and reversible oxidation signal corresponding to a one-electron couple Fc/Fc^+ (Figure 54 and 55). Half-width of the oxidation peak $E_p - E_{p/2}$ is 55-61 mV for all compounds with the $\Delta E = E_p^a - E_p^c \cong 59$ mV, attesting fast electron transfer kinetics in all cases.[185] The standard potentials E_o of these systems vary depending on the substituent(s) at the Cp ring(s) of Fc and on the presence of several ions. Standard potentials of substituted ferrocenes **1**, **2**, **5**–**8**, **12**–**14** alone and in the presence of different ions are collected in Table 5.

Table 5. Potentials (E_o, V[a]) of oxidation of Fc moiety in substituted ferrocenes **1**, **2**, **5**–**8**, **12**–**14**.

Compound	E_o	Li^+	Cl^-	F^- [b]
1	0.113	0.115 (+2)	0.094 (-20)	0.073 (*-40*) 0.108 (-5)
2	0.113	0.136 (+23)	0.102 (-34)	0.073 (*-40*) 0.117 (+4)
5	0.127	0.145 (+22)	0.124 (-21)	0.146 (+1)
6	0.122	0.148 (+26)		
7	0.219		0.205 (-20)	0.170 (*-49*) 0.225 (+6)
8	0.229			0.170 (*-59*) 0.219 (-10)
12	0.147			
13	0.099	0.103 (+5)	0.049 (-50)	0.023 (-26)
14	0.133	0.141 (+8)	0.058 (-73)	0.136 (+3)

[a] E^o in AN/0.1 M Bu_4NPF_6 *vs.* polypyrrole reference electrode. Li^+ as $LiClO_4$; Cl^- as $BzEt_3NCl$; F^- as Bu_4NF. In the parentheses, ion-induced shift of E_o (mV) is given. [b] First value corresponds to the pre-peak; second value is for the main Fc^+/Fc system.

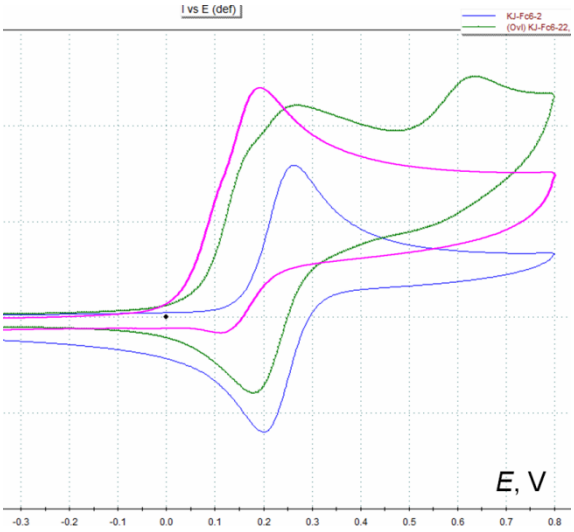

Figure 53. Oxidation of **8** (2 mmol L^{-1}) in CH_3CN/0.1 Bu_4NPF_6 M (blue); same solution after addition of F^- anion (green). *v* = 0.5 V/s. Magenta: oxidation of **1** in CH_3CN /0.1 Bu_4NPF_6 M after addition of F^- anion.

Two values are given for F^- anion because the shape of the oxidation curves of **1** and **8** changed in its presence (figure 53). Differential pulse voltammetry shows that new peak of **1** is double, with a pre-peak on the oxidation peak of the old system. Similar feature, even better pronounced, is observed for **8**. This pre-peak is tentatively ascribed to the oxidation of an intermediate with pentacoordinated tin atom; additional electron density from F^- anion makes its oxidation easier compared to the tetracoordinated form (the E_o shifts by –40 mV and –59 mV for **1** and **8**, respectively). Main peak, on the contrary, seems to be poorly sensible to the presence of this anion. Most pronounced in case of **13** and **14**, the addition of F^- anion also shifts the E^o toward less positive potentials, though to a much lesser extent than Cl^- (Table 5). When adding F^- after the addition of Cl^-, the E^o of both **13** and **14** remains practically unchanged, the opposite order of addition (Cl^- after F^-) provokes similar shift of E^o as Cl^- alone, visibly reflecting better coordinating ability of Cl^- anion. The addition of Li^+ is accompanied by the same anodic shift in E^o in both cases, - either before or after adding Cl^- or F^- anions (Figure 54 and 55).

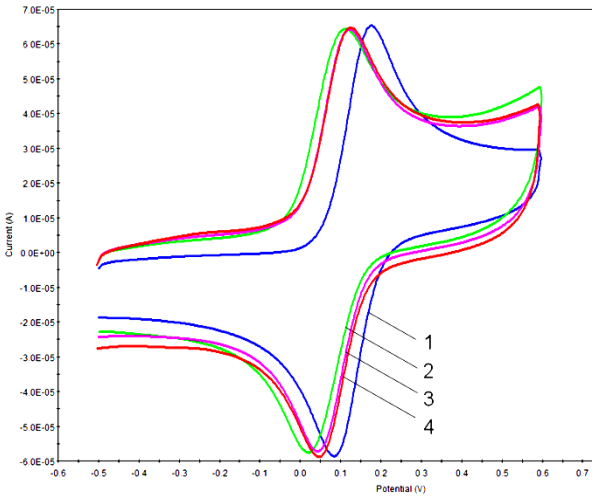

Figure 54. Voltammetry of **14** (2×10^{-3} mol L^{-1}) at a GC electrode in AN/0.1 M Bu_4NPF_6, *v* = 0.5 V/s. (1) – no additives, (2) – $(C_{16}H_{33})(C_6H_{13})Me_2NCl$ (4×10^{-3} mol L^{-1}) added, (3) – $(C_{16}H_{33})(C_6H_{13})Me_2NCl$ + $LiClO_4$ (4×10^{-3} mol L^{-1}), (4)– $(C_{16}H_{33})(C_6H_{13})Me_2NCl$ + $LiClO_4$ + Bu_4NF (4×10^{-3} mol L^{-1}).

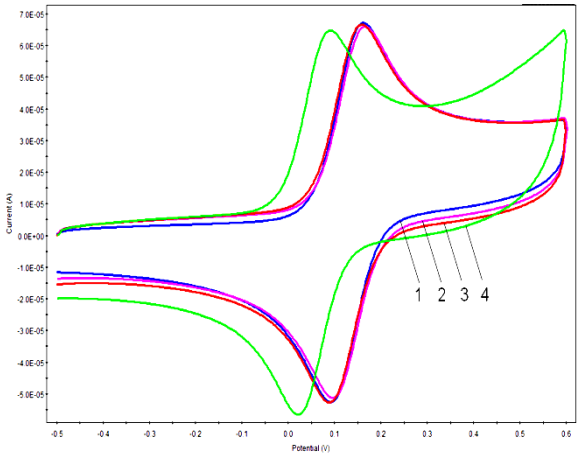

Figure 55. Voltammetry of **14** (2×10^{-3} mol L^{-1}) at a GC electrode in AN/0.1 M Bu_4NPF_6 with the reversed order of addition of ions. (1) – no additives, (2) – $LiClO_4$ (4×10^{-3} mol L^{-1}) added, (3) – $LiClO_4$ + Bu_4NF (4×10^{-3} mol L^{-1}), (4) – $LiClO_4$ + Bu_4NF + $(C_{16}H_{33})(C_6H_{13})Me_2NCl$ (4×10^{-3} mol L^{-1}). *v* = 0.5 V/s.

The addition of Li^+ (as $LiClO_4$) had little effect on E^o of these ferrocene derivatives compared to that provoked by Cl^- (Table 5 and Figure 56). The reason for this is probably that the complexation of Li^+ occurs at a remote crown-ether fragment whereas the coordination of the anion takes place at the tin atom being closer to Fc. Interestingly, the maximum effect of the added ion on the E^o of ferrocene **14** is

observed (Figure 56) at a more than 2:1 stoichiometric ratio (1:1 for **13**), the E^o becomes stable at ca. 20-fold excess of the ions. A possible explanation is that the results shown in Figure 56 are obtained with 1 minute delay after each addition of the corresponding ion; since the coordination is a thermodynamic equilibrium process, longer contact times are probably necessary.

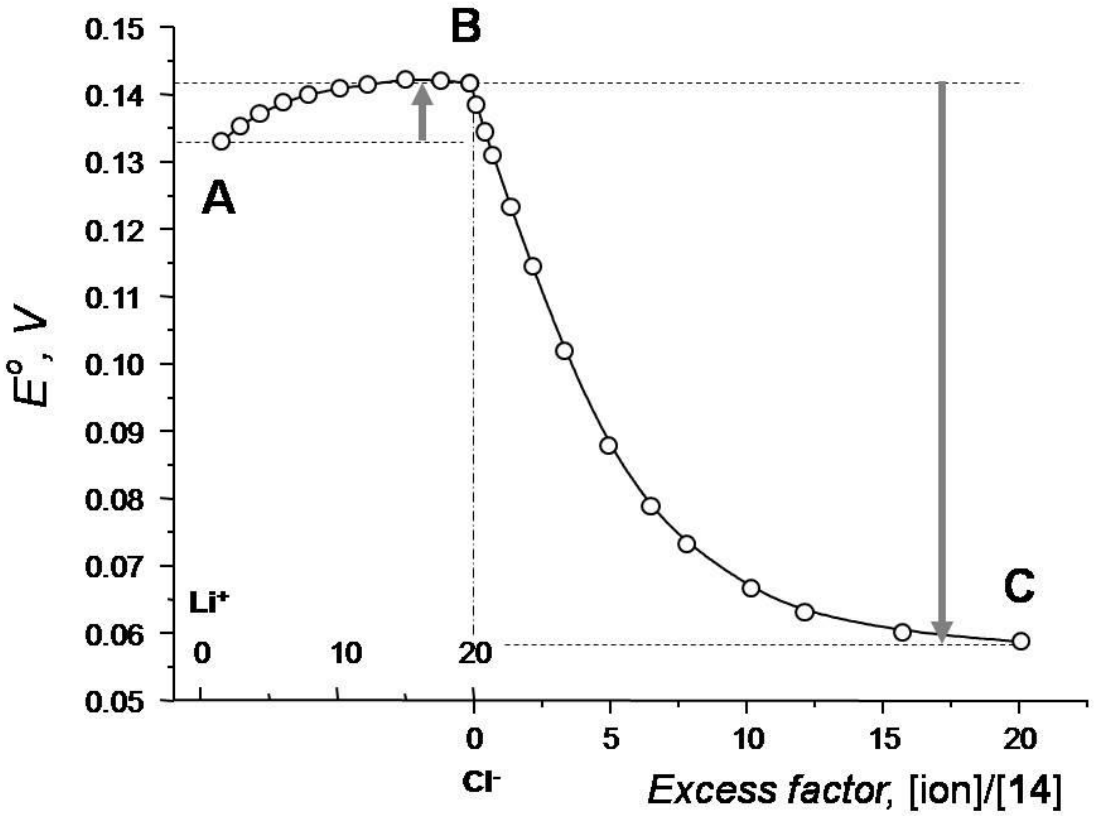

Figure 56. Variation of E^o of **14** with the concentration of added ions. A-B: addition of $LiClO_4$ (0-20 equiv), ΔE^o_{lim} = +8 mV. B-C: addition of $HexMe_2RNCl$ (0-20 equiv), ΔE^o_{lim} = -83 mV.

Non-substituted Fc under these conditions exhibits a reversible one-electron system with E^o = 0.082 V, which was used as a reference in the measurements. The observed difference in E^o of **13** and **14** relative to Fc corresponds to the electron-withdrawing effects exerted by the substituent(s). The apparent E^o of **13** is exactly half-way ($E^o_{\mathbf{13}} - E^o_{Fc}$ = 17 mV) between those of Fc and **8** ($E^o_{\mathbf{14}} - E^o_{Fc}$ = 34 mV), in agreement with cumulative effect of the substituents ($\sigma_{app} = 2\sigma$). Apparently, organometallic substituents in these ferrocene derivatives have a complex overall effect on the Fc core but its mechanism is not sensitive to steric demand.

2.2.9.2. Cathodic voltammetry and grafting to glassy carbon.

Grafting to glassy carbon was done by Prof. Dr. Viatcheslav Jouikov of the University of Rennes in France. On the cathodic branches of voltammograms of the compounds **5, 6, 13**, and **14** (Figure 57) there is a reduction peak supposedly corresponding to one-electron cleavage of Sn-Cl bond.[186] In the case of iodo-derivative **12**, this process occurs at less cathodic potential ($E_1 < E_2$) so as second cathodic peak (E_3) of the following reduction of stannyl radicals to the corresponding stannyl anions is also seen on the voltammogram (Figure 57).

and

$$R_3SnCl \xrightarrow{+e} R_3Sn^{\cdot} + Cl^- \qquad E_1$$

$$R_3SnI \xrightarrow{+e} R_3Sn^{\cdot} + I^- \qquad E_2$$

$$R_3Sn^{\cdot} \xrightarrow{+e} R_3Sn^- \qquad E_3$$

These peaks are absent on the voltammograms of fluorinated **7, 8** (E_p beyond -2.8 V) and of non-halogenated derivatives **1** and **2** (Figure 57 a).

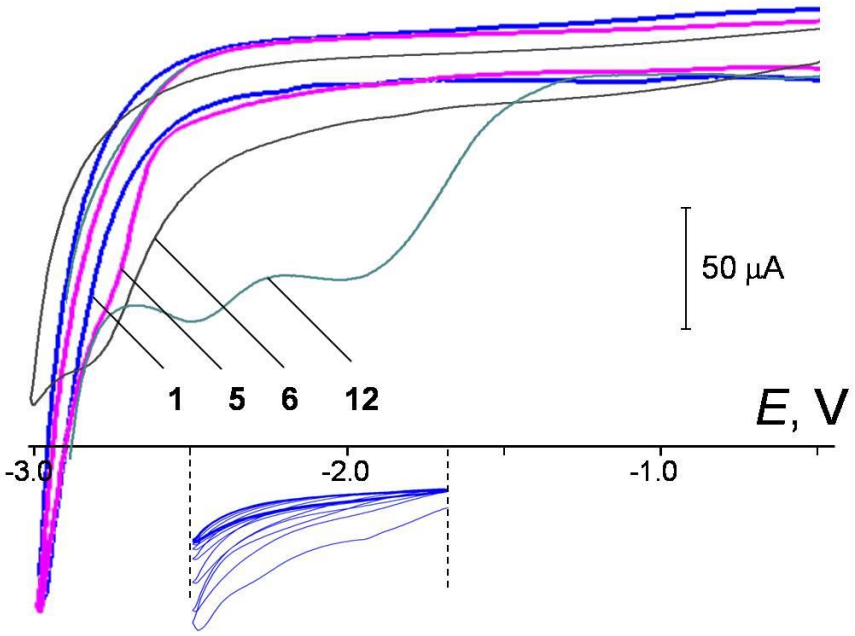

Figure 57. Cathodic voltammetry of substituted ferrocenes **1**, **5**, **6** and **12** (1 mmol L^{-1}) in CH_3CN/0.1 M Bu_4NPF_6 at a microdisk GC electrode. Scan rate *v* = 0.5 V/s. Below: first 15 scans of the cathodic grafting from **4** (E = –1.7…-2.5 V, *v* = 0.05 V/s).

One can see that the zone of cathodic charge of GC (reduction of graphitic C_{sp2} inclusions into a C_{sp3} lattice starting at E ≅ –1.7 V), leading to the induction of polynucleophilic sites at its surface,[187] is located before the potentials of own reduction of halostannanes. This fact permits generating carbanionic sites at the GC interface in the presence of halogenated ferrocene derivatives without the reduction of the latter. Thus produced interfacial C-nucleophiles substitute halogen atoms in Sn-Hal containing ferrocenes in a S_N2-like process resulting in the formation of a covalent bond (GC)C_{sp3}-Sn. Now, cycling the potential within the range of reduction of C_{sp2} inclusions in the GC (E = –1.7…–2.1 V) leads to a progressive coverage and inhibition of the GC interface by an organometallic layer covalently bound to the surface. This deposit remains at the surface after ultrasonic rinsing in acetonitrile and acetone attesting its non-adsorptional immobilization. Scheme 12 summarizes the formation of polynucleophilic sites at the GC surface and subsequent nucleophilic grafting of halogenated ferrocenes.

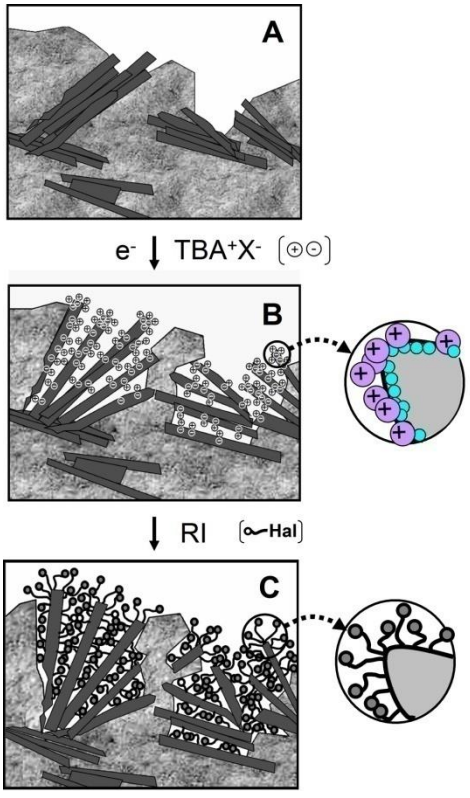

Scheme 12. Schematic representation of the grafting of R-Hal derivatives onto a glassy carbon (GC) surface (A) via cathodic charging (threshold potential, –1.7 V) of graphitized inclusions into GC (B). Nucleophilic substitution (S_N) of surface-induced nucleophilic sites on Sn-Hal bonds (C) starts at the charged graphite surface. GC: grey zones are those

with predominance of inert C_{sp3}, darker zones represent C_{sp2} graphitic inclusions (*Adapted from*[187]).

When cycling the potential in the cathodic domain, at E < –1.7 V, when C_{sp3} nucleophilic centers start to appear at the GC surface, the signal of reduction of **7** (2×10^{-3} mol L^{-1} in AN/0.1 M Bu_4NPF_6) progressively disappears displaying total passivation of the electrode. The anodic scan on this solution showed (Figure 58) that a new peak appeared at more positive potentials and the reverse peak of the reduction of free ferrocenium form is strongly displaced to more negative potentials reflecting strong impediment of the electron transfer. The electrode was then rinsed with acetone in an ultrasonic bath in order to remove adsorbed products. This procedure only removes soluble species and does not affect those covalently grafted to the GC surface. The voltammetry of thus obtained electrode in CH_3CN /0.1 M Bu_4NPF_6 is shown in Figure 58. During the anodic scan, a characteristic signal of oxidation of immobilized Fc is seen. Contrary to classical diffusion-like curve (Figure 54, 55 and 58), this signal is bell-shaped ("adsorption-like" peak), which is characteristic for the surface-immobilized redox systems. Covalent attachment of Fc moieties to the electrode surface also follows form linear (contrary to square root) dependence of the peak current i_p on the scan rate (Figure 58).

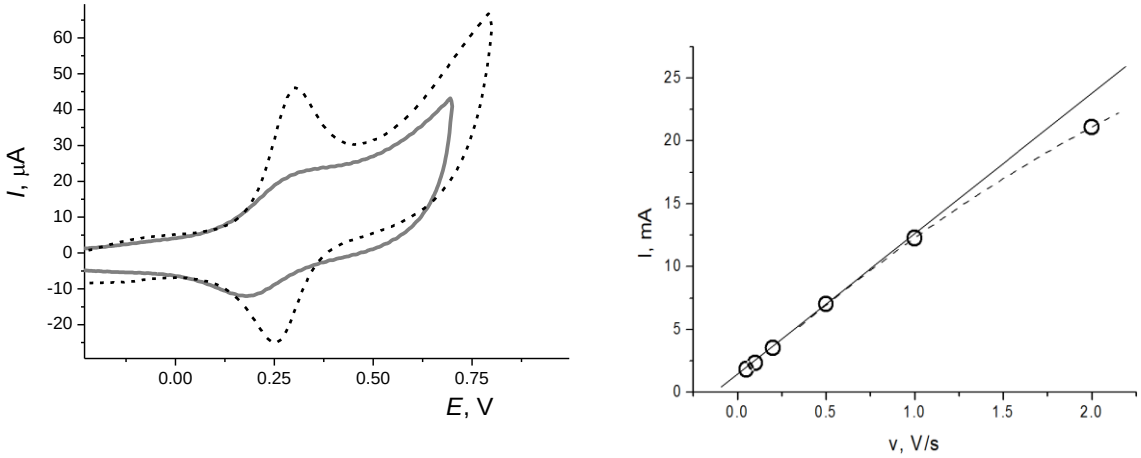

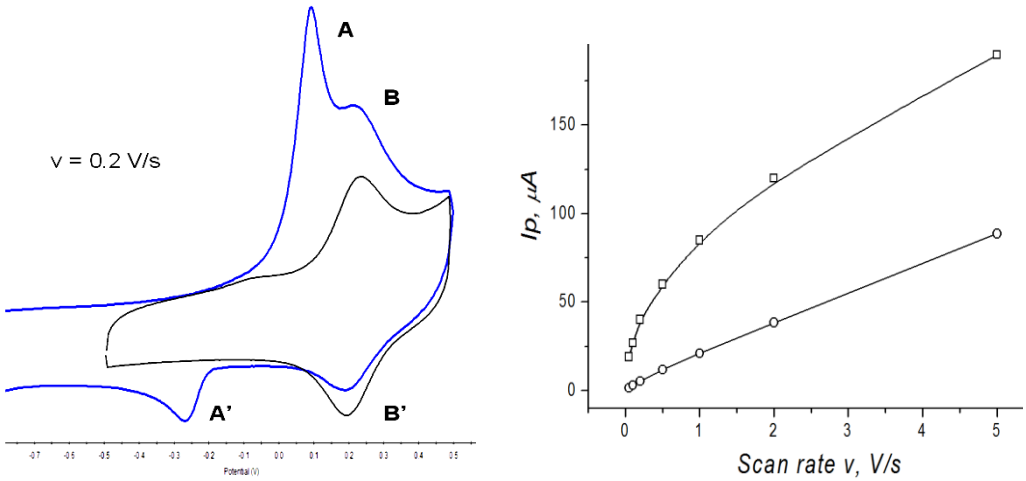

Figure 58. *Upper panels.* (*left*)- Responses of the GC electrode modified with **6** (broken line) and **8** (solid line). Solvent: CH_3CN/0.1 M Bu_4NPF_6. Scan rate *v* = 0.5 V/s. (*right*)- Peak current of the deposit from **6** versus scan rate. Linear "adsorption-like" (solid line) and $t^{-1/2}$ diffusional (broken line) dependencies at low and higher scan rates, respectively. *Bottom panels.* (*left*)-Voltammetry (anodic scan) of the GC electrode after cathodic grafting of ferrocenyl-crown compound (starting with **13**): A – (blue line) in the same solution (**13** in CH_3CN /0.1 M Bu_4NPF_6); well seen is the remarkable cathodic shift of the back peak (A') of reduction of free ferrocenium form in the solution. B – (black line) same electrode after ultrasonic cleansing, in CH_3CN /0.1 M Bu_4NPF_6; only grafted Fc is present. (*right*)-Peak currents of the oxidation of free (upper) and immobilized from **13** (lower) Fc moieties versus scan rate.

Thus immobilized organometallic layers bring an additional resistance to the electron transfer across the interface compared to an inhibited GC surface as can be seen from the depression of the reversible signal of reduction of *p*-chloranil taken as model compounds with fast electron transfer kinetics (Figure 59).

Quantitatively, charge transfer resistance (R_{CT}) brought to the interface by thus formed layer can be assessed by electrochemical impedance spectroscopy (EIS). A large demi-circle on the Nyquist plot (Figure 60) corresponds to the R_{CT} = 440 kohm for the freshly immobilized and non-oxidized layer and to Rct = 4.93 kohm for a layer subjected to several back-and-forth redox cycling between 0 and 0.6 V. Such a

cycling allows the counterions (anions of the supporting electrolyte) to enter the organometallic layer during the phase of oxidation of Fc to Fc^+ (and also the cations Bu_4N^+ during the reverse phase, see Scheme 13) in order to assure the electroneutrality of the whole system. Thus conditioned layer obtains the properties of a redox polymer saturated with supporting electrolyte.

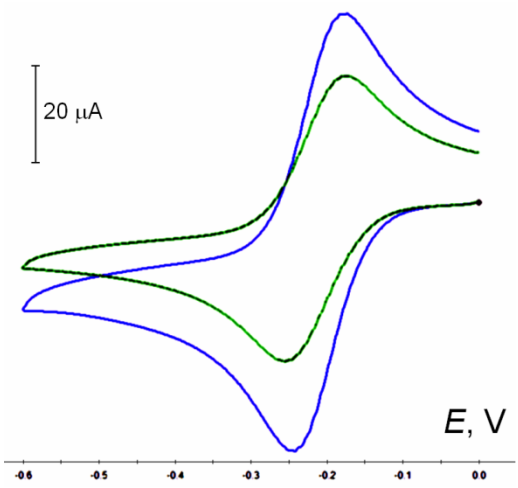

Figure 59. Depression of the reversible one-electron reduction of chloranil (2 mmol L^{-1}) on the layer grafted from **5** (green) in comparison with the reduction at a polished GC (blue). CH_3CN/0.1 M Bu_4NPF_6. *v* = 0.5 V/s.

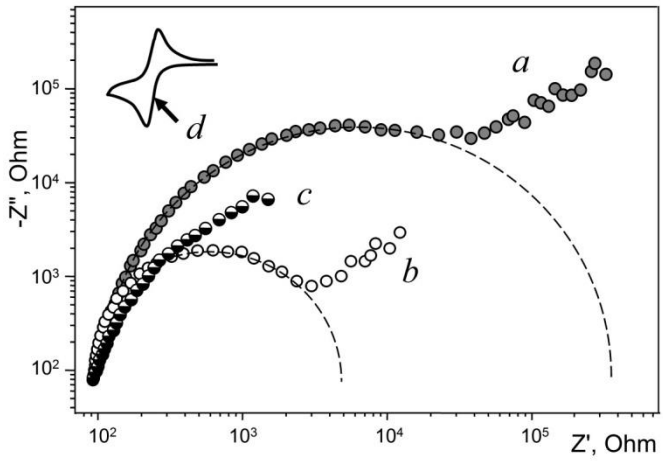

Figure 60. Nyquist plots for the reduction of *p*-chloranil (2.4 mmol L^{-1}) at the GC electrodes in CH_3CN/0.1 M Bu_4NPF_6. (a) GC electrode freshly grafted using 4. (b) Same electrode after 4 cycles between 0 and 0.6 V. (c) GC electrode after mechanical removal (polishing) of the immobilized layer. (d) The arrow shows the potential for EIS measurements. Frequency range from 1 MHz to 0.01 Hz; E_{app} = –0.2 V; ΔE = 10 mV.

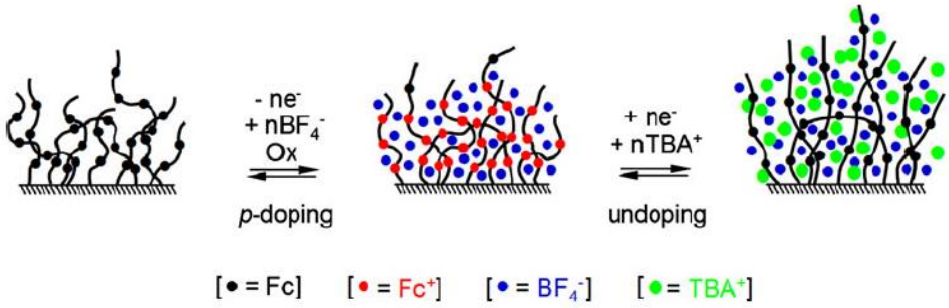

Scheme 13. Conditioning of the grafted redox layer: diffusion of counter ions during oxidation/reduction of the immobilized Fc sites (from[188]).

At low scan rates, a reversible pair of bell-shaped adsorption-like peaks (E_p^a = 0.221 and E_p^c = 0.207 V) appears on the voltammogram of the layer grafted from **12** (Figure 61). At higher scan rates, the peaks start moving apart with respect to the apparent E_o (at 1 V/s, E_p^a = 0.277 V) and their shape evolves obtaining more pronounced diffusional character ($I = f(t^{-1/2})$, Figure 58) due to the limitation of electron transfer by the diffusion of the counter anion of the supporting electrolyte to the oxidation sites (Fc within the grafted layer). On the back scan, - upon reduction of Fc^+ to neutral Fc, - diffusion of TBA^+ accounts for the diffusional trail on the voltammogram. The electrodeposited layer can be therefore characterized as rather thick and behaving as an electrode-immobilized redox polymer.

It is to note that redox response of the immobilized layer is sensitive to the presence of ions in solution: upon addition of the cations of Li^+ and Na^+, the E_o potential of the layer grafted from **12** shifts (Figure 62) by 7 and 27 mV, respectively.

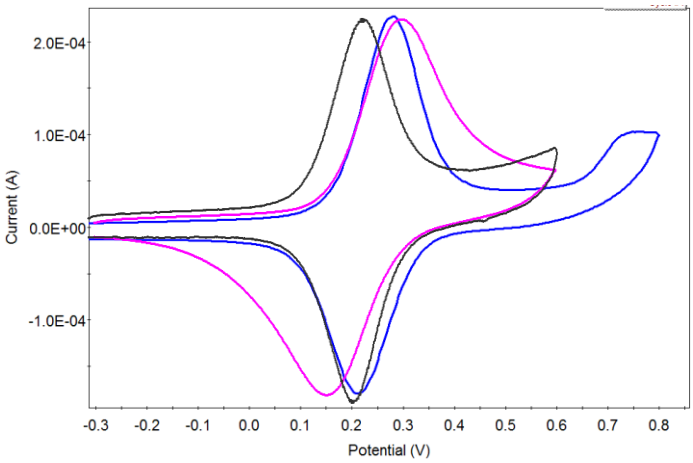

Figure **61**. Scan-rate normalized responses of the GC electrode modified with **12** at different scan rates. *v* = 0.2 (grey), 1 (blue) and 2 V/s (magenta). Apparent E_o = 0.214 V. Solvent: CH_3CN/0.1 M Bu_4NPF_6.

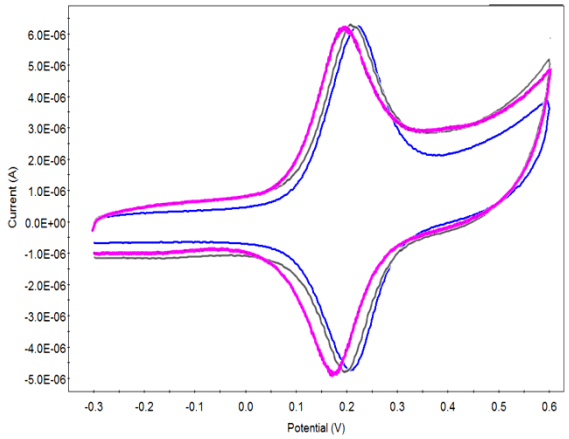

Figure 62. Voltammetry of **12** grafted onto G: (blue)-Freshly grafted electrode. (grey)-After the addition of $LiClO_4$. (magenta)-Same electrode after addition of $NaClO_4$. CH_3CN /0.1 M Bu_4NPF_6, *v* = 50 mV/s.

The grafted layer in the case of **6** has two redox responses: besides that of ferrocene (anodic, figure Q) there is also a cathodic adsorption-like signal corresponding to the reduction of surface-immobilized Sn-Cl groups (Figure 63). This signal, however, is less stable with time.

Grafting efficiency is not the same for different ferrocenes: smaller values are found for the compounds **6** and **8** (Figure 60) whereas largest extent of grafting was observed for **12**. Also, mono-substituted ferrocenes generally show lower surface coverage compared to di-substituted analogues, though not always by the factor 1/2. With the compounds where Sn is substituted with Ph group (**5**, **6** and **8**), poorest

grafting efficiency was observed. The reason of such variance is probably different steric accessibility of Sn for the nucleophilic attack by surface-located nucleophilic sites.

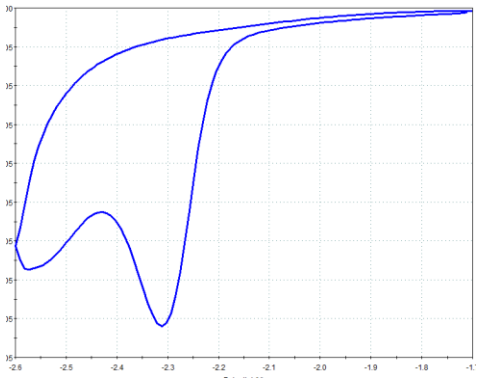

Figure 63. Cathodic voltammetry (first two scans) of the layer grafted onto GC from **6** (2 mmol L^{-1} solution in CH_3CN /0.1 M Bu_4NPF_6). *v* = 50 mV/s.

Integration of the oxidation current of Fc immobilized using **6** (Q = 34×10^{-6} coul) provided the amount of redox groups at the modified interface as $\Gamma_{Fc(\mathbf{4})}$ = 3.9×10^{-9} mol/cm^2. Assuming the radii of the immobilized moiety **6** as 7.5 Å, a monolayer coverage of the surface should then correspond to ca. 2.3×10^{-11} mol/cm^2. The experimental coverage value is approximately 170 times superior meaning that (even supposing surface roughness factor 3-5) a kind of multilayer was formed with in average 30-50 times more of Fc units as might be expected in the case of monolayer formation.

Scanning electron microscopy (SEM) of the modified surface (Figure 64) shows the formation of a thick layer covering the surface and smoothing not only its mechanical defects (Figure 64, C) but also the intrinsic roughness of GC (Figure 64, D). The analysis of this layer in back-scattered electrons confirmed the presence of Sn, Fe and Si atoms (Figure 65). Interestingly, morphology of the cathodically deposited layer depends on either mono- or di-substituted ferrocene was used as precursor for grafting.

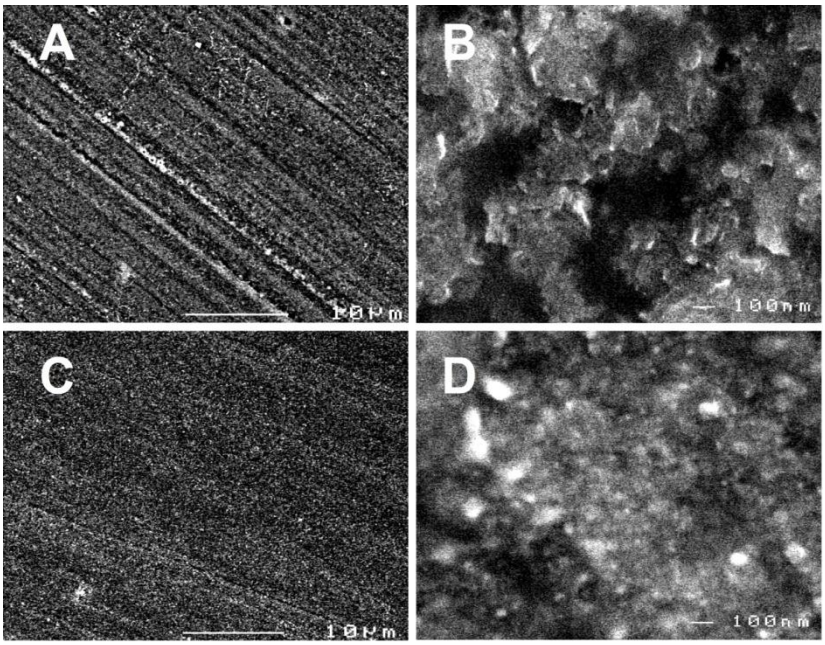

Figure 64. SEM photographs (secondary electrons) of the surface of GC electrode before (A, B) and after (C, D) immobilization of organometallic layer by cathodic cycling of potential (E = –1.7…-2.1 V) in the solution of **13** (2 mmol L^{-1}) in CH_3CN/0.1 M Bu_4BPF_6. Accelerating tension.7 kV.

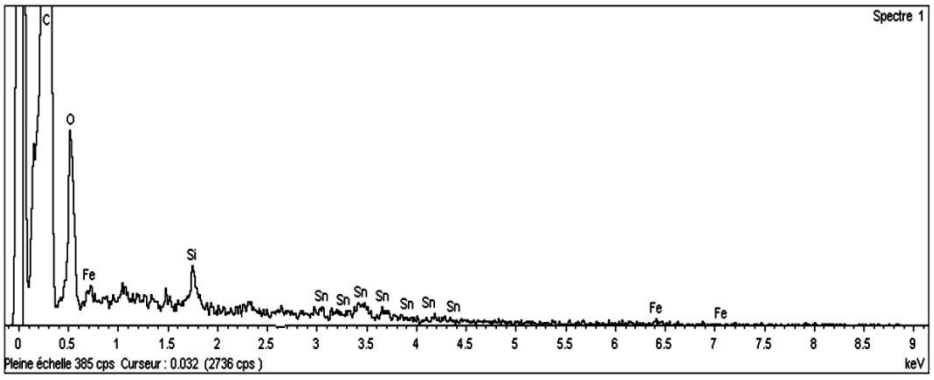

Figure 65. Elemental composition of the layer grafted from **13** by back-scattered electron spectroscopy. Tension 10 kV, integration over 20×30 μm area.

Figure 66 shows the SEM images of the surface of GC electrode modified using disubstituted derivative **14**. Though grafting procedure and conditions were similar to those used for grafting from **13**, a thick spongy layer was formed. The EIS study of this system revealed two time constants on Nyquist diagram; though the exact analysis of this system is complex, it corresponds to an equivalent circuit with dense and porous parallel components (supposedly corresponding to one of three possible models of non-perfect polymer coating, a "failed coating" model[189]). The formation of

this spongy layer is probably related to multi-functional character of **14** enabling the formation of polystannane links. Mechanically entangled Fc-containing strands seem to be as well present in the coating formed from **14** since the signal of immobilized Fc remarkably diminishes after several redox cyclings and ultrasonic cleaning of this surface.

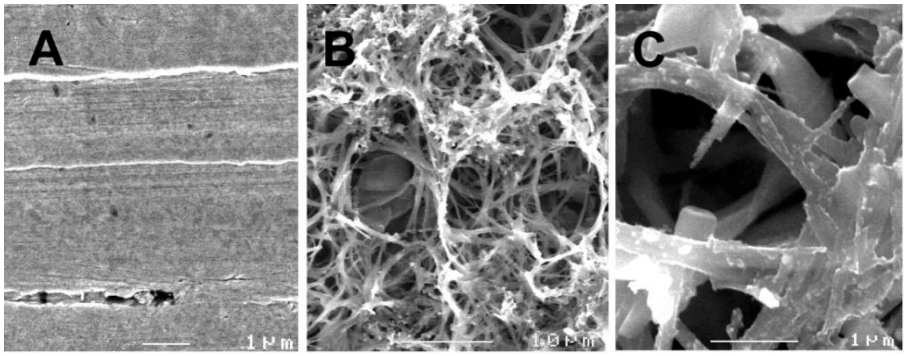

Figure 66. SEM photographs of the surface of GC electrode before (A) and after (B, C) immobilization of organometallic layer deposited from **14** under the same conditions as in Figure 64.

2.2.9.3. Conclusions.

Voltammograms (response of Fc) of all compounds show excellent reproducibility: no signs of adsorption or current depression were observed. Reduction of Cl and I-containing derivatives led to Sn-Hal bond reduction (oxidation peak of the eliminated Hal- is then seen in the anodic scan).

The E^o of Fc^+/Fc redox system is sensitive to the coordinating interactions, apparently both at the crown ether site and Sn atom, though the extent of these effects is dependent on the nature of the organometallic substituents and their number.

Electrochemically indiced nucleophilic sites in glassy carbon react with halogenated compounds of this reaction series leading to covalent grafting of these molecules, supposedly via the formation of C-Sn bonds, which allows one to immobilize Fc moiety at such surfaces in large amounts greatly superior to monolayer coverage. Redox response of embedded Fc in such organometallic deposits is also sensitive to the presence of the cations Li^+ and Na^+.

2.2.10. Molecular structure of the organotrichloridostannate complex [13·Cl]⁻.

Single crystals suitable for X-ray diffraction analysis were obtained by slow evaporation of the compound in ethanol. The compound crystallized in the triclinic space group *p-1* with two molecules per unit cell. The molecular structure of [**13**·Cl]⁻ is shown in Figure 67, and selected bond distances and bond angles are listed in Table 6.

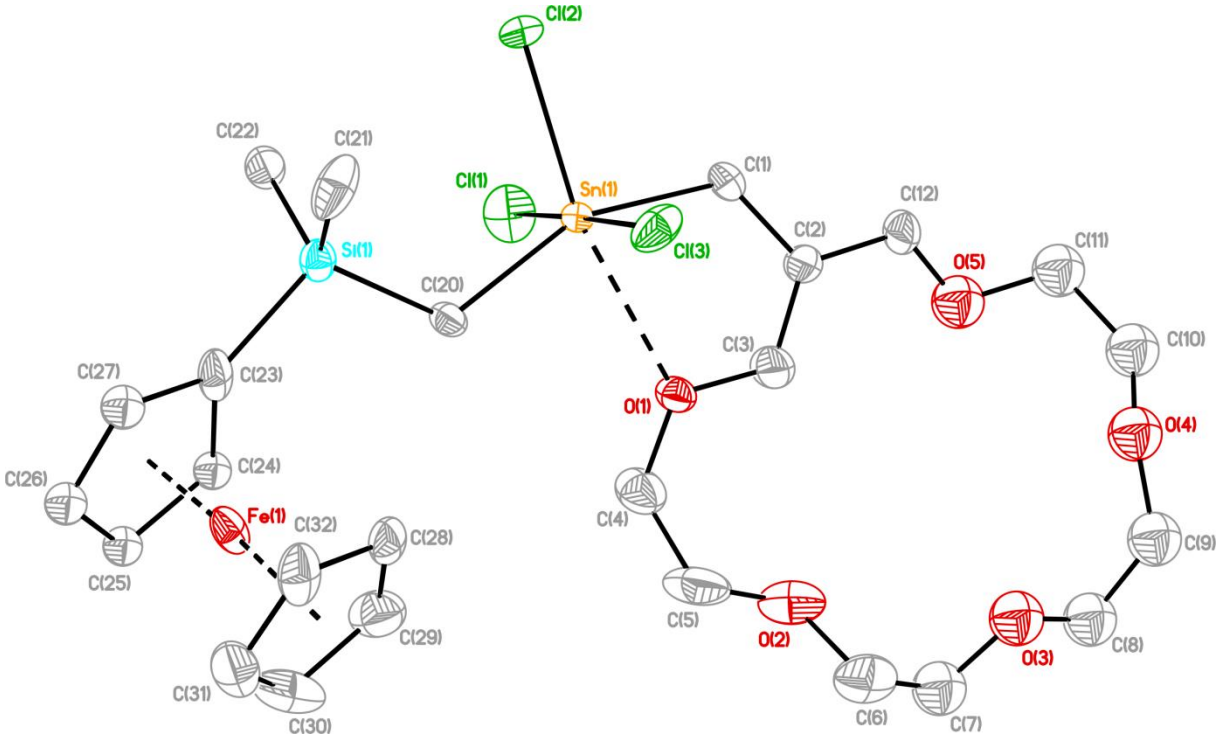

Figure 67. General view (SHELXTL) of a molecule of [**13**·Cl]⁻ showing 30% probability displacement ellipsoids and the crystallographic numbering scheme. The counter ion $[Bu_4P]^+$ is omitted for clarity.

Table 6. Selected bond lengths/Å and bond angles/° for [**13**·Cl]$^-$.

Bond lengths			
Sn(1)–C(1)	2.118(6)	Sn(1)–Cl(2)	2.4397(14)
Sn(1)–C(20)	2.115(5)	Sn(1)–Cl(3)	2.5697(15)
Sn(1)–Cl(1)	2.5595(18)	Sn(1)–O(1)	2.640(4)
Bond angles			
C(20)–Sn(1)–C(1)	155.6(2)	Cl(1)–Sn(1)–Cl(2)	92.94(7)
C(1)–Sn(1)–Cl(1)	89.5(2)	Cl(1)–Sn(1)–Cl(3)	90.5(2)
C(1)–Sn(1)–Cl(2)	96.78(17)	Cl(2)–Sn(1)–Cl(3)	88.84(6)
C(1)–Sn(1)–Cl(3)	90.5(2)	C(2)–C(1)–Sn(1)	117.6(4))
C(20)–Sn(1)–Cl(1)	88.74(16)	Si(1)-C(20)-Sn(1)	119.3(3)
C(20)–Sn(1)–Cl(2)	107.58(15)	C(3)–O(1)–Sn(1)	106.0(3)
C(20)–Sn(1)–Cl(3)	90.50(16)	C(4)–O(1)–Sn(1)	127.2(3)

The molecular structure of compound [**13**·Cl]$^-$ is similar to that of the analogue organotrichloridostannate complex [$PhCl_2SnCH_2$-[19]-crown-6·Cl]$^-$.[163] Thus, the tin atom in compound [**13**·Cl]$^-$ is hexacoordinated and adopts a distorted octahedral configuration with C(1) and C(20) occupying the axial and Cl(1), Cl(2), Cl(3) and O(1) occupying the equatorial positions. The distortion from the ideal geometry is the result of the streric hindrance of the ferrocene fragment and the crown ether unit and especially manifested by the C(20)–Sn(1)–C(1) angle of 155.6 (2) instead of 180°. The tin atom is displaced by 0.1215 Å of the equatorial plane in direction of C(20). However and in contrast to what was seen for the organotin substituted crown ether complex [$PhCl_2SnCH_2$-[19]-crown-6·Cl]$^-$[163], there is no loss of the intramolecular O(1)→Sn(1) coordination in [**13**·Cl]$^-$. Indeed, from the two intramolecular coordinations observed for the starting compound in the former complex, one of them is retained in the trichlorostannate complex [$PhCl_2SnCH_2$-[19]-crown-6·Cl]$^-$[163]. The preservation of the intramolecular O(1)→Sn(1) is probably the result of the competition between the ligands around the tin atom and the complex formed is stabilized by the intramolecular O(1)→Sn(1) coordination. The steric hindrance of the ferrocene fragment as well as the Sn(1)–O(1) coordination are likely keys factors which prevent intermolecular Cl→Sn interactions. The triochloroorganostannate

anion such as $[Et_2SnCl_3]^-$ exists as dimer.[190] The Sn(1)–O(1) distance of 2.640 (4) Å is considerably longer than the corresponding bond measured for the receptor **13** (2.480 (3) Å) and for the trichlorostannate complex $[PhCl_2SnCH_2$-[19]-crown-6·$Cl]^-$ (2.507 (4) Å)[163].

2.2.11. Molecular Structure of the Diaqua Complex 14·2H_2O.

The diaqua complex **14**·2H_2O was obtained as by-product from the reaction of **14** with Ph_4PCl. Single crystals suitable for X-ray diffraction analysis were obtained by slow evaporation of the compound in ethanol at room temperature. The compound crystallized monoclinically in the space group *p2/c* with two molecules per unit cell. The molecular structure of **14**·2H_2O is shown in Figure 68, and selected bond distances and bond angles are listed in Table 7.

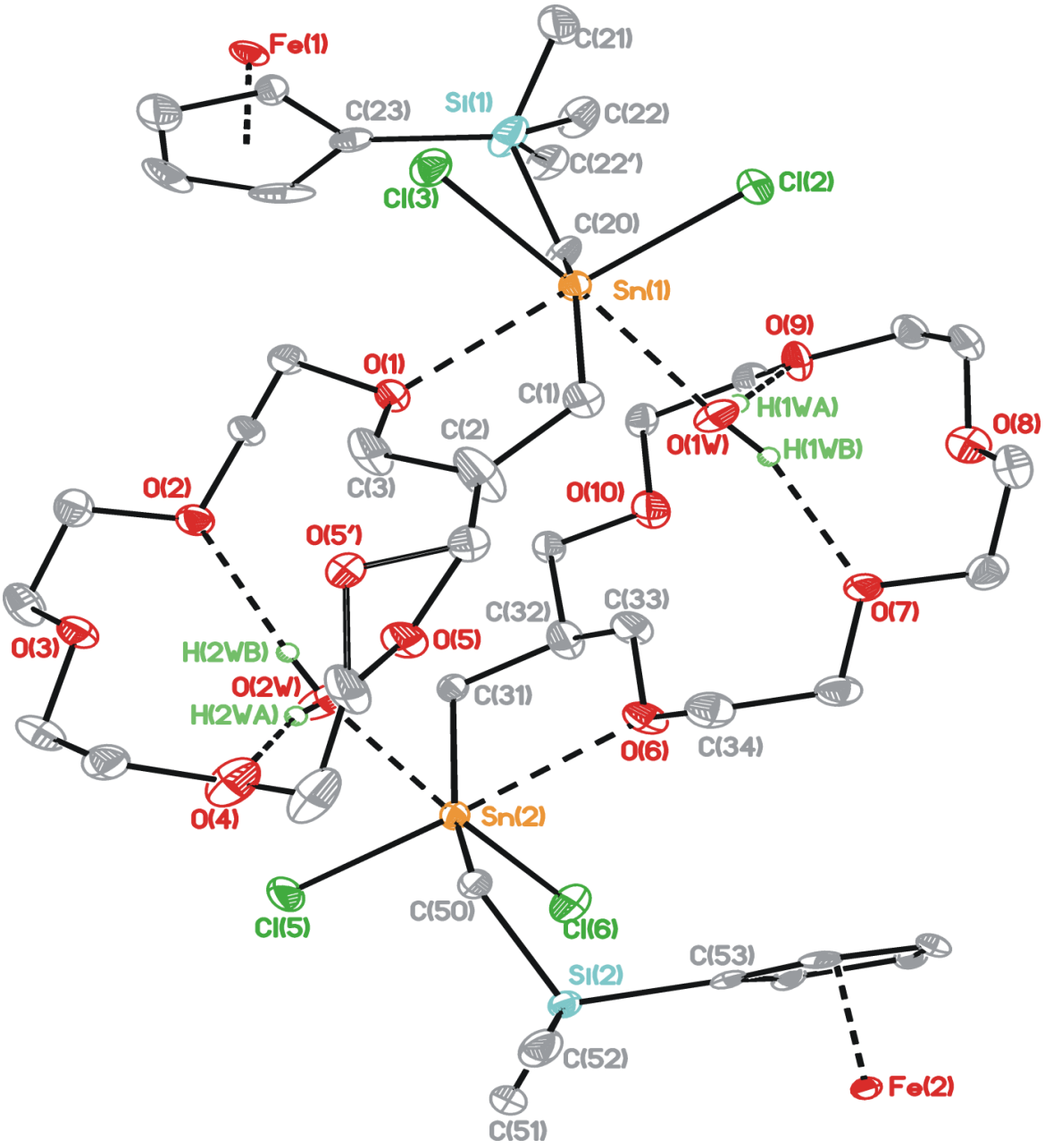

Figure 68. General view (SHELXTL) of a asymmetric unit of **14**·2H_2O showing 30% probability displacement ellipsoids and the crystallographic numbering scheme

Table 7. Selected bond lengths/Å and bond angles/° for **14**·H_2O.

Bond lengths			
Sn(1)–C(1)	2.122(4)	Sn(2)–C(50)	2.104(4)
Sn(1)–C(20)	2.092(4)	Sn(2)–C(31)	2.126(4)
Sn(1)–Cl(2)	2.4245(14)	Sn(2)–Cl(5)	2.4081(14)
Sn(1)–Cl(3)	2.4279(13)	Sn(2)–Cl(6)	2.4252(14)
Sn(1)–O(1)	2.541(3)	Sn(2)–O(2W)	2.572(4)
Sn(1)–O(1W)	2.634(4)	Sn(2)–O(6)	2.639(3)
Bond angles			
C(20)–Sn(1)–C(1)	149.31(19)	C(50)–Sn(2)–C(31)	147.77(18)
C(1)–Sn(1)–Cl(2)	99.18(14)	C(50)–Sn(2)–Cl(5)	100.66(13)
C(1)–Sn(1)–O(1)	74.12(14)	C(31)–Sn(2)–Cl(5)	101.14(13)
C(20)–Sn(1)–Cl(3)	104.49(13)	C(50)–Sn(2)–Cl(6)	106.80(12)
C(20)–Sn(1)–O(1)	87.16(14)	C(31)–Sn(2)–Cl(6)	95.89(13)
C(20)–Sn(1)–O(1W)	77.28(16)	Cl(5)–Sn(2)–Cl(6)	91.90(5)
C(20)–Sn(1)–Cl(2)	99.79(13)	C(50)–Sn(2)–O(2W)	79.26(16)
O(1)–Sn(1)–Cl(2)	172.99(8)	C(31)–Sn(2)–O(2W)	77.60(16)
O(1)–Sn(1)–Cl(3)	83.59(8)	Cl(5)–Sn(2)–O(2W)	89.22(12)
Cl(2)–Sn(1)–Cl(3)	95.41(5)	Cl(6)–Sn(2)–O(2W)	173.49(10)
C(1)–Sn(1)–Cl(3)	97.47(13)	C(50)–Sn(2)–O(6)	84.91(14)
C(1)–Sn(1)–O(1W)	79.89(16)	C(31)–Sn(2)–O(6)	73.91(14)
Cl(2)–Sn(1)–O(1W)	86.92(10)	Cl(5)–Sn(2)–O(6)	174.42(8)
Cl(3)–Sn(1)–O(1W)	176.75(9)	Cl(6)–Sn(2)–O(6)	86.13(8)
O(1)–Sn(1)–O(1W)	93.82(11)	O(2W)–Sn(2)–O(6)	92.17(14)

The asymmetric unit of **14**·2H_2O consists of two crown ethers and two half ferrocene units. Each tin atom is hexacoordinated by two oxygen, two halogen and two carbon atoms and exhibits a distorted octahedral configuration. As a result of the centrosymmetry adopted by the compound, all tin atoms are equivalent. The distortion result from the C(20)–Sn(1)–C(1) and C(50)–Sn(2)–C(31) angles of 149.0 (2) and 147.77°, which are below the ideal value 180°. Similarly, the C(1)–Sn(1)–Cl(3), C(1)–Sn(1)–Cl(2), C(31)–Sn(2)–Cl(6) and C(31)–Sn(2)–Cl(5) angles of

97.47(13), 99.18(14), 95.89(13) and 101.14(13)° are far above the value of 90°. The distortion came from the steric hindrance of the ferrocene fragment and the crown ether unit. The water molecules lie within the cavity of the crown ether ring and are coordinated by two oxygen atoms [O(2), O(4), and O(7), O(9)] of the crown ether ring, through hydrogen bonds and to the tin atom, respectively. The intermolecular Sn(1)–O(1W) and Sn(2)–O(2W) distances of 2.634 (4) and of 2.572 (4) Å as well as the intramolecular Sn(1)–O(1) and Sn(2)–O(6) distances of 2.541 (3) of 2.639 (3) Å distances are considerably longer than the corresponding distances found in Cl_3Sn-CH_2-[19]-crown-6·$2H_2O$ [Sn(1)–O(1W) (2.219(4) Å) and Sn(1)–O(1) (2.361(3) Å)] and in Cl_3Sn-CH_2-[19]-crown-6·$2H_2O$ [Sn(1)–O(1W) (2.2571(14) Å) and (2.3678(12) Å] .[153]

2.3. Novel Tin-Containing Crown Ether-Substituted Ferrocenophanes as Redox-Active Hosts for the Ditopic Complexation of Lithium Chloride.

2.3.1. Introduction.

The design and synthesis of ion pair receptors for selective recognition of anions and cations constitute an emerging field of research.[156,191-206] Such receptors have been reported to be able to diminish the effect of counterion observed for a monotopic or single ion receptors.[157,161,191] Heteroditopic receptors have applications in various fields, such as salt extraction, solubilization, membrane transport, ion sensing applications, and logic gates.[157,161,191] A search of the literature showed that many efforts have recently been devoted to the molecular recognition of lithium salts.[149,155,206-211] The growing interest in lithium salts is stimulated by their potential applications in high technology,[212] biological systems[213,214] and medicine.[215-219] Furthermore, lithium complexes of crown ethers have been reported as anionic conductors in manufacturing lithium-based rechargeable batteries and electrolytes,[220-225] and as anion activators in organic synthesis.[226-228] We present here other examples of ditopic receptors using an electrochemical reporter group coupled to the Lewis acidic organometallic moieties for sensing of ion pairs (Figure 69). Herein we show that the chloridotriorganotin-substituted [13]-crown-4 ether (Figure 69) can bind LiCl in solution and in the solid state. Its ability to sense LiCl electrochemically has also been investigated. Moreover, theoretical calculations have been performed on compounds shown in Figure 69.

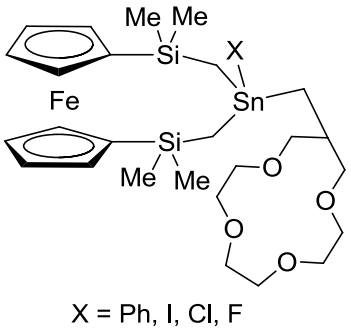

Figure 69. Tin-containing crown ether-substituted ferrocenophanes

2.3.2. Synthesis of the Crown Ether-substituted Tin-Containing Ferrocenophanes.

The reaction of diiodido(1,4,7,10-tetraoxacyclotridec-12-ylmethyl)phenylstannane[149] with $fc(Si(Me_2)CH_2MgCl)_2$[130] in THF afforded, after purification by column chromatography, the analytically pure ferrocenophane derivative **19** as a red oil (eq 19). Hereafter, fc refers to 1,1'-disubstituted ferrocene unit.

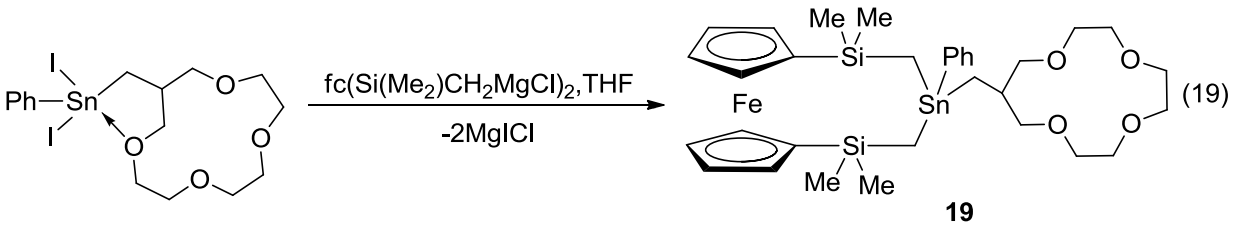

Treatment of the tetraorganostannane **19** with one mol equivalent of elemental iodine provided the triorganotin iodide **20**. The latter was reacted with an excess of silver chloride, AgCl, in acetonitrile in the dark to afford the organotin chloride derivative **21**. The corresponding organotin fluoride **22** was obtained by the reaction of compound **21** with an excess of potassium fluoride, KF, in the biphasic mixture CH_2Cl_2/H_2O for four days (Scheme 14).

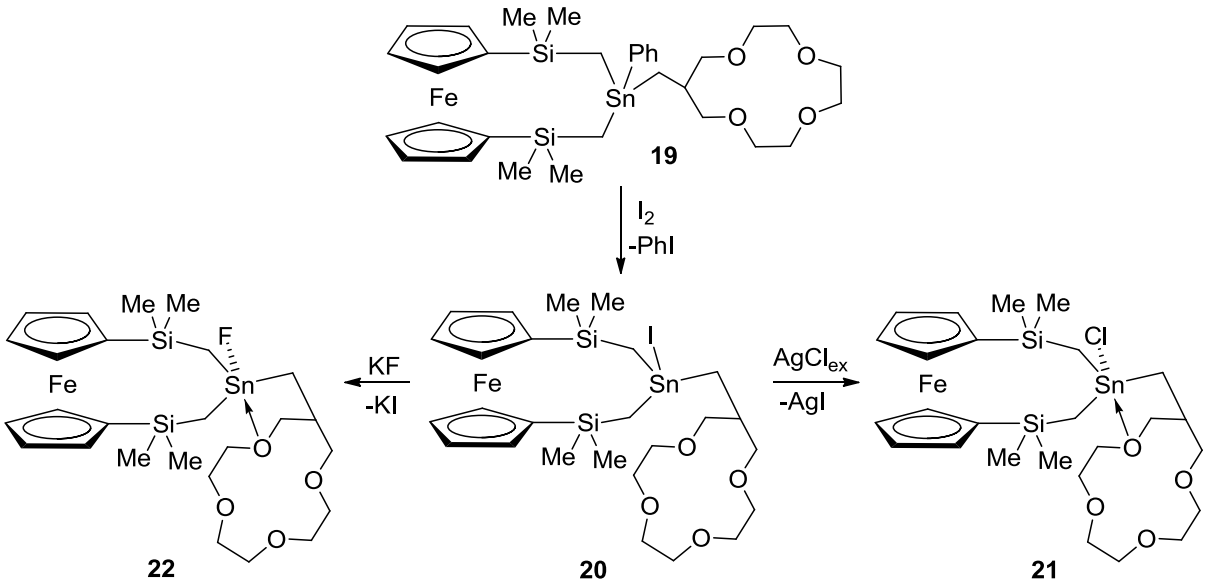

Scheme 14. Synthesis of compounds **20**–**22**.

The compounds **20** – **22** are orange crystalline materials that are soluble in organic solvents such as CH_2Cl_2, $CHCl_3$, and CH_3CN and that are stable under noninert conditions.

2.3.3. Molecular Structures of the Crown Ether-substituted Tin-Containing Ferrocenophanes.

Single crystals of **20** and **21** suitable for X-ray diffraction analysis were grown from ethanol solutions at –5°C, respectively, whereas those of **22** were obtained by slow evaporation from its toluene solution. Compound **20** crystallized in the triclinic space group $P\bar{1}$ with two molecules per unit cell, while compound **21** crystallized monoclinically in the space group $P2_1/c$ containing two crystallographic independent molecules A and B per asymmetric unit. Compound **22** crystallized in the orthorhombic space group $P2_12_12_1$ containing four molecules in the unit cell.

The molecular structures of compound **20** – **22** are shown in Figures 70 – 72. Selected bond distances and bond angles are collected in Tables 8, 9.

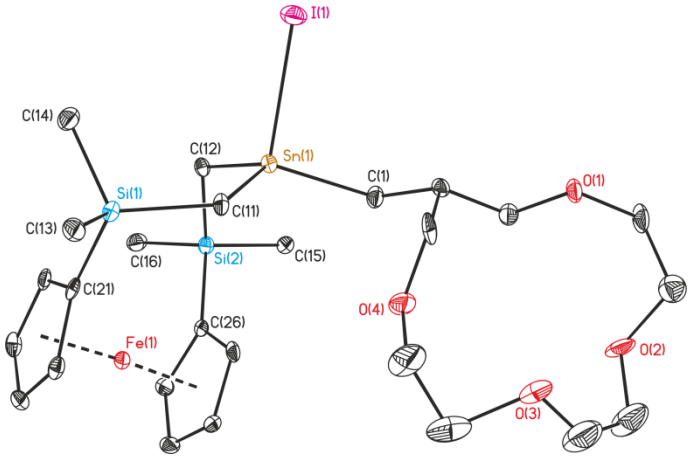

Figure 70. General view (SHELXTL) of a molecule of **20** showing 30% probability displacement ellipsoids. Hydrogen atoms are omitted for clarity.

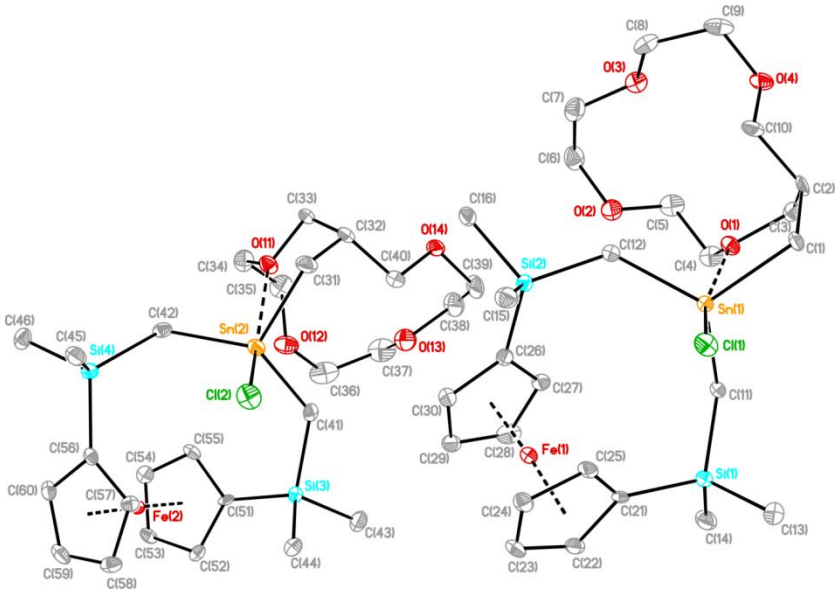

Figure 71. General view (SHELXTL) of the two crystallographic independent molecules A (right) and B (left) of **21** showing 30% probability displacement ellipsoids and the crystallographic numbering scheme.

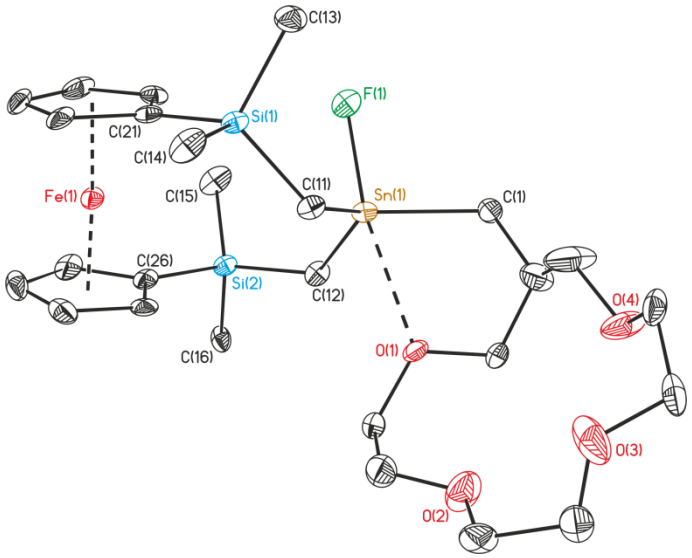

Figure 72. General view (SHELXTL) of a molecule of **22** showing 30% probability displacement ellipsoids. Hydrogen atoms are omitted for clarity.

Table 8. Selected interatomic distances (Å) for compounds **20**, **21**, and **22**.

	2	**3**	**4**
	X(1) = I	X(1) = Cl X(2) = Cl	X(1) = F
Sn(1)–C(1)	2.137(4)	2.124(3)	2.038(4)
Sn(1)–C(11)	2.123(4)	2.126(3)	2.124(4)
Sn(1)–C(12)	2.126(4)	2.155(3)	2.149(5)
Sn(1)–O(1)	3.6699(31)	2.629(2)	2.624(3)
Sn(1)–X(1)	2.7309(4)	2.4394(10)	2.031(2)
Sn(2)–C(31)		2.146(3)	
Sn(2)–C(41)		2.126(3)	
Sn(2)–C(42)		2.129(3)	
Sn(2)–X(2)		2.4383(11)	
Sn(2)–O(11)		2.739(2)	
Si(1)–C(11)	1.873(4)	1.854(3)	1.871(5)
Fe(1)–C(27)	2.029(4)	2.038(4)	2.036(5)

Table 9. Selected Bond Angles (deg) for compounds **20**, **21**, and **22**.

	2	**3**	**4**
	X(1) = I	X(1) = Cl X(2) = Cl	X(1) = F
C(1)–Sn(1)–C(11)	119.56(17)	115.65(13)	116.8(2)
C(1)–Sn(1)–C(12)	109.00(16)	117.08(12)	111.3(2)
C(11)–Sn(1)–C(12)	116.55(17)	117.02(12)	123.3(2)
C(1)–Sn(1)–X(1)	100.46(11)	93.24(10)	97.37(14)
C(11)–Sn(1)–X(1)	102.67(11)	105.97(10)	101.61(14)
C(12)–Sn(1)–X(1)	106.10(11)	102.95(10)	100.16(16)
C(1)–Sn(1)–O(1)		71.43(11)	72.87(14)
C(11)–Sn(1)–O(1)		82.61(11)	81.38(14)
C(12)–Sn(1)–O(1)		83.67(11)	85.86(16)
X(1)–Sn(1)–O(1)		164.62(5)	169.97(11)
C(41)–Sn(2)–C(42)		121.92(12)	
C(41)–Sn(2)–C(31)		114.55(13)	
C(42)–Sn(2)–C(31)		113.86(14)	
C(41)–Sn(2)–X(2)		101.60(10)	
C(42)–Sn(2)–X(2)		104.22(10)	
C(31)–Sn(2)– X(2)		94.98(11)	
C(41)–Sn(2)–O(11)		92.37(11)	
C(42)–Sn(2)–O(11)		77.94(11)	
C(31)–Sn(2)–O(11)		67.85(11)	
Cl(2)–Sn(2)–O(11)		161.43(6)	
Si(2)–C(12)–Sn(1)	118.0(2)	129.09(17)	128.5(2)
Si(1)–C(11)–Sn(1)	118.4(2)	129.00(19)	122.8(2)
C(21)–Si(1)–C(11)		113.48(16)	114.9(2)
C(11)–Si(1)–C(13)		109.65(15)	109.4(2)
C(51)–Si(3)–C(41)		108.61(15)	
C(41)–Si(3)–C(44)		114.55(16)	
Si(4)–C(42)–Sn(2)		126.63(18)	
Si(3)–C(41)–Sn(2)		128.23(17)	

The tin atom in compound **20** is four-coordinate and shows a distorted tetrahedral environment with angles varying between 119.6(2) (C(1)-Sn(1)-C(11)) and 100.5(1)° (C(1)-Sn(1)-I(1)). The distortion from the ideal geometry is mainly the result of the O(4) atom approaching the Sn(1) atom via the tetrahedral face defined by C(1), C(11), and I(1) at a distance of 3.670(3) Å. This distance is by 0.0200 Å shorter than the sum of the van der Waals radii[229] of tin (2.17 Å) and oxygen (1.52 Å). Most remarkably, the distance is significantly longer than the corresponding distances found in the tetraorganotin compounds Ph_3Sn-CH_2-[13]-crown-4 (2.976(16)) Å,[149] Ph_3Sn-CH_2-[16]-crown-5 (3.206(1) Å,[150] Ph_3Sn-CH_2-[19]-crown-6 (2.9820(13) and 2.9963(14) Å,[151] and in {$(Ph_3SnCH_2)_2$}-[26]-crown-8(3.1668(23) Å),[163] in the triorganotin iodide $Ph_2ISnCHCHC(OH)(Me)$-*t*-Bu (2.498(4), 2.550(4) Å)[230] and in the corresponding monoiodidotriorganotin-substituted crown ethers [Ph_2ISn-CH_2-[13]-crown-4, (2.466(2)Å)[149] Ph_2ISn-CH_2-[16]-crown-5, ((2.554(2)Å)[150] Ph_2ISn-CH_2-[19]-crown-6, ((2.610(2)Å)[151] and {$(PhISnCH_2)_2$}-[26]-crown-8 ((2.7985(19)Å).[163] Indeed, the tin atoms in the latter compounds are, in addition to the coordination to one iodine and three carbon atoms, intramolecularly coordinated to the oxygen atom of the crown ether ring. Compound **20** can be interpreted as a Frustrated Lewis Pair in which the Lewis base O(4) does not coordinate to the Lewis acidic Sn(1) atom. The origin for this somewhat unexpected behavior might be that the energy gained by the O→Sn coordination is not sufficient to overcome the ring strain that is associated with such coordination to a tin atom that itself is part of the ferrocenophane ring.

The tin atoms in compounds **21** and **22** are pentacoordinated and exhibit each a distorted trigonal-bipyramidal configuration (geometrical goodness $\Delta\Sigma(\theta)$[174] 47.6 and 49.5° (**21**), 52.26° (**22**) with C(1), C(11) and C(12) (**21**, molecule A; **22**) and C(31), C(41) and C(42) (**21**, molecule B) occupying the equatorial and O(1) and Cl(1) (**21**, molecule A), O(11) and Cl(2) (**21**, molecule B), and O(1) and F(1) (**22**) occupying the axial positions. The distortion is best reflected in the O(1)–Sn(1)–Cl(1) and O(11)–Sn(2)–Cl(2) (**21**) and O(1)–Sn(1)–F(1) (**22**) trans angles of 164.2 (5) (**21**, molecule A), 161.43 (6)° (**21**, molecule B) and of 169.97 (11)° (**22**), which deviate by 15.8, 18.57 and 10.03° from the ideal angle of 180°. The tin atoms are displaced by 0.3993 (3) Å (**21**, molecule A), 0.3867 (3) Å (**21**, molecule B) and 0.3632 (3) Å (**22**) from the trigonal planes defined by C(1), C(11), C(12) (molecule **A**)/ C(31), C(41), C(42) (molecule **B**) in the direction of Cl(1) (**21**, molecule **A**)/Cl(2) (**21**, molecule **B**) and F(1) (**22**).

In contrast to the triorganotin iodide **20**, the triorganotin chloride **21** and triorganotin fluoride **22** exhibit intramolecular O→Sn interactions at distances of 2.629(2) (Sn(1)–O(1), **21**, molecule A), 2.739(2) (Sn(1)–O(1), **21**, molecule B), and 2.624(3) Å (Sn(1)–O(1), **22**).These distances are longer than those found in other triorganotin halides having intramolecular O→Sn interaction such as 2,6-$(MeOCH_2)_2C_6H_3SnPh_2Cl$ (Sn–O(1) = 2.567(2) Å),[231] $Ph_2ClSnCH_2$-[16]-crown-5 (Sn–O(1) = 2.571(1) Å),[150] (*o*-$MeOC_6H_4)CH_2SnPh_2Cl$ (Sn–O(1) = 2.3991(10) Å),[232] and Ph_2FSn-CH_2-[16]-crown-5 (2.5301) (18) Å).[150] The last two distances [(2.739(2) (Sn(1)–O(1), **21**, molecule B) and 2.624(3) Å (Sn(1)–O(1), **22**) are the longest as compared with the intramolecularly coordinated chloridotriorganotin-and fluoridotriorganotin substituted crown ethers Ph_2ClSn-CH_2-[16]-crown-5 (2.571) (1) Å),[150] Ph_2ClSn-CH_2-[19]-crown-6 (2.606) (2) Å),[151] Ph_2FSn-CH_2-[16]-crown-5 (2.5301) (18) Å).[150] As expected, the Sn(1)–Cl(1) and Sn(2)–Cl(2) distances of 2.4394(10) and 2.4383 (11) Å in compound **21**, and the Sn(1)–F(1) distance of (2.031(2) Å in compound **22** are longer than the corresponding distances in tetracoordinated triorganotin chloride such as $[PhC(CH_3)_2CH_2]_3SnCl$ (Sn(1)–Cl(1) = 2.395(4) Å),[233] and triorganotinfluoride such as Mes_3SnF (Sn(1)–F(1) = 1.961(4) Å)[234], and $(PhMe_2Si)_3CSnMe_2F$ (Sn(1)–F(1) = 1.965(2) Å).[179] They exceed the sums of the covalent radii[181] of tin and chlorine by 0.049 and 0.048 Å, respectively, but are close to that of tin and fluorine (2.04 Å),[181] respectively.

The silicon atoms in compounds **20**–**22** each show a distorted tetrahedral configuration with bond angles ranging from 106.1 (2)° (C(12)–Si(2)–C(16))(**22**) to 114.9 (2)° (C(21)–Si(1)–C(11))(**22**). The Sn–C and Fe–C bond lengths in all these compounds are in the range to those found in the literature.[130,175-180]

2.3.4. Structures in solution of the Crown Ether-substituted Tin-Containing Ferrocenophanes.

The ^{119}Sn NMR spectra of compounds **19** and **20** in $CDCl_3$ at room temperature show resonances at δ –25 and 30, respectively, which are close to the ^{119}Sn chemical shifts reported for the tetracoordinated tetraorganotin compounds Me_3SnPh (δ –28.6),[235] $Me_3SnCH_2Bu^t$ (δ –14.4),[182] Et_3SnPh (δ –25.4),[236] and the trioganotin iodide Me_3SnI (δ 38.6),[237] respectively. This is evidence that the tin atoms in compounds **19** and **20** are four-coordinated, as observed in the solid state for **20**. Howewer, the tin atoms in the triorganotin chloride (**21**) and fluoride (**22**) are pentacoordinated, as it is

evidenced by the ^{119}Sn chemical shifts in $CDCl_3$ of δ 83.7(**21**) and 64 ($^1J(^{119}Sn–^{19}F)$ = 2210 Hz (**22**), respectively, being shifted to low frequency as compared with those having comparable substituent patterns at the tin atoms but lacking any chelation, such as Et_3SnCl (δ 155),[236] $(PhCMe_2CH_2)_3SnF$ (δ 139).[168] This observation suggests that the intramolecular O→Sn interaction found in the solid state for **21** and **22** is retained in solution. The ^{1}H NMR spectrum show AB-type resonances for the SiCH_2Sn protons at δ 0.28 (**19**) and δ 0.41 (**22**) and two resonances for the CH_3 protons at δ 0.12 and 0.20 (**19**) and 0.20 (and 0.34 (**22**).

The ESI-MS spectra in the positive mode of compounds **20–22** are characterized by the observation of a mass cluster centered at *m/z* 651.1 that is assigned to $\{fc[(Si(Me)_2CH_2)_2SnCH_2\text{-}[13]\text{-crown-4}]\}^+$. In addition, for **20** there are less intense mass clusters centered at *m/z* 668.1 and 691.1 that are assigned to $\{fc[(Si(Me)_2CH_2)_2SnCH_2\text{-}[13]\text{-crown-4}\cdot OH]\}^+$ and $\{fc[(Si(Me)_2CH_2)_2SnCH_2\text{-}[13]\text{-crown-4}]\cdot OH\cdot Na\}^+$, respectively. Furthermore, a mass cluster centered at *m/z* 670.1 is observed in the ESI-MS spectrum in the positive mode of compound **22** that is assigned to $\{fc[(Si(Me)_2CH_2)_2SnFCH_2\text{-}[13]\text{-crown-4}]\}^+$. No tin-containing mass cluster is observed in the ESI-MS spectrum in the negative mode of compound **20**, whereas an intense mass cluster centered at *m/z* 721.0 is observed in the ESI-MS spectrum (negative mode) of compound **21** that is assigned to $\{fc[(Si(Me)_2CH_2)_2SnClCH_2\text{-}[13]\text{-crown-4}\cdot Cl]\}^-$.

2.3.5. Complexation Studies of the Crown Ether-substituted Tin-Containing Ferrocenophanes

The ability of compounds **21** and **22** to complex salts was studied. Thus, the ^{119}Sn NMR spectrum of compound **22** in CD_3CN to which had been added one molar equivalent of tetraethylammonium fluoride, $Et_4NF\cdot 2H_2O$, showed no resonance at room temperature whereas at T = –84°C, a high field shifted triplet resonance at δ –121 ($^1J(^{119}Sn\text{-}^{19}F)$ 1737 Hz) was observed. The ^{19}F NMR spectrum at room temperature displayed a broad resonance at δ –116 ($\nu_{1/2}$ = 1612Hz). At T = –84°C, the signal sharpened (δ –113.6, $\nu_{1/2}$ = 99 Hz) and showed unresolved $^1J(^{19}F–^{117/119}Sn)$ satellites of 1748 Hz). These data indicate Sn–F exchange processes (Scheme 15) being fast at room and slow at low temperature on the corresponding NMR time scales.

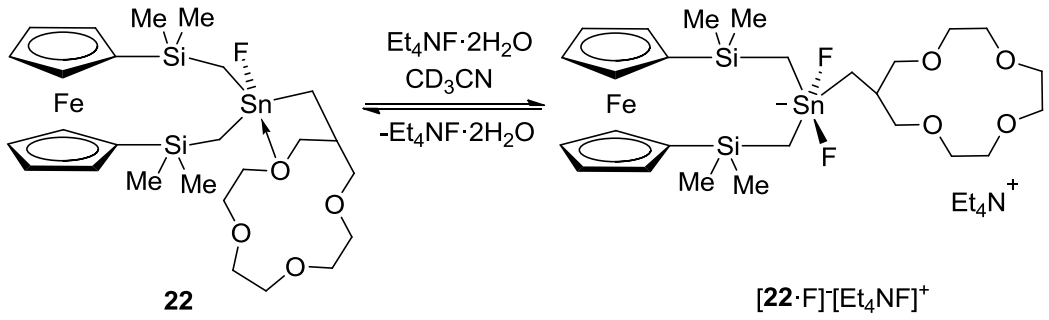

Scheme 15. Reaction of compound **22** with $Et_4NF{\cdot}2H_2O$ in CD_3CN.

Further evidence that compound **22** can complex the fluoride anion came from the ESI-MS analysis. The ESI-MS spectrum (positive mode) of compound **4** in CD_3CN to which had been added one molar equivalent of $Et_4NF{\cdot}2H_2O$ showed mass clusters centered at *m/z* 651.2 and 670.2 that are assigned to $\{fc[(Si(Me)_2CH_2)_2SnCH_2$-[13]-crown-4]$\}^+$ and $\{fc[(Si(Me)_2CH_2)_2SnFCH_2$-[13]-crown-4]$\}^+$, respectively. In the negative mode, there are mass clusters centered at *m/z* 689.1 and 729.1 that are assigned to $\{fc[(Si(Me)_2CH_2)_2SnFCH_2$-[13]-crown-4·F]$\}^-$ and $\{fc[(Si(Me)_2CH_2)_2SnFCH_2$-[13]-crown-4·F·OH·Na]$\}^-$, respectively. A less intense mass cluster was observed at *m/z* 1356.6 that corresponds to the species $\{[fc[(Si(Me)_2CH_2)_2Sn(\mu$–F)$CH_2$-[13]-crown-4]$_2{\cdot}H_2O]\}^-$.

The ^{119}Sn NMR as well as the ^{19}F NMR spectra at 22°C of a solution of **22** in CD_3CN to which had been added one molar equivalent of lithium fluoride, LiF, showed no change. This finding is fully in line with the result obtained for the reaction between the triorganotin fluoride, PhFSn-CH_2-[13]-crown-4[149] and LiF and reveal that compound **22** is not able to overcome the high lattice energy (1033 kJ/mol)[171] of LiF and to ditopically complex the latter. The ^{119}Sn and ^{19}F NMR spectra did not change after the same sample had been stored for three weeks indicating that the non-formation of a ditopic complex is not the result of kinetics.

The ^{119}Sn NMR spectrum of compound **21** in $CDCl_3$ at room temperature to which had been added excess of lithium chloride, LiCl, showed a single resonance at δ 84 indicating no formation of the corresponding chloride complex. Howewer, the ^{119}Sn NMR resonance is shifted from δ 67.0 to δ –27.8, when the reaction was carried out in CD_3CN indicating formation of the 1:1 ditopic complex [**21**·LiCl] shown in Scheme 16.

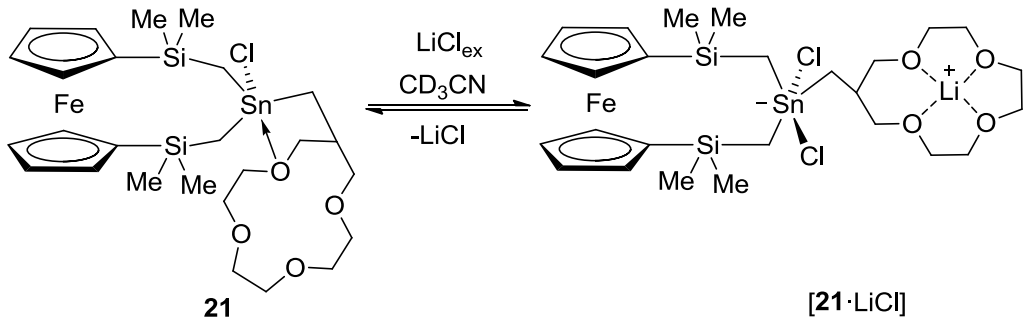

Scheme 16. Reaction of compound **21** with LiCl in CD_3CN.

Further experimental support for the formation of [**21**·LiCl] stems from the ^{1}H and ^{13}C NMR spectra and ESI-MS spectrometry. The ^{1}H NMR spectrum of [**21**·LiCl] in CD_3CN showed that the signals of the methine (HC_{12})and $SiCH_2Sn$ protons are low field shifted by 0.24 and 0.1 ppm, respectively, whereas that of the HC_{14} hydrogen atoms is moved by 0.06 ppm to high field. The ^{7}Li NMR spectrum shows a sharp singlet resonance at δ –1.1, indicating that LiCl is indeed dissolved as result of complexation by the crown ether. Appreciable changes in the ^{13}C NMR spectrum of **21** in CD_3CN were seen upon treatment with excess of LiCl. The resonances of the C11/C13, C14, $SiCH_2Sn$ carbon atoms are low field displaced by 5.46, 2.64, 5.24 ppm, respectively, while those of the C12 and C2–C9 crown ether carbon atoms moved by 0.59 and 1.57 ppm to low frequency, respectively. The ESI-MS spectum in the positive mode of compound [**21**·LiCl] showed an intense mass cluster centered at *m/z* 693.1 that is assigned to $\{fc[(Si(Me)_2CH_2)_2SnClCH_2\text{-}[13]\text{-crown-4}\cdot Li]\}^+$. A less intense mass cluster is observed at *m/z*1395.3 that is assigned to $\{[fc[(Si(Me)_2CH_2)_2Sn(\mu\text{–}Cl)CH_2\text{-}[13]\text{-crown-4}]_2\cdot Na]\}^+$. In the ESI-MS spectum (negative mode) of [**21**·LiCl], there is an intense mass cluster centered at *m/z* 721.1 that is assigned to $\{fc[(Si(Me)_2CH_2)_2SnClCH_2\text{-}[13]\text{-crown-4}\cdot Cl]\}^-$.

2.3.6. Molecular Structure of the Ditopic Complex [21.LiCl].

The formation of the ditopic complex [**21**·LiCl] was confirmed by X-ray diffraction analysis. Single crystals suitable for X-ray diffraction analysis were obtained by slow evaporation of a solution of [**21**·LiCl] at room temperature in acetonitrile. Compound [**21**·LiCl] crystallized in the monoclinic space group *P21* with two molecules per unit cell. The molecular structures of [**21**·LiCl] is shown in Figure 73. Selected bond distances and bond angles are collected in Table 10.

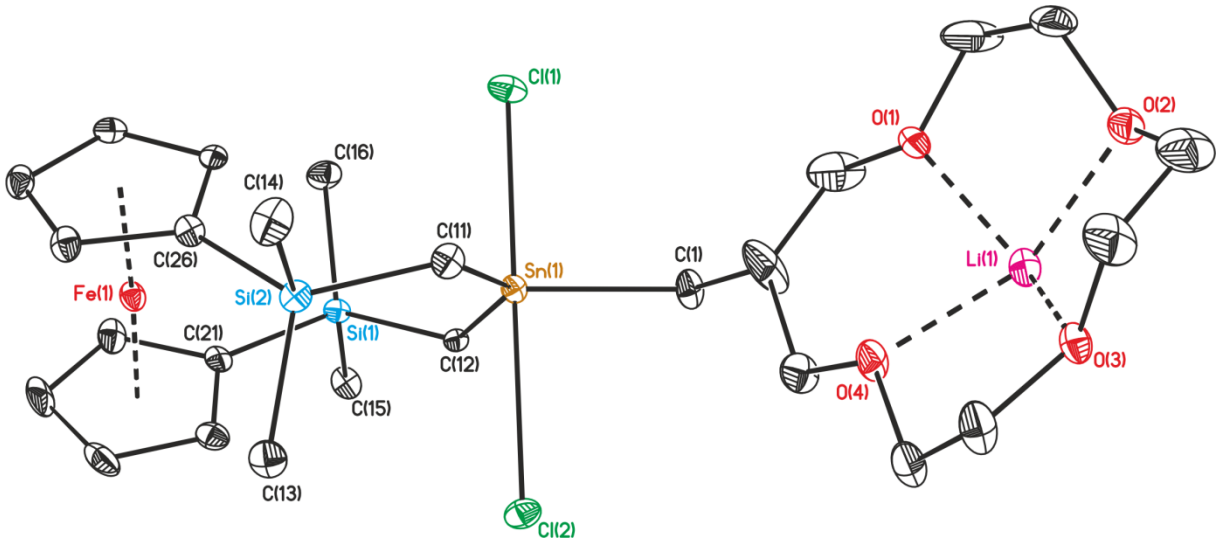

Figure 73. General view (SHELXTL) of a molecule of [**21**·LiCl] showing 30% probability displacement ellipsoids. Hydrogen atoms are omitted for clarity.

Table 10. Selected Bond Distances (Å) and Bond Angles (deg) for [**21**·LiCl][a]

Bond Distances			
Sn(1)–C(11)	2.133(4)	Li(1)–O(2)	2.021(8)
Sn(1)–C(12)	2.147(3)	Li(1)–O(3)	2.052(7)
Sn(1)–C(1)	2.149(4)	Li(1)–O(4)	2.031(7)
Sn(1)–Cl(1)	2.5287(11)	Li(1)–C(9)	2.739(8)
Sn(1)–Cl(2)	2.7706(11)	Li(1)–Cl(2b)	2.329(8)
Li(1)–O(1)	1.971(8)		
Bond Angles			
C(1)–Sn(1)–C(11)	115.14(15)	O(2)–Li(1)–O(3)	81.9(3)
C(11)–Sn(1)–C(12)	137.81(14)	O(4)–Li(1)–O(3)	80.0(3)
C(12)–Sn(1)–C(1)	106.12(15)	O(1)–Li(1)–Cl(2b)	114.5(3)
C(11)–Sn(1)–Cl(1)	92.69(11)	O(2)–Li(1)–Cl(2b)	113.8(3)
C(12)–Sn(1)–Cl(1)	95.09(11)	O(4)–Li(1)–Cl(2b)	105. 5(3)
C(1)–Sn(1)–Cl(1)	90.98(12)	O(3)–Li(1)–Cl(2b)	112.5(4)
C(11)–Sn(1)–Cl(2)	85.26(11)	O(1)–Li(1)–C(9)	112.8(3)
C(12)–Sn(1)–Cl(2)	87.15(11)	O(2)–Li(1)–C(9)	135.3(3)
C(1)–Sn(1)–Cl(2)	88.95(12)	O(4)–Li(1)–C(9)	29.28(16)

Cl(1)–Sn(1)–Cl(2)	177.69(3)	O(3)–Li(1)–C(9)	56.22(19)
Li(1a)–Cl(2)–Sn(1)	114.42(18)	Cl(2A)–Li(1)–C(9)	97.8(3)
O(1)–Li(1)–O(2)	82.9(3)	O(1)–Li(1)–C(4)	28.03(16)
O(1)–Li(1)–O(4)	84.1(3)	O(2)–Li(1)–C(4)	56.3(2)
O(2)–Li(1)–O(4)	140.5(4)	O(4)–Li(1)–C(4)	110.4(4)
O(1)–Li(1)–O(3)	132.8(4)	O(3)–Li(1)–C(4)	126.5(3)

[a]Symmetry codes: (a) –x, –0.5 + y, 1 – z; (b) –x, 0.5 + y, 1 – z

The molecular structure of [**21**·LiCl] shows that the LiCl salt is complexed as a host-separated ion pair with the lithium cation being bound inside the cavity of the crown ether and the chloride anion being bound to the tin atom. There is an intermolecular Cl(2)···Li(1A) interaction at a distance of 2.329(8) Å that is shorter than the sum of the van der Waals Radii[229] of Li (1.81 Å) and Cl (1.75 Å) even shorter than the Li···Cl distance in crystalline lithium chloride (2.565 Å),[238] which gives rise to formation of a one-dimensional polymeric chain structure (Figure 74). Such a binding mode was also reported by Reetz and coworkers for the complexation of potassium fluoride, KF, by a crown ether moiety coupled to a Lewis-acidic boron center.[143] Remarkably, and in contrast to the common crystal structures of lithium salts complexed by macrocyles,[149,238-240] there is no incorporation of water within the coordination sphere of Li^+. The lithium cation is five-coordinated and adopts a distorted square planar pyramidal environment, with the four crown ether oxygen atoms forming the base of the pyramid and the chloride anion of the neighbour molecule occupying the apical position. The lithium cation lies by 0.756(8) Å above the pyramid plane in the direction of Cl(2B). The average $Li–O_{crown}$ distance of 2.019 Å is close to the average standard Li–O (2.032 Å)[238] distance found for the Li^+ ionophores having a coordination number 5 and a square pyramidal coordination geometry.[149,241-244]

The tin atom is pentacoordinated and exhibits a distorted trigonal-bipyramidal configuration (geometrical goodness $\Delta\Sigma(\theta)$ 80.31°) with the C(1), C(11), and C(12) carbon atoms occupying the equatorial and Cl(1) and Cl(2) occupying the axial positions. The Sn(1) atom is displaced by 0.1156(2) Å from the trigonal plane in the direction of Cl(1). As result of the intermolecular Li(1A)···Cl(2) interaction, the Sn(1)–Cl(2) distance of 2.7706(11) Å is longer than the Sn(1)–Cl(1) distance of 2.5287(11)

Å. They are longer than those found in the parent compound **21** and the corresponding distances in the dichloridodiorganotin-substituted crown ether $PhCl_2Sn$-CH_2-[13]-crown-4 (2.4190)(5) Å).[149] Both distances exceed the sum of the covalent radii[181] of Sn (1.40 Å) and Cl (0.99 Å).

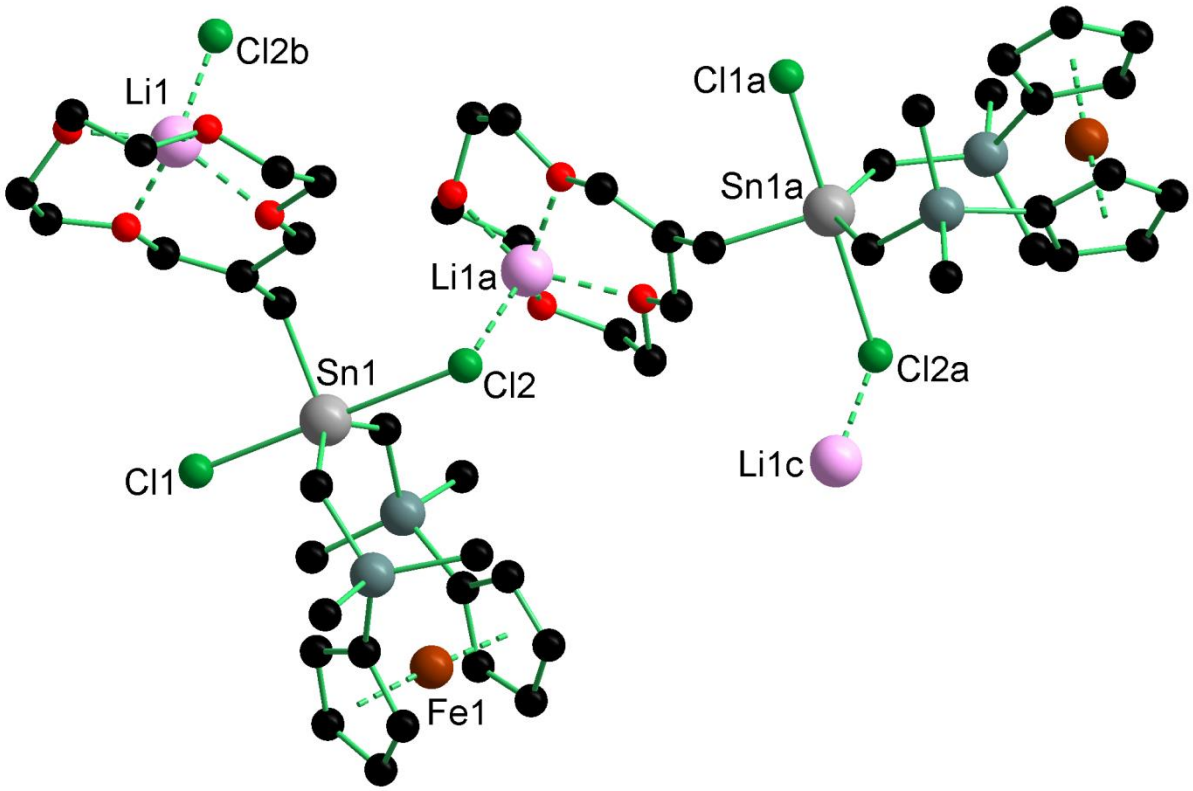

Figure 74. Ball- and- stick model of a one dimensional polymeric chain structure of [**21**·LiCl]. Hydrogen atoms are omitted for clarity. Symmetry code: (a) –x, -0.5 + y, 1–z; (b) –x, 0.5 + y, 1–z; (c) x, -1 + y, z.

2.3.7. Cyclic Voltammetry of the Crown Ether-substituted Tin-Containing Ferrocenophanes.

Electrochemical studies were done by Prof.Dr. V. Jouikov of the University of Rennes in France. Upon oxidation in CH_3CN/0.1 M Bu_4NPF_6 at a glassy carbon (GC) microdisk electrode, the compounds **21**, **22**, and [**21**·LiCl] show well-shaped reversible one-electron peaks (E_1) of the formation of corresponding ferricenium cations. Similar results were observed when using Bu_4NClO_4 as supporting salt: the E^o values remained practically unchanged, within ± 5 mV. The values of E^o of all three compounds are more positive than E^o of non-substituted ferrocene and are

close to those reported for other silyl-substituted ferrocenophanes,[130] 1,1'-bis[dimethyl(vinyl)silyl]ferrocenes[245,246] and 1,1'-Bis-silylferrocenylenes,[247] in accordance with electron-acceptor effects of tetracoordinate silyl substituents. A similar trend was earlier reported for $E_{1/2}$ of 1,1'-bissilyl ferrocenes substituted with $Si(OMe)_3$ or SiH_3.[248] The first oxidation step is followed by a second oxidation (E_2) at $E_p \cong 1.75$ V arising from the oxidation of crown ether moiety; the feature is common to all three compounds. In the cathodic scan, no reductions are observed up to ≅ –2.7 V, at lower negative potentials reductive cleavage of Sn–Cl bond occurs (E_3) which led to the appearance and growth of the oxidation peak of free Cl^- anion (E_4) on the anodic branch in the second and following scans. The peak at E_4 is not present in the original non-reduced system incurring that the hypercoordinate organotin chloride complex [**21**·LiCl] exists in solution in a non-dissociated form (Figure 75).

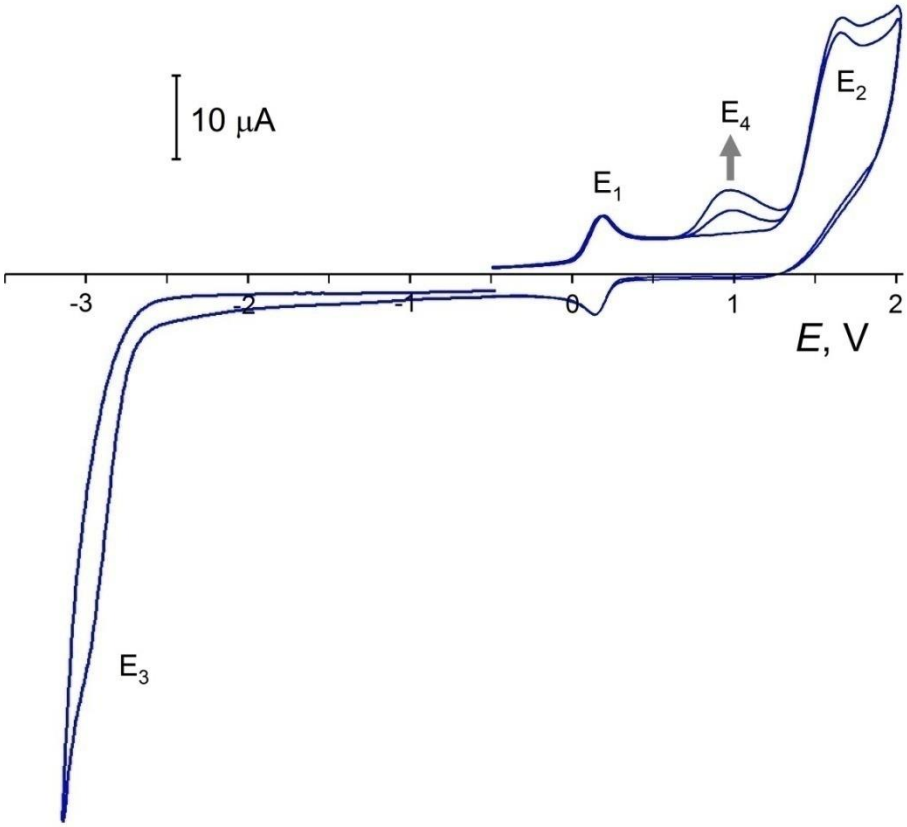

Figure 75. Voltammetry of the complex [**21**·LiCl] in CH_3CN/0.1 M Bu_4NPF_6 at a GC electrode. Scan starts from E = –0.5 to +1.9 V and then to –3.3 V. *v* = 0.5 V/s.

The E^o of [**21**·LiCl] is shifted by overall 58 mV to more positive potentials compared to E^o or ferrocene, primarily due to the electron-withdrawing effects of two substituents at cyclopentadienyl rings. In this difference two opposite shifts are also absorbed: to

less anodic potentials due to the coordination with Cl^- and to more positive potentials due to the complexation of Li^+.

The addition of two equivalents of LiCl to the solution of **21** (the same effect was observed upon stepwise addition: first of $LiClO_4$ and then of $HexMe_2(C_{16}H_{33})NCl$) caused a –66 mV cathodic shift of E^o(**21**) which now became exactly that of the ditopic complex [**21**·LiCl]; E^o(**21** + LiCl) = 0.155 V (Table 11).

Table 11. Standard oxidation potentials E^o (V *vs.* polypyrrole reference electrode) of the ferrocene derivatives alone and in the presence of the corresponding ions. AN/0.1 M Bu_4NPF_6 at a GC electrode (v = 500 mV/s, T = 20 °C); in parentheses, peak-to-peak separation, E_p^a-E_p^c, mV.

	Alone	Li^+ [a]	Cl^- [b]	F^- [c]
19	0.221 (62)	0.155 (59) [d]		0.165 (62)
20	0.154 (65)			0.164 (64)
21	0.121 (63)	0.155 (62)		0.191 (63)
Fc	0.096 (65)			

[a] As $LiClO_4$. [b] As $HexMe_2(C_{16}H_{33})NCl$. [c] As Bu_4NF. [d] Added as LiCl.

Ensuing addition of F^- anion (as Bu_4NF, 5 equivalents) to this solution caused two phenomena: (i) temporary appearance of a small signal of new ferrocene-related redox system (pre-peak) at remarkably negative potentials (E^o = –0.172 V, Figure 76) and (ii) the shift of E^o of complex [**21**·LiCl] by 30 mV to more positive potentials reaching E^o([**21**·LiCl]) = 0.185 V. Within several minutes, the system at –0.172 V progressively disappeared and the standard potential of the main redox couple shifted back becoming constant at E^o([**21**·LiCl]) = 0.165 V. These features probably reflect an additional coordination of F^- to the tin atom, the pre-peak being that of oxidation of the species with hexa-coordinate tin.

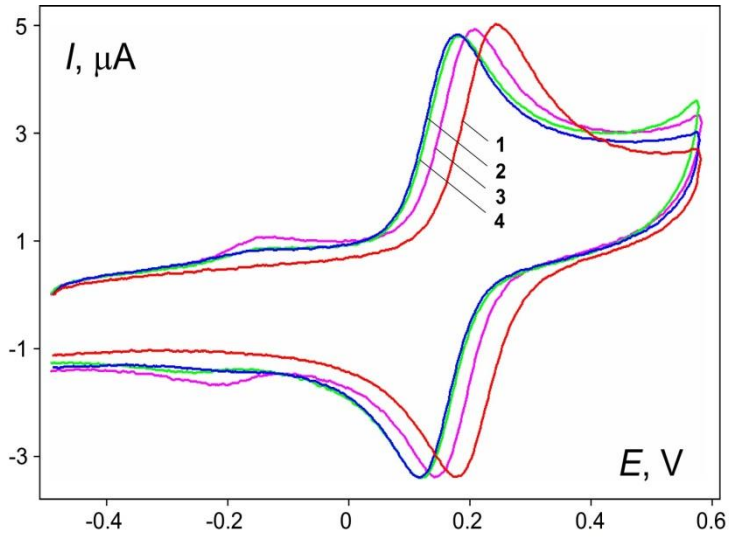

Figure 76. Voltammograms of oxidation of: (1)-compound **21** in CH_3CN/0.1 M Bu_4NPF_6 at a GC electrode. (2)-same solution, after the addition of LiCl. (3)-immediately after the addition of Bu_4NF. (4)-same as in (3) but after staying for 5 min. *v* = 0.5 V/s.

The fluorido-substituted derivative **22** has a lower oxidation potential compared to the chlorido-substituted derivative **21** (Table 11), which implies that the electronegativity of the halogen atom is not the major factor determining the electronic effects exerted by the substituent on the Fc moiety. The inverse order of E^o for **21** and **22** might arise from an additional back-bonding from the halogen lone pair to vacant orbitals of Sn, similarly to what was observed earlier for Sn–X electronic interactions in tricarbastannatranes.[ref 83b] The addition of lithium perchlorate, $LiClO_4$, to the solution of **22** caused the expected further increase in E^o which now became E^o = 0.155 V (Figure 77). The effect of Li^+ on E°(**22**) is stronger (ΔE° = +34 mV) than that on E°(**21**) and is additive whatever the order of its addition is (before or after Cl^- or F^- and whatever the order of addition of the anions). In contrast, the order of addition of anions and also whether Li^+ is present or not both affect the ΔE°(**22**) caused by Cl^- and F^-, so that no simple trend could be established. For instance, the addition of fluoride anion (as Bu_4NF) to the solution of (22 + Li^+) led to another increase of the oxidation potential, E^o = 0.191 V, whereas the addition of Cl^- caused a shift of –68 mV. This is quite unexpected because the coordination with anions is supposed to provide supplementary electron density to Sn and hence to decrease E^o. It is also to be noted that in the presence of F^-, a new oxidation peak with E_p = 0.6 V appeared (Figure 77).

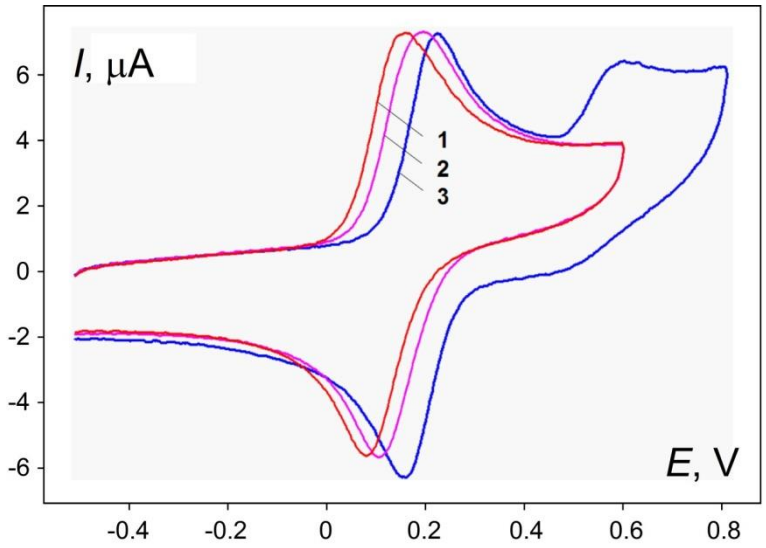

Figure 77. Voltammograms of oxidation of: (1)-compound **21** in CH_3CN/0.1 M Bu_4NPF_6 at a GC electrode. (2)-same solution, after the addition of $LiClO_4$. (3)-after the addition of Bu_4NF. *v* = 0.5 V/s.

Thus, the E^o of oxidation of these compounds is sensitive to the environment at the tin atom and to the coordination at both the Sn atom and the crown ether moiety so as ditopic complexation can be clearly characterized by means of voltammetry. However, additional experiments are needed to rationalize the situation with fluorido-substituted ferrocenophane **22**.

2.3.8. DFT calculations of the Crown Ether-substituted Tin-Containing Ferrocenophanes.

DFT Calculations were done by Prof. Dr. Viatcheslav Jouikov of the University of Rennes in France. The usual optimization approach (low level followed by high level calculations) proved unsuitable for **20-22**. In fact, although the 3-21G basis set includes the functions for Sn, enabling primary optimization of these compounds, it did not allow localizing O→Sn coordinated structures as minima: even starting from forcefully coordinated geometries, non-coordinated structures were obtained at HF/3-21G or DFT/3-21G levels. Only the optimization with a combined basis set treating at ECP LANL2DZ level all elements but Fe and Sn (for which split valence double zeta DGDZVP[249] or Ahlrichs' Def2-TZVP triple zeta valence balanced basis sets[250,251] are required) provided the experiment-consistent structures. The NBO[252] and CHelpG[253] population analyses have been then performed at the same level of theory on the optimized non-zero-frequency structures.

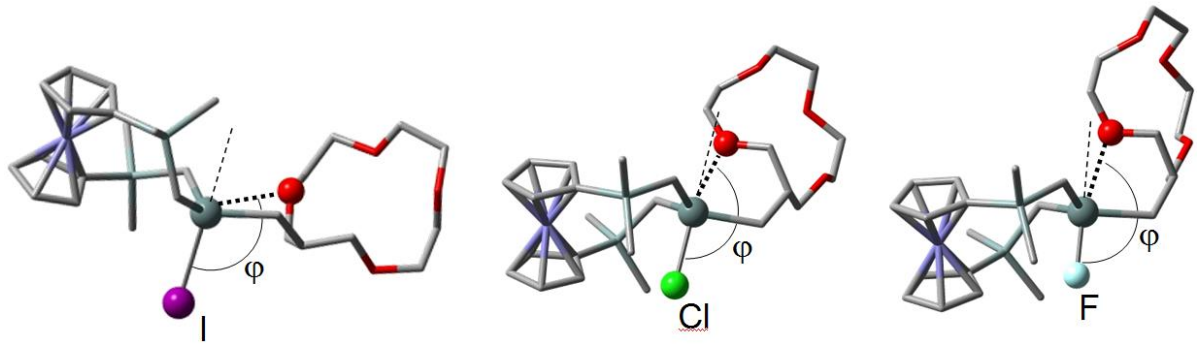

Figure 78. Optimized structures of ferrocenophanes **20**–**22** from DFT B3LYP/(LANL2DZ + Def2-TZVP).

The DFT trend in the O→Sn coordination is in line with the X-ray diffraction data: **21** and **22** are O→Sn coordinated whereas **20** is not (Figure 78). The *trans* O–Sn–X angles in **21** (161°) and **22** (166.52°) are smaller but still closer to ideal 180° than in **20**, for which it is closer to the right angle (105.73°). The sum of three C–Sn–C angles in **21** and **22** is also closer to 360° than in **20** (Table 12).

Atomic charges derived from different ways of partitioning electron density (Table 12) all converge in that the tin atom in **20** has the smallest positive charge in this reaction series and therefore have the weakest Lewis acidity for coordinating with O. For all compounds, the $q_{(Sn)}q_{(O)}$ energy components are attractive and increasing when going from **20** to **22**. Corresponding distance-dependent Coulomb energies q_+q_-/r and dipole moments also follow a similar trend.

Table 12. Distances (Å), angles (°), isotropic dipole moments (Debye) and charges for three ferrocenophanes from DFT B3LYP/(LANL2DZ + Def2-TZVP) calculations

	Sn-X	Sn-O	∠O-Sn-X	∑∠C-Sn-C	μ, D [a]	Charges (Sn, O)		
						*q*Mull	*q*NPA	*q*CHelpG
20	2.868	3.692	105.73	336.45	5.50	0.611	1.910	0.710
						-0.429	-0.633	-0.283
21	2.440	2.721	161.00	350.91	5.58	0.724	2.113	0.849
						-0.434	-0.645	-0.231
22	2.031	2.715	166.52	352.08	5.95	0.948	2.266	0.947
						-0.442	-0.677	-0.199

[a] μ from CHelpG (B3LYP/DGDZVP) charges fit to the electrostatic potential at the element's van der Waals radius according to Breneman scheme.[253]

From second order perturbation theory analysis, no direct dative interactions (above the threshold of 0.5 kcal/mol) are seen between Sn and O in compound **20**. The energy of σ(Sn–C)-σ*(O–C) orbital interactions and of p_z(O) with a vacant hybrid orbital of Sn is 1.34 kcal/mol only, too low to enable any efficient coordination. In **21**, there is an important two-electron stabilization due to electron delocalization from p_z(O) to the empty hybrid orbital of Sn amounting to 28.91 kcal/mol (27.28 kcal/mol in **22**) with additional 13.56 kcal/mol (12.12 kcal/mol in **22**) from the interactions of s and p lone pairs of O with three σ*(Sn-C) orbitals.

Thus both charge and orbital terms of the energy gain from O→Sn coordination are lowest for **20** compared to **21** and **22**. This attractive energy is opposed to steric strain of the ferrocenophane ring and steric repulsion of disilylferrocene and crown ether moieties. In **21** and **22,** this ratio is favorable for realizing stable O→Sn coordinated structures while steric forces prevail for **20**. A Fine interplay of these factors is also seen through DFT calculations. The simplified optimization procedures (freezing Fc fragment or setting it as ONIOM lower layer) do not converge to Sn–O coordinated structures, even for **21** and **22**, unless the Fe atom is treated at the same level as Sn (DGDZVP or Def2-TZVP). Although the difference is only about the energy of modification of the angle between two Cp rings and of their rotation about their axes relative to Fe atom, the flip of Fc moiety about two Sn–C bonds has an activation energy that delimitates coordinated and non-coordinated structures. In the solid state, both dihedral angles Si(1)–C(11)–Sn–X and Si(2)–C(12)–Sn–X in **21** and **22** are superior to 90° and are less than 90° in **20**. In DFT optimized structures of **21** and **22** (Figure 9) this angle is also > 90°, but only a half-flip is observed for **20** (Si(1)–C(11)–Sn-X < 90° and Si(2)–C(12)–Sn–X > 90°).

2.3.9. Conclusions

A series of novel silicon- and tin-containing ferrocenophanes was synthesized and completely characterized, and their ability in the ditopic complexation of lithium salts was investigated by NMR spectroscopy, cyclic voltammetry, and crystallography. In the solid state as well as in solution, the chlorido- and fluoridosubstituted derivatives **21** and **22**, respectively, show intramolecular O→Sn coordination, whereas the

iodido-substituted derivative **20** does not. This somewhat unexpected observation is confirmed by DFT calculations. It is the result of steric hindrance that in the case of 2 dominates the energy gain (smaller than in **21** and **22**) from the intramolecular O→Sn coordination. The chlorido-substituted ferrocenophane **21** is able to selectively complex lithium chloride in a ditopic fashion to give [**21**·LiCl]. However, in the solid state the charge separation induced by this complexation is compensated for by the formation of a coordination polymer via intermolecular Cl···Li interactions. Consequently, in order to achieve true charge separation the lithium cation should be encapsulated in a cryptand or a crown-4 derivative that is more protected by appropriate substituents. An interesting formal analogy can be drawn between [**21**·LiCl] and the zwitterionic 2-(N,N-dimethylammoniomethyl)phenyl-containing triorganodichloridostannate 2-$Me_2HNCH_2C_6H_4SnCl_2Ph_2$ and related derivatives.[254-256] In the latter compound, a proton is coordinated by the amine nitrogen atom (Lewis base) and a chloride anion is coordinated to a tin atom (Lewis acid). However, complete charge separation is not achieved, as the chloride anion intramolecularly interacts with the triorganoammonium moiety (N−H···Cl).

It is worth noting that an appropriate basis set with a fine combination of diffuse and polarization functions is needed for adequate rendering of the configurations and electronic effects in such ferrocenophane complexes.

2.4. Syntheses, Structures and Complexation Behaviour of Dibromido (1, 4, 7, 10, 13-pentaoxacyclohexadec-15-yl-methyl)phenylstannane.

2.4.1. Synthesis of Dibromido (1, 4, 7, 10, 13-pentaoxacyclohexadec-15-yl-methyl)phenylstannane (23).

In recent years, *Jurkschat* and coworkers reported the dihalogenidodiorganotin-substituted crown-4 and crown-6 compounds[149,163] shown in Figure 79 and demonstrated their affinity toward halogen salts. In a continuation of this work, we have prepared and structurally characterized the dibromidodiorganotin-substituted crown ether **23** (eq. 20). Its ability to bind halogen salts has been investigated.

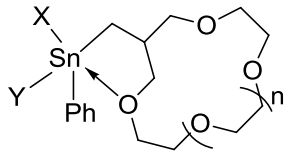

n = 1, 3; X = Y = I, Cl, Br

Figure 79. Dihalogenidodiorganotin-substituted crown-4 and crown-6 reported by *Jurkschat* and coworkers.

Compound **23** was obtained by reaction of (1,4,7,10,13-pentaoxacyclohexadec-15-yl-methyl)triphenylstannane[105] with two molar equivalents of bromine in dichloromethane at –55°C (eq. 20).

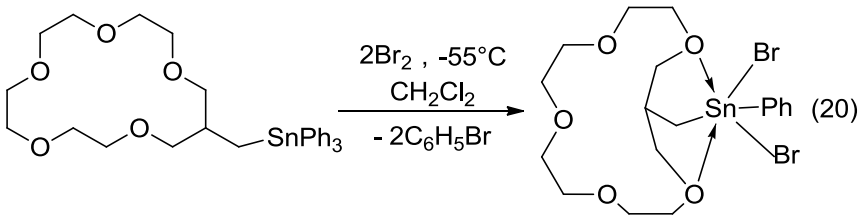

(20)

23

Compound **23** is a colorless air stable crystalline solid, which is insoluble in common organic solvents except dichloromethane.

2.4.2. Molecular Structure of the Dibromidodiorganostannane 23.

Suitable crystals for X-ray diffraction analysis were obtained by slow evaporation of a solution of compound in dichlomethane at room temperature. Compound **23** crystallized monoclinically in the space group $P2_1/c$ with four molecules per unit cell. The molecular structure of **23** is shown in Figure 80, and selected bond distances and bond angles are listed in Table 13.

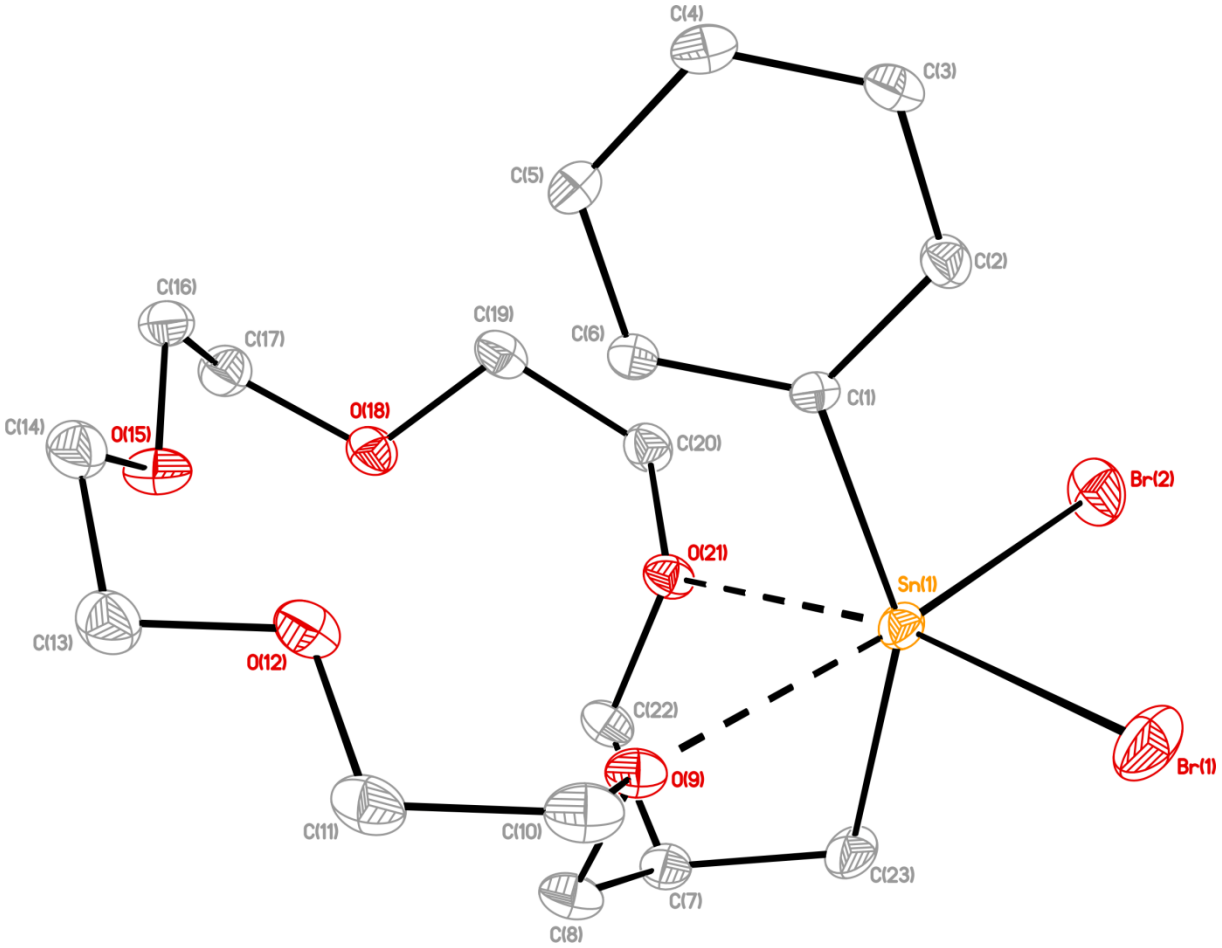

Figure 80. Molecular structure of **23**.

Table 13. Selected Bond Distances (Å) and Bond Angles (deg) for **23**.

Bond lengths			
Sn(1)–C(1)	2.126(3)	Sn(1)–O(21)	2.474(2)
Sn(1)–C(23)	2.135(3)	Sn(1)–Br(1)	2.5749(5)
Sn(1)–O(9)	2.513(3)	Sn(2)–Br(2)	2.5767(5)
Bond angles			
C(1)–Sn(1)–O(21)	72.74(12)	O(9)–Sn(1)–Br(1)	95.95(6)
C(1)–Sn(1)–C(23)	151.41(14)	O(9)–Sn(1)–Br(2)	164.87(6)
C(1)–Sn(1)–Br(1)	98.81(9)	O(21)–Sn(1)–Br(1)	168.91(6)
C(1)–Sn(1)–Br(2)	98.47(9)	O(21)–Sn(1)–Br(2)	91.30(6)
C(1)–Sn(1)–O(9)	84.89(10)	C(2)–C(1)–Sn(1)	118.4(2)
C(1)–Sn(1)–O(21)	85.55(10)	C(6)–C(1)–Sn(1)	122.3(2)

C(23)–Sn(1)–Br(1)	99.61(11)	C(7)–C(23)–Sn(1)	107.6(2)
C(23)–Sn(1)–Br(2)	100.35(12)	C(8)–O(9)–Sn(1)	111.0(2)
C(23)–Sn(1)–O(9)	71.63(13)	C(10)–O(9)–Sn(1)	128. 7(2)
C(23)–Sn(1)–O(21)	72.74(12)	C(20)–O(21)–Sn(1)	111.0(2)
Br(1)–Sn(1)–Br(2)	98.086(19)	C(22)–O(21)–Sn(1)	111.0(2)

The molecular structure of compound **23** is similar to those observed for the corresponding dihalogenidodiorganotin-substituted crown ethers PhX_2Sn-CH_2-[16]-crown-5 (X = I, Cl)[150] and PhX_2Sn-CH_2-[19]-crown-6 (X = I, Br).[163] Thus, as expected, the tin atom in compound **23** adopts a distorted octahedral *trans-cis-cis* configuration. The deviation of the O(9)–Sn(1)–O(21) and Br(1)–Sn(1)–Br(2) *cis*-angles from 90° to 74.19(8)° and 98.086(19)°, respectively, and of the C(1)–Sn(1)–C(23) *trans*- angle from 180° to 151.41(14)° are the main causes of the distortion. The intramolecular Sn(1)–O(21) and Sn(1)–O(9) distances of 2.474(2) and 2.513(3) Å fall in the range of those found in PhX_2Sn-CH_2-[16]-crown-5 (X = Cl, 2.522(1) and 2.4793(9) Å, X = I, 2.482(2) Å), PhX_2Sn-CH_2-[19]-crown-6 (X = I, 2.525(3) and 2.554(3) Å, X = Br, 2.516(3) and 2.506(3)) Å), $H_3COOCC_2H_4)_2SnBr_2$ (2.529(3) and 2.533(3) Å)[257] and in $(MeO_2CCH_2CH_2)_2SnI_2$ (2.522(8) and 2.528(7) Å).[258] The Sn(1)–Br(1) and Sn(1)–Br(2) bond distances of 2.575 (5) and 2.578 (5) Å are close to the corresponding distances found for $PhBr_2Sn$-CH_2-[19]-crown-6 (2.5701(6) and 2.5793(7) Å) and longer than that reported in the tetrahedrally configurated diorganotin dibromide Et_2SnBr_2 (2.505(4) Å)[259]

2.4.3. Structure of the Diorganotindibromide 23 in Solution.

A ^{119}Sn NMR spectrum of **23** in CD_2Cl_2 displayed a single resonance at δ –162, which is close to δ –147 found for $PhBr_2Sn$-CH_2-[19]-crown-6.[163] It is low-frequency shifted in comparison to 1,2-bis(diphenylbromostannyl)ethane $(Ph_2BrSnCH_2)_2$ (δ –5)[167] and to 1,2-bis(dibromophenylstannyl)methane, $(PhBr_2Sn)_2CH_2$ (δ –33),[165] in which no intramolecular or intermolecular coordination takes place. This is an evidence of the intramolecular O→Sn coordination found in the solid state is preserved in solution. A ^{13}C NMR spectrum of **23** in CD_2Cl_2 at room temperature showed for the crown ether carbon atoms six instead of eleven resonances that would be expected from the molecular structure in the solid state (Figure 81). This

result is fully in line with what was seen with other related organotin-substituted crown ether compounds,[148-151,170,260] and indicate, on the ^{13}C NMR time scale, a symmetric structure in solution in contrast to the unsymmetrical structure observed in the solid state.

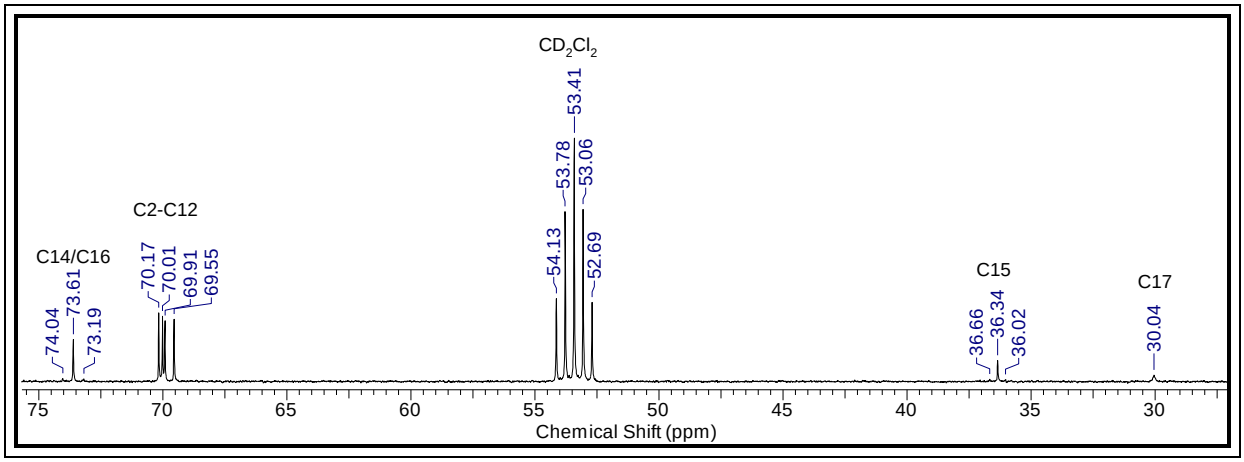

Figure 81. ^{13}C NMR spectrum showing the crown ethers carbon atoms of **23**.

2.4.4. Complexation Behavior of the Dibromidodiorganotin 23 toward Bromide Salts.

The ^{119}Sn NMR spectrum at room temperature of a solution of the dibromidodiorganotin **23** in CD_2Cl_2 to which had been added one molar equivalent of tetraphenylphosphonium bromide, Ph_4PBr, displayed a resonance at δ –235 ($\nu_{1/2}$ = 144 Hz) that is high field shifted ($\Delta\delta$ 73) in comparison to the chemical shift of pure **23** (δ –162). This finding is in agreement with the behaviour found for $PhBr_2Sn$-CH_2-[19]-crown-6 ($\Delta\delta$ 40)[163] and can be interpreted in terms of the equilibrium shown in scheme 17. The equilibrium is fast on the ^{119}Sn NMR time scale at room temperature and shifted toward **23**.

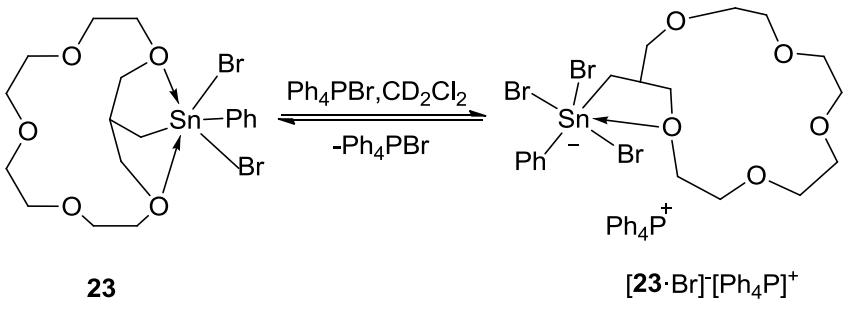

Scheme 17. Reaction of **23** with Ph_4PBr in CD_2Cl_2.

The ability of the receptor **23** to ditopically complex NaBr and LiBr, respectively, has been also studied. Thus, the ^{119}Sn NMR spectra at room temperature of a solution of the dibromidodiorganotin **23** in CD_2Cl_2 to which had been added an excess of sodium and lithium bromide, respectively, showed no significant shift of the resonances, δ –163 (238 Hz) and –169 (575 Hz), respectively. These observations are consistent with the non-formation of the corresponding ditopic complex [**23**·NaBr] and [**23**·LiBr], respevtively. The non appreciable change in the ^{119}Sn NMR spectra of **23** + NaBr, and **23** + LiBr show that the complexation ability of **23** is not strong enough to overcome the lattice energy of sodium bromide (741 kJ/mol)[171] and lithium bromide (803 kJ/mol)[171] and to give the corresponding ditopic complexes [**23**·NaBr] and [**23**·LiBr], respectively. The increase of the Lewis acidity at the tin atom in **23** seems to be an efficient method in order to ditopically complex NaBr and LiBr, respectivelly; that is, the tribromidomonorganotin Br_3Sn-CH_2-[16]-crown-5[154] has shown the ability to ditopically complex the latter salts.[154]

2.5. Molecular Structure of 12-({dichloro[(dichlorophenylstannyl)methyl)-1,4,7,10-tetraoxacyclononadecane.

Compound **24** ($PhI_2SnCH_2SnI_2CH_2$-[13]-crown-4)[163] (eq 21.) has been previously synthesized and structurally characterized by NMR spectroscopy and elemental analysis. Its complexation properties toward lithium chloride was also reported.

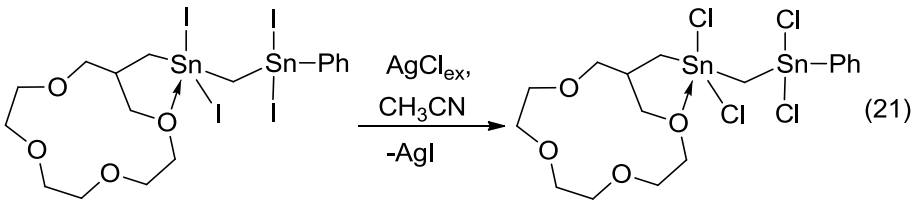

(21)

24

However, full characterization of **24** by single crystal X-ray diffraction analysis was unsuccessful. At our hand**,** single crystals suitable for X-ray diffraction analysis were grown by slow evaporation of compound **24** in dichloromethane/*n*-hexane. The compound crystallized monoclinically in the space group P2(1)/n with four molecules per unit cell. The molecular structure of **24** is shown in Figure 82, and selected bond distances and bond angles are listed in Table14.

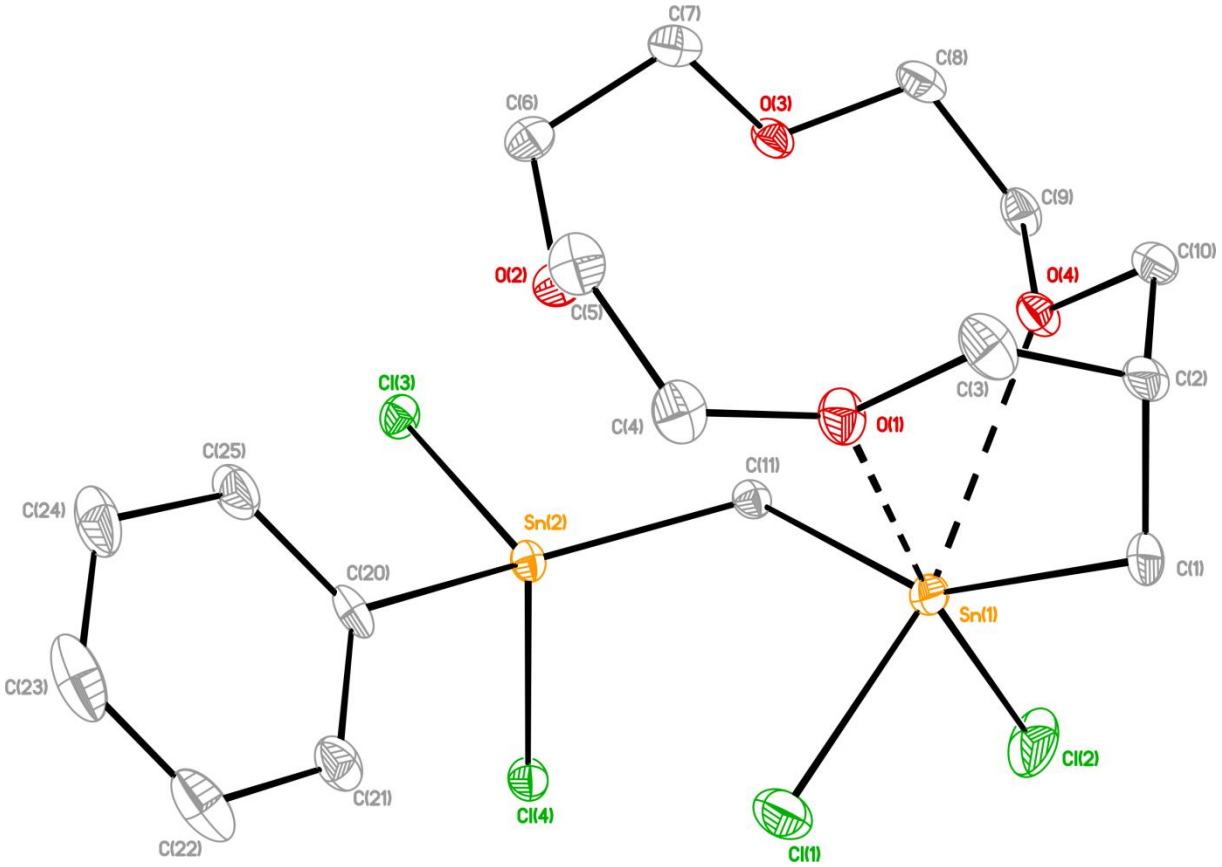

Figure 82. General view (SHELXTL) of a molecule of **24** showing 30% probability displacement ellipsoids and the crystallographic numbering scheme.

Table 14. Selected bond lengths/Å and bond angles/° for **24**.

Bond lengths			
Sn(1)–C(1)	2.112(4)	Sn(2)–C(11)	2.088(3)
Sn(1)–C(11)	2.093(3)	Sn(2)–C(20)	2.112(4)
Sn(1)–Cl(1)	2.4072(13)	Sn(2)–Cl(3)	2.3607(10)
Sn(1)–Cl(2)	2.4119(12)	Sn(2)–Cl(4)	2.3759(10)
Sn(1)–O(1)	2.446(3)	Sn(2)–O(2)	2.773(3)
Sn(1)–O(4)	2.633(3)		
Bond angles			
C(1)–Sn(1)–Cl(1)	104.77(14)	Cl(2)–Sn(1)–O(4	105.05(7)
C(1)–Sn(1)–Cl(2)	99.81(12)	C(11)–Sn(2)–C(20)	142.21(15)
C(1)–Sn(1)–O(1)	73.77(13)	C(11)–Sn(2)–Cl(3)	105.11(11)

C(1)–Sn(1)–O(4)	70.38(14)	C(11)–Sn(2)–Cl(4)	99.32(10)
C(1)–Sn(1)–C(11)	148.27(15)	C(11)–Sn(2)–O(2)	76.04(11)
C(11)–Sn(1)–O(1)	87.57(12)	C(20)–Sn(2)–Cl(3)	102.33(11)
C(11)–Sn(1)–Cl(1)	99.31(11)	C(20)–Sn(2)–Cl(4)	101.97(12)
C(11)–Sn(1)–Cl(2)	97.63(11)	C(20)–Sn(2)–O(2)	80.87(13)
C(11)–Sn(1)–O(4)	79.60(12)	Cl(3)–Sn(2)–Cl(4)	98.16(4)
O(1)–Sn(1)–Cl(1)	86.49(8)	Cl(3)–Sn(2)–O(2)	85.32(6)
O(1)–Sn(1)–O(2)	71.88(9)	Cl(4)–Sn(2)–O(2)	174.85(6)
O(1)–Sn(1)–Cl(2)	173.45(7)	C(2)–C(1)–Sn(1)	108.8(3)
Cl(1)–Sn(1)–Cl(2)	96.54(5)	C(4)–O(1)–Sn(1)	129.3(2)
Cl(1)–Sn(1)–O(4)	158.36(7)	C(3)–O(1)–Sn(1)	111.2(2)

The Sn(1) atom in **24** is hexacoordinated by two carbon, two halogen and two oxygen atoms and exhibits a real structure along the path trigonal bipyramid to octahedron. This configuration is similar to that found for the analogous bis(diiodidodiorganostannyl)methane substituted crown ether $PhI_2SnCH_2SnI_2CH_2$-[13]-crown-4.[149] The configuration observed for the Sn(1) atom in **24** contrast well with the distorted trigonal-bipyramidal geometry adopted by the Sn(1) atom in the corresponding bis(dichloridodiorganostannyl)methane substituted crown ether $PhCl_2SnCH_2SnCl_2CH_2$-[19]-crown-6[163]. The distortion is best reflected by (i) the decrease of the C(1)–Sn(1)–C(11) angle from 180° to 148.27(15)° and by (ii) the increase of Cl(1)–Sn(1)–Cl(2) angle from 90° to 96.54(5)°. The intramolecular Sn(1)–O(1) distance of 2.446(3) Å is considerably shorter than the intramolecular Sn(1)–O(4) coordination of 2.633(3) Å. The Sn(1)–Cl(2) distance of 2.4119(12) Å is longer than the Sn(1)–Cl(1) (2.4072(13)Å) distance and exceed the sum of the covalent radii[181] of Sn(1.40 Å) and Cl(0.99). The Sn(1)–O(1) distance of 2.446(3) Å is slightly shorter than the corresponding bond found in $PhCl_2SnCH_2SnCl_2CH_2$-[19]-crown-6 (2.491(2) Å).

The Sn(2) atom in **24** shows a distorted trigonal-bipyramidal configuration (geometrical goodness[174] $\Delta\Sigma(\theta)$ 50.2°) with C(11),C(20),and Cl(3) occupying the equatorial and O(2) and Cl(4) occupying the axial positions. The distortion is manifested by the Cl(4)–Sn(2)–O(2) angle of 174.85(6)°, which deviates by 5.15° from the ideal 180°. The Sn(2) atom is displaced by 0.3774(3) Å from the trigonal plane in the direction of Cl(4). This configuration contrasts well with the distorted

tetrahedral geometry exhibited by the Sn(2) atom in the corresponding bis(diiodidodiorganostannyl)methane substituted crown ether $PhI_2SnCH_2SnI_2CH_2$-[13]-crown-4.[149] The difference of configuration observed is an evidence of the increase in the Lewis acidity at the Sn(2) atom in **24**. The Sn(2)–O(2) distance of 2.773(3) Å is longer than the Sn(1)–O(1) (2.446(3) Å) and Sn(1)–O(4) (2.633(3) Å) distances. The lengthening of the Sn(2)–O(2) distance is the result of the influence of the phenyl group, which decreased the Lewis acidity of the Sn(2) atom. Due to the trans influence of the crown ether oxygen atom O(2), the Sn(2)–Cl(2) (2.3759(10) Å) distance is longer than the Sn(2)–Cl(3) (2.3607(10) Å). Both distances are below the sum of the covalent radii[181] of Sn (1.40 Å) and Cl (0.99 Å).

Unlike to the formation of the one-dimensional chain structure found in $PhCl_2SnCH_2SnCl_2CH_2$-[19]-crown-6[163], no self association was observed in **24**, although they have same substituent pattern around the tin atoms.

2.6. Syntheses, Structures and Complexation Behaviour of (dichloridodiorganostannyl)-substituted [26]-crown-8.

2.6.1. Synthesis of the Bis (dichloridodiorganostannyl)-substituted [26]-crown-8.

The bis(dichloridodiorganostannyl)-substituted [26]-crown-8 was obtained by the reaction of the bis(diiodidodiorganostannyl)-substituted [26]-crown-8[163] with an excess of silver chloride in acetonitrile over a period of 14 days in the dark (eq. 22).

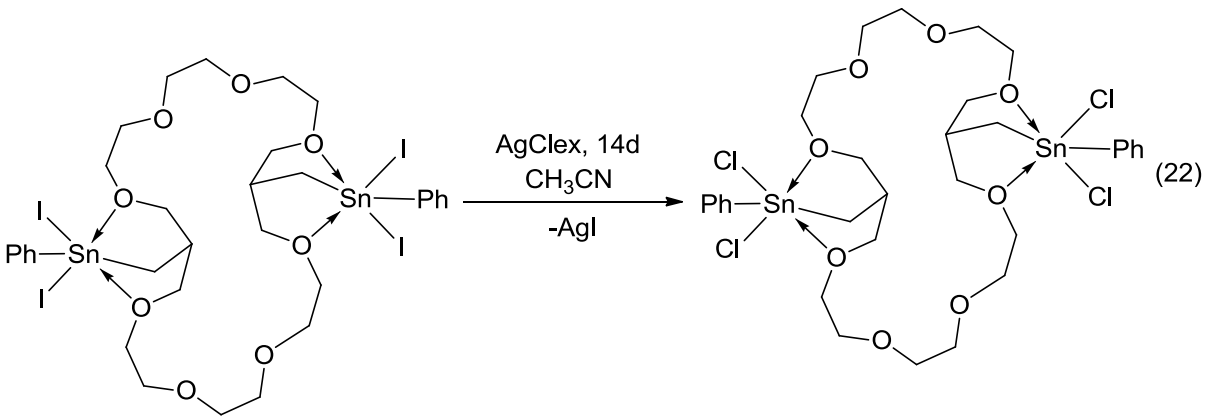

(22)

25

Compound **25** is air and moisture stable and shows good solubility in chlorinated solvents.

2.6.2. Molecular Structure of the Bis (dichloridodiorganotin)-substituted [26]-Crown-8.

Single crystals suitable for X-ray diffraction analysis were grown by slow evaporation of compound **25** in dichloromethane/n-hexane. The compound crystallized monoclinically in the space group P2(1)/c with two molecules per unit cell. The molecular structure of **25** is shown in Figure 83, and selected bond distances and bond angles are listed in Table 15.

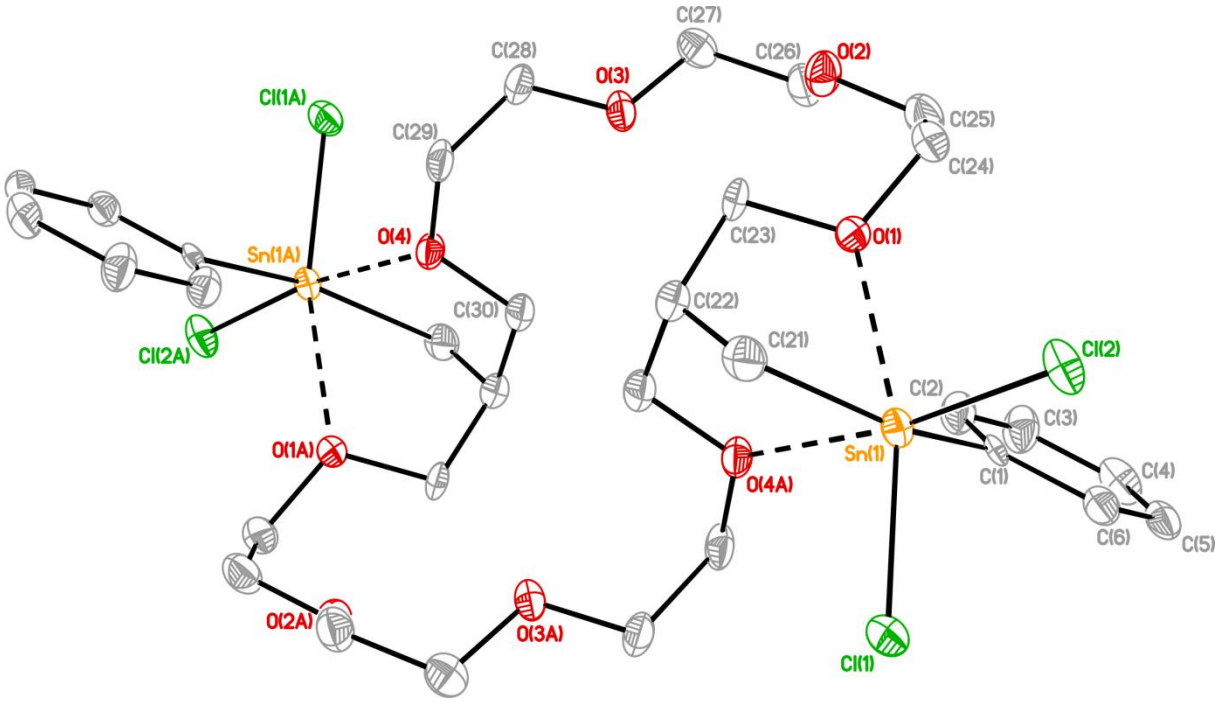

Figure 83. General view (SHELXTL) of a molecule of **25** showing 30% probability displacement ellipsoids and the crystallographic numbering scheme.

Table 15. Selected bond lengths/Å and bond angles/° for **25**.

Bond lengths			
Sn(1)–C(1)	2.111(5)	Sn(1)–O(4A)	2.402(3)
Sn(1)–C(21)	2.126(2)	Sn(1)–Cl(1)	2.4051(12)
Sn(1)–O(1)	2.493(3)	Sn(1)–Cl(2)	2.4099(13)
Bond angles			
C(1)–Sn(1)–C(21)	152.03(16)	O(1)–Sn(1)–O(4A)	75.34(11)
C(1)–Sn(1)–Cl(1)	98.13(9)	O(1)–Sn(1)–Cl(1)	164.38(10)
C(1)–Sn(1)–Cl(2)	97.85(10)	O(1)–Sn(1)–Cl(2)	97.66(9)
C(1)–Sn(1)–O(1)	85.17(12)	Cl(1)–Sn(1)–O(4A)	89.67(8)
C(1)–Sn(1)–O(4A)	85.14(13)	Cl(2)–Sn(1)–O(4A)	172.20(9)
C(21)–Sn(1)–Cl(1)	99.83(13)	Cl(2)–Sn(1)–Cl(1)	97.01(4)
C(21)–Sn(1)–Cl(2)	101.04(14)	C(2)–C(1)–Sn(1)	122.6(2)
C(21)–Sn(1)–O(1)	72.06(15)	C(24)–O(1)–Sn(1)	128.7(3)
C(21)–Sn(1)–O(4A)	73.72(16)	C(22)–C(21)–Sn(1)	105.8(3)

The molecular structure of compound **25** is similar to that of the corresponding bis(diiodidoorganotin)-substituted [26]-crown-8.[163] Thus, it shows a centrosymmetric structure with an inversion center at the middle of the crown ether ring. The presence of the electron withdrawing Cl-substituents induce intramolecular Sn–O interactions between the crown ether oxygen and the tin atoms. As consequence, the tin atom is hexacoordinated and exhibits a distorted octahedral environment. The decrease of the C(21)–Sn(1)–C(1) angle from 180° to 152.03(16)° reflects the distortion. The latter angle is close to that observed for the corresponding angles in [(PhI_2SnCH_2)$_2$]-[26]-crown-8 (150.78(19)°],[163] [PhX_2Sn-CH_2-[16]-crown-5 (X = I, 151.000(6)°, X = Cl, 150.00(18)°].[150]

The intramolecular Sn–O distances of 2.402(3) and 2.493(3) Å are shorter than the corresponding distances in the bis(diiodidoorganotin)-substituted-[26]-crown-8 [(PhI_2SnCH_2)$_2$]-[26]-crown-8 (2.471(3) and 2.560(3) Å)].[163] The difference is the result of the increase of the Lewis acidity at the tin atom in **25** in comparison with that of PhI_2SnCH_2)$_2$]-[26]-crown-8.[163] The Sn(1)–Cl(1) and Sn(1)–Cl(2) distances of

2.4099(13) and 2.4051(12) are by 0.0199 and 0.0151 Å, respectively, longer than the sum of the covalent radii of Sn and Cl (2.39 Å).[181]

2.6.3. Structure of the Bis (dichloridodiorganotin)-substituted [26]-crown-8 in Solution.

A ^{119}Sn NMR spectrum at room temperature of compound **25** in $CDCl_3$ displayed only one resonance at δ –111 indicating the magnetic equivalence of the two tin atoms, which result from a centrosymmetric structure in solution. This signal is high field shifted in comparison with the ^{119}Sn chemical shifts of the four-coordinated organotin dichloride $(PhCl_2Sn)_2CH_2$ (δ 8)[261]. This observation shows that the tin atoms are hypercoordinated and the intramolecular O→Sn interaction found in the solid state being retained in solution. In addition to their centrosymmetric nature, compounds **25** exhibits a C_{2h} symmetry in solution supported by their ^{13}C NMR spectrum that showed exactly eight resonances for the crown ether carbon atoms.

2.7. Experimental section

General methods

The solvents were dried and distilled from the appropriate desiccants prior to use. All manipulations were performed under an inert atmosphere of argon. Elemental iodine (I_2), elemental bromine (Br_2), AgCl, AgF, KF, $Et_4NF{\cdot}2H_2O$, $Bu_4NF{\cdot}3H_2O$, CsF, NaCl, NaF, LiF and LiCl were commercially available. Literature procedure were used to prepare $FcSi(Me_2)CH_2MgCl$,[130] $fc(Si(Me_2)CH_2MgCl)_2$[130], (1,4,7,10,13-pentaoxacyclohexadec-15-ylmethyl)-triphenylstannane,[150] Iodo(1,4,7,10,13-pentaoxacyclohexadec-15-ylmethyl)diphenylstannane,[130] and diiodo(1,4,7,10-tetraoxacyclotridec-12-ylmethyl)diphenylstannane,[149] 12,25-bis{[diiodophenylstannyl]methyl}-1,4,7,10,14,17,20,23-octaoxa-cyclohexacosane.[163] The atom numbering of the crown ether fragments and of the organtin fragment is shown in Scheme 18.

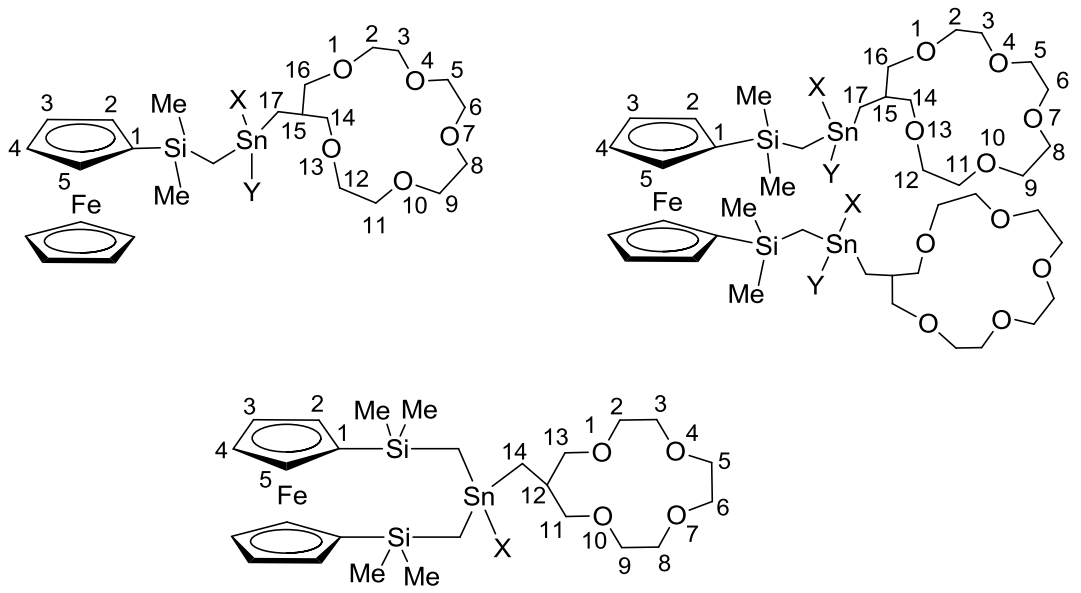

Scheme 18. Atoms numbering of the crown ether moiety, the organotin fragment and the ferrocene fragment.

NMR Spectroscopy. The NMR spectra were recorded on Bruker DRX 400, DPX 300 spectrometers with broad band decoupling of ^{119}Sn at 111.92 MHz and ^{13}C at 100.61 MHz. Chemical shifts δ are given in ppm and referenced to tetramethylstannane (^{119}Sn), trichlorofluoromethane (^{19}F) and tetramethylsilane (^{29}Si, ^{1}H, ^{13}C).

Electrospray mass spectra were recorded on a Thermoquest-Finnigan instrument using CH_3CN as the mobile phase. The samples were introduced as solution in CH_3CN via a syringe pump operating at 0.5µL/min. The capillary voltage was 4.5 kV while the cone skimmer voltage varied between 50 and 250 kV. Identification of the expected ions was assisted by comparison of experimental and calculated isotope distribution patterns. The m/*z* values reported correspond to those of the most intense peak in the corresponding isotope pattern. **Elemental analyses** were performed on a LECO-CHNS-932 Analyser. **Melting points** were determined using a Büchi Melting Point M-560.

Voltammetry and DFT Calculations. Cyclic voltammetry has been carried out using a PAR 2273A digital potentiostat piloted by PowerSuite software. A standard 5 mL three-electrode electrochemical cell was used with the auxiliary electrode (Pt wire) separated from the analyte by a sintered-glass tube. Bu_4NPF_6, $HexMe_2(C_{16}H_{33})NCl$, LiCl, and $LiClO_4$ (Aldrich) were dried under vacuum and kept over P_2O_5. Bu_4NF (Aldrich) was used as a 1 M solution in THF. All experiments were performed in dry CH_3CN. For DFT modeling, the Gaussian-03 package[262] and its facilities for structure optimization, NBO,[252] and CHelpG[253] charge calculations were used.

Synthesis of ferrocenyl{[(dimethylsilyl)methyl][1,4,7,10,13-Pentaoxacyclohexadec-15-ylmethyl]diphenylstannylmethane}, $FcMe_2SiCH_2SnPh_2CH_2$-[16]-crown-5 (1).

A solution of $FcSiMe_2CH_2MgCl$ prepared from $FcSiMe_2CH_2Cl$ (1.09 g, 3.72 mmol) and Mg (0.18 g, 7.42 mmol) in THF (20 mL), was added dropwise to a stirred solution of Ph_2ISnCH_2-[20]-crown-5 (2.40 g, 3.09 mmol) in THF (40 mL) for a period of 2h. After the addition had been completed, the reaction mixture was heated at reflux overnight and then cooled to room temperature. Cold water (50 mL) was added and the mixture was extracted two times with 50 mL of dichloromethane. The combined organic phases were dried with $MgSO_4$ and filtered, and the solvents evaporated *in vacuo* to give the crude product. The latter was purified by column chromatography [SiO_2, cyclohexane/ethyl acetate (4/1)] to yield 1.86 g (64%) of pure **1** as viscous red oil.

^{1}H NMR ($CDCl_3$, 300.13 MHz, 296 K) *δ*: 0.14 (s, 6H, CH_3), 0.36 (s, $^{2}J(^{1}H–^{119/117}Sn)$ = 75Hz, 2H, $SnCH_2Si$), 1.14 (d, $^{3}J(^{1}H–^{1}H)$ = 9.0Hz, $^{2}J(^{1}H–^{117}Sn)$ = 54 Hz, $^{2}J(^{1}H–^{119}Sn)$ = 66 Hz, 2H, $SnCH_2$), 2.17 (m, 1H, CH), 3.29-3.59 (complex pattern, 20H, CH_2-O-CH_2), 3.98 (m, 2H, Hcp-2,5), 4.05 (s, 5H, Hcp), 4.26 (m, 2H, Hcp-3,5), 7.30–7.48 (complex pattern,10H, Ph). **^{13}C{^{1}H} NMR** ($CDCl_3$, 100.63 MHz, 300 K) *δ*: -4.2 ($^{1}J(^{13}C–^{117}Sn)$ = 250Hz, $^{1}J(^{13}C–^{119}Sn)$ = 262Hz, $SnCH_2Si$), –0.7 ($^{3}J(^{13}C–^{117/119}Sn)$ = 12 Hz, CH_3), 20.9 (C17), 37.1 ($^{2}J(^{13}C–^{117/119}Sn)$ = 19 Hz, C15), 68.0 (Ccp), 69.6–70.6(C2-C12), 70.7($C_{cp-3,4}$), 72.8 ($C_{cp-2,5}$), 73.2 ($^{3}J(^{13}C–^{117/119}Sn)$ = 25 Hz, 74.0 ($^{3}J(^{13}C-^{117/119}Sn)$ = 48 Hz, C14/C16), 127.9 ($^{3}J(^{13}C–^{117/119}Sn)$ = 44 Hz, Cm), 128.1(C_p), 136.5 ($^{2}J(^{13}C–^{117/119}Sn)$ = 34 Hz, Co), 141.9 ($^{3}J(^{13}C–^{117/119}Sn)$ = 445/467 Hz, Ci). **^{29}Si{^{1}H} NMR** (CDCl3, 59.63 MHz, 295 K) *δ*: –1.0. **^{119}Sn{^{1}H} NMR** ($CDCl_3$, 111.89 MHz, 295 K) *δ*: –66.3. Anal. Calcd for $C_{37}H_{50}O_5FeSiSn$ (777.35): C 57.2; H 6.5. Found 57.5; H 6.7.

Synthesis of 1,1'-Bis{[(1,4,7,10,13-Pentaoxacyclohexadec-15-ylmethyl)diphenylstannyl)methyl]dimethylsilyl}ferrocene $fc(Me_2SiCH_2SnPh_2CH_2$-[16]-crown-5)$_2$ (2).

A solution of $Fc(SiMe_2CH_2MgCl)_2$ prepared from $Fc(SiMe_2CH_2Cl)_2$ (1.0 g, 2.55 mmol) and Mg (0.25 g, 10 mmol) in THF (20 mL), was added dropwise to a stirred solution of Ph_2ISnCH_2-[16]-crown-5 (3.3 g, 3.09 mmol) in THF (45 mL) for a period of 2h. After addition had been completed, the reaction mixture was heated at reflux overnight and then cooled to room temperature. Cold water (50 mL) was added and the mixture was extracted two times with 50 mL of dichloromethane. The combined organic phases were dried with $MgSO_4$ and filtered, and the solvents evaporated *in vacuo* to give the crude product. The latter was purified by column chromatography [Al_2O_3, Cyclohexane/Ethylacetate (4/1)] to yield 2.41 g (69%) of pure **5** as viscous red oil.

^{1}H NMR ($CDCl_3$, 300.13 MHz, 296 K) *δ*: 0.12 (s, 12H, CH_3), 0.32 (s, $^{1}J(^{1}H–^{117/119}Sn)$ = 75Hz 4H, $SnCH_2Si$), 1.13 (d, $^{3}J(^{1}H–^{1}H)$ = 9.0Hz, $^{2}J(^{1}H–^{117/119}Sn)$ = 54 Hz, 4H, $SnCH_2$), 2.16 (m, 2H, CH), 3.30–3.61 (complex pattern, 40H, CH_2-O-CH_2), 3.90 (s, 4H, $Hcp_{-2,5}$), 4.16(s, 4H, $Hcp_{-3,4}$), 7.30-7.48 (complex pattern, 20H, Ph). **^{13}C{^{1}H} NMR** ($CDCl_3$, 125.68 MHz, 300 K) *δ*: 0.0 ($SiCH_2Sn$), 4.9 ($^{3}J(^{13}C–^{117/119}Sn)$ = 11 Hz, CH_3), 15.9 (CH_2Sn), 41.2 ($^{2}J(^{13}C–^{117/119}Sn)$ = 19 Hz, C15), 73.8–74.8(C2-C16), 75.1($C_{cp-3,4}$), 76.9 ($C_{cp-2,5}$), 77.3 (Ccp_{-1}), 131.9 ($^{3}J(^{13}C–^{117/119}Sn)$ =14 Hz, Cm), 132.1(C_p), 132.3

($^2J(^{13}C–^{117/119}Sn)$ =11 Hz, Co), 140.7 ($^3J(^{13}C–^{117/119}Sn)$ = 35 Hz, Ci). **$^{29}Si\{^1H\}$ NMR** ($CDCl_3$, 59.63 MHz, 295 K) *δ*: –0.80. **$^{119}Sn\{^1H\}$ NMR** ($CDCl_3$, 111.89 MHz, 295 K) *δ*: –65.82.

Synthesis of ferrocenyl{[(dimethylsilyl)methyl][1,4,7,10,13-Pentaoxacyclohexadec-15-ylmethyl]phenyliodidostannylmethane}: $FcMe_2SiCH_2SnPhICH_2$-[16]-crown-5 (3).

Over a period of three hours, iodine (0.17 g, 0.68 mmol) was added in small portions at 0°C to a stirred solution of **1** (0.53 g, 0.68 mmol) in CH_2Cl_2 (25 mL). Stirring was continued and the reaction mixture was warmed to room temperature overnight. Dichloromethane and iodobenzene were removed *in vacuo* (10^{-3} mm Hg) to give 440 mg (79 %) of **3** as viscous red oil.

^1H NMR ($CDCl_3$, 300.13 MHz, 294 K) *δ*: 0.48 (s, 3H, CH_3), 0.52 (s, 3H, CH_3) 0.80/0.93 ABX-type resonance, $^2J(^1H–^1H)$ = 12.0Hz, $^4J(^1H–^1H)$ = 12.0Hz, $^2J(^1H–^{117}Sn)$= 80.0 Hz, $^2J(^1H–^{119}Sn)$ = 104.0 Hz, 2H, $SnCH_2Si$), 1.33/1.52 (ABX-type resonance, $^2J(^1H–^1H)$ = 8.0Hz, $^3J(^1H–^1H)$ = 12.0Hz, $^2J(^1H–^{117}Sn)$ = 56.0 Hz, $^2J(^1H–^{119}Sn)$ = 80.0 Hz, 2H, $SnCH_2$), 2.33 (m, 1H, CH), 3.26-3.61 (complex pattern, 20H, CH_2-O-CH_2), 4.06 (s, 1H, H_{cp-2}), 4.16 (s, 5H, H_{cp}), 4.26 (s, 1H, H_{cp-5}), 4.34 (s, 1H, H_{cp-3}), 4.36 (s, 1H, H_{cp-4}), 7.32–7.62 (complex pattern, 5H, Ph). **$^{13}C\{^1H\}$ NMR** ($CDCl_3$, 100.63 MHz, 300 K) *δ*: 1.4 (CH_3), 1.6 (CH_3), 4.6 ($SnCH_2Si$), 21.3 (C17), 38.0 (C15), 68.7 (Ccp), 70.0–71.3 (C2-C12), 73.5 ($C_{cp-3,4}$), 74.0 ($C_{cp-2,5}$), 74.6 (C14/C16), 128.7 ($^3J(^{13}C–^{117/119}Sn)$ = 59 Hz, Cm), 130.7(C_p), 135.6 ($^2J(^{13}C–^{117/119}Sn)$ = 48 Hz, Co), 143.0 (Ci). **$^{29}Si\{^1H\}$ NMR** ($CDCl_3$, 59.63 MHz, 294 K) *δ*: –0.94. **$^{119}Sn\{^1H\}$ NMR** ($CDCl_3$, 111.89 MHz, 294 K) *δ*: –72.0. Anal. Calcd for $C_{31}H_{45}O_5FeISiSn$ (827.2): C 45.0; H 5.5. Found 45.5; H 5.8.

Synthesis of 1,1'-Bis{[(iodido(1,4,7,10,13-Pentaoxacyclohexadec-15-ylmethyl)phenylstannyl)methyl]dimethylsilyl}ferrocene fc($Me_2SiCH_2SnPhICH_2$-[16]-crown-5)$_2$ (4).

Over a period of three hours, iodine (0.32 g, 0.23 mmol) was added in small portions at 0 °C to a stirred solution of **2** (0.12 g, 0.47 mmol) in CH_2Cl_2 (25 mL). Stirring was continued and the reaction mixture was warmed to room temperature overnight. Dichloromethane and iodobenzene were removed *in vacuo* (10^{-3} mm Hg) to give 260 mg (76 %) of **4** as viscous red oil.

^{1}H NMR ($CDCl_3$, 400.13 MHz, 300 K) *δ*: 0.45 (s, 12H, CH_3), 0.81 (complex pattern, 4H, $SnCH_2Si$), , 1.27 (s, 2H, $SnCH_2$), 1.37 (complex pattern, 4H, $SnCH_2$), 2.27 (m, 2H, CH), 3.29-3.71 (complex pattern, 40H, CH_2-O-CH_2), 4.00 (s, 2H, Hcp_{-2}), 4.19 (s, 2H, Hcp_{-5}), 4.28 (s, 4H, $Hcp_{-3,4}$), 7.26–7.67 (complex pattern, 10H, Ph). **^{13}C{^{1}H} NMR** ($CDCl_3$, 100.63 MHz, 300 K) *δ*: 1.1 (CH_3), 4.18 ($SiCH_2Sn$), 20.9 ($SnCH_2$), 37.5 ($^{3}J(^{13}C–^{117/119}Sn)$ = 23 Hz, C15), 69.5–70.7 (C2–C12), 71.4($^{3}J(^{13}C–^{117/119}Sn)$ = 46 Hz, C14/C16), 72.5 ($^{3}J(^{13}C–^{117/119}Sn)$ = 34 Hz Ccp-1), 73.1 (C_{cp-3}), 73.4 (C_{cp-4}), 74.1 (C_{cp-2}), 74.4 (C_{cp-5}), 128.3 ($^{3}J(^{13}C–^{117/119}Sn)$ = 58 Hz, C_m), 130.2 (C_p), 135.1 ($^{2}J(^{13}C–^{117/119}Sn)$ = 45 Hz, C_o), 142.3 (C_i). **^{29}Si{^{1}H} NMR** ($CDCl_3$, 59.63 MHz, 295 K) *δ*: –0.74. **^{119}Sn{^{1}H} NMR** ($CDCl_3$, 111.89 MHz, 295 K) *δ*: –72.16.

Synthesis of ferrocenyl{[(dimethylsilyl)methyl][1,4,7,10,13-Pentaoxacyclohexadec-15-ylmethyl]phenylchloridostannylmethane}: $FcMe_2SiCH_2SnPhClCH_2$-[16]-crown-5 (5).

To a solution of **3** (0.39 g, 0.47 mmol) in CH_3CN (20 mL) was added excess silver chloride, AgCl (0.20 g, 1.41 mmol). The resulting mixture was stirred at room temperature and in the dark for 14 days. After the AgI formed and the non reacted AgCl had been removed by filtration, the solvent was evaporated under vacuum to give 0.29 g (83%) of **5** as viscous red oil.

^{1}H NMR (CD_3CN, 400.13 MHz, 300 K) *δ*: 0.45 (s, 6H, CH_3), 0.16/0.65 ABX-type resonance, $^{2}J(^{1}H–^{1}H)$ = 8.0Hz, $^{4}J(^{1}H–^{1}H)$ = 12.0Hz, $^{2}J(^{1}H–^{117/119}Sn)$ = 88.0 Hz, 2H, $SnCH_2Si$), 1.15/1.30 (ABX-type resonance, $^{2}J(^{1}H–^{1}H)$ = 8.0Hz, $^{3}J(^{1}H–^{1}H)$ = 12.0Hz, $^{2}J(^{1}H–^{117/119}Sn)$ = 80.0 Hz, 2H, $SnCH_2$), 2.34 (m, 1H, CH), 3.26-3.66 (complex pattern, 20H, CH_2-O-CH_2), 4.19 (s, 7H, $H_{cp-2,5,}$ H_{cp}), 4.38 (s, 2H, $H_{cp-3,4}$), 7.42–7.68 (complex pattern, 5H, Ph). **^{13}C{^{1}H} NMR** (CD_3CN, 100.63 MHz, 300 K) *δ*: 0.77 (CH_3), 3.2 ($SnCH_2Si$), 18.5 (C17), 37.2 ($^{2}J(^{13}C–^{117/119}Sn)$ = 23 Hz, C15), 68.6 (Ccp), 69.9–70.7 (C2-C12), 71.2 (C14/C16), 73.6 ($C_{cp-3,4}$), 74.4 ($C_{cp-2,5}$), 128.8 ($^{3}J(^{13}C–^{117/119}Sn)$ = 58 Hz, Cm), 129.5(C_p), 135.6 ($^{2}J(^{13}C–^{117/119}Sn)$ = 47 Hz, Co), 144.4 (Ci). **^{29}Si{^{1}H} NMR** (CD_3CN, 59.63 MHz, 295 K) *δ*: –1.1. **^{119}Sn{^{1}H} NMR** (CD_3CN, 111.89 MHz, 295 K) *δ*: –17.0. **ESI-MS** (MeCN, *m/z*); positive mode: 736.2 $\{FcMe_2SiCH_2Sn(OH)PhCH_2$-[16]-crown-5·$H_2O\}^{+}$, 759.2 $\{FcMe_2SiCH_2Sn(OH)PhCH_2$-[16]-crown-5·$CH_3CN\}^{+}$, negative mode: 771.1 $\{Fc(Me_2SiCH_2SnClPhCH_2$-[16]-crown-5·$Cl\}^{-}$ Anal. Calcd for $C_{31}H_{45}O_5FeClSiSn$ (735.7): C 50.6; H 6.2. Found 50.1; H 6.4.

Synthesis of the ditopic complex {$FcMe_2SiCH_2SnPhClCH_2$-[16]-crown-5·LiCl} [5·LiCl].

Lithium Chloride (0,006 g, 0.16 mmol) was added to a solution of **3** (0.04 g, 0.05 mmol) in CH_3CN (5 mL) and the mixture was stirred at room temperature for two days. The reaction mixture was filtered and the solvent was evaporated under vacuo to give 49 mg (66%) of pure **5**·LiCl as an amorph solid.

^{1}H NMR (CD_3CN, 300.13 MHz, 295.16 K) *δ*: 0.23 (s, 6H, CH_3), 0.70 (s, $^2J(^1H–^{119/117}Sn)$ = 93.0Hz 2H, $SnCH_2Si$), 1.31 (d, $^3J(^1H–^1H)$ = 9.0Hz, $^2J(^1H–^{117}Sn)$ = 69.0 Hz, $^2J(^1H–^{119}Sn)$ = 81.0 Hz 2H, $SnCH_2$), 2.64 (m, 2H, CH), 3.40–3.58 (complex pattern, 20H, CH_2-O-CH_2), 4.28 (s, 4H, $Hcp_{-2,5}$), 4.41 (s, 4H, $Hcp_{-3,4}$), 7.32–8.11 (complex pattern, 5H, Ph). **$^{13}C\{^1H\}$ NMR** (CD_3CN, 75.47 MHz, 295.16 K) *δ*: 0.33 (CH_3), 9.6 ($SiCH_2Sn$), 24.8 (C17), 36.0 ($^2J(^{13}C–^{117/119}Sn)$ = 24 Hz, C15), 65.3 (C_{cp1}), 68.1–69.2 (C2–C12), 71.7 ($C_{cp-3,4}$) , 74.1 ($C_{cp-3,4}$), 77.3 (C14/C16, $^3J(^{13}C-^{117/119}Sn)$ = 70 Hz), 127.5 ($^3J(^{13}C–^{117/119}Sn)$ = 63 Hz, Cm), 128.1 (C_p), 136.8 ($^2J(^{13}C–^{117/119}Sn)$ = 51 Hz, Co), 146.8 (Ci). **$^{29}Si\{^1H\}$ NMR** (CD_3CN, 59.63 MHz, 294.16 K) *δ*: –1.79. **$^{119}Sn\{^1H\}$ NMR** (CD_3CN, 111.92 MHz, 294.16 K) *δ*: –106.1. **ESI-MS** (MeCN, *m/z*); positive mode: 736.2 $FcSi(Me_2)CH_2Sn(OH)PhCH_2$-[16]-crown-5·$H_2O\}^+$, 759.2 {$FcSi(Me_2)CH_2Sn(OH)PhCH_2$-[16]-crown-5·$CH_3CN\}^+$ negative mode: 771.1 {$FcSi(Me_2)CH_2SnClPhCH_2$-[16]-crown-5·$Cl\}^-$ **Anal. Calcd** for $C_{40}H_{70}O_{10}FeCl_4Si_2Sn_2$ (1202.17): C 39.9; H 5.9. Found 39.8; H 6.0.

Synthesis of the trichlordiorganostannate complex {$FcMe_2SiCH_2SnCl_2CH_2$-[16]-crown-5·Cl}$^-${$Bu_4P\}^+$ [5·Cl]$^-$[Bu_4P]$^+$.

Tetrabutylphosphonium chloride (0,04 g, 0,14 mmol) was added to a solution of **5** (0,1 g, 0,14 mmol) in CH_3CN (10 mL) and the mixture was stirred at room temperature over night. The solvent were removed in Vacuo to give an orange solid. Single crystals suitable for X-ray diffraction analysis were obtained by slow evaporation of the compound in ethanol to give 0.08 g (57%) of [**5**·Cl]$^-$[Bu_4P]$^+$ as orange crystals, mp 112° C.

$^{119}Sn\{^1H\}$ NMR ($CDCl_3$, 111.89 MHz, 295 K) δ: –25.3. **ESI-MS** (MeCN, *m/z*); negative mode: 711.1 {$FcMe_2SiCH_2SnCl_2CH_2$-[16]-crown-5·$OH\}^-$, 729.1 {$FcMe_2SiCH_2SnCl_2CH_2$-[16]-crown-5·$Cl\}^-$.

Synthesis of 1,1'-Bis{[(chlorido(1,4,7,10,13-Pentaoxacyclohexadec-15-ylmethyl)phenylstannyl)methyl]dimethylsilyl}ferrocene fc($Me_2SiCH_2SnPhClCH_2$-[16]-crown-5)$_2$ (6).

To a solution of **4** (0.35 g, 0.24 mmol) in CH_3CN (20 mL) was added excess silver chloride, AgCl (0.20 g, 1.41 mmol). The resulting mixture was stirred at room temperature and in the dark for 14 days. After the AgI formed and the non reacted AgCl had been removed by filtration, the solvent was evaporated under vacuo to give 0.24 g (78%) of **6** as viscous red oil.

^{1}H NMR (CD_3CN, 400.13 MHz, 300 K) *δ*: 0.46 (s, 12H, CH_3), 0.23/0.66, ABX-type resonance, $^2J(^1H–^1H)$ = 8.0Hz, $^4J(^1H–^1H)$ = 12.0Hz, $^2J(^1H–^{117/119}Sn)$ = 88.0 Hz, 4H, $SnCH_2Si$),1.12/1.28, (ABX-type resonance, $^2J(^1H–^1H)$ = 8.0Hz, $^3J(^1H–^1H)$ = 12.0 Hz, $^2J(^1H–^{117}Sn)$ = 64.0 Hz, $^2J(^1H–^{119}Sn)$ = 96.0 Hz, 4H, $SnCH_2$), 2.26 (m, 2H, CH), 3.27-3.65 (complex pattern, 40H, CH_2-O-CH_2), 4.21 (s, 4H, $H_{cp-2,5}$), 4.39 (complex pattern, 4H, $H_{cp-3,4}$), 7.40–7.69 (complex pattern, 10H, Ph). **^{13}C{^{1}H} NMR** (CD_3CN, 100.63 MHz, 300 K) *δ*: 0.8 (CH_3), 3.4 ($SiCH_2Sn$), 18.7 ($SnCH_2$), 37.2 ($^2J(^{13}C–^{117/119}Sn)$ = 24 Hz , C15), 69.9–70.7 (C2–C12), 71.9 ($^3J(^{13}C–^{117/119}Sn)$ = 34 Hz, C14/C16), 73.2 (Ccp_{-1}) 73.7 ($C_{cp-3,4}$), 74.5 ($^4J(^{13}C–^{117/119}Sn)$ = 73.5 Hz, $C_{cp-2,5}$), 128.8 ($^3J(^{13}C–^{117/119}Sn)$ = 60 Hz, Cm), 129.5 (C_p), 135.7 ($^2J(^{13}C–^{117/119}Sn)$ = 45 Hz, Co), 144.4 (Ci). **^{29}Si{^{1}H} NMR** (CD_3CN, 59.63 MHz, 296.16 K) *δ*: –0.85. **^{119}Sn{^{1}H} NMR** (CD_3CN, 111.89 MHz, 296.16 K) *δ*: –18.2. **ESI-MS** (MeCN, *m/z*); negative mode: 1321.4 $\{Fc(Me_2SiCH_2SnPhClCH_2\text{-}[16]\text{-}crown\text{-}5)_2 \cdot Cl\}^-$, positive mode: 1284.4 $\{Fc(Me_2SiCH_2SnPhCH_2\text{-}[16]\text{-}crown\text{-}5)_2 \cdot OH \cdot H_2O\}^+$ **Anal. Calcd** for $C_{52}H_{80}O_{10}FeCl_2Si_2Sn_2$ (1285.5): C 48.6; H 6.3. Found 47.2; H 6.2.

Synthesis of the ditopic complex fc($Me_2SiCH_2SnPhClCH_2$)$_2$-[16]-crown-5·LiCl (6·2LiCl).

Lithium Chloride (0,003 g, 0.06 mmol) was added to a solution of **8** (0.04 g, 0.03 mmol) in CH_3CN (5 mL) and the mixture was stirred at room temperature for two days. The reaction mixture was filtered and the solvent was evaporated under vacuo to give 25 mg (58%) of pure **8**·LiCl as amorph solid.

^{1}H NMR ($CDCl_3$, 400.13 MHz, 300 K) *δ*: 0.29 (s, 12H, CH_3), 0.81 (s, $^2J(^1H–^{119/117}Sn)$ = 96.0Hz 4H, $SnCH_2Si$), 1.32 (d, $^3J(^1H–^1H)$ = 8.0Hz, $^2J(^1H–^{117}Sn)$ = 68.0 Hz, $^2J(^1H–^{119}Sn)$ = 68.0 Hz 4H, $SnCH_2$), 2.77 (m, 2H, CH), 3.45–3.67 (complex pattern, 40H,

CH_2-O-CH_2), 4.18 (s, 4H, $Hcp_{-2,5}$), 4.40 (s, 4H, $Hcp_{-3,4}$), 7.31–8.21 (complex pattern, 10H, Ph). **$^{13}C\{^1H\}$ NMR** ($CDCl_3$, 100.63 MHz, 300 K) *δ*: 0.8 (CH_3), 11.4 ($SiCH_2Sn$), 26.2 (C17), 36.2 ($^2J(^{13}C–^{117/119}Sn)$ = 24 Hz, C15), 68.3–69.6 (C2–C12), 72.0 ($C_{cp-3,4}$) , 71.8 ($C_{cp-3,4}$), 73.7 ($C_{cp-2,5,}$ C_{cp-1}), 78.3 (C14/C16, $^3J(^{13}C-^{117/119}Sn)$ = 70 Hz), 127.8 ($^3J(^{13}C–^{117/119}Sn)$ = 63 Hz, Cm), 128.3(C_p), 137.5 ($^2J(^{13}C–^{117/119}Sn)$ = 49 Hz, Co), 147.8 (Ci). **$^{29}Si\{^1H\}$ NMR** ($CDCl_3$, 59.63 MHz, 294.16 K) *δ*: –1.67. **$^{119}Sn\{^1H\}$ NMR** ($CDCl_3$, 111.92 MHz, 294.16 K) *δ*: –123.6. **ESI-MS** (MeCN, *m/z*); positive mode: 1249.3 $\{fc(Si(Me_2)CH_2SnPhCH_2\text{-}[16]\text{-}crown\text{-}5)_2 \cdot OH \cdot H_2O\}^+$ negative mode: 1321.4 $\{fc(Si(Me_2)CH_2SnPhClCH_2\text{-}[16]\text{-}crown\text{-}5)_2 \cdot Cl\}^-$.

In situ synthesis of the dichlordiorganostannate complex $\{fc(Me_2SiCH_2SnPhClCH_2\text{-}[16]\text{-}crown\text{-}5)_2 \cdot 2Cl\}^-\{2Ph_4P\}^+$ ($[6 \cdot 2Cl]^-[\ 2Ph_4P]^+$).

Tetraphenylphosphonium chloride (38 mg, 0,01 mmol) was added to a solution of **6** (65 mg, 0.05 mmol) and the mixture was studied by NMR spectroscopy.

^1H NMR (CD_3CN, 300.13 MHz, 300 K) *δ*: 0.33 (s, 12H, CH_3), 0.71 (s, $^2J(^1H–^{119/117}Sn)$ = 90.0Hz 4H, $SnCH_2Si$), 1.33 (d, $^3J(^1H–^1H)$ = 6.0Hz, $^2J(^1H–^{117}Sn)$ = 69.0 Hz, $^2J(^1H–^{119}Sn)$= 84.0 Hz 4H, $SnCH_2$), 2.39 (m, 2H, CH), 3.31-3.56 (complex pattern, 40H, CH_2-O-CH_2), 4.08 (s, 4H, $Hcp_{-2,5}$), 4.28 (s, 4H, $Hcp_{-3,4}$), 7.23-7.94 (complex pattern, 40H, Ph_4P). **$^{29}Si\{^1H\}$ NMR** (CD_3CN, 59.63 MHz, 294.16 K) *δ*: –1.36. **$^{119}Sn\{^1H\}$ NMR** (CD_3CN, 111.92 MHz, 294.16 K) *δ*: –83.19.

Synthesis of ferrocenyl{[(dimethylsilyl)methyl][1,4,7,10,13-Pentaoxacyclohexadec-15-ylmethyl]phenylfluoridostannylmethane}: $FcMe_2SiCH_2SnPhFCH_2$-[16]-crown-5 (7).

A solution of **3** (0,42 g, 0,58 mmol) in CH_2Cl_2 (20 mL) was mixed with a solution of KF (0,44 g, 7,62 mmol) in water (25 mL). The biphasic mixture was stirred at room temperature for two days. The organic phase was then separated dried over $MgSO_4$, and filtered. The filtrate was evaporated in *vacuo* to give 0,29 g (79 %) of **7** as a viscous red oil.

^1H NMR ($CDCl_3$, 400.13 MHz, 300 K) *δ*: 0.42 (s, 3H, CH_3), 0.46 (s, 3H, CH_3) 0.33/054 ABX-type resonance, $^2J(^1H–^1H)$ = 8.0Hz, $^4J(^1H–^1H)$ = 12.0Hz, $^2J(^1H–^{117}Sn)$= 72.0 Hz, $^2J(^1H–^{119}Sn)$ = 104.0 Hz, 2H, $SnCH_2Si$), 1.02/1.18 (ABX-type resonance, $^2J(^1H–^1H)$ = 8.0Hz, $^3J(^1H–^1H)$ = 12.0Hz, $^2J(^1H–^{117}Sn)$ = 56.0 Hz, $^2J(^1H–^{119}Sn)$ = 88.0

Hz, 2H, $SnCH_2$), 2.36 (m, 1H, CH), 3.33–3.78 (complex pattern, 20H, CH_2-O-CH_2), 4.06 (s, 1H, H_{cp-2}), 4.14 (s, 5H, H_{cp}), 4.22 (s, 2H, H_{cp-5}), 4.32 (s, 2H, H_{cp-3}), 4.34 (s, 2H, H_{cp-4}), 7.37–7.63 (complex pattern, 5H, Ph). **$^{13}C\{^1H\}$ NMR** ($CDCl_3$, 100.63 MHz, 300 K) *δ*: 0.3 (CH_3), 0.5 (CH_3), 2.4 ($SiCH_2Sn$), 2.5 ($SiCH_2Sn$), 15.4 (C17), 15.5 (C17), 36.4 (C15), 68.1 (Ccp), 69.4–70.7 (C2–C12), 70.33 ($Ccp_{3,4}$), 72.6 (Ccp_{-1}), 73.0 ($C_{cp-3,4}$), 73.2 ($C_{cp-2,5}$), 74.4 (C14/C16), 74.5 ($^3J(^{13}C–^{117/119}Sn)$ = 68 Hz, C14/C16), 128.3 ($^3J(^{13}C–^{117/119}Sn)$ = 61 Hz, C_m), 129.0 (C_p), 135.4 ($^2J(^{13}C–^{117/119}Sn)$ = 45 Hz, C_o), 143.2 (C_i), 143.3 (C_i). **$^{19}F\{^1H\}$ NMR** ($CDCl_3$, 282.36 MHz, 295 K) *δ*: -183.93 ($^1J(^{19}F–^{117}Sn)$ = 2086 Hz, ($^1J(^{19}F–^{119}Sn)$ = 2182 Hz) **$^{29}Si\{^1H\}$ NMR** ($CDCl_3$, 59.63 MHz, 295 K) *δ*: –1.23. **$^{119}Sn\{^1H\}$ NMR** ($CDCl_3$, 111.89 MHz, 295 K) *δ*: –22.4 ($^1J(^{119}Sn–^{19}F)$ = 2184 Hz). **ESI-MS** (MeCN, *m/z*); positive mode: 701.2 {$FcMe_2SiCH_2SnPhCH_2$-[16]-crown-5}$^+$. Anal. Calcd for $C_{31}H_{45}O_5FeFSiSn$ (719.3): C 51.8; H 6.3. Found 52.0; H 6.8.

Synthesis of 1,1'-Bis{[(fluorido(1,4,7,10,13-Pentaoxacyclohexadec-15-ylmethyl)phenylstannyl)methyl]dimethylsilyl}ferrocene. fc($Me_2SiCH_2SnPhFCH_2$-[16]-crown-5)$_2$ (8).

A solution of **4** (0,26 g, 0,18 mmol) in CH_2Cl_2 (20 mL) was mixed with a solution of KF (0,15 g, 0,26 mmol) in water (25 mL). The biphasic mixture was stirred at room temperature for two days. The organic phase was then separated dried over $MgSO_4$, and filtered. The filtrate was evaporated in *vacuo* to give 0,16 g (73%) of **8** as viscous red oil.

^1H NMR ($CDCl_3$, 400.13 MHz, 300 K) *δ*: 0.39 (complex pattern, 12H, CH_3), 0.30/0.48 (ABX-type resonance, $^2J(^1H–^1H)$ = 8.0Hz, $^4J(^1H–^1H)$ = 12.0 Hz, $^2J(^1H–^{117}Sn)$ = 88.0 Hz, $^2J(^1H–^{119}Sn)$ = 112.0 Hz, 4H, $SnCH_2Si$), 0.98/1.16 (ABX-type resonance, $^2J(^1H–^1H)$ = 8.0Hz, $^3J(^1H–^1H)$ = 12.0Hz, $^2J(^1H–^{117}Sn)$ = 80.0 Hz, $^2J(^1H–^{119}Sn)$= 96.0 Hz, 4H, $SnCH_2$), 2.33 (m, 2H, CH), 3.29–3.76 (complex pattern, 40H, CH_2-O-CH_2), 4.08 (complex pattern, 4H, $H_{cp-2,5}$), 4.27 (complex pattern, 4H, $H_{cp-3,4}$), 7.08–7.70 (complex pattern, 10H, Ph). **$^{13}C\{^1H\}$ NMR** ($CDCl_3$, 100.63 MHz, 300 K)) *δ*: 0.9 (CH_3), 1.0 (CH_3), 2.9 ($SiCH_2Sn$) 3.0 ($SiCH_2Sn$), 15.8 (C17), 16.0 (C17), 36.9 ($^3J(^{13}C–^{117/119}Sn)$ = 23 Hz, C15), 68.4 (Ccp_{-1}), 68.6 (Ccp_{-1}), 69.9–71.8 (C2–C12), 70.8 ($C_{cp-3,4}$) 73.1 ($^4J(^{13}C–^{117/119}Sn)$ = 27 Hz, $C_{cp-2,5}$), 73.5 ($C_{cp-3,4}$), 73.6 ($C_{cp-2,5}$), 74.8 (C14/C16), 74.9 ($^3J(^{13}C–^{117}Sn)$ = 42 Hz, $^3J(^{13}C–^{119}Sn)$ = 71 Hz, C14/C16), 128.7 ($^3J(^{13}C–^{117/119}Sn)$ = 59 Hz, C_m), 129.5 (C_p), 135.9 ($^2J(^{13}C–^{117/119}Sn)$ = 46 Hz, C_o), 143.7 (C_i), 143.8 (C_i).

$^{19}F\{^{1}H\}$ NMR ($CDCl_3$, 282.36 MHz, 295 K) *δ*: –183.64 ($^{1}J(^{19}F–^{117}Sn)$ = 2090 Hz, ($^{1}J(^{19}F–^{119}Sn)$ = 2186 Hz). **$^{29}Si\{^{1}H\}$ NMR** ($CDCl_3$, 59.63 MHz, 295 K) *δ*: –1.06. **$^{119}Sn\{^{1}H\}$ NMR** ($CDCl_3$, 111.89 MHz, 295 K) *δ*: –23.02 (d,$^{1}J(^{119}Sn–^{19}F)$ = 2181 Hz). **ESI-MS** (MeCN, *m/z*); positive mode: 1231.4 $\{Fc(Me_2SiCH_2SnPhCH_2$-[16]-crown-$5)_2\}^+$. **Anal. Calcd** for $C_{55}H_{80}O_{10}FeF_2Si_2Sn_2$ (1252.6): C 49.9; H 6.4. Found C 48.7; H 6.3.

Synthesis of the difluordiorganostannate complex $\{fc(Me_2SiCH_2SnFPhCH_2$-[16]-crown-$5)_2 \cdot 2F\}^-\{2Bu_4N\}^+$ $[8 \cdot 2F]^-[2Bu_4N]^+$.

Tetrabutylammoniumfluorid (0,04 g, 0,01 mmol) was added to a solution of **8** (0,07 g, 0,05 mmol) in CH_3CN (8 mL) and the mixture was stirred at room temperature over night. The reaction mixture was filtered and the solvent was evaporated under vacuo to give 0,04 g (55%) of pure $[\mathbf{8} \cdot 2F]^-[2Bu_4N]^+$ as viscous red oil.

$^{19}F\{^{1}H\}$ NMR (CH_3CN, 282.36 MHz, 295.16 K) *δ*: –132.99 (s,$^{1}J(^{19}F–^{117}Sn)$ = 1818 Hz, ($^{1}J(^{19}F–^{119}Sn)$ = 1895 Hz). $^{29}Si\{^{1}H\}$ NMR (CH_3CN, 59.63 MHz, 295.16 K). **$^{29}Si\{^{1}H\}$ NMR** (CH_3CN, 59.63 MHz, 294.16 K) *δ*:–1.53. $^{119}Sn\{^{1}H\}$ NMR (CH_3CN, 111.89 MHz, 295.16 K) *δ*: –207.56 (t, $^{1}J(^{119}Sn–^{19}F)$ =1893 Hz).

In situ reaction of 8 with two molar equivalent of NaF in CD_3CN.

NaF (4 mg, 0,10 mmol) was added to a solution of **8** (60 mg, 0,05 mmol) in CD_3CN (600 µL) and the mixture was studied by NMR spectroscopy.

$^{19}F\{^{1}H\}$ NMR (CD_3CN, 282.40 MHz, 294.16 K) *δ*: –179.82 ($^{1}J(^{19}F–^{117}Sn)$ = 2095 Hz, ($^{1}J(^{19}F–^{119}Sn)$ = 2191 Hz). **$^{29}Si\{^{1}H\}$ NMR** (CD_3CN, 59.63 MHz, 294.16 K) *δ*: –1.03. **$^{119}Sn\{^{1}H\}$ NMR** (CD_3CN, 111.92 MHz, 294.16 K) *δ*: –25.09 (d,$^{1}J(^{119}Sn–^{19}F)$ = 2189Hz).

In situ reaction of 8 with one molar equivalent of CsF in $CD_3CN/CDCl_3$ (2/1).

CsF (12 mg, 0,08 mmol) was added to a solution of **8** (100 mg, 0,08 mmol) in $CD_3CN/CDCl_3$ (2/1) (600 µL) and the mixture was studied by NMR spectroscopy.

^{1}H NMR ($CD_3CN/CDCl_3$ (2/1), 400.13 MHz, 300 K) *δ*: 0.28 (s, 12H, CH_3), 0.45 (s, $^{2}J(^{1}H–^{119/117}Sn)$ = 88.0Hz 4H, $SnCH_2Si$),), 1.06 (d, $^{3}J(^{1}H–^{1}H)$ = 8.0Hz, $^{2}J(^{1}H–^{117}Sn)$ = 32.0 Hz, $^{2}J(^{1}H–^{119}Sn)$ = 40.0 Hz 4H, $SnCH_2$), 2.37 (m, 2H, CH), 3.40-3.55 (complex pattern, 40H, CH_2-O-CH_2), 4.08 (s, 4H, $Hcp_{-2,5}$), 4.24 (s, 4H, $Hcp_{-3,4}$), 7.30-

7.84(complex pattern, 10H, Ph). **^{13}C{^{1}H} NMR** ($CD_3CN/CDCl_3$ (2/1), 100.63 MHz, 300 K) *δ*: 1.35 (CH_3), 3.7 ($SiCH_2Sn$), 20.4 (C17), 36.7 (C15), 68.5 (C_{cp-1}), 69.4–69.9 (C2–C12), 71.2 ($C_{cp-3,4}$), 73.6 ($C_{cp-2,5}$), 75.6 ($^{3}J(^{13}C–^{119/117}Sn)$ = 57 Hz, C14/C16). **^{19}F{^{1}H} NMR** ($CD_3CN/CDCl_3$ (2/1), 282.40 MHz, 241.16 K) *δ*: –117.9 ($^{1}J(^{19}F_b–^{119}Sn$ = 1310 Hz), *δ*: –137.1 ($^{1}J(^{19}F_a–^{119}Sn$ = 1903 Hz). **^{29}Si{^{1}H} NMR** ($CD_3CN/CDCl_3$ (2/1), 59.63 MHz, 295.16 K) *δ*: –6.85. **^{119}Sn{^{1}H} NMR** ($CD_3CN/CDCl_3$ (2/1), 111.92 MHz, 241.16 K) *δ*: –144.9 (dd, ($^{1}J(^{119}Sn–^{19}F_a$) = 1936 Hz; $^{1}J(^{119}Sn–^{19}F_b$) = 1316 Hz).

Synthesis of ferrocenyl{[(dimethylsilyl)methyl][1,4,7,10,13-Pentaoxacyclohexadec-15-ylmethyl]diiodidostannylmethane}: $FcMe_2SiCH_2SnI_2CH_2$-[16]-crown-5 (11).

Over a period of three hours, iodine (0.29 g, 0.37 mmol) was added in small portions at 0 °C to a stirred solution of **1** (0.09 g, 0.75 mmol) in CH_2Cl_2 (25 mL). Stirring was continued and the reaction mixture was warmed to room temperature overnight. Dichloromethane and iodobenzene were removed *in vacuo* (10^{-3} mm Hg) to give 0.26 g (78 %) of **11** as viscous red oil.

^{1}H NMR ($CDCl_3$, 300.13 MHz, 294 K) *δ*: 0.45 (s, $^{2}J(^{1}H–^{29}Si)$ = 90.0Hz 6H, CH_3), 1.40 (s, $^{2}J(^{1}H–^{119/117}Sn)$ = 36.0Hz, 2H, $SnCH_2Si$), 1.63 (d, $^{3}J(^{1}H–^{1}H)$ = 9.0Hz, $^{2}J(^{1}H–^{117}Sn)$ = 63 Hz, $^{2}J(^{1}H–^{119}Sn)$ = 81.0 Hz, 2H, $SnCH_2$), 2.22 (m, 1H, CH), 3.27–3.65 (complex pattern, 20H, CH_2-O-CH_2), 4.13 (s, 5H, H_{cp}), 4.21 (s, 1H, $H_{cp-2,5}$), 4.36 (s, 2H, $H_{cp-2,5}$). **^{13}C{^{1}H} NMR** ($CDCl_3$, 100.63 MHz, 300 K) *δ*: –1.0 (CH_3), 16.4 (C17), 29.7 ($SnCH_2Si$), 38.0 (C15), 68.9 (Ccp), 70.2–70.8 (C2-C12), 71.1 (C14/C16), 71.7 ($C_{cp-3,4}$), 73.5 ($C_{cp-2,5}$), 74.1 (C_{cp-1}), **^{29}Si{^{1}H} NMR** ($CDCl_3$, 59.63 MHz, 296.16 K) *δ*: –1.59. **^{119}Sn{^{1}H} NMR** ($CDCl_3$, 111.89 MHz, 294 K) *δ*: –203.57. **ESI-MS** (MeCN, *m/z*); positive mode: 641.1 $[FcSiMe_2Sn(OH)CH_2$-[16]-crown-5$]^+$; 901.0 $[FcSiMe_2SnI_2CH_2$-[16]-crown-5·Na$]^+$ **Anal. Calcd** for $C_{25}H_{40}O_5FeI_2SiSn$ (877.03): C 34.2.; H 4.6. Found. C 35.2.; H 5.0.

In situ reaction of 11 with one molar equivalent of *n*-Bu_4NI in $CDCl_3$.

Bu_4NI (26 mg, 0,07 mmol) was added to a solution of **11** (61 mg, 0,07 mmol) in $CDCl_3$ (600 µL) and the mixture was studied by NMR spectroscopy.

^{119}Sn{^{1}H} NMR ($CDCl_3$, 111.88 MHz, 294.16 K) *δ*: –202.26.

In situ reaction of 11 with two molar equivalent of *n*-Bu_4NI in $CDCl_3$.

Bu_4NI (52 mg, 0,14 mmol) was added to a solution of **11** (61 mg, 0,07 mmol) in $CDCl_3$ (600 µL) and the mixture was studied by NMR spectroscopy.

$^{119}Sn\{^1H\}$ NMR ($CDCl_3$, 111.88 MHz, 294.16 K) *δ*: –199.66.

Synthesis of 1,1'-Bis{[(diiodido(1,4,7,10,13-Pentaoxacyclohexadec-15-ylmethyl)stannyl)methyl]dimethylsilyl}ferrocene.
$fc(Me_2SiCH_2SnI_2CH_2$-[16]-crown-5)$_2$ (12).

Over a period of three hours, iodine (0.52 g, 2.04 mmol) was added in small portions at 0 °C to a stirred solution of **2** (0.70 g, 0.51 mmol) in CH_2Cl_2 (35 mL). Stirring was continued and the reaction mixture was warmed to room temperature overnight. Dichloromethane and iodobenzene were removed *in vacuo* (10^{-3} mm Hg) to afford an orange solid. Recrystallisation from ethanol at –5°C gave 0.67 g (84 %) of **12** as orange crystals, mp 142.6° C.

^1H NMR ($CDCl_3$, 400.13 MHz, 400 K) *δ*: 0.53 (s, $^2J(^1H–^{29}Si)$ = 120.0Hz, 12H, CH_3), 1.46 (s, $^2J(^1H–^{119/117}Sn)$ = 100.0Hz 4H, $SnCH_2Si$),), 1.71 (d, $^3J(^1H–^1H)$ = 8.0Hz, $^2J(^1H–^{117}Sn)$ = 64.0 Hz, $^2J(^1H–^{119}Sn)$ = 80.0 Hz, 4H, $SnCH_2$), 2.30 (m, 2H, CH), 3.36-3.72 (complex pattern, 40H, CH_2-O-CH_2), 4.23 (s, 4H, $Hcp_{-2,5}$), 4.38 (s, 4H, $Hcp_{-3,4}$). **$^{13}C\{^1H\}$ NMR** ($CDCl_3$, 100.63 MHz, 300 K) *δ*: 1.1 (CH_3), 16.2 (C17), 29.8 ($SiCH_2Sn$), 38.1 (C15), 70.2–70.8 (C2–C16), 72.3($C_{cp-3,4}$), 73.5 ($C_{cp-2,5}$), 74.1 (C_{cp-1}). **$^{29}Si\{^1H\}$ NMR** ($CDCl_3$, 59.63 MHz, 295.16 K) *δ*: –1.27. **$^{119}Sn\{^1H\}$ NMR** ($CDCl_3$, 111.89 MHz, 295.16 K) *δ*: –206.7. ESI-MS (MeCN, *m/z*); negative mode: 1694.2 $[Fc(Me_2SiCH_2SnI_2CH_2$-[16]-crown-5)$_2$·I]$^-$ **Anal. Calcd** for $C_{40}H_{70}O_{10}FeI_4Si_2Sn_2$ (1567.97): C 30.7; H 4.5. Found 31.1; H 4.6.

In situ reaction of 12 with one molar equivalent of CsF in $CDCl_3$.

CsF (4 mg, 0,03mmol) was added to a solution of **12** (40 mg, 0,03 mmol) in $CDCl_3$ (600 µL) and the mixture was studied by NMR spectroscopy.

$^{119}Sn\{^1H\}$ NMR ($CDCl_3$, 111.89 MHz, 294.16 K) *δ*: –197.53.

Reaction of 12 with two molar equivalent of NaI.

NaI (12 mg, 0,08 mmol) was added to a solution of **12** (63 mg, 0,04 mmol) and the mixture was stirred at room temperature over night. The solvent was evaporated in vacuo to give an orange solid.

^{1}H NMR ($CDCl_3$, 300.13 MHz, 295.16 K) *δ*: 0.48 (s, 12H, CH_3), 1.58 (s, 4H, $SnCH_2Si$),), 1.90 (d, $^{3}J(^{1}H–^{1}H)$ = 6.0Hz, 4H, $SnCH_2$), 2.30 (m, 2H, CH), 3.51-3.84 (complex pattern, 40H, CH_2-O-CH_2), 4.16 (s, 4H, $Hcp_{-2,5}$), 4.32 (s, 4H, $Hcp_{-3,4}$). **^{13}C{^{1}H} NMR** ($CDCl_3$, 100.63 MHz, 300 K) *δ*: 1.1 (CH_3), 17.02 (C17), 28.42 ($SiCH_2Sn$), 38.58 (C15), 68.30 (C_{cp-1}) 69.30–70.91 (C2–C16), 72.35 ($C_{cp-3,4}$), 74.10 ($C_{cp-2,5}$). **^{29}Si{^{1}H} NMR** ($CDCl_3$, 59.63 MHz, 295.16 K) *δ*: –1.06. **^{119}Sn{^{1}H} NMR** ($CDCl_3$, 111.92 MHz, 295.16 K) *δ*: –152.01.

Synthesis of ferrocenyl{[(dimethylsilyl)methyl][1,4,7,10,13-Pentaoxacyclohexadec-15-ylmethyl]dichloridostannylmethane}: $FcMe_2SiCH_2SnCl_2CH_2$-[16]-crown-5 (13).

To a solution of **11** (0.39 g, 0.47 mmol) in CH_3CN (20 mL) was added excess silver chloride, AgCl (0.20 g, 1.41 mmol). The resulting mixture was stirred at room temperature and in the dark for 14 days. After the AgI formed and the non reacted AgCl had been removed by filtration, the solvent was evaporated under vacuo to give 0.29 g (83%) of **13** as viscous red oil. The oil was dissolved in ethanol. Cooling the solution at -5°C gave 0.29 g (83%) of **13** as pure orange crystals, mp 83.6° C.

^{1}H NMR ($CDCl_3$, 400.13 MHz, 300 K) *δ*: 0.43 (s, 6H, CH_3), 0.90 (s, $^{2}J(^{1}H–^{119/117}Sn)$ = 111.0Hz 2H, $SnCH_2Si$), 1.30 (d, $^{3}J(^{1}H–^{1}H)$ = 9.0Hz, $^{2}J(^{1}H–^{117}Sn)$ = 75.0 Hz, $^{2}J(^{1}H–^{119}Sn)$ = 93.0 Hz, 2H, $SnCH_2$), 2.22 (m, 1H, CH), 3.33-3.65 (complex pattern, 20H, CH_2-O-CH_2), 4.18 (s, 5H, H_{cp}), 4.25 (s, 2H, $H_{cp-2,5}$), 4.40 (s, 2H, $H_{cp-3,5}$). **^{13}C{^{1}H} NMR** ($CDCl_3$, 75.47 MHz, 300 K) *δ*: 0.2 ($^{3}J(^{1}H–^{117/119}Sn)$ = 28.7 Hz, CH_3), 14.5 (C17), 26.6 ($SiCH_2Sn$), 35.9 ($^{2}J(^{13}C–^{117/119}Sn)$ = 33.2 Hz,C15), 68.8 (Ccp), 69.7–70.6 (C2–C16), 71.6 ($C_{cp-3,4}$), 73.5 (Ccp_{-1}), 73.8 ($C_{cp-2,5}$). **^{29}Si{^{1}H} NMR** ($CDCl_3$, 59.63 MHz, 297.16 K) *δ*: –2.3. **^{119}Sn{^{1}H} NMR** ($CDCl_3$, 111.89 MHz, 295 K) *δ*: –8.2. **ESI-MS** (MeCN, *m/z*); positive mode: 681.1 $\{FcMe_2SiCH_2Sn(OH)_2CH_2$-[16]-crown-5·Na$\}^{+}$, negative mode: 729.0 $\{FcMe_2SiCH_2SnCl_2CH_2$-[16]-crown-5·Cl$\}^{-}$ Anal. Calcd for $C_{25}H_{40}O_5FeCl_2SiSn$ (694.13): C 43.3; H 5.8. Found 43.3; H 5.9.

Synthesis of the ditopic complex $FcMe_2SiCH_2SnCl_2CH_2$-[16]-crown-5·LiCl (13·LiCl).

Lithium Chloride (15 mg, 0.35 mmol) was added to a solution of **13** (0.09 g, 0.13 mmol) in CH_3CN (8 mL) and the mixture was stirred at room temperature for two days. The reaction mixture was filtered and the solvent was evaporated under vacuo to give viscous orange oil. The latter was recrystallized from CH_3CN to give 66 mg (69%) of pure **5**·LiCl as red oil.

^{1}H NMR (CD_3CN, 400.13 MHz, 300 K) *δ*: 0.39 (s, $^2J(^1H–^{29}Si)$ = 117.0Hz 6H, CH_3), 1.12 (s, $^2J(^1H–^{119/117}Sn)$ = 102.0Hz 2H, $SnCH_2Si$), 1.47 (d, $^3J(^1H–^1H)$ = 9.0Hz, $^2J(^1H–^{117}Sn)$ = 72.0 Hz, $^2J(^1H–^{119}Sn)$ = 90.0 Hz, 2H, $SnCH_2$), 2.72 (m, 1H, CH), 3.62-3.72 (complex pattern, 20H, CH_2-O-CH_2), 4.21 (s, 7H, H_{cp}) $H_{cp-2,5}$,), 4.37 (s, 2H, $H_{cp-3,5}$). **^{29}Si{^{1}H} NMR** (CD_3CN, 59.63 MHz, 296.16 K) *δ*: –3.0. **^{119}Sn{^{1}H} NMR** (CD_3CN, 111.89 MHz, 295.16 K) *δ*: –124.2. **ESI-MS** (*m/z*); negative mode: 729.0 $\{FcMe_2SiCH_2SnCl_2CH_2$-[16]-crown-5·Cl$\}^–$, 736.1 $\{FcMe_2SiCH_2SnCl_2CH_2$-[16]-crown-5·LiCl$\}^-$ positive mode: 701.1 $\{FcMe_2SiCH_2SnCl_2CH_2$-[16]-crown-5·Li$\}^+$.

Synthesis of the trichlordiorganostannate complex $\{FcMe_2SiCH_2SnCl_2CH_2$-[16]-crown-5·Cl$\}^–\{Bu_4P\}^+$ $[13·Cl]^–[Bu_4P]^+$.

Tetrabutylphosphonium chloride (0,04 g, 0,14 mmol) was added to a solution of **13** (0,1 g, 0,14 mmol) in CH_3CN (10 mL) and the mixture was stirred at room temperature over night. The solvent was removed in vacuo to give an orange solid. Single crystals suitable for X-ray diffraction analysis were obtained by slow evaporation of the compound in ethanol to give 0.08 g (57%) of $[\mathbf{10}·Cl]^–[Bu_4P]^+$ as orange crystals, mp 112°C.

^{119}Sn{^{1}H} NMR ($CDCl_3$, 111.89 MHz, 295 K) *δ*: –25.3. **ESI-MS** (MeCN, *m/z*); negative mode: 711.1 $\{FcMe_2SiCH_2SnCl_2CH_2$-[16]-crown-5·OH$\}^–$, 729.1 $\{FcMe_2SiCH_2SnCl_2CH_2$-[16]-crown-5·Cl$\}^–$.

Synthesis of the trichloridorganostannate complex $\{FcMe_2SiCH_2SnCl_2CH_2$-[16]-crown-5·Cl$\}^–\{Ph_4P\}^+$ $[13·Cl]^–[Ph_4P]^+$.

Tetraphenylphosphonium chloride (0,05 g, 0,13 mmol) was added to a solution of **13** (0,09 g, 0,13 mmol) in CH_3CN (10 mL) and the mixture was stirred at room temperature over night. The reaction mixture was filtered and the solvent was

evaporated in vacuo to give 0.08 g (59%) of [**10**·Cl]$^-$[Ph_4P]$^+$ as a orange solid, mp 114°C.

^{119}Sn{^{1}H} NMR ($CDCl_3$, 111.89 MHz, 295 K) *δ*: –50.4.

In situ synthesis of the trichloridorganostannate complex {$FcMe_2SiCH_2SnCl_2CH_2$-[16]-crown-5·Cl}$^-${$(Ph_3P)_2N$}$^+$ ([13·Cl]$^-$[$(Ph_3P)_2N$]$^+$).

Bis(triphenylphosphonium)ammonium chloride (70 mg, 0.12 mmol) was added to a solution of **13** (80 mg, 0.12 mmol) in $CDCl_3$ (600 µL) and the mixture was studied by NMR spectroscopy.

^{119}Sn{^{1}H} NMR ($CDCl_3$, 111.92 MHz, 295.16 K) *δ*: –48.42.

Synthesis of 1,1'-Bis{[(dichlorido(1,4,7,10,13-Pentaoxacyclohexadec-15-ylmethyl)stannyl)methyl]dimethylsilyl}ferrocene fc($Me_2SiCH_2SnCl_2CH_2$-[16]-crown-5)$_2$ (14).

To a solution of **12** (0.25 g, 0.16 mmol) in CH_3CN (20 mL) was added excess silver chloride, AgCl (0.27 g, 1.91 mmol). The resulting mixture was stirred at room temperature and in the dark for 14 days. After the AgI formed and the non reacted AgCl had been removed by filtration, the solvent was evaporated under vacuo to give a viscous red oil. The oil was dissolved in ethanol. Cooling the solution at –5°C gave 0.16 g (84%) of **14** as orange crystals, mp 107.9°C.

^{1}H NMR ($CDCl_3$, 400.13 MHz, 300 K) *δ*: 0.50 (s, ^2J(^{1}H–^{29}Si) = 120.0Hz, 12H, CH_3), 0.94 (s, ^2J(^{1}H–$^{119/117}$Sn) = 108.0Hz 4H, $SnCH_2Si$), 1.34 (d, ^3J(^{1}H–^{1}H) = 8.0Hz, ^2J(^{1}H–^{117}Sn) = 80.0 Hz, ^2J(^{1}H–^{119}Sn) = 96.0 Hz 4H, $SnCH_2$), 2.25 (m, 2H, CH), 3.40-3.67 (complex pattern, 40H, CH_2-O-CH_2), 4.21 (s, 4H, $Hcp_{-2,5}$), 4.38 (s, 4H, $Hcp_{-3,4}$). **^{13}C{^{1}H} NMR** ($CDCl_3$, 100.63 MHz, 300 K) *δ*: 0.3 (CH_3), 14.3 (C17), 26.6 ($SiCH_2Sn$), 38.9 (^2J(^{13}C–$^{117/119}$Sn) = 29 Hz, C15), 69.6–70.5 (C2–C16), 71.3 (C_{cp-1}), 71.8 ($C_{cp-3,4}$), 73.4 ($C_{cp-2,5}$). **^{29}Si{^{1}H} NMR** ($CDCl_3$, 59.63 MHz, 294.16 K) *δ*: –2.03. **^{119}Sn{^{1}H} NMR** ($CDCl_3$, 111.89 MHz, 294.16 K) *δ*: –9.9. **ESI-MS** (MeCN, *m/z*); positive mode: 1093.3, [Fc($Me_2SiCH_2SnOHCH_2$-[16]-crown-5)$_2$]$^{2+}$, negative mode: 1237.2 [Fc($Me_2SiCH_2SnCl_2CH_2$-[16]-crown-5)$_2$·Cl]$^-$. **Anal. Calcd** for $C_{40}H_{70}O_{10}FeCl_4Si_2Sn_2$ (1202.17): C 39.9; H 5.9. Found 39.8; H 6.0.

Synthesis of the diaqua complex 14·2H_2O.

14·2H_2O was obtained as byproduct from the reaction of **6** with 2 molar equivalents of tetraphenylphosphonium chloride. Single crystals suitable for X-ray diffraction analysis were obtained by slow evaporation of the compound in ethanol at room temperature. mp 107.8°C.

^{1}H NMR (CD_3CN, 500.13 MHz, 300 K) *δ*: 0.49 (s, $^2J(^1H–^{29}Si)$ = 120.0Hz, 12H, CH_3), 1.06 (s, $^2J(^1H–^{119/117}Sn)$ = 110.0Hz 4H, $SnCH_2Si$), 1.40 (d, $^3J(^1H–^1H)$ = 5.0Hz, $^2J(^1H–^{117}Sn)$ = 85.0 Hz, $^2J(^1H–^{119}Sn)$ = 95.0 Hz 4H, $SnCH_2$), 2.28 (m, 2H, CH), 3.44-3.62 (complex pattern, 40H, CH_2-O-CH_2), 4.26 (s, 4H, $Hcp_{-2,5}$), 4.43 (s, 4H, $Hcp_{-3,4}$). **^{13}C{^{1}H} NMR** (CD_3CN, 125.77 MHz, 300 K) *δ*: 0.3 (CH_3), 15.1 (C17), 28.1 ($SiCH_2Sn$), 36.2 (C15), 70.2–70.6 (C2–C16), 72.2 (C_{cp-1}), 73.7 ($C_{cp-3,4}$), 73.8 ($C_{cp-2,5}$). **^{29}Si{^{1}H} NMR** (CD_3CN, 59.63 MHz, 294.16 K) *δ*: –1.96. **^{119}Sn{^{1}H} NMR** (CD_3CN, 111.92 MHz, 294.16 K) *δ*: –27.1. **Anal. Calcd** for $C_{80}H_{144}O_{10}Fe_2Cl_8Si_4Sn_4$ (2440.39): C 39.4; H 5.9. Found 39.4; H 5.9.

Synthesis of the ditopic complex fc($Me_2SiCH_2SnCl_2CH_2$-[16]-crown-5)$_2$·LiCl (14·2LiCl).

Lithium Chloride (0,01 g, 0.23 mmol) was added to a solution of **14** (0.07 g, 0.06 mmol) in CH_3CN (7 mL) and the mixture was stirred at room temperature for two days. The reaction mixture was filtered and the solvent was evaporated under vacuo to give 49 mg (66%) of pure **6**·2LiCl as a red oil.

^{1}H NMR (CD_3CN, 400.13 MHz, 400 K) *δ*: 0.42 (s, $^2J(^1H–^{29}Si)$ = 120.0Hz, 12H, CH_3), 1.16 (s, $^2J(^1H–^{119/117}Sn)$ = 120.0Hz, 4H, $SnCH_2Si$), 1.48 (d, $^3J(^1H–^1H)$ = 8.0Hz, $^2J(^1H–^{117}Sn)$ = 80.0 Hz, $^2J(^1H–^{119}Sn)$ = 88.0 Hz 4H, $SnCH_2$), 2.79 (m, 2H, CH), 3.60-3.78 (complex pattern, 40H, CH_2-O-CH_2), 4.25 (s, 4H, $Hcp_{-2,5}$), 4.44 (s, 4H, $Hcp_{-3,4}$). **^{13}C{^{1}H} NMR** (CD_3CN, 100.63 MHz, 300 K) *δ*: 0.9 (CH_3), 23.2 (C17), 35.3 ($SiCH_2Sn$), 35.8 (C15), 68.3–69.8 (C2–C12), 72.28($C_{cp-3,4,}$ C_{cp-1}), 74.1 ($C_{cp-2,5}$), 77.5 ($^3J(^{13}C–^{119/117}Sn)$ = 95 Hz, C14/16). **^{29}Si{^{1}H} NMR** (CD_3CN, 59.63 MHz, 294.16 K) *δ*: –2.64. **^{119}Sn{^{1}H} NMR** (CD_3CN, 111.89 MHz, 294.16 K) *δ*: –129.1. **ESI-MS** (MeCN, *m/z*); positive mode: 1237.2 $\{Fc(Me_2SiCH_2SnCH_2$-[16]-crown-5)$_2$·$(CH_2Cl_2)_2$·$Li\}^{2+}$, negative mode: 1257.2 $\{Fc(Me_2SiCH_2SnCl_2CH_2$-[16]-crown-5)$_2$·Cl·$H_2O$·$H_2\}^-$. **Anal. Calcd** for $C_{40}H_{70}O_{10}FeCl_6Si_2Sn_2$·2$H_2O$ (1323.04): C 36.3; H 5.7. Found 36.5; H 5.9.

In situ synthesis of the triichlordiorganostannate complex {fc($Me_2SiCH_2SnCl_2CH_2$-[16]-crown-5)$_2$·Cl}$^-${Bu_4P}$^+$ ([14·Cl]$^-$[Bu_4P]$^+$.

Tetrabutylphosphonium chloride (40 mg, 0.02 mmol) was added to a solution of **14** (90 mg, 0.08 mmol) in CD_3CN (600 µL) and the mixture was studied by NMR spectroscopy.

^{119}Sn{^{1}H} NMR (CD_3CN, 111.89 MHz, 294.16 K) *δ*: –199.45.

Reaction of 14 with two molar equivalent of Ph_4PCl.

Tetraphenylphosphonium chloride (81 mg, 0,22 mmol) was added to a solution of **14** (130 mg, 0.11 mmol) and the mixture was stirred at room temperature over night. The reaction mixture was filtered and the solvent was evaporated in vacuo to give 0,08 g (31%) of pure **14**·2H_2O as orange solid. mp = 107,5°C.

^{1}H NMR (CD_3CN, 500.13 MHz, 300 K) *δ*: 0.49 (s, ^4J(^{1}H–$^{117/119}$Sn) = 120.0Hz, 12H, CH_3), 1.06 (s, ^2J(^{1}H–$^{119/117}$Sn) = 110.0Hz 4H, $SnCH_2Si$), 1.40 (d, ^3J(^{1}H–^{1}H) = 5.0Hz, ^{2}J(^{1}H–^{117}Sn) = 85.0 Hz, ^2J(^{1}H–^{119}Sn) = 95.0 Hz 4H, $SnCH_2$), 2.28 (m, 2H, CH), 3.44-3.62 (complex pattern, 40H, CH_2-O-CH_2), 4.26 (s, 4H, $Hcp_{-2,5}$), 4.43 (s, 4H, $Hcp_{-3,4}$). **^{13}C{^{1}H} NMR** (CD_3CN, 100.63 MHz, 300 K) *δ*: 0.1 (CH_3), 16.0 (C17), 28.1 ($SiCH_2Sn$), 36.2 (C15), 69.6–70.5 (C2–C16), 72.2 ($C_{cp-3,4}$), 73.7 (C_{cp-1}), 73.8 ($C_{cp-2,5}$). **^{29}Si{^{1}H} NMR** (CD_3CN,, 59.63 MHz, 294.16 K) *δ*: –1.96. **^{119}Sn{^{1}H} NMR** (CD_3CN, 111.89 MHz, 294.16 K) *δ*: –27. Anal. Calcd for $C_{80}H_{144}O_{22}Fe_2Cl_8Si_4Sn_4$ (1202.17): C 39.4; H 5.9. Found 39.4; H 5.9.

Synthesis of the trichloridorganostannate complex {Fc($Me_2SiCH_2SnCl_2CH_2$-[16]-crown-5)$_2$·2Cl}$^-${2($Ph_3P)_2N$}$^+$ ([14·Cl]$^-$[2($Ph_3P)_2N$]$^+$).

Bis(triphenylphosphonium)ammonium chloride (50 mg, 0.09 mmol) was added to a solution of **14** (50 mg, 0.04 mmol) in $CDCl_3$ (600 µL) and the mixture was studied by NMR spectroscopy.

^{1}H NMR ($CDCl_3$, 300.13 MHz, 294.16 K) *δ*: 0.40 (s, 12H, CH_3), 0.94 (s, ^2J(^{1}H–$^{119/117}$Sn) = 120.0Hz 4H, $SnCH_2Si$), 1.32 (d, ^3J(^{1}H–^{1}H) = 9.0Hz, ^2J(^{1}H–^{117}Sn) = 84.0 Hz, ^2J(^{1}H–^{119}Sn) = 96.0 Hz 4H, $SnCH_2$), 2.35 (m, 2H, CH), 3.32-3.51 (complex pattern, 40H, CH_2-O-CH_2), 4.05 (s, 4H, $Hcp_{-2,5}$), 4.22 (s, 4H, $Hcp_{-3,4}$). 7.38-7.56

(complex pattern, 60H, Ph_3P). **$^{29}Si\{^1H\}$ NMR** ($CDCl_3$, 59.63 MHz, 294.16 K) *δ*: –2.22. **$^{119}Sn\{^1H\}$ NMR** ($CDCl_3$, 111.92 MHz, 294.16 K) *δ*: –67.

In situ synthesis of the triichlordiorganostannate complex $\{Fc(Me_2SiCH_2SnCl_2CH_2\text{-}[16]\text{-crown-}5)_2\cdot 2Cl\}^-\{2Ph_4P\}^+$ ($[14\cdot Cl]^-[\ 2Ph_4P]^+$).

Tetraphenylphosphonium chloride (31 mg, 0,08 mmol) was added to a solution of **14** (50 mg, 0.04 mmol) and the mixture was studied by NMR spectroscopy.

$^{119}Sn\{^1H\}$ NMR ($CDCl_3$, 111.88 MHz, 294.16 K) *δ*: –186.

In situ reaction of 14 with two molar equivalent of NaCl in CD_3CN.

NaCl (6 mg, 0,12 mmol) was added to a solution of **14** (70 mg, 0,06 mmol) in CD_3CN (600 µL) and the mixture was studied by NMR spectroscopy.

$^{119}Sn\{^1H\}$ NMR ($CDCl_3$, 111.88 MHz, 294.16 K) *δ*: –11.

In situ reaction of 14 with four molar equivalent of NaCl in CD_3CN.

NaCl (13 mg, 0,23 mmol) was added to a solution of **14** (70 mg, 0,06 mmol) in CD_3CN (600 µL) and the mixture was studied by NMR spectroscopy.

$^{119}Sn\{^1H\}$ NMR (CD_3CN, 111.92 MHz, 294.16 K) *δ*: – 41.

In situ reaction of 14 with two molar equivalent of CsCl in CD_3CN.

CsCl (17 mg, 0,09 mmol) was added to a solution of **14** (59 mg, 0,05 mmol) in CD_3CN (600 µL) and the mixture was studied by NMR spectroscopy.

$^{119}Sn\{^1H\}$ NMR ($CDCl_3$, 111.89 MHz, 295.16 K) *δ*: –35.

Synthesis of 1-phenyl-1-(1,4,7,10-tetraoxacyclotridec-12-ylmethyl)-3,3,14,14-tetramethyl-3,14-disila-1-stanna[5,5]-ferrocenophane, $fc[(Si(Me)_2CH_2)_2SnPhCH_2$-[13]-crown-4] (19).

A Solution of $fc(SiMe_2CH_2MgCl)_2$ prepared from $fc(SiMe_2CH_2Cl)_2$[130] (0,48 g, 1,23 mmol) and magnesium (0,12 g, 4,9 mmol) in THF (20 mL), was added dropwise to a stirred solution of PhI_2SnCH_2-[13]-crown-4[149] (0,80 g, 1,23 mmol) in THF (40 mL). After the addition had been completed, the reaction mixture was heated at reflux overnight and then cooled to room temperature. Cold water (30 mL) was added and

the mixture was extracted two times with 40 mL of dichloromethane. The combined organic phases were dried with $MgSO_4$ and filtered, and the solvents evaporated in *vacuo* to give the crude product. The latter was purified by column chromatography [SiO_2, isohexane/ethylacetate (3/1)] to yield 0.36 g (40%) of pure **19** as red viscous oil.

^{1}H NMR ($CDCl_3$, 400.13 MHz, 300 K) *δ*: 0.12 (s, 6H, CH_3), 0.20 (s, 6H, CH_3), 0.33/0.42 (AB type resonance, $^2J(^1H–^1H)$ = 36.0Hz, 2H, $SnCH_2Si$), 1.13 (d, $^3J(^1H–^1H)$ = 8.0Hz, $^2J(^1H–^{117}Sn)$ = 48.0 Hz, $^2J(^1H–^{119}Sn)$ = 64.0 Hz, 2H, $SnCH_2$), 2.10 (m, 1H, CH), 3.35–3.60 (complex pattern, 16H, CH_2-O-CH_2), 4.09 (s, 4H, $H_{Cp–2,5}$), 4.30 (complex pattern, 4H, $H_{Cp–3,4}$), 7.26–7.61(m, 5H, Ph). **^{13}C{^{1}H} NMR** ($CDCl_3$, 100.63 MHz, 300 K) *δ*: –3.6 (CH3), 2.0 ($^1J(^{13}C–^{117/119}Sn)$ = 22 Hz, $SiCH_2Sn$), 2.27 ($^1J(^{13}C–^{117/119}Sn)$ = 20 Hz, $SiCH_2Sn$), 13.5 (C14), 37.3 ($^2J(^{13}C–^{117/119}Sn)$ = 18 Hz, C12), 69.1–70.0 (C2–C9), 70.1($C_{cp–1}$), 70.3 ($C_{cp–1}$), 71.5 ($^3J(^{13}C–^{117}Sn)$ = 43 Hz, $^3J(^{13}C–^{119}Sn)$ = 51 Hz, C11/C13), 73.5 ($C_{cp–3,4}$), 73.9 ($C_{cp–2,5}$), 127.9 ($^3J(^{13}C–^{117}Sn)$ = 46 Hz, Cm), 128.0 (Cp), 135.7 ($^3J(^{13}C–^{117}Sn)$ = 34 Hz, C_o), 143.2. **^{29}Si{^{1}H} NMR** ($CDCl_3$, 59.63 MHz, 296 K) *δ*: 0.1. **^{119}Sn{^{1}H} NMR** ($CDCl_3$, 111.92 MHz, 296 K) *δ*: –25. Anal. Calcd for $C_{32}H_{48}FeO_4Si_2Sn$ (727.37): C 52.8; H 6.7. Found: C 52.0; H 6.7.

Synthesis of 1-Iodido-1-(1,4,7,10-tetraoxacyclotridec-12-ylmethyl)-3,3,14,14-tetramethyl-3,14-disila-1-stanna[5,5]-ferrocenophane, fc[(Si(Me)$_2$CH$_2$)$_2$SnICH$_2$-[13]-crown-4] (20).

Over a period of two hours, iodine (42 mg, 0.17 mmol) was added in small portions at 0°C to a stirred solution of **19** (0.12 g, 0.17 mmol) in CH_2Cl_2 (20 mL). Stirring was continued and the reaction mixture was warmed to room temperature overnight. Dichloromethane and iodobenzene were removed in *vacuo* (10^{-3} mmHg) to afford an orange solid. Recrystallization from ethanol at –5°C gave 0.12 g (92%) of pure **20** as orange crystals. mp 122.6 °C.

^{1}H NMR ($CDCl_3$, 400.13 MHz, 300 K) *δ*: 0.23 (s, 6H, CH_3), 0.36 (s, 6H, CH_3), 0.92 (d, $^3J(^1H–^1H)$ = 8.0Hz,$^2J(^1H–^{117/119}Sn)$ = 88.0 Hz, 4H, $SnCH_2Si$), 1.50 (d, $^3J(^1H–^1H)$ = 4.0Hz, $^2J(^1H–^{117}Sn)$ = 40.0 Hz, $^2J(^1H–^{119}Sn)$ = 56.0 Hz, 2H, $SnCH_2$), 2.43 (m, $^3J(^1H–^{117/119}Sn)$ = 84.0 Hz, 1H, CH), 3.48–3.76 (complex pattern, 16H, CH_2-O-CH_2), 4.02 (s, 2H, $H_{Cp–2}$), 4.33 (s, 2H, $H_{Cp–5}$), 4.35 (s, 4H, $H_{Cp–3,4}$). **^{13}C{^{1}H} NMR** ($CDCl_3$, 100.63 MHz, 300 K) *δ*: 2.2 (CH_3), 2.9 (CH_3), 6.9 ($SiCH_2Sn$), 21.9 (C14), 38.3 ($^2J(^{13}C–$

$^{117/119}$Sn) = 26 Hz, C12), 69.7–71.2 (C2–C9), 71.3 (C_{cp-1}), 71.6 ($^3J(^{13}C–^{117/119}Sn)$ = 52 Hz, C11/C13), 73.7 ($C_{cp-3,4}$), 74.5 ($C_{cp-2,5}$). **^{29}Si {^{1}H} NMR** ($CDCl_3$, 59.63 MHz, 296 K) *δ*: –0.8. **^{119}Sn {^{1}H} NMR** ($CDCl_3$, 111.92 MHz, 296 K) *δ*: 31. **ESI-MS** (MeCN, *m/z*); positive mode: 651.1 $\{Fc[Si(Me)_2(CH_2)_2SnCH_2$-[13]-crown-4]$\}^+$, 668.1 $\{Fc[Si(Me)_2(CH_2)_2SnCH_2$-[13]-crown-4·OH]$\}^+$, 691·1 $\{Fc[Si(Me)_2(CH_2)_2SnCH_2$-[13]-crown-4·OH·Na]$\}^+$. Anal. Calcd for $C_{26}H_{43}FeIO_4Si_2Sn$ (777.22): C 40.2; H 5.6. Found: C 40.3; H 5.6.

Synthesis of 1-Chlorido-1-(1,4,7,10-tetraoxacyclotridec-12-ylmethyl)-3,3,14,14-tetramethyl-3,14-disila-1-stanna[5,5]-ferrocenophane, fc[$(Si(Me)_2CH_2)_2SnClCH_2$-[13]-crown-4] (21).

A solution of **20** (0.52 g, 0.67 mmol) in CH_3CN (25 mL) was added excess silver chloride, AgCl (0.29 g, 2 mmol). The resulting mixture was stirred at room temperature and in dark for 14 days. After the AgI formed and the non-reacted AgCl had been removed by filtration the solvent was evaporated in *vacuo* (10^{-3} mmHg) to afford an orange solid. Recrystallisation from ethanol at –5°C gave 0.4 g (87%) of pure **21** as orange crystals. mp 131.5 °C.

^{1}H NMR ($CDCl_3$, 400.13 MHz, 300 K) *δ*: 0.23 (s, 6H, CH_3), 0.37 (s, 6H, CH_3), 0.59 (s, $^2J(^1H–^{117}Sn)$ = 72.0 Hz, $^2J(^1H–^{119}Sn)$ = 96.0 Hz, 4H, $SnCH_2Si$), 1.28 (d, $^3J(^1H–^1H)$ = 8.0Hz, $^2J(^1H–^{117}Sn)$ = 64.0 Hz, $^2J(^1H–^{119}Sn)$ = 72.0 Hz, 2H, $SnCH_2$), 2.24 (m, $^3J(^1H–^{117/119}Sn)$ = 120.0 Hz, 1H, CH), 3.59–3.73 (complex pattern, 16H, CH_2-O-CH_2), 4.06 (s, 2H, H_{Cp-2}), 4.35 (s, 4H, $H_{Cp-3,4}$), 4.52 (s, 2H, H_{Cp-5}). **^{13}C{^{1}H} NMR** ($CDCl_3$, 100.63 MHz, 300 K) *δ*: -2.04 (CH_3), 3.46 (CH_3), 6.35 ($^1J(^{13}C–^{117}Sn)$ = 306 Hz, $^1J(^{13}C–^{119}Sn)$ = 322 Hz $SnCH_2Si$), 22.79 ($^1J(^{13}C–^{117}Sn)$ = 427 Hz, $^1J(^{13}C–^{119}Sn)$ = 447 Hz, C14), 37.2 ($^3J(^{13}C–^{117/119}Sn)$ = 24 Hz, C12), 69.6–70.6 (C2–C9), 71.4 (C_{cp-1}), 71.8 ($^3J(^{13}C–^{117/119}Sn)$ = 40 Hz,C11/C13), 74.1 ($C_{cp-2,5,}$ $C_{cp-3,4}$). **^{29}Si{^{1}H} NMR** ($CDCl_3$, 59.63 MHz, 294.16 K) *δ*: 0.0. **^{119}Sn{^{1}H} NMR** ($CDCl_3$, 111.92 MHz, 294.16 K) *δ*: 84 **ESI-MS** (MeCN, *m/z*); positive mode: 651.1 $\{fc[Si(Me)_2(CH_2)_2SnCH_2$-[13]-crown-4]$\}^+$; negative mode: 721.0, $\{fc[(Si(Me)_2CH_2)_2SnClCH_2$-[13]-crown-4·Cl]$\}^-$. Anal. Calcd for $C_{26}H_{43}FeClO_4Si_2Sn$(685.77): C 45.5; H 6.3. Found: C 45.2; H 6.3.

Synthesis of 1-Fluorido-1-(1,4,7,10-tetraoxacyclotridec-12-ylmethyl)-3,3,14,14-tetramethyl-3,14-disila-1-stanna[5,5]-ferrocenophane, fc[(Si(Me)$_2$CH$_2$)$_2$SnFCH$_2$-[13]-crown-4] (22).

A solution of **20** (0.11 g, 0.14 mmol) in CH_2Cl_2 (10 mL) was mixed with a solution of KF (0.08 g, 1.42 mmol) in water (15 mL). The biphasic mixture was stirred at room temperature for four days. The organic phase was then separated, dried over $MgSO_4$, and filtered. Removing the solvent in vacuo afforded orange viscous oil. The latter was dissolved in toluene. Slow evaporation of this solution afforded 0.06 g (63%) of **22** as orange crystals. mp 127.4°C.

^{1}H NMR ($CDCl_3$, 400.13 MHz, 300 K) *δ*: 0.20 (s, 6H, CH_3), 0.34 (s, 6H, CH_3), 0.41 (complex pattern, 4H, $SnCH_2Si$), 1.11 (d, $^3J(^1H–^1H)$ = 8.0Hz, $^2J(^1H–^{117}Sn)$ = 72.0 Hz, $^2J(^1H–^{119}Sn)$ = 80.0 Hz, 2H, $SnCH_2$), 2.24 (m, $^3J(^1H–^{117/119}Sn)$ = 136.0 Hz , 1H, CH), 3.46–3.72 (complex pattern, 16H, CH_2-O-CH_2), 4.08 (s, 2H, $H_{Cp–2}$), 4.31 (s, 2H, $H_{Cp–3}$), 4.34 (s, 2H, $H_{Cp–4}$), 4.62 (s, 2H, $H_{Cp–5}$).**^{13}C{^{1}H} NMR** ($CDCl_3$, 100.63 MHz, 300 K) *δ*: 1.5 (CH3), 1.6 ($^3J(^{13}C–^{117/119}Sn)$ = 91Hz, CH3), 4.7 ($SiCH_2Sn$), 4.8 ($^1J(^{13}C–^{119}Sn)$ = 306 Hz, $SiCH_2Sn$), 18.5 (C14), 18.6 ($^1J(^{13}C–^{117}Sn)$ = 497 Hz, $^1J(^{13}C–^{119}Sn)$ = 527 Hz, C14), 36.6 ($^3J(^{13}C–^{117/119}Sn)$ = 25 Hz, C12), 36.7 ($^3J(^{13}C–^{117/119}Sn)$ = 25 Hz, C12), 66.27 (Cp_{-1}), 69.4–72.0 (C2–C9), 71.8 ($^3J(^{13}C–^{117}Sn)$ = 43 Hz,C11/C13), 73.8 ($C_{cp–3,4}$), 74.0 ($C_{cp–2,5}$), 74.1 ($^3J(^{13}C–^{117}Sn)$ = 20 Hz,C11/C13),). **^{19}F{^{1}H} NMR** ($CDCl_3$, 282.40 MHz, 295 K) *δ*: –176.0 ($^1J(^{19}F–^{117}Sn)$ = 2115 Hz, ($^1J(^{19}F–^{119}Sn)$ = 2214 Hz), **^{29}Si{^{1}H} NMR** ($CDCl_3$, 59.63 MHz, 295.16 K) *δ*: – 0.1. **^{119}Sn{^{1}H} NMR** ($CDCl_3$, 111.92 MHz, 296 K) *δ*: 64 ($^1J(^{119}Sn–^{19}F)$ = 2210 Hz). **ESI-MS** (MeCN, *m/z*); positive mode: 651.1 {fc[Si(Me)$_2$(CH$_2$)$_2$SnCH$_2$-[13]-crown-4]}$^+$, 670.1 {fc[(Si(Me)$_2$CH$_2$)$_2$SnCH$_2$-[13]-crown-4]}$^+$ Anal. Calcd for $C_{26}H_{43}FFeO_4Si_2Sn$ (669.32): C 46.7; H 6.5. Found: C 46.6; H 6.5.

Synthesis of the Ditopic Complex fc[(Si(Me)$_2$CH$_2$)$_2$SnClCH$_2$-[13]-crown-4·LiCl] ([21·LiCl]).

Lithium chloride (0.02 g, 0.47 mmol) was added to a solution of **21** (0.14 g, 0.20 mmol) in CH_3CN (8 mL), and the mixture was stirred at room temperature over night. After filtration of excess salt, slow evaporation of acetonitrile at room temperature provided 0.09 g (61 %) of pure [**21**·LiCl] as orange crystals, mp 211.7° C.

^{1}H NMR (CD_3CN, 400.13 MHz, 300 K) *δ*: 0.27 (s, $^{2}J(^{1}H–^{29}Si)$ = 120.0 Hz, 12H, CH_3), 0.74 (s, $^{2}J(^{1}H–^{117/119}Sn)$ = 96.0 Hz, 4H, $SnCH_2Si$), 1.17 (d, $^{3}J(^{1}H–^{1}H)$ = 8.0Hz, $^{2}J(^{1}H–^{117}Sn)$ = 56.0 Hz, $^{2}J(^{1}H–^{119}Sn)$ = 72.0 Hz, 2H, $SnCH_2$), 2.68 (m, $^{3}J(^{1}H–^{117/119}Sn)$ = 80.0 Hz, 1H, CH), 3.42–3.79 (complex pattern, 16H, CH_2-O-CH_2), 4.33 (s, 2H, $H_{Cp–2,5}$), 4.43 (s, 4H, $H_{Cp–3,4}$). **^{13}C{^{1}H} NMR** (CD_3CN, 100.63 MHz, 300 K) *δ*: 2.3 (CH3), 10.9 ($SnCH_2Si$), 25.4 (C14), 36.6 ($^{3}J(^{13}C–^{117/119}Sn)$ = 21 Hz, C12), 67.9–68.6 (C2–C9), 70.9 ($C_{cp–3,4}$), 72.1 ($C_{cp–1}$), 74.2 ($C_{cp–2,5}$),76.6 ($^{3}J(^{13}C–^{117/119}Sn)$= 51 Hz,C11/C13). **^{29}Si{^{1}H} NMR** (CD_3CN, 59.63 MHz, 294.16 K) *δ*: –1.1. **^{119}Sn{^{1}H} NMR** (CD_3CN, 111.92 MHz, 294.16 K) *δ*: –27.84. **ESI-MS** (MeCN, *m/z*); positive mode: 693.1 {fc[$Si(Me)_2(CH_2)_2SnCH_2$-[13]-crown-4]·Li}$^{+}$, 1395.3 {[fc[$(Si(Me)_2CH_2)_2Sn$(*μ*–Cl)CH_2-[13]-crown-4]$_2$·Na]}$^{–}$ **ESI-MS** (MeCN, *m/z*); negative mode: 721.1 {fc[$Si(Me)_2(CH_2)_2SnClCH_2$-[13]-crown-4]·Cl}$^{-}$, 728.1 {fc[$Si(Me)_2(CH_2)_2SnClCH_2$-[13]-crown-4]·LiCl}$^{-}$ Anal. Calcd for $C_{26}H_{43}Cl_2FeLiO_4Si2Sn$ (728.16): C 42.9; H 6.0. Found: C 42.8; H 6.1.

In situ reaction of 22 with one molar equivalent of $Et_4NF·2H_2O$ in CD_2Cl_2.

$Et_4NF·2H_2O$ (14 mg, 0,08 mmol) was added to a solution of **22** (50 mg, 0,08 mmol) in CD_2Cl_2 (600 µL) and the mixture was studied by NMR spectroscopy.

^{19}F{^{1}H} NMR (CD_2Cl_2, 282.40 MHz, 189 K) *δ* –113.6 (s, $^{1}J(^{19}F–^{117/119}Sn$ = 1748 Hz Hz). **^{119}Sn{^{1}H} NMR** (CD_2Cl_2, 111.92 MHz, 189 K) *δ* –121 (t, $^{1}J(^{119}Sn–^{19}F)$ = 1737 Hz).

In situ reaction of 22 with one molar equivalent of LiF in CD_3CN.

LiF (1.6 mg, 0,06 mmol) was added to a solution of **22** (40 mg, 0,06 mmol) in CD_3CN (600 µL) and the mixture was studied by NMR spectroscopy.

^{19}F{^{1}H} NMR (CD_3CN, 282.36 MHz, 295.16 K) *δ* –113.6 (s, $^{1}J(^{19}F–^{117}Sn$ = 2115 Hz, $^{1}J(^{19}F–^{119}Sn$ = 2214 Hz). **^{119}Sn{^{1}H} NMR** (CD_3CN, 111.92 MHz, 295.16 K) *δ* –60 (d, $^{1}J(^{119}Sn–^{19}F)$ = 2209 Hz).

Synthesis of Dibromo(1,4,7,10,13-pentaoxacyclohexadec-15-yl-methyl)phenylstannane, $PhBr_2SnCH_2$-[16]-crown-5 (23)

To a cooled solution (–55°C) of Ph_3SnCH_2-[16]-crown-5 (2 g, 3.35 mol) in dichloromethane (60 mL) was added drop-wise a solution of bromide (1.07 g, 6.70

mol) in dichloromethane (20 mL). After the addition had been completed, the mixture was stirred and warmed to room temperature overnight. From the slightly yellow solution obtained, the solvent and the bromobenzene were removed in vacuo (10^{-3} mmHg) to afford a yellow solid. Crystals of **23** (1.29 g, 64%) suitable for X-ray diffraction analysis were obtained by slow evaporation of a solution of the compound in CH_2Cl_2 at room temperature. mp 185°C.

^{1}H NMR (CD_2Cl_2, 300.13 MHz, 276.16 K) *δ*: 1.98 (d, $^{3}J(^{1}H–^{1}H)$ = 6.0Hz, $^{2}J(^{1}H–^{117}Sn)$ = 90.0 Hz, $^{2}J(^{1}H–^{119}Sn)$ = 96.0 Hz, 2H, $SnCH_2$), 2.63 (m, 1H, C15), 3.46-3.94 (complex pattern, 20H, CH_2-O-CH_2), 7.39–7.90 (complex pattern, 5H, Ph). **^{13}C{^{1}H} NMR** (CD_2Cl_2, 75.47 MHz, 276.16 K) *δ*: 30.04 (C17), 36.34 ($^{2}J(^{13}C–^{117/119}Sn)$ = 48.3 Hz, C15), 69.55–70.17 (C2–C12), 73.61 ($^{3}J(^{13}C–^{117/119}Sn)$ = 64.1 Hz, C14/C16), 128.51 ($^{3}J(^{13}C–^{117}Sn)$ = 90,6 Hz, $^{3}J(^{13}C–^{119}Sn)$ = 94,3 Hz, C_m), 130.10($^{4}J(^{13}C–^{117/119}Sn)$ = 19,6 Hz C_p), 135.85 ($^{2}J(^{13}C–^{117/119}Sn)$ = 67.2 Hz, C_o), 143.73 (C_i). **^{119}Sn{^{1}H} NMR** (CD_2Cl_2, 111.92 MHz, 296.16 K) *δ*: –168.13. **Anal. Calcd** for $C_{18}H_{28}Br_2O_5Sn$ (602.9): C 35.9; H 4.7. Found 35.8; H 4.8.

In situ reaction of 23 with two molar equivalent of Ph_4PhBr in CD_2Cl_2

Ph_4PhBr (35 mg, 0,08 mmol) was added to a solution of **23** (50 mg, 0,08 mmol) in CD_2Cl_2 (600 µL) and the mixture was studied by NMR spectroscopy.

^{119}Sn{^{1}H} NMR (CD_2Cl_2, 111.92 MHz, 295.16 K) *δ*: –235.

In situ reaction of 23 with two molar equivalent of NaBr in CD_2Cl_2.

NaBr (9 mg, 0,08 mmol) was added to a solution of **23** (50 mg, 0,08 mmol) in CD_2Cl_2 (600 µL) and the mixture was studied by NMR spectroscopy.

^{119}Sn{^{1}H} NMR (CD_2Cl_2, 111.92 MHz, 295.16 K) *δ*: –162.

In situ reaction of 23 with two molar equivalent of LiBr in CD_2Cl_2

LiBr (7 mg, 0,08 mmol) was added to a solution of **23** (50 mg, 0,08 mmol) in CD_2Cl_2 (600 µL) and the mixture was studied by NMR spectroscopy.

^{119}Sn{^{1}H} NMR (CD_2Cl_2, 111.92 MHz, 295.16 K) *δ*: –169.

Synthesis of 12,25-bis{[dichlorophenylstannyl]methyl}-1,4,7,10,14,17,20,23-octaoxa-cyclohexacosane, [($PhCl_2SnCH_2)_2$]-[26]-crown-8 (25).

To a solution of [($PhI_2SnCH_2)_2$]-[26]-crown-8 (0.13 g, 0.10 mmol) in CH_3CN (15 mL) was added excess silver chloride, AgCl (0.17 g, 1.2 mmol). The resulting mixture was stirred at room temperature and in the dark for 14 days. After the AgI formed and the non-reacted AgCl had been removed by filtration, the solvent was evaporated in vacuo to afford a white solid. Recrystallization from CH_2Cl_2/*n*-Hexane by slow evaporation at room temperature gave 0.04g (44%) of {($PhCl_2SnCH_2)_2$}-[26]-crown-8 as colorless crystalline solid, m.p. 154°C.

^{1}H-NMR ($CDCl_3$, 300.13 MHz, 297 K) *δ*: 1.87 (d, $^3J(^1H–^1H)$ = 6.0 Hz, $^2J(^1H–^{117}Sn)$ = 78.0 Hz, $^2J(^1H–^{119}Sn)$ = 96.0 Hz, 4H, Sn-CH_2), 2.60 (m, 2H, CH), 3.50–3.71 (complex pattern, 32H, CH_2-O-CH_2), 7.42–7.95 (m, 10H, Ph). **^{13}C{^{1}H}-NMR** ($CDCl_3$, 125.68 MHz, 300 K) *δ*: 25.6 (C27/C28), 36.5 (C12/C25), 69.1–69.6 (C2–C22), 72.9 (C11/C13, C24/C26), 127.9 ($^3J(^{13}C–^{117/119}Sn)$ = 11 Hz, Cm), 129.4 (Cp), 134.0 (65 Hz, Co), 134.1 (Ci). **^{119}Sn{^{1}H}-NMR** ($CDCl_3$, 111.89 MHz, 295 K) *δ*: -111.

2.8. References

(1) Pedersen, C. J. *J. Am. Chem. Soc.,* **1967**, *89*, 2495.

(2) Lehn, J.-M. *Supramolecular Chemistry: Concepts and Perspectives*; VCH ed. Weinheim, **1995**.

(3) Steed, J. W.; Atwood, J. L. *Supramolecular Chemistry: An Introduction*; Wiley ed. Chichester, **2000**.

(4) Gokel, G. W. *Molecular Recognition Receptors for Cationic Guests, in Comprehensive Supramolecular Chemistry*; Lehn, J.-M; Atwood, J. L, Davies, J. E. D; MacNicol; D. D; Vogtle, F; Pergamon. ed. Oxford, **1996**; Vol. 1.

(5) Dietrich, B.; Lehn, J. M.; Sauvage, J. P. *Tetrahedron Lett.,* **1969**, *10*, 2885.

(6) Trueblood, K. N.; Knobler, C. B.; Maverick, E.; Helgeson, R. C.; Brown, S. B.; Cram, D. J. *J. Am. Chem. Soc.,* **1981**, *103*, 5594.

(7) Gutsche, C. D.; Muthukrishnan, R. *J. Org. Chem.,* **1978**, *43*, 4905.

(8) Gokel, G. W.; Leevy, W. M.; Weber, M. E. *Chem. Rev.,* **2004**, *104*, 2723.

(9) Thuery, P.; Nierlich, M.; Lamare, V.; Dozol, J.-F.; Asfari, Z.; Vicens, J. *J. Inclusion Phenom. Macrocyclic. Chem.,* **2000**, *36*, 375.

(10) Casnati, A.; Sansone, F.; Dozol, J.-F.; Rouquette, H.; Arnaud-; Neu, F.; Byrne, D.; Fuangswasdi, S.; Schwing-Weill, M.-J.; Ungaro, R. *J. Inclusion. Phenom. Macrocyclic. Chem.* **2001**, *41*, 193.

(11) Gorbunova, M. G.; Bonnesen, P. V.; Engle, N. L.; Bazelaire, E.; Delmau, L. t. H.; Moyer, B. A. *Tetrahedron Lett.,* **2003**, *44*, 5397.

(12) Guillon, J.; Sonnet, P.; Malval, J.-P.; Massip, S. p.; Gosse, I.; Leger, J.-M.; Lapouyade, R.; Rochette, J.; Monti, J.-P.; Jarry, C. *Supramolecular Chem.,***2002**, *14*, 437.

(13) Haverlock, T. J.; Bonnesen, P. V.; Sachleben, R. A.; Moyer, B. A. *Radiochim. Acta* ,**1997**, *76*, 103-108.

(14) Talanov, V. S.; Talanova, G. G.; Gorbunova, M. G.; Bartsch, R. A. *J. Chem. Soc., Perkin Trans. 2,* **2002**, *0*, 209.

(15) Thuéry, P.; Nierlich, M.; Saadioui, M.; Asfari, Z.; Vicens, J. *Acta Cryst. C,* **1999**, *55*, 443.

(16) Dubberley, S. R.; Blake, A. J.; Mountford, P. *Dalton Trans.,* **2003**, *0*, 2418.

(17) Marchand, A. P.; Chong, H.-S.; Pavan Kumar, T.; Huang, Z.; Alihodzic, S.; Watson, W. H.; Ejsmont, K. *Tetrahedron,* **2002**, *58*, 10205.

(18) Tongraung, P.; Chantarasiri, N.; Tuntulani, T. *Tetrahedron Lett.,* **2003**, *44*, 29.

(19) Tuntulani, T.; Thavornyutikarn, P.; Poompradub, S.; Jaiboon, N.; Ruangpornvisuti, V.; Chaichit, N.; Asfari, Z.; Vicens, J. *Tetrahedron,* **2002**, *58*, 10277.

(20) Akkus, G. U.; Memon, S.; Yilmaz, M. *Polycyclic Aromat. Compd.* **2002**, *22*, 1075.

(21) Reynier, N.; Dozol, J.-F. o.; Saadioui, M.; Asfari, Z.; Vicens, J. *Tetrahedron Lett.,* **1998**, *39*, 6461.

(22) Chen, L.; He, X.; Zhang, H.; Liu, Y.; Hu, X.; Sheng, Y. *Anal. Lett.,* **2001**, *34*, 2237-2248.

(23) Choi, M. J.; Kim, M. Y.; Chang, S.-K. *Chem. Commun.,* **2001**, *0*, 1664.

(24) Thuery, P.; Nierlich, M.; Arnaud-Neu, F.; Souley, B.; Asfari, Z.; Vicens, J. *Supramolecular Chem.,* **1999**, *11*, 143.

(25) Atwood, J. L.; Barbour, L. J.; Dalgarno, S.; Raston, C. L.; Webb, H. R. *J. Chem. Soc, Dalton Trans.,* **2002**, *0*, 4351.

(26) Dalgarno, S. J.; Hardie, M. J.; Makha, M.; Raston, C. L. *Chem. Eur. J.* **2003**, *9*, 2834.

(27) De Salvo, G.; Gattuso, G.; Notti, A.; Parisi, M. F.; Pappalardo, S. *J. Org. Chem.,* **2002**, *67*, 684.

(28) Fraternali, F. W., G. *Anal.Quim., Int. Ed.,* **1997**, *93*, 376.

(29) Gokel, G. W. *Chem. Soc. Rev.,* **1992**, *21*, 39.

(30) Gokel, G. W.; Dishong, D. M.; Diamond, C. J. *J. Chem. Soc., Chem. Commun.,* **1980**, *0*, 1053.

(31) Echegoyen, L.; Kaifer, A.; Durst, H.; Schultz, R. A.; Dishong, D. M.; Goli, D. M.; Gokel, G. W. *J. Am. Chem. Soc.,* **1984**, *106*, 5100.

(32) Potvin, P. G.; Lehn, J.-M. *In Synthesis of Macrocycles. The Design of Selective Complexing Agents*; Izatt, R. M., Christensen, J. J ed. New York, **1987**.

(33) Lindoy, L. F. *The Chemistry of Macrocyclic Ligand Complexes*; University Press ed. Cambridge, **1989**.

(34) Dietrich, B.; Viout, P.; Lehn, J.-M. *Aspect de la Chimie des Composés Macrocycliques* Paris, **1991**.

(35) Gokel, G. *Crown Ethers and Cryptandts*; Royal Society of Chemistry ed. Cambridges, **1994**.

(36) Cram, D. J.; Cram, J., M. *Container Molecules and Their Guests, Monographs in Supamolecular Chemistry*; Stoddart, J. F, The Royal Society of Chemistry ed. Cambridge, **1994**.

(37) Cram, D. J. *From Design to Discovery*; American Chemistry Society ed. Washington, **1991**.

(38) Cao, J.; Jiang, Y.; Zhao, J.-M.; Chen, C.-F. *Chem. Commun.,* **2009**, *0*, 1987.

(39) Bourgeois, J.-P.; Fujita, M.; Kawano, M.; Sakamoto, S.; Yamaguchi, K. *J. Am. Chem. Soc.,* **2003**, *125*, 9260.

(40) Marcos, P. M.; Felix, S.; Ascenso, J. R.; Segurado, M. A. P.; Thuery, P.; Mellah, B.; Michel, S.; Hubscher-Bruder, V.; Arnaud-Neu, F. *New J. Chem.,***2007**, *31*, 2111.

(41) Even, P.; Boitrel, B. *Coord. Chem. Rev.,* **2006**, *250*, 519.

(42) Diederich, F. *In Modern Cyclophane Chemistry: Molecular Recognition Studies with Cyclophane Receptors in Aqueous Solutions*; Gleiter, R., Hopf, H; Wiley-VCH ed. Weinheim, **2004**.

(43) Lee, J. W.; Samal, S.; Selvapalam, N.; Kim, H.-J.; Kim, K. *Acc. Chem. Res.,* **2003**, *36*, 621.

(44) Lagona, J.; Mukhopadhyay, P.; Chakrabarti, S.; Isaacs, L. *Angew. Chem. Int. Ed.,* **2005**, *44*, 4844.

(45) Nakamura, H.; Takagi, M.; Ueno, K. *Talanta,* **1979**, *26*, 921.

(46) Takagi, M.; Nakamura, M.; Ueno, K. *Anal. Lett.,* **1977**, *10*, 115.

(47) de Silva, A. P.; de Silva, S. A. *J. Chem. Soc., Chem. Commun.,* **1986**, *0*, 1709.

(48) Saji, T.; Kinoshita, I. *J. Chem. Soc., Chem. Commun.,* **1986**, *0*, 716.

(49) Saji, T. *Chem. Lett.,* **1986**, 275.

(50) Beer, P. D.; Danks, J. P.; Hesek, D.; McAleer, J. F. *J. Chem. Soc., Chem. Commun.,* **1993**, *0*, 1735.

(51) Beer, P. D. *J. Chem. Soc., Chem. Commun.,* **1985**, *0*, 1115.

(52) Beer, P. D.; Crane, C. G.; Keefe, A. D.; Whyman, A. R. *J. Organomet. Chem.,* **1986**, *314*, C9.

(53) Beer, P. D.; Sikanyika, H.; Slawin, A. M. Z.; Williams, D. J. *Polyhedron* **1989**, *8*, 879.

(54) Beer, P. D.; Keefe, A. D.; Sikanyika, H.; Blackburn, C.; McAleer, J. F. *J. Chem. Soc., Dalton Trans.,* **1990**, *0*, 3289.

(55) Chen, Z.; Pilgrim, A. J.; Beer, P. D. *J. Chem. Soc., Faraday Trans.,* **1995**, *91*, 4331.

(56) Chen, Z.; Pilgrim, A. J.; Beer, P. D. *J. Electroanal. Chem.,* **1998**, *444*, 209.

(57) Beer, P. D.; Crowe, D. B.; Ogden, M. I.; Drew, M. G. B.; Main, B. *J. Chem. Soc., Dalton Trans.,* **1993**, *0*, 2107.

(58) Hall, C. D.; Sharpe, N. W.; Danks, I. P.; Sang, Y. P. *J. Chem. Soc., Chem. Commun.,***1989**, *0*, 419.

(59) Medina, J. C.; Goodnow, T. T.; Rojas, M. T.; Atwood, J. L.; Lynn, B. C.; Kaifer, A. E.; Gokel, G. W. *J. Am. Chem. Soc.,* **1992**, *114*, 10583.

(60) Plenio, H.; Aberle, C. *Organometallics,* **1997**, *16*, 5950.

(61) Chesney, A.; R. Bryce, M.; S. Batsanov, A.; A. K. Howard, J.; M. Goldenberg, L. *Chem. Commun.,* **1998**, *0*, 677.

(62) D. Beer, P.; K. Smith, D. *J. Chem. Soc., Dalton Trans.,* **1998**, *0*, 417.

(63) Tendero, M. J. L.; Benito, A.; Martinez-Manez, R.; Soto, J.; Paya, J.; Edwards, A. J.; Raithby, P. R. *J. Chem. Soc., Dalton Trans.,* **1996**, *0*, 343.

(64) Benito, A.; Martinez-Manez, R.; Soto, J.; Tendero, M. J. L. *J. Chem. Soc., Faraday Trans.,* **1997**, *93*, 2175.

(65) E. Padilla-Tosta, M.; Martinez-Manez, R.; Pardo, T.; Soto, J.; Jose L. Tendero, M. *Chem. Commun.,* **1997**, *0*, 887.

(66) Plenio, H.; Burth, D. *Organometallics,* **1996**, *15*, 4054.

(67) Lopez, J. L.; Tárraga, A.; Espinosa, A.; Velasco, M. D.; Molina, P.; Lloveras, V.; Vidal-Gancedo, J.; Rovira, C.; Veciana, J.; Evans, D. J.; Wurst, K. *Chem. Eur. J.,* **2004**, *10*, 1815.

(68) Tarraga, A.; Molina, P.; Lopez, J. L.; Velasco, M. D. *Dalton Trans.,* **2004**, *0*, 1159.

(69) Sessler, J. L.; Gale, P. A. *Anion receptor chemistry*; Royal Society of Chemistry ed. Cambridge, **2006**.

(70) Filby, M. H.; Steed, J. W. *Coord. Chem. Rev.,* **2006**, *250*, 3200.

(71) Katayev, E. A.; Ustynyuk, Y. A.; Sessler, J. L. *Coord. Chem. Rev.,* **2006**, *250*, 3004.

(72) Schmuck, C. *Coord. Chem. Rev.,* **2006**, *250*, 3053.

(73) Davis, A. P.; Sheppard, D. N.; Smith, B. D. *Chem. Soc. Rev.,* **2007**, *36*, 348.

(74) Gale, P. A.; Garcia-Garrido, S. E.; Garric, J. *Chem. Soc. Rev.,* **2008**, *37*, 151.

(75) Lee, C.-H.; Miyaji, H.; Yoon, D.-W.; Sessler, J. L. *Chem. Commun.,* **2008**, *0*, 24.

(76) Okunola, O. A.; Santacroce, P. V.; Davis, J. T. *Supramolecular Chem.,* **2008**, *20*, 169.

(77) Kim, S. K.; Lee, D. H.; Hong, J.-I.; Yoon, J. *Acc.Chem. Res.,* **2008**, *42*, 23.

(78) Cametti, M.; Rissanen, K. *Chem. Commun.,* **2009**, *0*, 2809.

(79) Katayev, E. A.; Kolesnikov, G. V.; Sessler, J. L. *Chem. Soc. Rev.,* **2009**, *38*, 1572.

(80) Gale, P. A.; Gunnlaugsson, T. *Chem. Soc. Rev.,* **2010**, *39*, 3595.

(81) Park, C. H.; Simmons, H. E. *J. Am. Chem. Soc.,* **1968**, *90*, 2431.

(82) Yoon, D.-W.; Gross, D. E.; Lynch, V. M.; Sessler, J. L.; Hay, B. P.; Lee, C.-H. *Angew. Chem. Int. Ed.,* **2008**, *47*, 5038.

(83) Li, Y.; Flood, A. H. *Angew. Chem. Int. Ed.,* **2008**, *47*, 2649.

(84) Gale, P. A.; Hiscock, J. R.; Moore, S. J.; Caltagirone, C.; Hursthouse, M. B.; Light, M. E. *Chem. An Asian J.,* **2010**, *5*, 555.

(85) Ball., P. *A Biography of water*; Phoenix ed. London, **2000**.

(86) Mateus, P.; Delgado, R.; Brandaì f o, P.; Fel• lix, V. t. *J. Org. Chem.,* **2009**, *74*, 8638.

(87) Mateus, P.; Delgado, R.; Brandao, P.; Carvalho, S.; Felix, V. *Org. Biomol. Chem.,* **2009**, *7*, 4661.

(88) Azuma, Y.; Newcomb, M. *Organometallics*, **1984**, *3*, 9.

(89) Newcomb, M.; Madonik, A. M.; Blanda, M. T.; Judice, J. K. *Organometallics,* **1987**, *6*, 145.

(90) Newcomb, M.; Horner, J. H.; Blanda, M. T.; Squattrito, P. J. *J. Am. Chem. Soc.,* **1989**, *111*, 6294.

(91) Katz, H. E. *J. Am. Chem. Soc.,***1986**, *108*, 7640.

(92) Yang, X.; Knobler, C. B.; Zheng, Z.; Hawthorne, M. F. *J. Am. Chem. Soc.,* **1994**, *116*, 7142.

(93) Aoyagi, S.; Ogawa, K.; Tanaka, K.; Takeuchi, Y. *J. Chem. Soc., Perkin Trans. 2,* **1995**, *0*, 355.

(94) Jung, M. E.; Xia, H. *Tetrahedron Lett.,* **1988**, *29*, 297.

(95) Jurkschat, K.; Kuivila, H. G.; Liu, S.; Zubieta, J. A. *Organometallics,* **1989**, *8*, 2755.

(96) Jacobson, S.; Pizer, R. *J. Am. Chem. Soc.,* **1993**, *115*, 11216.

(97) Lacy, S. M.; Rudkevich, D. M.; Verboom, W.; Reinhoudt, D. N. *J. Chem. Soc., Perkin Trans. 2,* **1995**, *0*, 135.

(98) Yamaguchi, S.; Akiyama, S.; Tamao, K. *J. Am. Chem. Soc.,* **2001**, *123*, 11372.

(99) Yamaguchi, S.; Akiyama, S.; Tamao, K. *J. Am. Chem. Soc.,* **2000**, *122*, 6793.

(100) Aldridge, S.; Fallis, I. A.; Howard, S. T. *Chemical Commun.,* **2001**, *0*, 231.

(101) Nicolas, M.; Fabre, B.; Marchand, G.; Simonet, J. *Eur. J. Org. Chem.,* **2000**, *2000*, 1703.

(102) Sasaki, S.-i.; Amano, T.; Ozawa, S.; Masuyama, T.; Citterio, D.; Hisamoto, H.; Hori, H.; Suzuki, K. *J. Chem. Soc., Perkin Trans. 1,* **2001**, *0*, 1366.

(103) Schulte, M.; Schürmann, M.; Jurkschat, K. *Chem. Eur. J.,* **2001**, *7*, 347.

(104) Blanda, M. T.; Herren, M. A. *Chem. Commun.,* **2000**, *0*, 343.

(105) Lee, H.; Diaz, M.; Knobler, C. B.; Hawthorne, M. F. *Angew. Chem. Int. Ed.,* **2000**, *39*, 776.

(106) Sole, S.; Gabbai, F. P. *Chem. Commun.,* **2004**, *0*, 1284.

(107) Nicolas, M.; Fabre, B.; Simonet, J. *Chem. Commun.,* **1999**, *0*, 1881.

(108) Schulte, M.; Gabriele, G.; Schürmann, M.; Jurkschat, K.; Duthie, A.; Dakternieks, D. *Organometallics,* **2002**, *22*, 328.

(109) Chiu, C.-W.; Gabbai, F. *Dalton Trans.,* **2008**, *0*, 814.

(110) Dakternieks, D.; Jurkschat, K.; Zhu, H.; Tiekink, E. R. T. *Organometallics,* **1995**, *14*, 2512.

(111) Huh, J. O.; Do, Y.; Lee, M. H. *Organometallics,* **2008**, *27*, 1022.

(112) Hudnall, T. W.; Kim, Y.-M.; Bebbington, M. W. P.; Bourissou, D.; Gabbai, F. o. P. *J. Am. Chem. Soc.,* **2008**, *130*, 10890.

(113) Bresner, C.; Day, J. K.; Coombs, N. D.; Fallis, I. A.; Aldridge, S.; Coles, S. J.; Hursthouse, M. B. *Dalton Trans.,* **2006**, *0*, 3660.

(114) Hudnall, T. W.; Chiu, C.-W.; Gabbai, F. *Acc. Chem. Res.,* **2009**, *42*, 388.

(115) Wuest, J. D. *Acc. Chem. Res.,* **1998**, *32*, 81.

(116) Williams, V. C.; Piers, W. E.; Clegg, W.; Elsegood, M. R. J.; Collins, S.; Marder, T. B. *J. Am. Chem. Soc.,***1999**, *121*, 3244.

(117) Sun, Y.; Ross, N.; Zhao, S.-B.; Huszarik, K.; Jia, W.-L.; Wang, R.-Y.; Macartney, D.; Wang, S. *J. Am. Chem. Soc.,* **2007**, *129*, 7510.

(118) Bayer, M. J.; Jalisatgi, S. S.; Smart, B.; Herzog, A.; Knobler, C. B.; Hawthorne, M. F. *Angew. Chem. Int. Ed.,* **2004**, *43*, 1854.

(119) Kim, Y.; Kim, M.; Gabbai, F. *Org. Lett.,* **2010**, *12*, 600.

(120) Kim, Y.; Gabbai, F. *J. Am. Chem. Soc.,* **2009**, *131*, 3363.

(121) Chaniotakis, N.; Jurkschat, K.; Müller, D.; Perdikaki, K.; Reeske, G. *Eur. J. Inorg. Chem.,* **2004**, *2004*, 2283.

(122) Schulte, M.; Gabbaï, F. P. *Chem. Eur. J.,* **2002**, *8*, 3802.

(123) Kawachi, A.; Tani, A.; Shimada, J.; Yamamoto, Y. *J. Am. Chem. Soc.,* **2008**, *130*, 4222.

(124) Hoefelmeyer, J. D.; Gabbai, F. P. *Chem. Commun.,* **2003**, *0*, 712.

(125) Melaimi, M.; Gabbai, F. *J. Am. Chem. Soc.,* **2005**, *127*, 9680.

(126) McNally, B. A.; Koulov, A. V.; Lambert, T. N.; Smith, B. D.; Joos, J.-B.; Sisson, A. L.; Clare, J. P.; Sgarlata, V.; Judd, L. W.; Magro, G.; Davis, A. P. *Chem. Eur. J.,* **2008**, *14*, 9599.

(127) Beer, P. D.; Keefe, A. D. *J. Organomet. Chem.,* **1989**, *375*, C40.

(128) Beer, P. D.; Graydon, A. R.; Johnson, A. O. M.; Smith, D. K. *Inorg. Chem.,* **1997**, *36*, 2112.

(129) Dusemund, C.; Sandanayake, K. R. A. S.; Shinkai, S. *J. Chem. Soc., Chem. Commun.,* **1995**, *0*, 333.

(130) Altmann, R.; Gausset, O.; Horn, D.; Jurkschat, K.; Schürmann, M.; Fontani, M.; Zanello, P. *Organometallics,* **2000**, *19*, 430.

(131) Shukla, R.; Kida, T.; Smith, B. D. *Org. Lett.,* **2000**, *2*, 3099.

(132) Ikeda, A.; Shinkai, S. *Chem. Rev.,* **1997**, *97*, 1713.

(133) Kim, J. S.; Quang, D. T. *Chem. Rev.,* **2007**, *107*, 3780.

(134) Beer, P. D.; Gale, P. A. *Angew. Chem.Int. Ed.,* **2001**, *40*, 486.

(135) Gale, P. A.; Quesada, R. *Coord. Chem. Rev.,* **2006**, *250*, 3219.

(136) Caltagirone, C.; Gale, P. A. *Chem. Soc., Rev.,* **2009**, *38*, 520.

(137) Martinez-Manez, R. n.; Sancenon, F. l. *Chem. Rev.,* **2003**, *103*, 4419.

(138) Bianchi, K.; K.Bowman-James; E.Garcia-Espana; *Supramolecular Chemistry of Anions*; Wiley-VCH ed. New York, **1997**.

(139) Gale, P. A. *The Encyclopedia of Supramolecular Chemistry*; J. L. Atwood; J. W. Steed; Dekker ed. New York, **2004**.

(140) Suksai, C.; Leeladee, P.; Jainuknan, D.; Tuntulani, T.; Muangsin, N.; Chailapakul, O.; Kongsaeree, P.; Pakavatchai, C. *Tetrahedron Lett.,* **2005**, *46*, 2765.

(141) Arafa, E. A.; Kinnear, K. I.; Lockhart, J. C. *J. Chem. Soc., Chem. Commun.,* **1992**, *0*, 61.

(142) de Silva, A. P.; McClean, G. D.; Pagliari, S. *Chem. Commun.,* **2003**, *0*, 2010.

(143) Reetz, M. T.; Niemeyer, C. M.; Harms, K. *Angew. Chem. Int. Ed.,* **1991**, *30*, 1472.

(144) Cametti, M.; Nissinen, M.; Dalla Cort, A.; Mandolini, L.; Rissanen, K. *J. Am. Chem. Soc.,* **2005**, *127*, 3831.

(145) Kim, Y.-H.; Hong, J.-I. *Chem. Commun.,* **2002**, *0*, 512.

(146) D. Beer, P.; W. Dent, S. *Chem. Commun.,* **1998**, *0*, 825.

(147) Kemmer, M.; Biesemans, M.; Gielen, M.; Martins, J. C.; Gramlich, V.; Willem, R. *Chem. Eur. J.,* **2001**, *7*, 4686.

(148) Reeske, G.; Schürmann, M.; Costisella, B.; Jurkschat, K. *Eur. J. Inorg. Chem.,* **2005**, *2005*, 2881.

(149) Tagne Kuate, A. C.; Iovkova, L.; Hiller, W.; Schürmann, M.; Jurkschat, K. *Organometallics,* **2010**, *29*, 5456.

(150) Reeske, G.; Schürmann, M.; Costisella, B.; Jurkschat, K. *Organometallics,* **2007**, *26*, 4170.

(151) Tagne Kuate, A. C.; Reeske, G.; Schürmann, M.; Costisella, B.; Jurkschat, K. *Organometallics,* **2008**, *27*, 5577.

(152) Reeske, G.; Bradtmöller, G.; Schürmann, M.; Jurkschat, K. *Chem. Eur. J.,* **2007**, *13*, 10239.

(153) Arens, V. Diplomarbeit, TU-Dortmund, **2008**.

(154) Arens, V. Ph.D. Thesis, Technische Universität Dortmund, **2012**.

(155) Mahoney, J. M.; Beatty, A. M.; Smith, B. D. *Inorg. Chem.,* **2004**, *43*, 7617.

(156) Smith, B. D. *Macrocyclic Chemistry: Current Trends and Future Perspectives* Springer, Dordrecht, **2005**.

(157) Kim, S. K.; Sessler, J. L. *Chem. Soc. Rev.,* **2010**, *39*, 3784.

(158) J. White, D.; Laing, N.; Miller, H.; Parsons, S.; A. Tasker, P.; Coles, S. *Chem. Commun.,* **1999**, *0*, 2077.

(159) Webber, P. R. A.; Beer, P. D. *Dalton Trans.,* **2003**, *0*, 2249.

(160) Chrisstoffels, L. A. J.; de Jong, F.; Reinhoudt, D. N.; Sivelli, S.; Gazzola, L.; Casnati, A.; Ungaro, R. *J. Am. Chem., Soc.,* **1999**, *121*, 10142.

(161) McConnell, A. J.; Beer, P. D. *Angew. Chem. Int. Ed.,* **2012**, *51*, 5052.

(162) Beer, P. D.; Chen, Z.; Ogden, M. I. *J. Chem. Soc., Faraday Trans.,* **1995**, *91*, 295.

(163) Tagne Kuate, A. C. Ph.D. Thesis, Technische Universität Dortmund, **2009**.

(164) Hunter, B. K. R., L. W. *Can. J. Chem.,* **1968**, *46*, 1399.

(165) Gielen, M.; Jurkschat, K. *J. Organomet. Chem.,* **1984**, *273*, 303.

(166) Reeske, G., Technische Universität Dortmund, **2004**.

(167) Jurkschat, K.; Hesselbarth, F.; Dargatz, M.; Lehmann, J.; Kleinpeter, E.; Tzschach, A.; Meunier-Piret, J. *J. Organometal. Chem.,* **1990**, *388*, 259.

(168) McFarlane, W.; Wood, R. J. *J. Organometal. Chem.,* **1972**, *40*, C17.

(169) Reeske, G.; Schürmann, M.; Costisella, B.; Jurkschat, K. *Organometallics,* **2007**, *26*, 4170.

(170) Reeske, G.; Schürmann, M.; Jurkschat, K. *Dalton Trans.,* **2008**, 3398.

(171) Cubicciotti, D. *J. Chem. Phys.,* **1959**, *31*, 1646.

(172) Ohtsu, K. K., T.; Ozutsumi, K. *Anal. Sci.,* **1996**, *12*, 37.

(173) Altmann, R.; Jurkschat, K.; Schümann, M.; Dakternieks, D.; Duthie, A. *Organometallics,* **1998**, *17*, 5858.

(174) Kolb, U.; Dräger, M.; Jousseaume, B. *Organometallics* ,**1991**, *10*, 2737.

(175) MacLachlan, M. J.; Lough, A. J.; Geiger, W. E.; Manners, I. *Organometallics,* **1998**, *17*, 1873.

(176) Cervantes-Lee, F.; Sharma, H. K.; Pannell, K. H.; Derecskei-Kovacs, A.; Marynick, D. S. *Organometallics,* **1998**, *17*, 3701.

(177) Gausset, O.; Delpon-Lacaze, G.; Schürmann, M.; Jurkschat, K. *Acta Cryst. C,* **1998**, *54*, 1425.

(178) Davies, A. G.; Tse, M.-W.; Kennedy, J. D.; McFarlane, W.; Pyne, G. S.; Ladd, M. F. C.; Povey, D. C. *J. Chem. Soc., Perkin Trans. 2,* **1981**, 369.

(179) Al-Juaid, S. S.; Dhaher, S. M.; Eaborn, C.; Hitchcock, P. B.; Smith, J. D. *J. Organometal. Chem.,***1987**, *325*, 117.

(180) Seiler, P.; Dunitz, J. D. *Acta Cryst.B,* **1979**, *35*, 1068.

(181) Holleman, A. F. W., E. *Inorganic Chemistry*; Wiberg N., Ed.; Academic Press ed. London, **2001**.

(182) Mitchell, T. N.; Amamria, A.; Fabisch, B.; Kuivila, H. G.; Karol, T. J.; Swami, K. *J. Organometal. Chem.,* **1983**, *259*, 157.

(183) Kennedy, J. D.; McFarlane, W.; Pyne, G. S.; Clarke, P. L.; Wardell, J. L. *J. Chem. Soc., Perkin Trans. 2,* **1975**, 1234.

(184) Nicholson, J. W. *Coord. Chem. Rev.,* **1982**, *47*, 263.

(185) Hammerich, O. *Methods for studies of electrochemical reactions. In: Organic Electrochemistry*; 4th ed. Lund, H.; Hammerich, O. Eds.; Dekker, M.M.: New York, Basel, **2001**, 95-182.

(186) Michman, M. *The electrochemistry of alkyl compounds of germanium, tin and lead. In: Tche chemistry of organic germanium, tin, and lead compounds* / Ed. S. Patai. V.1, John Wiley, New York, **1995**, 665-722.

(187) Jouikov, V.; Simonet, J. *Langmuir,* **2012**, *28*, 931-938.

(188) Jouikov, V.; Simonet, J. *J. Appl. Electrochem.,* **2012**, *42*, 527-537.

(189) Orazem, M. E.; Tribollet, B. *Electrochemical impedance spectroscopy,* John Wiley and Sons, Inc., New Jersey, **2008**.

(190) Matsubayashi, G.-e.; Shimizu, R.; Tanaka, T. *J. Chem. Soc., Dalton Trans.,* **1987**, 1793.

(191) Kirkovits, G. J.; Shriver, J. A.; GALE, P. A.; Sessler, J. L. **2001**, *41*, 69-75.

(192) Alfonso, M.; Espinosa, A.; Tarraga, A.; Molina, P. *Chem. Commun.,* **2012**, *48*, 6848.

(193) Chailap, B.; Tuntulani, T. *Org. Biomol. Chem.,* **2012**, *10*, 3617.

(194) Bernier, N.; Esteves, C. V.; Delgado, R. *Tetrahedron,* **2012**, *68*, 4860.

(195) Chawla, H. M.; Sahu, S. N.; Shrivastava, R.; Kumar, S. *Tetrahedron Lett.,* **2012**, *53*, 2244.

(196) Appelt, C.; Slootweg, J. C.; Lammertsma, K.; Uhl, W. *Angew. Chem. Int. Ed.,* **2012**, *51*, 5911.

(197) Kriz, J.; Dybal, J. A.; Makrlik, E.; Sedlakova, Z. k. *Chem. Phys.,* **2012**, *400*, 19.

(198) Xia, Y.; Wang, X.; Zhang, Y.; Luo, B.; Liu, Y. *J. Mol. Model.,* **2011**, *18*, 2291-2299.

(199) Valderrey, V.; Escudero-AdÃ¡n, E. C.; Ballester, P. *J. Am. Chem. Soc.,* **2012**, *134*, 10733.

(200) Ciardi, M.; Tancini, F.; Gil-Ramirez, G. n.; Escudero Adan, E. C.; Massera, C.; Dalcanale, E.; Ballester, P. *J. Am. Chem. Soc.,* **2012**, *134*, 13121.

(201) Puchnin, K.; Zaikin, P.; Cheshkov, D.; Vatsouro, I.; Kovalev, V. *Chem. Eur. J*., **2012**, *18*, 10954.

(202) Perraud, O.; Robert, V.; Gornitzka, H.; Martinez, A.; Dutasta, J.-P. *Angew. Chem. Int. Ed.,* **2012**, *51*, 504.

(203) Picot, S. C.; Mullaney, B. R.; Beer, P. D. *Chem. Eur. J.,* **2012**, *18*, 6230.

(204) Kim, S. K.; Vargas-Zuniga, G. I.; Hay, B. P.; Young, N. J.; Delmau, L. t. H.; Masselin, C.; Lee, C.-H.; Kim, J. S.; Lynch, V. M.; Moyer, B. A.; Sessler, J. L. *J. Am. Chem. Soc.,* **2012**, *134*, 1782.

(205) Park, I.-W.; Yoo, J.; Kim, B.; Adhikari, S.; Kim, S. K.; Yeon, Y.; Haynes, C. J. E.; Sutton, J. L.; Tong, C. C.; Lynch, V. M.; Sessler, J. L.; Gale, P. A.; Lee, C.-H. *Chem. Eur. J.,* **2012**, *18*, 2514.

(206) Gavette, J. V.; Lara, J.; Reling, L. L.; Haley, M. M.; Johnson, D. W. *Chem. Sc.,* **2013**, *4*, 585.

(207) Otón, F.; Ratera, I.; Espinosa, A.; Wurtz, K.; Parella, T.; Tárraga, A.; Veciana, J.; Molina, P. *Chem. Eur. J.,* **2010**, *16*, 1532.

(208) Sarauli, D.; Popova, V.; Zahl, A.; Puchta, R.; Ivanovic-Burmazovic, I. *Inorg. Chem.,* **2007**, *46*, 7848.

(209) Chenthamarakshan, C. R.; Eldo, J.; Ajayaghosh, A. *Macromolecules,* **1999**, *32*, 5846.

(210) Chenthamarakshan, C. R.; Ajayaghosh, A. *Tetrahedron Lett.,* **1998**, *39*, 1795.

(211) Reetz, M. T.; Johnson, B. M.; Harms, K. *Tetrahedron Lett.,* **1994**, *35*, 2525.

(212) Song, M.-K.; Park, S.; Alamgir, F. M.; Cho, J.; Liu, M. *Mater. Sci. Eng. R,* **2011**, *72*, 203.

(213) Citterio, D.; Takeda, J.; Kosugi, M.; Hisamoto, H.; Sasaki, S.-i.; Komatsu, H.; Suzuki, K. *Anal. Chem.,* **2006**, *79*, 1237.

(214) Balkhi, S. E.; Megarbane, B.; Poupon, J. l.; Baud, F. d. r. J.; Galliot-Guilley, M. *Clin. Toxicol.,* **2009**, *47*, 8.

(215) Bartsch, R. A.; Ramesh, V.; Bach, R. O.; SHono, T.; Kimura, K. *In Lithium Chemistry-A Theoretical and Experimental Overview*; Sapse, A.-M., Schleyer, P. v. R., ed.; Wiley: New York, Chapter 10, **1995**.

(216) *Lithium-Current Applications in science, Medecine, and Technology*; Bach, R. O. ed.; Wiley-Interscience: New York, **1985**.

(217) Tosteson, D. *Sci. Am.,* **1981**, *244*, 164-175.

(218) Lazarus, J. H.; Collard, K. J. *Endocrine and Metabolic Effects of lithium*; Plenum: New York, **1986**.

(219) Bach, R. O. *Med. Hypotheses,* **1987**, *23*, 157.

(220) Fujimoto, M.; Nogami, T.; Mikawa, H. *Chem. Lett.,* **1982**, *11*, 547.

(221) Lee, H. S.; Yang, X. Q.; McBreen, J.; Choi, L. S.; Okamoto, Y. *J. Electrochem. Soc.,* **1996**, *143*, 3825-3829.

(222) Danil de Namor, A. F.; Tanco, M. A. L.; Joe, C. Y. N.; Salomon, M. *Pure Appl. Chem.,* **1995**, *67*, 1095.

(223) Pokhodenko, V. D.; Koshechko, V. G.; Krylov, V. A. *J. Power Sources,* **1993**, *45*, 1.

(224) Newman, D. S.; Lee, C.-M. *Proc.-Electrochem. Soc*.,**1990**, *90*, 743.

(225) Matsuda, Y.; Morita, M. *J. Power Sources,* **1987**, *20*, 273.

(226) Bajaj, A. V.; Poonia, N. S. *Coord. Chem. Rev.,* **1988**, *87*.

(227) Hay, B. P.; Rustad, J. R. *J. Am. Chem. Soc.,* **1994**, *116*, 6316.

(228) Gokel, G. W.; Durst, H. D. *Synthesis,* **1976**, *168*.

(229) Mantina, M.; Chamberlin, A. C.; Valero, R.; Cramer, C. J.; Truhlar, D. G. *J. Phys. Chem. A,* **2009**, *113*, 5806.

(230) Kayser, F.; Biesemans, M.; Delmotte, A.; Verbruggen, I.; De Borger, I.; Gielen, M.; Willem, R.; Tiekink, E. R. T. *Organometallics,* **1994**, *13*, 4026.

(231) Jambor, R.; Dostál, L.; Růžička, A.; Císařová, I.; Brus, B.; Holčapek, M.; Holeček, J. *Organometallics,* **2002**, *21*, 3996.

(232) Munguia, T.; Lopez-Cardoso, M.; Cervantes-Lee, F.; Pannell, K. H. *Inorg. Chem.,* **2007**, *46*, 1305.

(233) Schomburg, D.; Link, M.; Linoh, H.; Tacke, R. *J. Organometal. Chem.,* **1988**, *339*, 69.

(234) Reuter, H.; Puff, H. *J. Organometal. Chem.,* **1989**, *379*, 223.

(235) Kroth, H. J.; Schumann, H.; Kuivila, H. G.; Schaeffer, C. D.; Zuckerman, J. J. *J. Am. Chem. Soc.,* **1975**, *97*, 1754.

(236) McFarlane, W.; Maire, J. C.; Delmas, M. *J. Chem. Soc., Dalton Trans.,* **1972**, 1862.

(237) Van Den Berghe, E. V.; Van Der Kelen, G. P. *J. Organometal. Chem.,* **1971**, *26*, 207.

(238) Olsher, U.; Izatt, R. M.; Bradshaw, J. S.; Dalley, N. K. *Chem. Rev.,* **1991**, *91*, 137.

(239) Boulatov, R.; Du, B.; Meyers, E. A.; Shore, S. G. *Inorg. Chem.,* **1999**, *38*, 4554.

(240) Chivers, T.; Downard, A.; Parvez, M.; Schatte, G. *Inorg. Chem.,* **2001**, *40*, 1975.

(241) Metzger, E.; Aeschimann, R.; Egli, M.; Suter, G.; Dohner, R.; Ammann, D.; Dobler, M.; Simon, W. *Helv. Chim. Acta.,* **1986**, *69*, 1821.

(242) Kitazawa, S.; Kimura, K.; Yano, H.; Shono, T. *J. Am. Chem. Soc.,* **1984**, *106*, 6978.

(243) Kimura, K.; Yano, H.; Kitazawa, S.; Shono, T. *J. Chem. Soc., Perkin Trans. 2,* **1986**, 1945.

(244) Kimura, K.; Oishi, H.; Miura, T.; Shono, T. *Anal. Chem.,* **1987**, *59*, 2331.

(245) Jain, R.; Choi, H.; Lalancette, R. A.; Sheridan, J. B. *Organometallics,* **2005**, *24*, 1468.

(246) Garcia, B. n.; Casado, C. M.; Cuadrado, I.; Alonso, B.; Moran, M. s.; Losada, J. *Organometallics,* **1999**, *18*, 2349.

(247) Zhao, X.; Sharma, H. K.; Cervantes-Lee, F.; Pannell, K. H.; Long, G. J.; Shahin, A. M. *J. Organometal. Chem.,* **2003**, *686*, 235.

(248) Cerveau, G.; Chuit, C.; Colomer, E.; Corriu, R. J. P.; Reye, C. *Organometallics* , **1990**, *9*, 2415.

(249) Sosa, C.; Andzelm, J.; Elkin, B. C.; Wimmer, E.; Dobbs, K. D.; Dixon, D. A. *J. Phys. Chem.,* **1992**, *96*, 6630.

(250) Weigend, F.; Ahlrichs, R. *Phys. Chem. Chem. Phys.,* **2005**, *7*, 3297.

(251) Metz, B.; Stoll, H.; Dolg, M. *J. Chem. Phys.,* **2000**, *113*, 2563.

(252) Glendening, E. D.; Reed, A. E.; Carpenter, J. E.; Weinhold, F. *NBO version 3.1*, **2003**.

(253) Breneman, C. M.; Wiberg, K. B. *J. Comput. Chem.,* **1990**, *11*, 361.

(254) Svec, P.; Cernoskova, E.; Padelkova, Z. k.; Ruzicka, A.; Holecek, J. *J. Organometal. Chem.,* **2010**, *695*, 2475.

(255) Svec, P.; Ruzicka, A. *Main Group Met. Chem.,* **2011**, *34*, 7.

(256) Dannappel, K. Doctoral Thesis, TU Dortmund, **2007**.

(257) Schlecht, S.; Dinnebier, R.; Friese, K. *Z. Anorg. Allg. Chem.,* **2002**, *628*, 725.

(258) Balasubramanian, R.; Chohan, Z. H.; Doidge-Harrison, S. M. S. V.; Howie, R. A.; Wardell, J. L. *Polyhedron,* **1997**, *16*, 4283.

(259) Alcock, N. W.; Sawyer, J. F. *J. Chem. Soc., Dalton Trans.,* **1977**, 1090.

(260) Tagne Kuate, A. C.; Schürmann, M.; Schollmeyer, D.; Hiller, W.; Jurkschat, K. *Chem. Eur. J.,* **2010**, *16*, 8140.

(261) Dakternieks, D.; Jurkschat, K.; Wu, H.; Tiekink, E. R. T. *Organometallics*, **1993**, *12*, 2788.

(262) Frisch, M. J.; Trucks, G. W.; Schlegel, H. B.; Scuseria, G. E.; Robb, M. A.; Cheeseman, J. R.; Montgomery, Jr., J. A.; Vreven, T.; Kudin, K. N.; Burant, J.

C.; Millam, J. M.; Iyengar, S. S.; Tomasi, J.; Barone, V.; Mennucci, B.; Cossi, M.; Scalmani, G.; Rega, N.; Petersson, G. A.; Nakatsuji, H.; Hada, M.; Ehara, M.; Toyota, K.; Fukuda, R.; Hasegawa, J.; Ishida, M.; Nakajima, T.; Honda, Y.; Kitao, O.; Nakai, H.; Klene, M.; Li, X.; Knox, J. E.; Hratchian, H. P.; Cross, J. B.; Adamo, C.; Jaramillo, J.; Gomperts, R.; Stratmann, R. E.; Yazyev, O.; Austin, A. J.; Cammi, R.; Pomelli, C.; Ochterski, J. W.; Ayala, P. Y.; Morokuma, K.; Voth, G. A.; Salvador, P.; Dannenberg, J. J.; Zakrzewski, V. G.; Dapprich, S.; Daniels, A. D.; Strain, M. C.; Farkas, O.; Malick, D. K.; Rabuck, A. D.; Raghavachari, K.; Foresman, J. B.; Ortiz, J. V.; Cui, Q.; Baboul, A. G.; Clifford, S.; Cioslowski, J.; Stefanov, B. B.; Liu, G.; Liashenko, A.; Piskorz, P.; Komaromi, I.; Martin, R. L.; Fox, D. J.; Keith, T.; Al-Laham, M. A.; Peng, C. Y.; Nanayakkara, A.; Challacombe, M.; Gill, P. M. W.; Johnson, B.; Chen, W.; Wong, M. W.; Gonzalez, C.; Pople, J. A. *Gaussian 03,* Revision B.01, Gaussian, Inc., Pittsburgh PA, **2003**.

3. On the Reaction of the Monorganotin Salts $[HOSnCH_2[16]\text{-crown-}5][CF_3SO_3]_2$ with *p*-MeC_6H_4SH, $Ph_2P(S)SH$ and $NEt_3 \cdot HF$

3.1. Monoorganotin-substituted Crown Ether Cations and Dimeric Monoorganotin Sulfide Derivative

3.1.1. Introduction

The design and development of synthetic macrocyclic compounds capable of molecular recognition of ionic and neutral substrates was firstly highlighted by C. J *Pedersen* with the discovery of cyclic polyethers.[1] The latter are able to complex selectively cations by charge transfer interactions through the electron donor ability of the oxygen groups and also to encapsulate neutral substrates by hydrogen bonding interactions.[2-22]

Among the examples of interactions between crown ethers and cationic substrates listed in the literature, only very few cases concern the complexation of cationic organometallic compounds even though the stabilization of such species and their isolation as air stable materials are of fundamental interest, notably due to their potential in organic synthesis.

Complexes of crown ether encapsulating methyl magnesium or dimethylaluminium, [MeMg-([15]crown-5)][23] or $[AlMe_2([15]crown\text{-}5)]$[24] have been reported, in which the metal atom is within the cavity of the crown ether ring and coordinated by all the crown ether oxygen atoms. Organotin(IV) cations have also been successfully complexed by crown ethers, as demonstrated by P. R. *Shukla* et al. They showed by using IR and ^1H NMR spectroscopy, that the diorganotin cation $[SnPh_2]^+$ is complexed by [12]-crown-4, [15]-crown-5 and [18]-crown-6 and the tin atom in each case is inside the cavity and coordinated by four oxygen atoms.[25]

Very recently, our research group was able to provide for the first time structurally characterized (by X-ray diffraction analysis) cationic di- and monoorganotin complexes of crown ethers[26] [Scheme 1, **1**-**3**], in which the tin atom is coordinated by all the five oxygen atoms of the crown ether ring. This coordination mode corroborates the suggestion of P.R *Shukla* with the difference here that all the five oxygen atoms are involved in the interactions with the tin atoms.

Moreover, compounds **1** and **2** are so far the only second examples of a monoorganotin(IV) cation and the first ones that are monomeric in the solid state. Both compounds also represent rare examples of monomeric monoorganotin hydroxide and the presence of the SnOH groups is of particular interest, as they can be used for further reactions. In the general context of our work on organotin-substituted crown ethers,[27-32] we were interested on the reactivity of compound **1** toward Brønsted acids. Their reaction with thioalcohol groups and the formation of the derivatives **4–6** (Scheme 1) will be presented. A mechanism of formation of the neutral compound **6** is also proposed.

Scheme 1

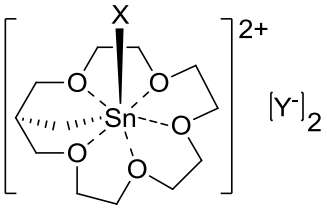

1, X = OH, Y = CF_3SO_3
2, X = OH, Y = ClO_4
3, X = Ph, Y = ClO_4

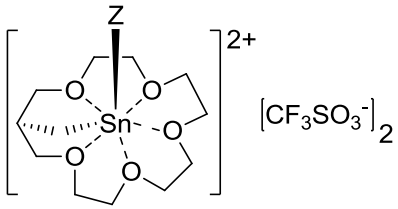

4, Z = SPhMe
5, Z = SC_8H_{10}

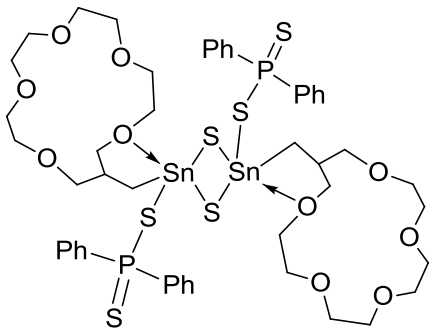

6

3.1.2. Synthesis of the Monoorganotin-substituted Crown Ether Cations 4 and 5 and the Dimeric Monoorganotin Sulfide Derivative 6.

The reaction of Hydroxy(1,4,7,10,13-pentaoxacyclohexadec-15-methyl)stannylium-bis-triflat (**1**)[26] with three molar equiv of 4-methylthiophenol or 2-naphtalene thiol at room temperature for three hours gave, after recrystallisation from CH_3CN/diethyl ether in the presence of air moisture, the crown ether substituted monoorganotin dications **4** and **5**, respectively, in moderate yield, (eq. 1).

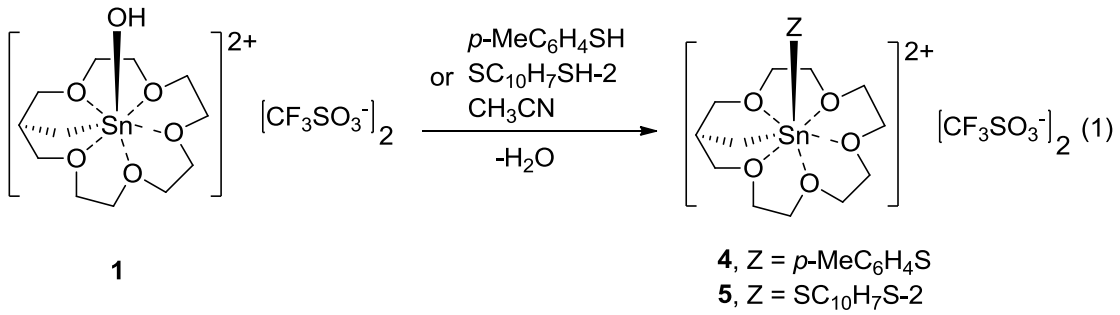

Scheme 2

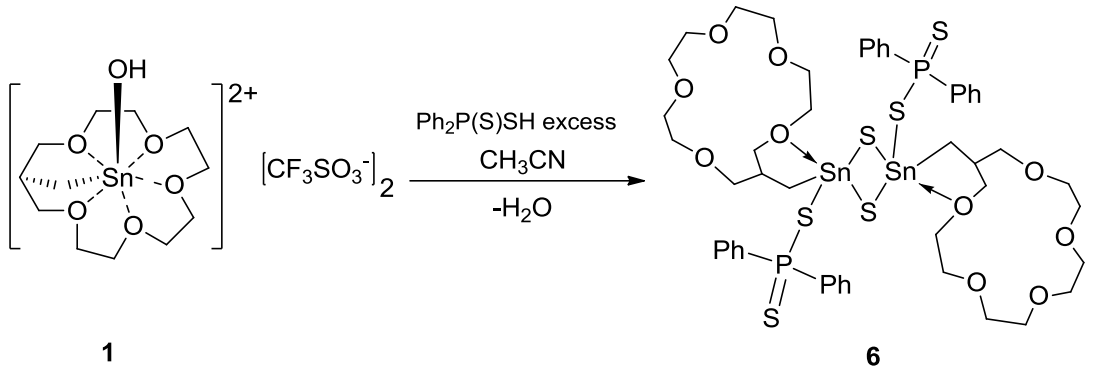

Similarly, the treatment of **1** with three molar equiv diphenyldithiophosphonic acid provided the neutral dimeric monoorganotin sulfide derivative **6** in low yield (Scheme 2). Compounds **4–6** are colourless and air stable crystalline materials. They are soluble in organic solvents such as DMSO, CH_3OH, CH_3CN.

3.1.3. Molecular Structure of the Monoorganotin-substituted Crown Ether Cations 4 and 5 and the Dimeric Monoorganotin Sulfide Derivative 6.

Single crystals of **4** suitable for X-ray diffraction analysis were grown by slow evaporation of the solution of compound in CH_3CN/Et_2O, whereas those of **6** were obtained by slow evaporation from its acetontrille solution. Compound **4** crystallized in the orthorhombic space group *Cmc21* with four molecules per unit cell. Compound **6** crystallized in the triclinic space group *P-1* with one molecule per unit cell and with one molecule of acetonitrile per asymmetric unit. The molecular structures of compounds **4** and **6** are represented in Figures 1 and 2. Selected geometrical data are collected in Tables 1 and 2.

Compounds **4** consists of the dication $[MePhSSnCH_2([16]crown-5)]^{2+}$ and two symmetrical triflates anions. The overall structure of **4** closely resemble that of **1**-**3,**[26] with the difference that the axially bonded phenyl or hydroxyl substituent is replaced

by a para methylthiophenolate group in **4**. As described for compounds **1**–**3**,[26] an interesting point in the structure of **4** is the distorted pentagonal bipyramidal environment of the tin atom. The latter is located inside the crown ether cavity and coordinated by the five oxygen atoms. The distortion is best reflected in the C(1)-Sn(1)-S(1) angle of 159.81(15)° which deviate by 20.19° from the ideal angle 180°. The consecutive O-Sn-O angles range from 71.04(6)° (O(3)-Sn(1)-O(2)) to 73.57(11)° (O(1A)-Sn(1)-O(1)) and their average value (72.31°) is close to those reported in compounds **1**–**3** [71.04(7)°(O(3)-Sn(1)-O(4)), 74.20(7)°(O(1)-Sn(1)-O(5)), average 72.34° (**1**); 70.80(12)° (O(12)-Sn(2)-O(13)), 74.70(13)° (O(11)-Sn(2)-O(15)), average 72.28° (**2**); 69.72(5)° (O(2)-Sn(1)-O(3)), 76.37(5)° (O(1)-Sn(1)-O(5)), average 72.12° (**3**)]. The Sn–O bond lengths in **4** range from 2.233(4) (Sn(1)-O(3)) to 2.329(2) (Sn(1)-O(1)) Å. They are longer than the intramolecular Sn–O distances found in **1** (2.242(2), (2.273(2) Å), and notably longer than those measured in **2** (2.252(3), 2.280(3) Å) and in **3** (2.2612(14), 2.3561(14) Å).[26] The Sn(1)–S(1) bond distance of (2.3691(17) Å) found for complex **4** is slightly shorter than the sum the covalent radii[33] of Sn(1.40) and S(1.04 Å).

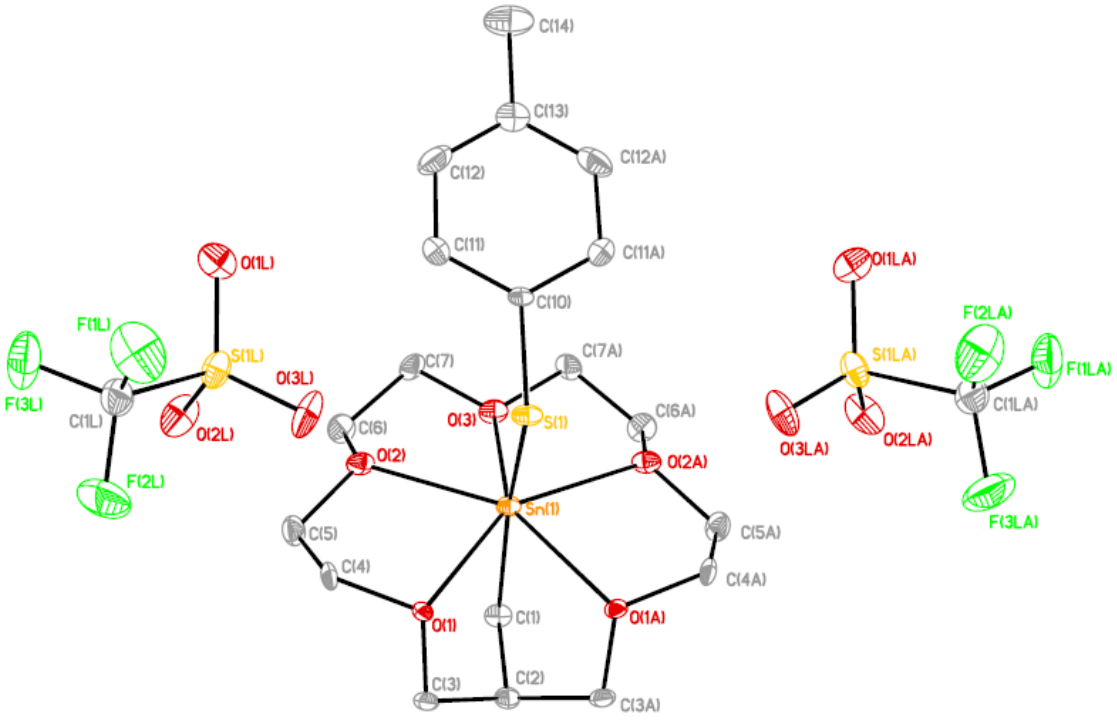

Figure 1. Molecular structure of **4** showing 30% probability displacement ellipsoids and the crystallographic numbering scheme.

Table 1. Selected bond lengths [Å] for compounds **4** and **6**.

	4	**6**
S(1)–C(1)	2.090(5)	2.138(2)
Sn(1)–O(1)	2.329(2)	2.776(2)
Sn(1)–O(2)	2.285(2)	
Sn(1)–O(3)	2.233(4)	
Sn(1)–S(1)	2.3691(17)	2.4374(6)
Sn(1)–S(3A)		2.4286(6)
Sn(1)–S(3)		2.3957(6)
S(1)–P(1)		2.0676(8)
S(2)–P(1)		1.9490(9)

Table 2. Selected bond angles [°] for compounds **4** and **6**.

	4	**6**
S(1)–Sn(1)–C(1)	159.81(15)	
O(1)–Sn(1)–O(2)	72.93(8)	
O(3)–Sn(1)–O(1A)	141,56(7)	
O(1A)–Sn(1)–C(1)	77.75(15)	
O(3)–Sn(1)–O(2A)	71.04(6)	
C(1)–Sn(1)–O(2A)	96.39(12)	
O(2)–Sn(1)–O(1A)	146.47(7)	
O(2A)–Sn(1)–O(1A)	72.93(8)	
O(1A)–Sn(1)–O(1)	73.57(11)	
O(2)–Sn(1)–O(2A)	140.50(11)	
O(1)–Sn(1)–S(1)	86.14(11)	80.06(4)
O(2)–Sn(1)–S(1)	90.32(11)	
Sn(1)–C(1)–C(2)	103,0(3)	115.08(14)
Sn(1)–S(1)–C(10)	104.70(18)	
O(3)–Sn(1)–S(1)	106.87(9)	
O(3)–Sn(1)–C(1)	93.32(16)	

Sn(1)–S(1)–P(1)	97.49(3)
S(3)–Sn(1)–S(1)	105.09(2)
C(1)–Sn(1)–S(1)	116.81(7)
C(1)–Sn(1)–S(3)	120.79(6)
C(1)–Sn(1)–S(3A)	110.96(6)
S(3)–Sn(1)–S(3A)	92.95(2)
S(1)–Sn(1)–S(3A)	107.13(2)
Sn(1)–S(3)–S(1A)	87.05(2)
S(3A)–Sn(1)–O(1)	170.30(4)
S(3)–Sn(1)–O(1)	78.68(4)

Compound **6** is a centrosymmetric dimer consisting of a fully planar and rectangular four-membered ring, Sn_2S_2,[34] as evidenced by the sum of the angles in the four- ring being 360°. The tin atoms are pentacoordinated and exhibit each a distorted trigonal-bipyramidal environment (geometrical goodness $\Delta\Sigma(\theta)$[35] 31.64 with S(1), C(1) and S(3), occupying the equatorial and O(1) and S(3A) occupying the axial positions. The distortion is especially manifested by S(3A)–Sn(1)–O(1) angle of 170.30(4)°, which deviate by 9.70° from the ideal value 180°. The tin atom is displaced by 0.3993 (3) Å from the trigonal planes defined by S(1), C(1), S(3), in the direction of S(3A). The S(3)–Sn(1)–S(3A) angle of 92.95(2)° is comparable to those found in $[(Me_2NCH_2CH_2CH_2)_2SnS]_2$ [S(3)-Sn(1)-S(3A) = 92.7 (1)°].[34] The Sn–S bonds distances in compound **6** [Sn(1)–S(1) = 2.4374(6); Sn(1)–S(3) = 2.3957(6); Sn(1)–S(3A) = 2.4286(6) Å] are longer than the value found in compound **4** (2.3691(17) Å) and lie within the range of the analogous pentacoordinated compounds such as $[MeN(CH_2CH_2CH_2)_2SnS]_2$ [(Sn(1)–S(1))(2.395(1))Å, (Sn(2)–S(1))(2.526(2)) Å].[36] The intramolecular Sn(1)–O(1) distance of (2,776(2)) Å is longer than the corresponding distances found in related five coordinate tin compounds having Sn–O chelation such as 2,6-$(MeOCH_2)_2C_6H_3SnPh_2Cl$ (Sn–O(1) = 2.567(2) Å),[37] Ph_2ClSn-CH_2-[16]-crown-5 (Sn–O(1) = (2.571)(1) Å),[28] and Ph_2FSn-CH_2-[16]-crown-5 (2.5301) (18) Å).[28]

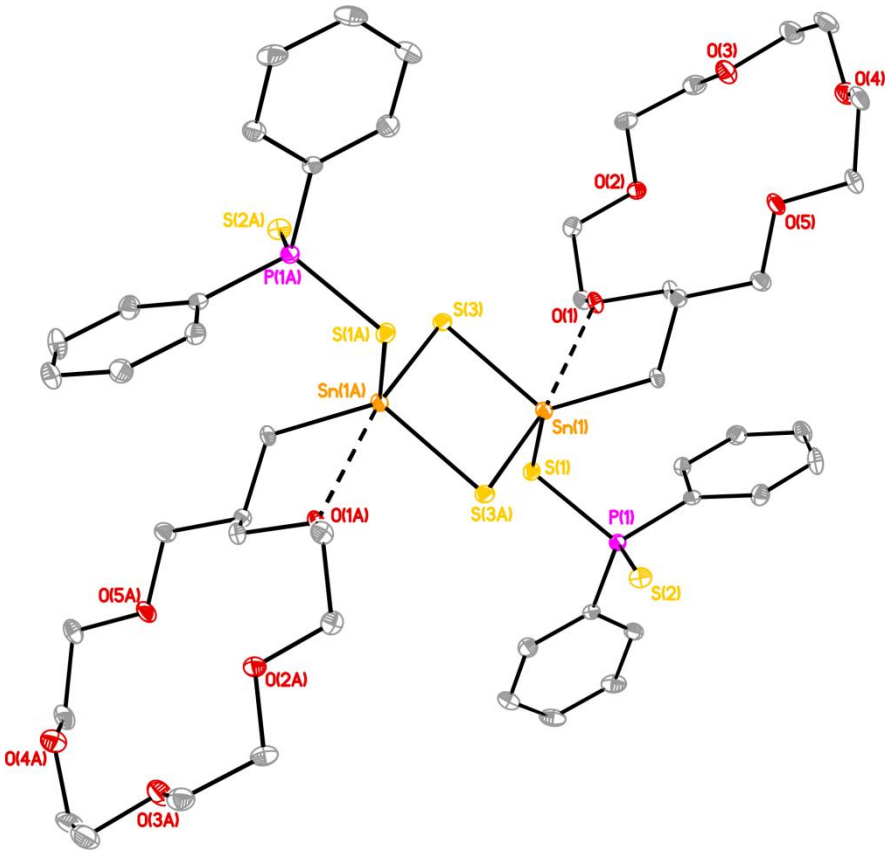

Figure 2. Molecular structure of **6** showing 30% probability displacement ellipsoids Acetonitrile molecules were omitted for clarity.

3.1.4. ^{119}Sn Mössbauer Spectroscopic Measurements on Compounds 1 and 4.

The ^{119}Sn Mössbauer spectra were recorded by Pr.Dr. Rainer Pöttgen of the Universität Münster. The ^{119}Sn Mössbauer spectrum of **1** is presented in Figure 3 together with a transmission integral fit. The corresponding fitting parameters are listed in Table 3. The spectrum was well reproduced by a superposition of two quadrupole-split signals. The main signal at ca. 85 % intensity shows an isomer shift of δ = 1.03(1) mm s^{-1} and a large quadrupole splitting parameter ΔE_Q = 3.54(1) mm s^{-1}, reflecting the non-cubic site symmetry of the tin atom. The isomer shift is in line with the tetravalent character of tin. The superimposed signal with an intensity of around 15 % can be attributed to a small impurity. The identity of which was not uncovered.

Table 3. Fitting parameters of ^{119}Sn Mössbauer spectroscopy measurements on **1** at 78 K. δ = isomer shift, ΔEQ = electric quadrupole splitting, *Γ* = experimental line width. Parameters marked with asterisk were kept fixed during the fitting procedure.

Signal	*Δ*(mm s^{-1})	ΔE_Q(mm s^{-1})	*Γ*(mm s^{-1})	*Area*(%)
1	1.03(1)	3.54(1)	0.85*	85(1)
2	0.78(6)	2.07(9)	0.85*	15(1)

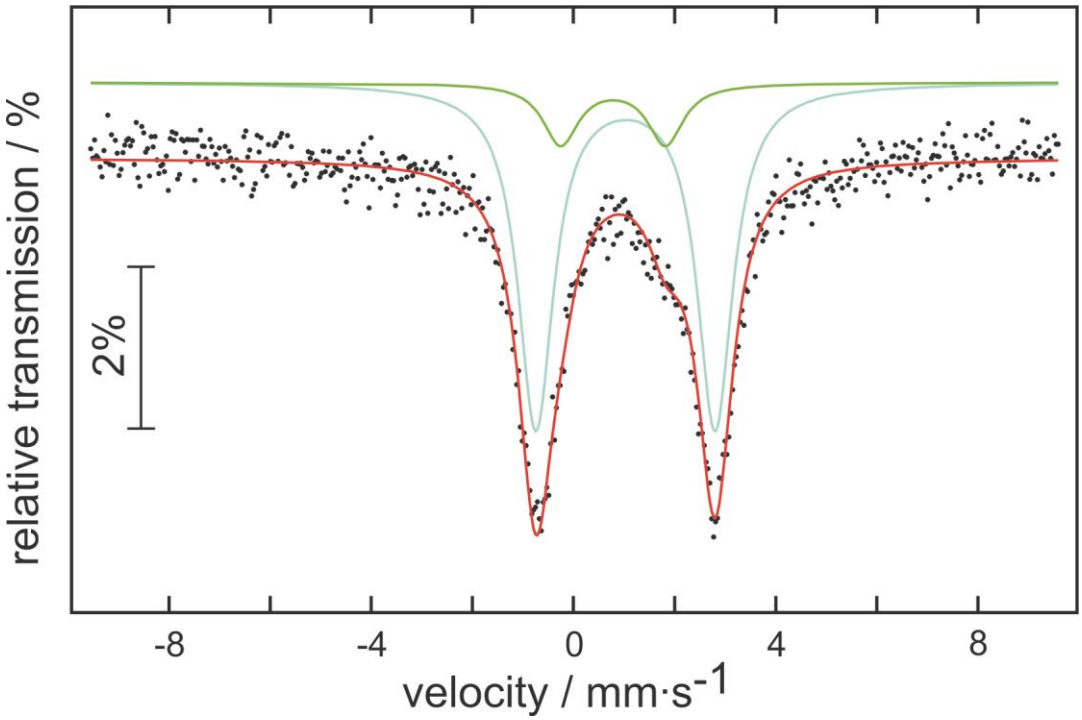

Figure 3. Experimental (data points) and simulated (continuous lines) ^{119}Sn Mössbauer spectrum of **1** at 78 K.

The ^{119}Sn Mössbauer spectrum of **4** recorded at 78 K is shown in Figure 4 together with a transmission integral fit. The spectrum was well reproduced by a single signal at δ = 1.38(1) mm/s, subjected to substantial quadrupole splitting of ΔE_Q = 3.47(1) mm/s, a result of the strong deviation from cubic site symmetry. The experimental line width of *Γ* = 0.79(1) mm/s is in the usual range. This spectrum shows a small anisotropy (η = 0.86(1)), most likely due to the Gol'danskii-Karyagin effect (anisotropy of atomic vibrations), similar to $[H_3Pt(SnCl_3)_5]\cdot 3(C_{10}H_8N_2)$,[38] $C_{22}H_{50}Cl_4N_2O_4Pt_2S_2Sn_2\cdot CH_2Cl_2$,[39] and $C_{28}H_{44}Cl_2N_8O_6S_4SiSn$.[40]

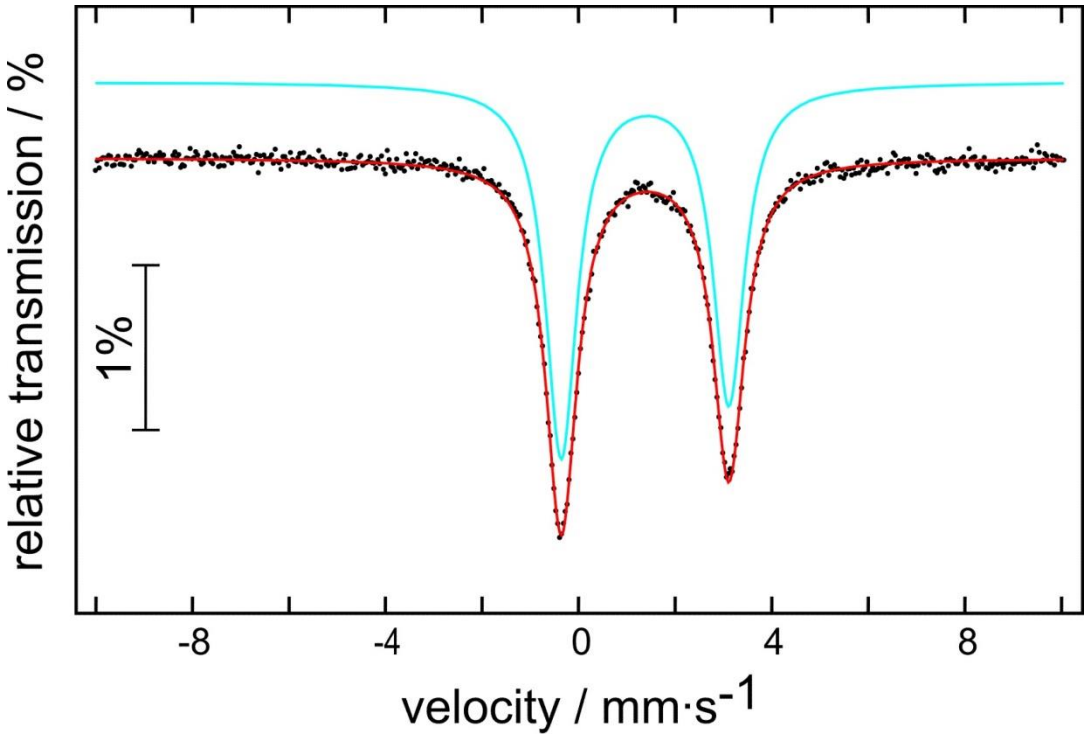

Figure 4. Experimental and simulated ^{119}Sn Mössbauer spectrum of **4** at 78 K.

3.1.5. Structures in Solution of the Monoorganotin-substituted Crown Ether Cations 4 and 5 and the Dimeric Monoorganotin Sulfide Derivative 6.

The structures in solution of compounds **4** and **5** are similar to those of the parent compounds **1** and **2**.[31] Thus, as expected, the intramolecular encapsulation of the tin atom in the monorganotin compounds **4** and **5** is retained in solution, as evidenced by the ^{119}Sn NMR chemical shifts δ –497 , which is in the range of those of the parent compound (**1,** δ –550)[26] and of related heptacoordinated tin atoms such as {[MeSn(OC_2H_4)$_3$N]$_3$ (δ –537)}[41-43] and {*n*-BuSn(Oxinate)$_3$(δ –561)}.[44] The ^{13}C NMR spectra showed for each compound six resonances for the crown ether carbon atoms (C15, C14/C16, C2/C12, C3/C11, C5/C9, C6/C8) (according to numbering scheme shown in Scheme 5). The ^1J(^{13}C–$^{117/119}$Sn) coupling constants of 923/965 Hz is by 333/209 Hz bigger with respect to the parent compound **1**, and is close to that of the diorganotin(IV) complex of the crown ether [PhSnCH_2([16]crown-5)][ClO_4]$_2$.[26] The ^{1}H NMR (400.13 MHz, CD_3CN) spectra of **4** and **5** showed for the SnCH_2 and CH protons a doublet and a multiplet resonances at δ 1.67 (^3J(^{1}H–^{1}H) = 4 Hz, ^2J(^{1}H–$^{117/119}$Sn) = 80 Hz) (**4**) and 1,75 (^3J(^{1}H–^{1}H) = 4 Hz, ^2J(^{1}H–$^{117/119}$Sn) = 80 Hz) (**5**), and

δ 2.98 ($^3J(^1H–^{117/119}Sn)$ = 480 Hz) (**4**, **5**), respectively (Figure 5). Compound **5** is used as a representative example for **4** and **5**). The chemical shifts as well as the magnitude of the coupling constant are close to those found for the parent compound **1** {δ 1.67 ($^3J(^1H–^1H)$ = 4 Hz, $^2J(^1H–^{117/119}Sn)$ = 106 Hz) and δ = 2.92 ($^3J(^1H–^{117/119}Sn)$ = 480 Hz)}. In addition, for compounds **4** and **5** a multiplet resonance for the OCH_2 protons is observed at δ 3.59–4.45 ppm.

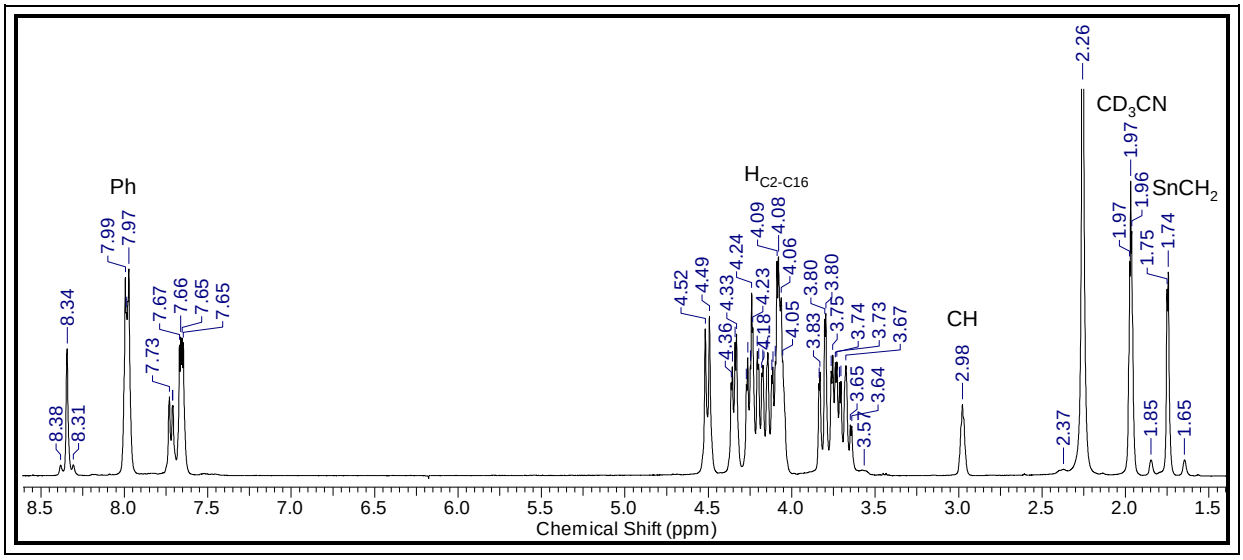

Figure 5. ^1H NMR spectrum of **5** showing the $SnCH_2$, CH, H_{C2-C16} and Ph protons in CD_3CN.

The ^1H NMR (499.79 MHz, CD_3CN) spectrum of **6** showed a complex pattern for the OCH_2 protons at δ 3.37–3.67. The $SnCH_2$ and CH protons appear as doublet and multiplet resonances at δ 1.80 ($^3J(^1H–^1H)$ = 5 Hz, $^2J(^1H–^{117/119}Sn)$ = 64 Hz) and δ = 2.57, respectively. They are respectively shifted by 0.13 and 0.41 ppm to low field, in comparison with the parent compound **1**[26], respectively (Figure 6).

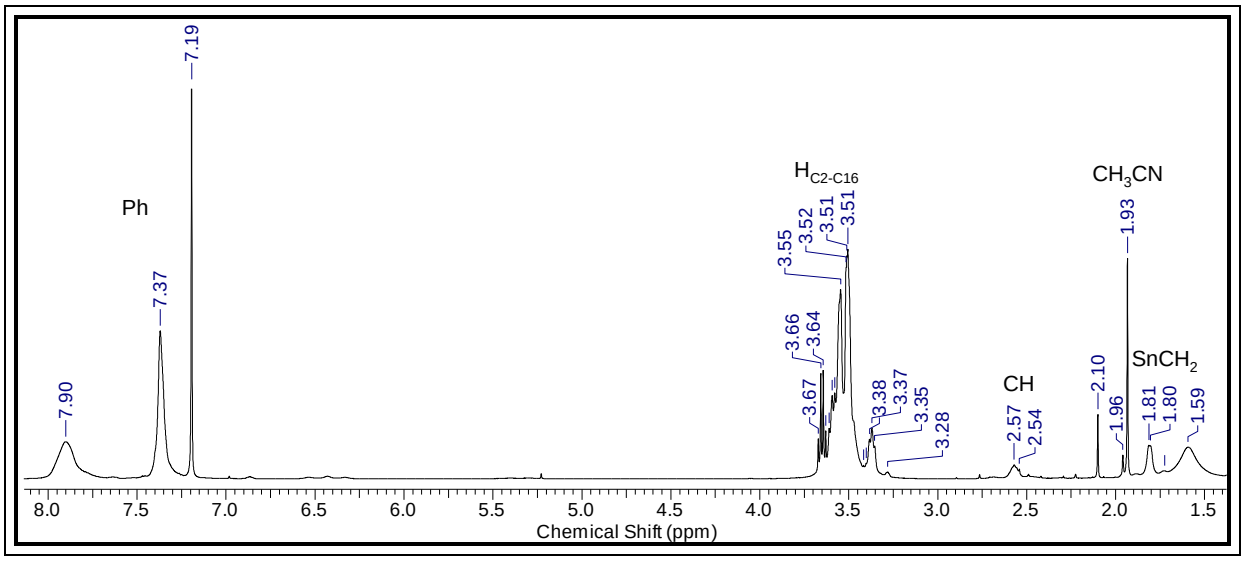

Figure 6. ^{1}H NMR spectrum of **6** showing the resonances for the $SnCH_2$, CH, $H_{C2\text{-}C16}$ and Ph protons in CD_3CN.

The ^{13}C NMR spectrum (CD_3CN) of **6** showed two complex patterns at 69.65–71.07 and at 128.21–131.16 ppm that are assigned to the crown ether and the phenyl carbon atoms, respectively. Two other signals belonging to the CH (crown ether) and $SnCH_2$ carbon atoms appear at 18.43 and 36.68 ppm, respectively (Figure 7).

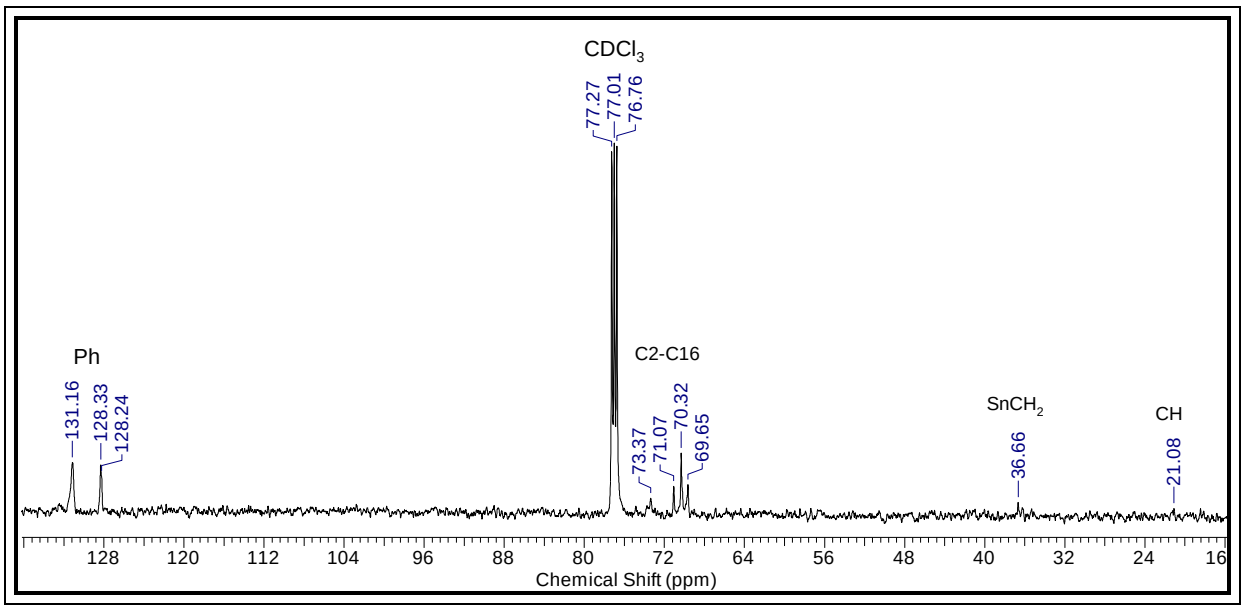

Figure 7. ^{13}C NMR spectrum of **6** showing the resonances for the CH, $SnCH_2$, C2-C16 and Ph carbon in CD_3CN.

Crude reaction mixture according to equation 2 gave in the ^{31}P NMR spectrum in CD_3CN one signal at δ 55.9 and one resonance at δ –455.5 in the ^{119}Sn NMR spectrum in the same solvent. From this reaction mixture, we isolated single crystals of **6** suitable for X-ray diffraction analysis (Figure 2).

The ^{31}P NMR spectrum ($CDCl_3$) of **6** at room temperature showed two signals at δ 57 and 58 in an almost 100 : 75 ratio, respectively, which are assigned to trans and cis isomers, respectively (Scheme 3). No resonance was observed in the ^{119}Sn NMR of **6** in $CDCl_3$. The cis-trans isomerisation shown in Scheme 3 might be one explanation of the difference observed.

Scheme 3

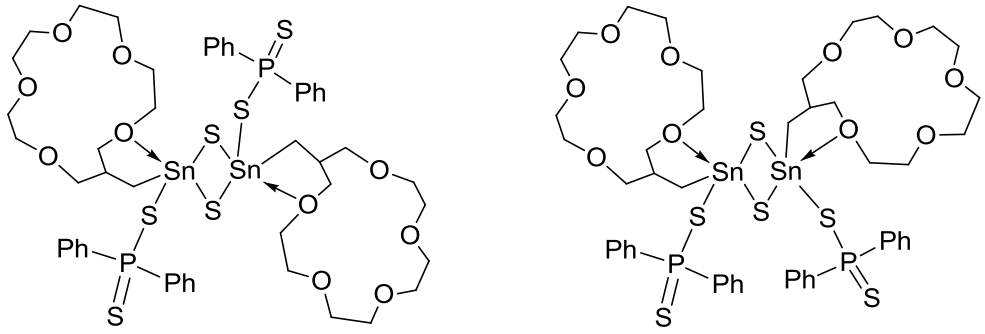

6-trans **6**-cis

The ES-IMS spectra of compounds **4** and **5** in the positive mode displayed an intense mass cluster centered at *m/z* 639.1 and *m/z* 675.1 that is assigned to $[MePhSSnCH_2([16]\text{-crown-}5)\cdot O_3SCF_3]^+$ and $[C_{10}H_8SSnCH_2([16]\text{-crown-}5)\cdot O_3SCF_3]^+$, respectively. The ESI-MS spectrum of compound **6** in the positive mode showed a mass cluster centered at *m/z* 1045.2 that is assigned to $\{[([16]\text{-crown-}5)SnS(Ph_2PS_2)]_2\text{-}Ph_2PS_2\}^+$.

The ^{31}P NMR spectrum of $Ph_2P(S)SH$ in CD_3CN showed three signals at δ 57, 62 and 70 in an almost 17 : 80 : 3 ratio, respectively. $Ph_2P(S)OP(S)Ph_2$ (**7**) was obtained as a byproduct from the reaction shown in equation 3. Compound **7** crystallized in the monoclinic space C1 2/c1 with 4 molecules per unit cell. The molecular structure of compound **7** is shown in Figure 8. Selected bond distances and bond angles are collected in Table 4.

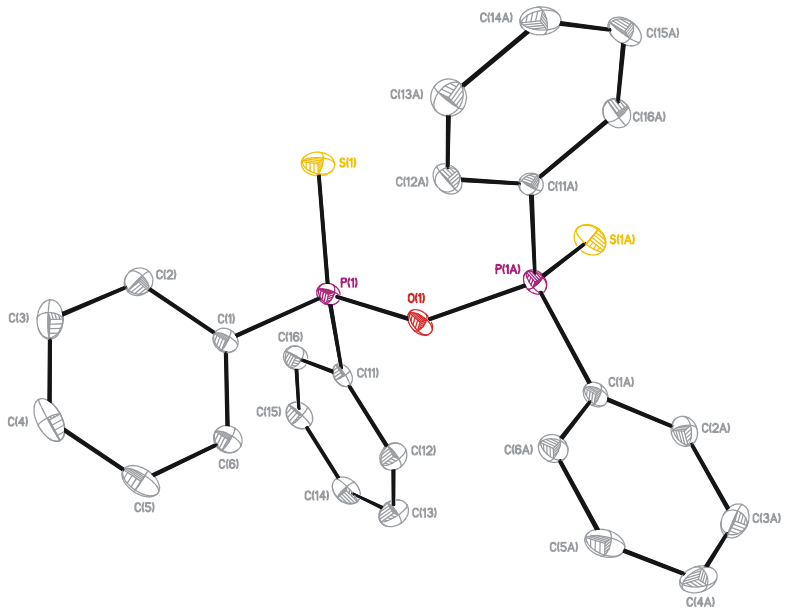

Figure 8. General view (SHELXTL) of a molecule of **7** showing 30% probability displacement ellipsoids and the crystallographic numbering scheme.

Table 4. Selected Bond Distances (Å) and Bond Angles (deg) for **7**.

Bond lengths			
P(1)–O(1)	1.6217(8)	P(1)–S(1)	1.9171(7)
P(1)–C(1)	1.7999(19)	C(11)–C(12)	1.388(3)
P(1)–C(11)	1.8009(18)		
Bond angles			
O(1)–P(1)–C(1)	98.75(8)	C(11)–P(1)–S(1)	115.25(6)
O(1)–P(1)–C(11)	102.96(6)	P(1)–O(1)–P(1A)	134.88(12)
C(1)–P(1)–C(11)	105.93(8)	C(12)–C(11)–P(1)	122.13(14)
O(1)–P(1)–S(1)	116.88(6)	C(16)–C(11)–P(1)	118.57(14)
C(1)–P(1)–S(1)	115.03(7)	C(2)–C(1)–P(1)	120.25(15)

The phosphorus atom in compound **7** is four-coordinate and adopts a distorted tetrahedral configuration with angles varying between 98.75(8) (O(1)–P(1)–C(1)) and 116.88(6)° (O(1)–P(1)–S(1)). The distortion is mainly reflected by the O(1)–P(1)–C(1) angle of 98.75(8)° which deviate from the ideal value by 8.75°. The P(1)–S(1) distance of 1.9171(7) Å is close to that found in compound **6** (1.9490(9) Å) and is in

the range of the reference bond length of phosphor and sulfur double bond (P=S, 1.92 Å).[46] The P(1)–O(1) distance of 1.6217(8) Å is slightly longer than the reference P–O single bond (P–O, 1.56 Å)[46] and falls in the range of the analogues compounds having a single phosphor oxygen bond such as $S[(t\text{-}Bu)_2C_6H_2O]_2P(OPh)_3$ {P–O(1) = 1.676(3) Å},[47] $S(t\text{-}Bu)MeC_6H_2O)_2P(OPh)_3$ {P–O(1) = 1.681(3) Å},[47] $S(Me_2C_6H_2O)_2P(OPh)_3$ {P–O(1) = 1.656(2) Å }.[47]

2.1.6. Reaction of 1 with 1,4-benzenedithiol.

Reaction of two molar equivalent of compound **1** with one molar equivalent of 1,4-benzenedithiol showed in the ^{119}Sn NMR spectrum two resonances at δ 499 and 497 in an almost 72 : 28 ratio. In course of our attempts to grow single crystals of **9** (scheme 2), we isolated instead a crystalline material that was identified to be the compound **8**.

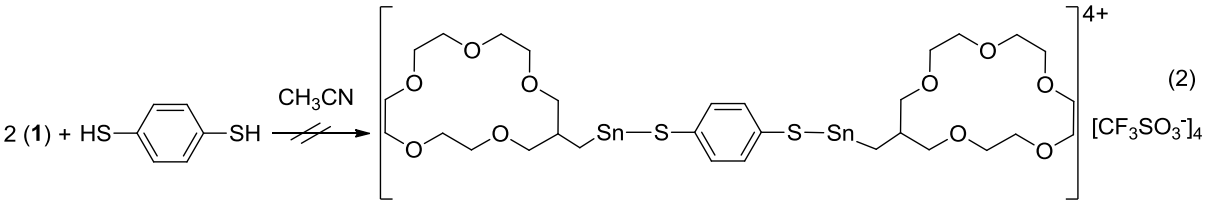

8 **9**

Compound **8** crystallized in the monoclinic space P2(1)/c with 2 molecules per unit cell. The molecular structure of compound **8** is shown in Figure 9. Selected bond distances and bond angles are collected in Table 5.

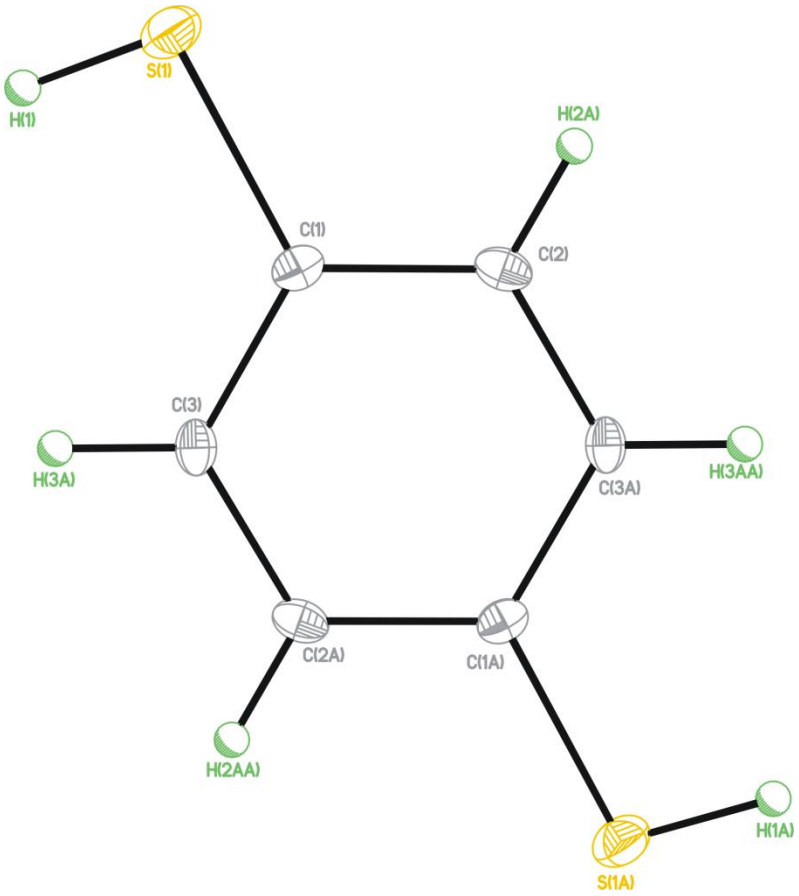

Figure 9. General view (SHELXTL) of a molecule of **8** showing 30% probability displacement ellipsoids and the crystallographic numbering scheme.

Table 5. Selected Bond Distances(Å) and Bond Angles(deg) for **8**.

Bond lengths			
S(1)–C(1)	1.7709(19)	C(2)–C(3A)	1.385(3)
S(1)–H(1)	1.100(16)	C(2)–H(2A)	0.9500
C(1)–C(2)	1.384(3)	C(3)–C(2A)	1.385(3)
C(1)–C(3)	1.397(3)	C(3)–H(3A)	0.9500
Bond angles			
C(1)–S(1)–H(1)	98.2(10)	C(1)–C(2)–C(3A)	120.82(18)
C(2)–C(1)–C(3)	119.53(18)	C(1)–C(2)–H(2A)	119.6
C(2)–C(1)–S(1)	118.51(15)	C(2A)–C(3)–C(1)	119.7(2)
C(3)–C(1)–S(1)	121.94(17)	C(1)-C(3)-H(3A)	120.2

3.1.7. Conclusions

Novel organotin(IV) cations intramolecularly encapsulated by crown ethers (**4**,**5**) have been synthesized and characterized. The molecular structure of compound **4** indicates a coordination of the tin atom by all five oxygen atoms of the ring. We found that the tin atom is evicted of the cavity of the crown ether when the incoming group is relativily large and a dimeric compound (**6**) is formed. We also noticed that the substitution of the OH function by other group is only possible for more acidic compound than alcohol. Consequently, the replacement of the terminal OH group by the fluoride anion using an appropriate fluoride source should allow to obtain monoorganotin(IV) fluoride.

3.2. Synthesis and Characterization of F_3SnCH_2-[16]-crown-5: A rare example of monoorganotin-trifluoride.

3.2.1. Introduction

Compounds that incorporated in their framework tin-fluorine bonds are often only slightly soluble in common organic solvents and usually give rise to polymeric compounds as result of intermolecular Sn−F−Sn bridges.[48-52] In order to avoid the formation of the latter and to facilitate the studies of organotin fluorides in solution, bulky organic substituents and/or chelating ligands are generally used.[53-59] Monomeric organotin(IV) fluorides continue to receive great interest over the years owing to their use for fluoride exchange with different kinds of organometallic halides.[60-62] Among the numerous reports dealing with organotin(IV) fluorides, only one example of a monomeric monoorganotin(IV) trifluoride, namely $[(2,6-OMe)_2C_6H_3]_3CSnF_3$,[63] has been reported and characterized in the solid state. The tin atom in this compound is heptacoordinated and exhibits a distorted monocapped-trigonal-antiprismatic environment. The authors were unable to record the ^{119}Sn NMR spectrum due to the poor solubility of the trifluoride compound.

Several years ago, our research group has been involved in the design, synthesis and structures of organotin-substituted crown ethers and the studies of their complexation behaviour towards inorganic salts.[26,28-32] Very recently, we employed the triiodidomonoorganotin-substituted crown ether I_3SnCH_2-[16]-crown-5[64] to synthesize the first examples of a structurally characterized cationic monomeric

monoorganotin(IV) complexes of crown ethers, $[HOSnCH_2([16]crown\text{-}5][Y^-]_2$ ($Y=ClO_4$ or CF_3SO_3).[26] In these compounds, the tin atoms are intramolecularly encapsulated by the five crown ether oxygen atoms. Of particular importance is the SnOH functional group, which opens the possibility for further reactions.

In this context and as a continuation of this work, we present here an efficient method to prepare (in solution and in the solid state) a monomeric monoorganotin (IV) trifluoride with terminal Sn−F bond starting from the cationic monoorganotin(IV) hydroxide.[26]

3.2.2. Synthesis of the Trifluoridomonoorganotin-substituted-[16]-Crown-5 (10).

The reaction of hydroxyl (1,4,7,10,13)-pentaoxacyclohexadec-15-methyl)stannylium-bis-triflat[26] (**1**) with $NEt_3{\cdot}HF$ in acetonitrile afforded the monoorganotin trifluoride **10** in moderate yield (eq. 4). In contrast to $[(2,6{-}OMe)_2C_6H_3]_3CSnF_3$,[63] compound **10** is soluble in methanol and has a relatively low melting point (90 °C for **10** and 219°C for $[(2,6{-}OMe)_2C_6H_3]_3CSnF_3$].[63]

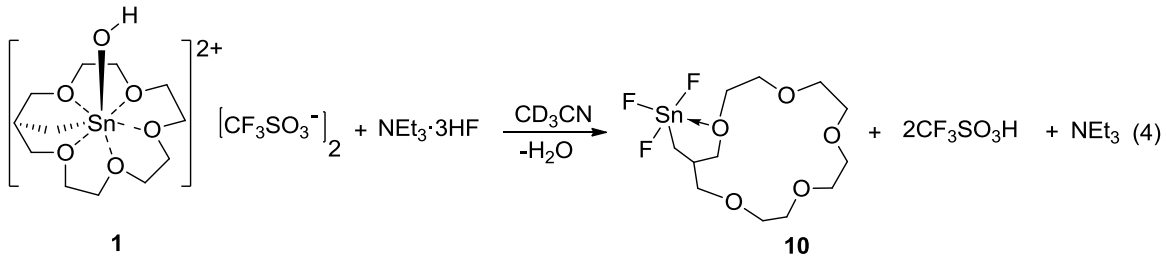

1 **10**

3.2.3. Molecular Structure of the Trifluoridomonoorganotin-substituted-[16]-Crown-5.

Single crystals suitable for X-ray analysis were obtained by keeping the concentrated acetonitrile solution at −5 °C. Crystals of **10** were isolated as its aqua complex acetonitrile solvate, hereafter referred to **10**$\cdot H_2O\cdot 2CH_3CN$. The molecular structure of compound **10** is represented in Figure 10. Selected bond distances and bond angles are listed in Table 6.

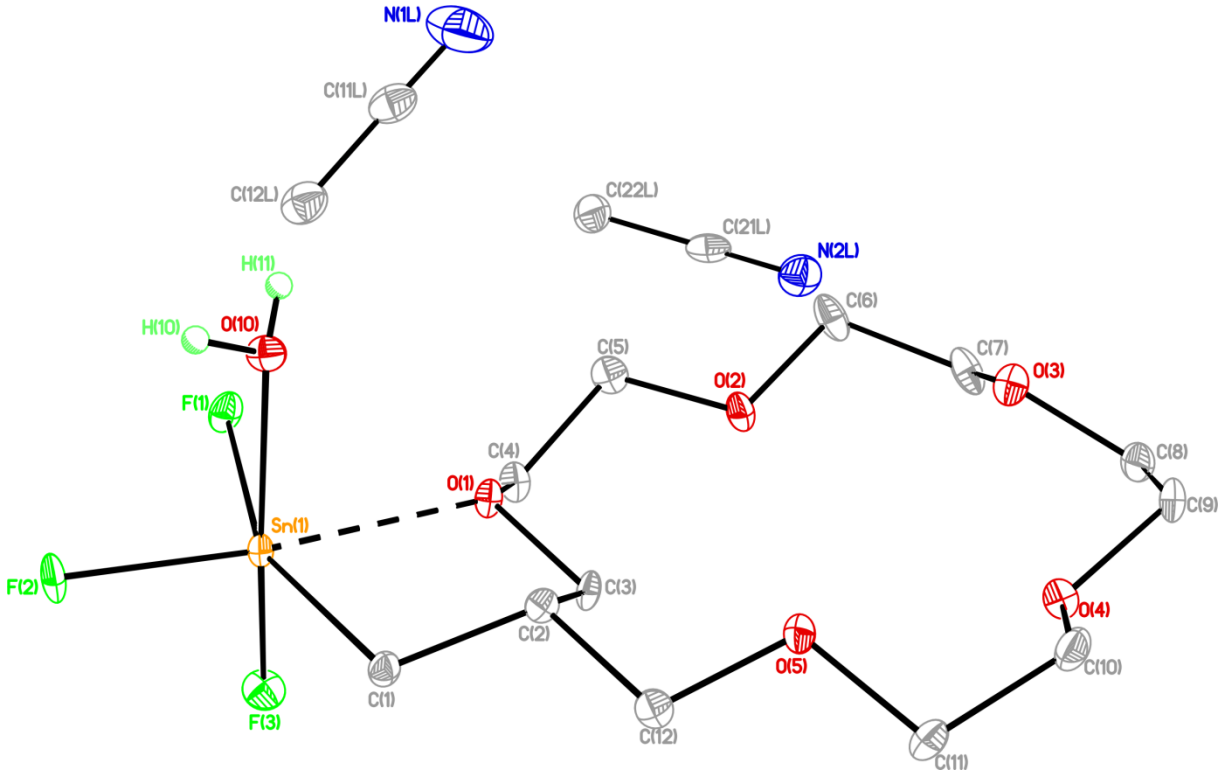

Figure 10. Molecular structure of **10**·H_2O·$2CH_3CN$ showing 30% probability displacement ellipsoids and the crystallographic numbering scheme.

Compound **10**·H_2O·$2CH_3CN$ crystallized in the triclinic space group *P*–1 with two acetonitrile molecules per unit cell.

The tin atom is hexacoordinated and exhibits a distorted octahedral environment, with C(1) and F(1) being respectively above and below the equatorial plane formed by O(1), F(2), F(3) and O(10). The distortion is especialy manifested in (i) the decrease of the F(1)−Sn(1)−C(1) angle from 180° to 157.29 (10)° which is almost the same than that observed for the monorganotin trichloride mono and di-aqua-complexes Cl_3SnCH_2-[16]-crown-5·H_2O (158.89(5)°)[64] and Cl_3SnCH_2-[16]-crown-6·$2H_2O$ (157.94(14)°),[65] (ii) the decrease of the C(1)−Sn(1)−O(1) angle from 90° to 78.64(10)° and (iii) the increase of the F(1)−Sn(1)−F(2) and F(2)−Sn(1)−F(3) angles from 90° to 92.91(7)° and 94.12(8)°, respectively. The distortion of the octahedron is, however, more accentuated for compounds without intermolecular O→Sn interactions. Indeed, the C–Sn–X angle for I_3SnCH_2-[16]-crown-5 (149.69(12)°)[64] deviates more from the ideal 180° than the corresponding angle in Cl_3SnCH_2-[16]-crown-5·H_2O (158.89(5)°)[64] and in F_3SnCH_2-[16]-crown-5·H_2O·$2CH_3CN$ (157.29(10)°).

Table 6. Selected bonds lengths [Å] and bond angles [°] for compound **10**·H_2O·2CH_3CN.

Bonds lengths			
Sn(1)–F(1)	1.9303(14)	Sn(1)–C(1)	2.127(3)
Sn(1)–F(2)	1.9371(18)	Sn(1)−O(10)	2.197(2)
Sn(1)–F(3)	1.9641(16)	Sn(1)−O(1)	2.316(2)
Bond angles			
F(1)–Sn(1)–F(2)	92.91(7)	F(1)–Sn(1)–C(1)	157.29(10)
F(1)–Sn(1)–F(3)	89.39(7)	F(2)–Sn(1)–C(1)	107.49(10)
F(2)–Sn(1)–F(3)	94.12(8)	F(3)–Sn(1)–C(1)	98.76(9)
F(1)–Sn(1)–O(10)	81.68(8)	F(3)–Sn(1)–C(1)	90.18(9)
F(3)–Sn(1)–O(10)	170.28(9)	C(1)–Sn(1)–O(10)	88.21(10)
F(1)–Sn(1)–O(1)	80.74(7)	F(2)–Sn(1)–O(1)	173.60(6)
F(3)–Sn(1)–O(1)	86.63(7)	C(1)–Sn(1)–O(1)	78.64(10)
O(10)–Sn(1)–O(1)	88.14(9)	C(3)–O(1)–Sn(1)	108.31(16)
C(2)–C(1)–Sn(1)	108.63(18)	C(3)–O(1)–C(4)	114.2(2)
		C(4)–O(1)–Sn(1)	121.12(17)

The intramolecular Sn(1)−O(1) distance of 2.316(2) Å is shorter than the corresponding Sn−O distances found in I_3SnCH_2-[16]-crown-5 (2.432(3), 2.470(3)Å)[64] and close to those observed in Cl_3SnCH_2-[19]-crown-6·2H_2O (2.361(3) Å,[65] Cl_3SnCH_2-[16]-crown-5·H_2O (2.3678(12)Å).[64] This shows that the Lewis acidity at the tin atoms is nearly equal in the trifluorido- and the trichloridomonoorganotin compounds.

A characteristic feature of compound **10**·H_2O·2CH_3CN is the intermolecular O→Sn coordination involving a water molecule. The hydrogen-atoms of the latter are involved in intermolecular interactions with two crown ether oxygen atoms (O(3) and O(5)) of a neighbour molecule and give rise to the formation of a head-to-tail dimer in the crystal lattice (Figure 11).

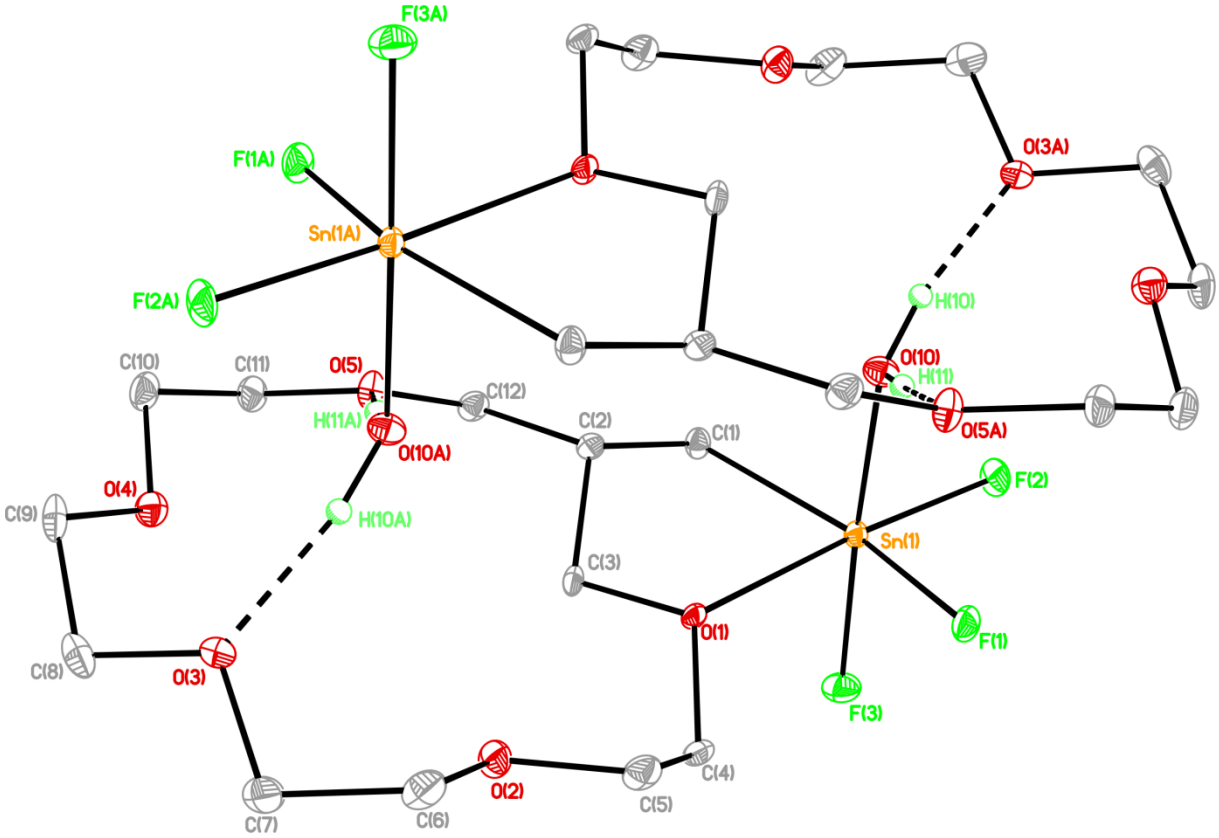

Figure 11. Dimeric chain structure of **10**·H_2O·$2CH_3CN$.

Notably, the tin atom in compound **10**·H_2O·$2CH_3CN$ is coordinated by only one oxygen atom from the crown ether ring and contrasts well with that observed for the corresponding dichloridodiorganotin- and triiodidomonoorganotin-substituted crown ethers $PhCl_2SnCH_2$-[16]-crown-5[28] and I_3SnCH_2-[16]-crown-5.[64] Indeed, the tin atoms in the two latter compounds are also hexacoordinated, but are intramolecularly coordinated by two oxygen atoms of the crown ether ring. The shortening of the intermolecular Sn(1)−O(10) distance of 2.197(2) Å is an evidence of a water molecule being strongly bound to the tin atom and can be explained by the existence of only one intramolecular O→Sn coordination in compound **10**·H_2O·$2CH_3CN$. This value is close to the sum of the covalent radii[33] of Sn and O (2.10 Å) and is slightly shorter than that found for Cl_3SnCH_2-[19]-crown-6·$2H_2O$ (2.219(4) Å).[65] The Sn(1)−F(1) (1.9303(14) Å), Sn(2)−F(2) (1.9371(18) Å) and Sn(1)−F(3) (1.9641(16) Å) bond lengths of **10**·H_2O·$2CH_3CN$ are in the range to those found in the monoorganotin(IV) trifluoride $[(2,6\text{−}OMe)_2C_6H_3]_3CSnF_3$ with terminal fluorine atoms (Sn−F(1) = 1.956(6) Å, Sn−F(2) = 1.948(7)Å, Sn−F(3) = 1.975(6)Å.[63] Among the Sn−F bonds distances of compound **10**·H_2O·$2CH_3CN$, only one is close to the standard covalent Sn−F bond length (1.96 Å).[54] In contrast to the analogous

Cl_3SnCH_2-[16]-crown-5·H_2O[64] and Cl_3SnCH_2-[19]-crown-6·$2H_2O$,[65] the tin−halogen distances are more affected by the intermolecular O→Sn coordination from the water molecules than the intramolecular O→Sn from the crown ether oxygen atoms. Indeed, the Sn−F(2) bond distance of 1.9371(18) Å is shorter than the Sn−F(3) of 1.9641(16) Å. The lengthening of the latter bond is the result of its *trans* position to the oxygen atom of the water molecule with this effect being stronger than the corresponding one from the crown ether oxygen atoms.

3.2.4. Structures in Solution of the Trifluoridomonoorganotin-substituted-[16]-Crown-5.

The ^{119}Sn NMR spectrum (CD_3OD) at room temperature of the trifluoridomonoorganotin-substituted crown ether **10** showed no signal and the ^{19}F NMR spectrum displayed broad and unresolved resonances in the area of δ –130 to –140 and –150 to –162. These results indicated the exchange processes in solution being fast at room temperature on the ^{119}Sn and ^{19}F NMR time scales. The ^{119}Sn NMR spectrum of **10** in CD_3OD at –60 °C showed a resonance at δ –573 that looks like a quartet ($^1J(^{119}Sn–^{19}F)$ = 2723 Hz) (Figure 12).

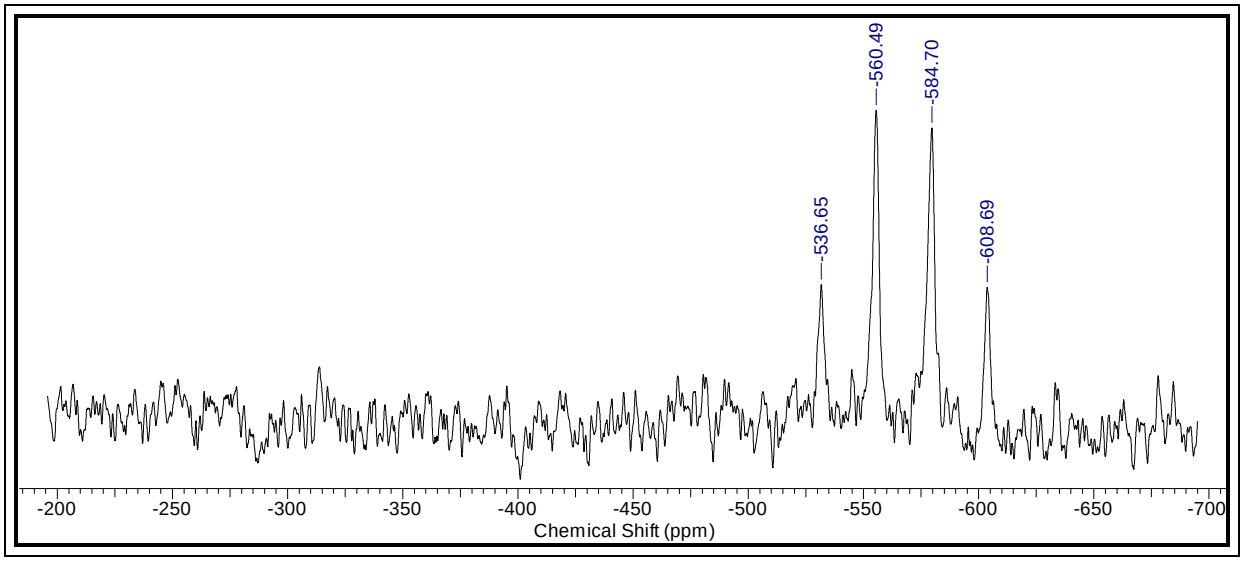

Figure 12. ^{119}Sn NMR spectrum of **10** in CD_3OH at –60 °C.

The ^{19}F NMR spectrum at –62°C showed a broad signal at δ –156 ($\nu_{1/2}$ = 752 Hz) for which the $^{117/119}$Sn satellites are hardly visible ($^1J(^{19}F–^{119}Sn)$ = 2683 Hz (Figure 13). The latter coupling constant is smaller than that found in the monoorganotin (IV) fluoride $[(2,6-OMe)_2C_6H_3]_3CSnF_3$ ($^1J(^{19}F–^{119}Sn)$ = 3390 Hz.[63] The ^{119}Sn and ^{19}F

chemical shifts observed contrast well with the structure in the solid state. Indeed, it would be expected three ^{19}F resonances and a doublet of doublet of doublet resonance in the ^{119}Sn NMR spectrum of **10**. This indicates that the structure observed in the solid state is not retained in solution.

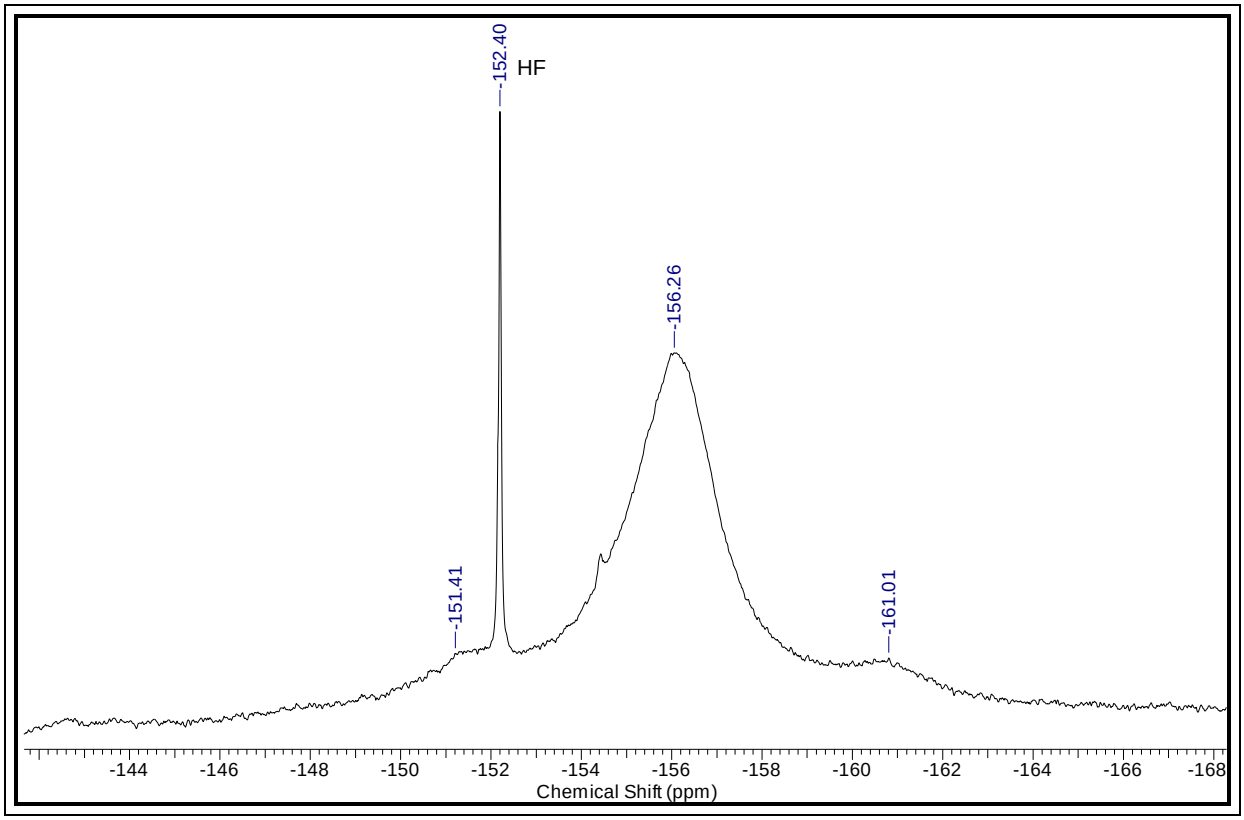

Figure 13. ^{19}F NMR spectrum of **10** in CD_3OD at –62 °C.

The ^{1}H NMR (300.13 MHz, CD_3OD) spectrum of **10** showed complex pattern for OCH_2 protons at δ 3.53−3.86. It is high field shifted and showed significant restricted distribution than the parent compound **1** (δ 3.72−4.50). The $SnCH_2$ and CH protons appear as a doublet and unresolved multiplet resonances at δ 1.13 ppm ($^{3}J(^{1}H-^{1}H)$ = 9.0 Hz, $^{2}J(^{1}H-^{117}Sn)$ = 129.0 Hz, $^{2}J(^{1}H-^{119}Sn)$ = 141.0 Hz) and δ 2.31−2.45, respectively (Figure 14), that are, with respect to the parent compound **1**, shifted by δ 0.54 and 0.60 to high field.

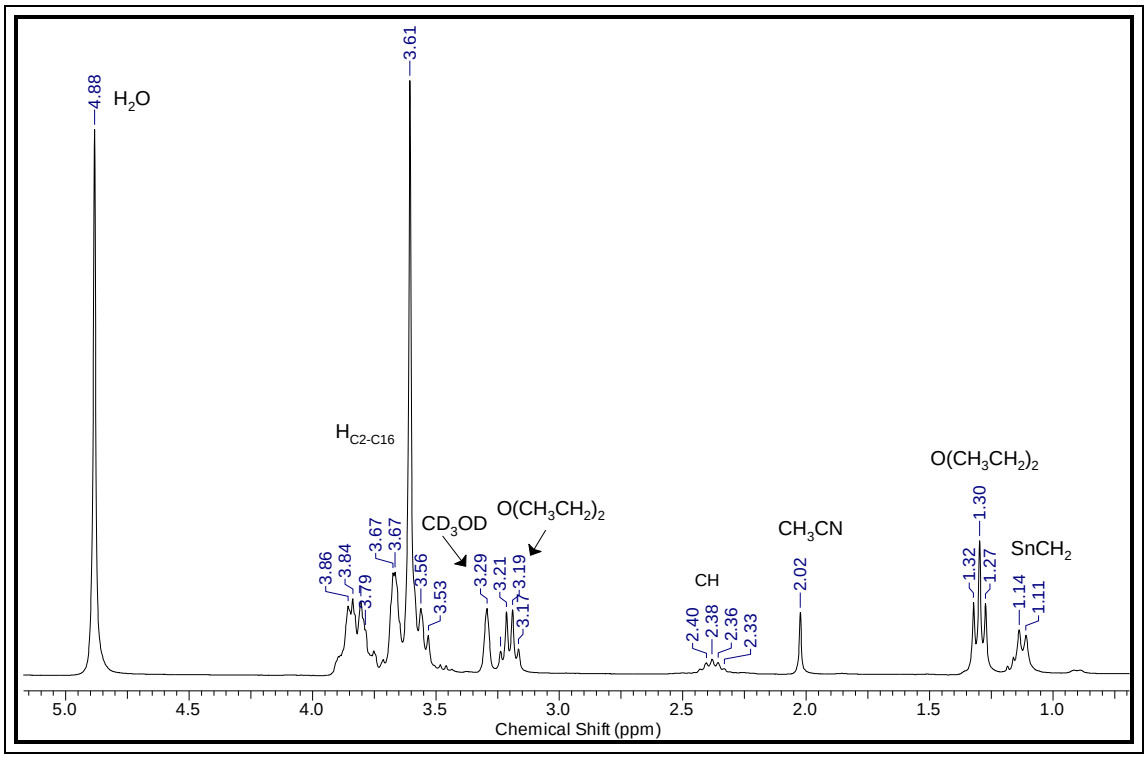

Figure 14. ^{1}H NMR spectrum of **10** showing the resonances for the $SnCH_2$, CH, and $H_{C2\text{-}C16}$ in CD_3OD.

The ^{13}C NMR (75.48 MHz, CD_3OD) spectrum of **10** displayed upfields shifts for the C1 ($\Delta\delta$ = 9.8 ppm) and C3/C12 ($\Delta\delta$ = 1.5 ppm) carbon atoms and downfield shifts for the C2 carbon atom ($\Delta\delta$ = 2.6 ppm) (Figure 15) with respect to the parent compound **1**.

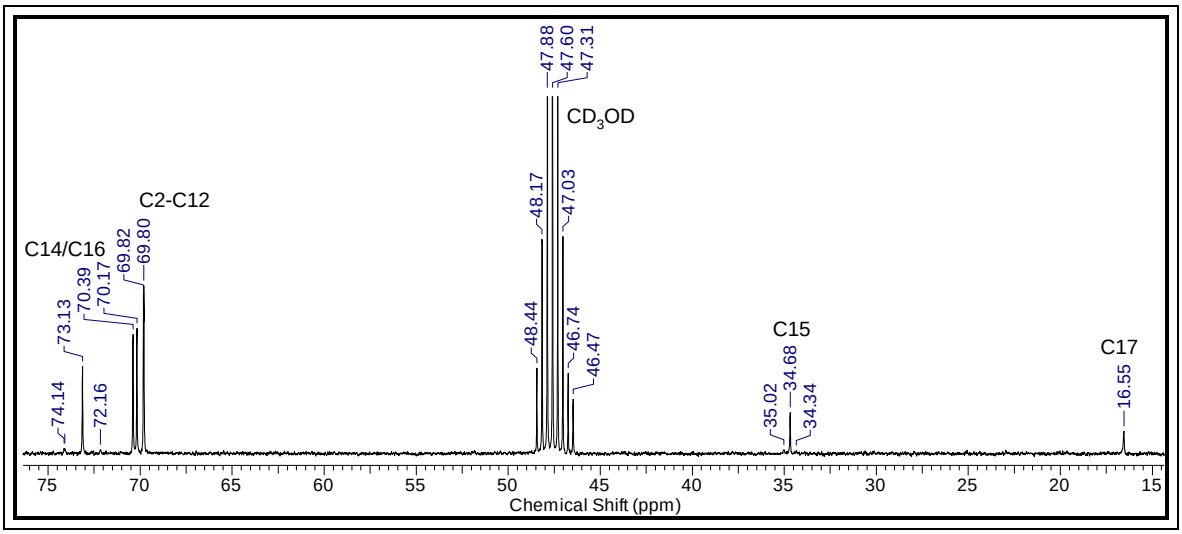

Figure 15. ^{13}C NMR spectrum of **10** showing the resonances for the C15, C17 and C2-C16 carbon in CD_3OD.

The ESI-MS spectrum of compound **10** in the negative mode is characterized by the observation of a mass cluster centered at m/z 443.0 that is assigned to $[\{(F_3(H_2O)SnCH_2\text{-}[16]\text{-crown-}5)(2CH_3CN)\}–H_2O–2CH_3CN\cdot F]^-$.

3.2.5. Complexation studies of the Trifluoridomonoorganotin-substituted-[16]-Crown-5

The addition of one molar equiv of $Et_4NF\cdot 2H_2O$ to a solution of **10** in CD_3OD (Scheme 4) causes no change to the ^{119}Sn and ^{19}F NMR spectra. This is a proof that the coordination of the fluoride anion is most probably inhibited by the intramolecular O→Sn interactions and/or by the coordination of water or methanol to the tin atom. Moreover, the reaction of **10** with deuterated water, D_2O, showed no evidence of formation of the resulting hydroxides. This demonstrates the stability of **10** toward hydrolysis (Scheme 4).

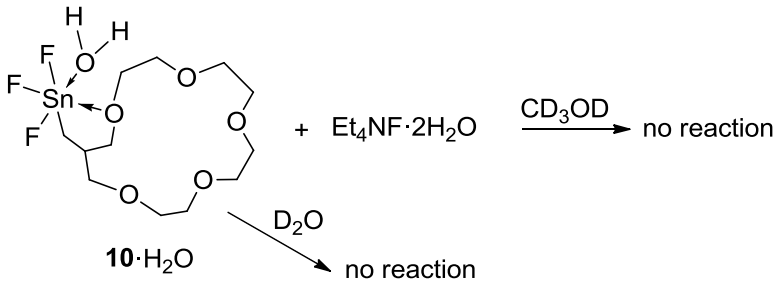

Scheme 4. Reaction of **10·H₂O** with $Et_4NF\cdot 2H_2O$ and D_2O, respectively.

3.2.6. Conclusions

An example of monoorganotin (IV) trifluoride stabilized by intra- and intermolecular O→Sn bonds has been synthesized and characterized. The strong O→Sn coordinations is not broken by addition of fluoride anion. The search for appropriate methods to synthesize trihydroxytin-substituted crown ether starting from the monoorganotin(IV) trifluoride represent further aims in this area.

3.3. Experimental Section

General methods. The solvents were dried and distilled from the appropriate desiccants prior to use. All manipulations were performed under an inert atmosphere of argon. Literature procedures were used to prepare $[HOSnCH_2([16]crown-5][CF_3SO_3^-]_2$.[26] The atom numbering of the crown ether fragments is shown in scheme 5.

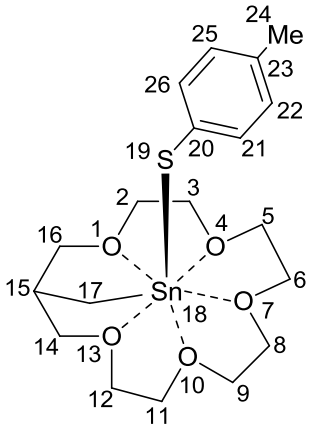

Scheme 5. Numbering scheme for the crown ether ring (1-17) in **4–6** and **10** and for **4** also 19-25.

NMR Spectroscopy. NMR spectra were recorded on Bruker DRX 400, DPX 300 spectrometers with broad band decoupling of ^{119}Sn at 111.92 MHz and ^{13}C at 100.61 MHz. Chemical shifts δ are given in ppm and referenced to tetramethylstannane (^{119}Sn), trichlorofluoromethane (^{19}F) and tetramethylsilane (^{1}H, ^{13}C).

Electrospray mass spectra were recorded on a Thermoquest-Finnigan instrument using CH_3CN as the mobile phase. The samples were introduced as solution in CH_3CN via a syringe pump operating at 0.5µL/min. The capillary voltage was 4.5 kV while the cone skimmer voltage varied between 50 and 250 kV. Identification of the expected ions was assisted by comparison of experimental and calculated isotope distribution patterns. The m/*z* values reported correspond to those of the most intense peak in the corresponding isotope pattern. **Elemental analyses** were performed on a LECO-CHNS-932 Analyser. **Melting points** were determined using a Büchi Melting Point M-560.

^{119}Sn Mössbauer spectroscopy

A $Ca^{119m}SnO_3$ source was used for the ^{119}Sn Mössbauer spectroscopic investigation. The sample was placed within a thin-walled glass container at a

thickness of about 10 mg Sn/cm^2. A palladium foil of 0.05 mm thickness was used to reduce the tin K X-rays concurrently emitted by this source. The measurement was conducted in the usual transmission geometry at 78 K with a total counting time of one day.

Synthesis of 4. *Para*-methylthiobenzene (0.11 g, 0.881 mmol) was added to a solution of **1**[26] (0.2 g, 0.294 mmol) in CH_3CN (25 mL) and the mixture was stirred for 3 h. The solvent was removed in vacuo to give colorless solid materials. Single crystals of **4** suitable for X-ray diffraction analysis were obtained by vapour diffusion of Et_2O into a solution of the compound in CH_3CN, yield 39 %; mp. 230°C.

^{1}H NMR (400,13 MHz, CD_3CN, 27°C, TMS): δ 1,67 (d, ^3J(H–H) = 4.0, ^2J(^{1}H–$^{117/119}$Sn) = 80.0Hz, 2H; $SnCH_2$), 2.35 (s, ^1J(^{1}H–^{13}C) = 24 Hz, 3H; CH_3), 2.91-2.94 (m, ^3J(^{1}H–$^{117/119}$Sn) = 480.0 Hz, 1H; CH), 3.59–4.45 ppm (m, 20H; O-CH_2), 7.25 (d, ^3J(^{1}H–^{1}H) = 8.0, 2H; HC22/HC25), 7.54 (d, ^3J(^{1}H–^{1}H) = 8.0, 2H; HC21/HC26); **^{13}C NMR** (100.63 MHz, CD_3CN, 27°C, TMS): δ = 20.2 (C_{17}), 20.7 (CH_3), 32.3 (^2J(^{13}C–$^{117/119}$Sn) = 76.5 Hz; C_{15}), 68.5–69.8 (C_2-C_{12}), 75.6 (^3J(^{13}C–$^{117/119}$Sn) = 47.3 Hz; C_{14}/C_{16}), 119.4 ppm (C_1 triflate), 120.8 ppm (C_{20}), 130.5 ppm (^1J(^{13}C–^{1}H) = 28.2 Hz; C_{21}/C_{26}), 137.29 ppm (^1J(^{13}C–^{1}H) = 34.2 Hz, C_{22}/C_{25}), 141.2 ppm (C23); **^{119}Sn{^{1}H} NMR** (300 MHz, CD_3CN, 20 °C): δ = –497 **Anal. Calcd** (%) for $C_{21}H_{30}F_6O_{11}S_3Sn$ (787.32): C 32.0, H 3.8; found C 31.9, H 4.0.

Synthesis of 5. *2*-Naphtholthiobenzene (0.13 g, 0.79 mmol) was added to a solution of **1**[26] (0.18 g, 0.26 mmol) in CH_3CN (20 mL) and the mixture was stirred for 3 h. The solvent was removed in vacuo to give colorless solid materials. Yield 47%; mp. 238.4°C. The ^{1}H, ^{13}C and ^{119}Sn data are identical with those of compound 4. **Anal.** calcd (%) for $C_{24}H_{30}F_6O_{11}S_3Sn$ (823.32): C 35.0, H 3.7; found C 34.8, H 3.6.

Synthesis of 6. Diphenyldithiophosphonic acid (0.22 g, 0.88 mmol) was added to a solution of **1**[26] (0.2 g, 0.294 mmol) in CH_3CN (25 mL) and the mixture was stirred for 3 h. The 3/4 of the solvent was removed in vacuo and the concentrated solution was kept at room temperature for a long period to afford colorless crystals of **6**, yield 21%; mp. 126 °C.

^{1}H NMR (499,79 MHz, CD_3CN, 27°C, TMS): δ 1.80 (d, $^{3}J(^{1}H–^{1}H)$ = 5 Hz, $^{2}J(^{1}H–^{117/119}Sn)$ = 64 Hz, 2H, CH_2), 2.54–2.58 (m, 1H, CH), 3.37–3.67 ppm (m, 20H; O-CH_2), 7.37-7.90 (m, 10H; Ph), **^{13}C NMR** (125.68 MHz, CD_3CN, 27°C): δ = 21.1 (C_{17}), 36.7 (C_{15}), 69.7–71.1 (C_2-C_{12}), 128.3–131.2 (phenyl), **^{119}Sn{^{1}H} NMR** (300 MHz, $CDCl_3$, δ : –366.24. **^{31}P NMR** (300 MHz, CD_3CN, 23°C): δ 57 and 58 (P*cis* and P*trans*). **Anal. Calcd** (%) for $C_{52}H_{72}N_2O_{10}P_2S_6Sn2$ (1376.80): C 41.9, H 4.8; found C 42.4, H 4.

Synthesis of 10·H_2O·2CH_3CN.

To a stirred solution of $[HOSnCH_2([16]crown-5)][CF_3SO_3]_2$[26] (0.156 g, 0.229 mmol) in CH_3CN (7 mL) was added dropwise to a solution of NEt_3·3HF (0.012 mL, 0.074 µmol). The mixture was stirred at room temperature overnight. The solution was then kept at –5°C for several days to afford 0.06 g (50%) of pure **11** as colorless crystals, mp. 90 °C.

^{1}H NMR (CD_3OD, 300.13 MHz, 295K) δ: 1.13 (d, $^{3}J(^{1}H–^{1}H)$ = 9.0 Hz, $^{2}J(^{1}H–^{117}Sn)$ = 129.0 Hz, $^{2}J(^{1}H–^{119}Sn)$ = 141.0 Hz, 2H, Sn-CH_2), 2.38 (m, 1H, CH), 3.53−3.86 (complex pattern, 20H, CH_2−O−CH_2), 4.88 (H_2O). **^{13}C{^{1}H} NMR** (CD_3OD, 75.48 MHz, 295 K) δ : 16.6 (C17), 34.7 ($^{2}J(^{13}C–^{117/119}Sn)$ = 51 Hz, C15), 69.8−70.4 (C2−C12), 73.2 ($^{3}J(^{13}C–^{117/119}Sn)$ = 149 Hz, C14/C16). $^{19}F\{^{1}H\}$ NMR (CD_3OD, 282.4 MHz, 211 K) δ: –156.3 ($^{1}J(^{19}F–^{117/119}Sn)$ = 2683 Hz). **^{119}Sn{^{1}H} NMR** (CD_3OD, 111.87 MHz, 213 K) δ: –572 (q, $^{1}J(^{119}Sn–^{19}F)$ = 2723 Hz). **Anal. Calcd.** for $C_{12}H_{23}F_3O_5Sn$ (424.1), Cacld : C 34.0 ; H 5.5. Found: C 34.1; H 6.2%.

2.4. References

(1) Pedersen, C. J. *J. Am. Chem. Soc.,* **1967**, *89*, 2495.

(2) Kolthoff, I. M.; Chantooni, M. K.; Roland, G. *J. Coord. Chem.,* **1999**, *48*, 207.

(3) Karkhaneei, E.; Afkhami, A.; Shamsipur, M. *J. Coord. Chem.,* **1996**, *39*, 33.

(4) D'Aprano, A.; Salomon, M.; Mauro, V. *J. Solution Chem.,* **1995**, *24*, 685-702.

(5) Ohtsu, K. K., T.; Ozutsumi, K. *Anal. Sci.,* **1996**, *12*, 37.

(6) Buschmann, H. J.; Cleve, E.; Schollmeyer, E. *Thermochim. Acta,* **1992**, *207*, 329.

(7) Wagner-Czauderna, E.; Koczorowska, A.; Kalinowski, M. K. *J. Coord. Chem.,* **1999**, *46*, 265.

(8) Wenz, G.; Buschmann, H. J.; Schollmeyer, E. *J. Coord. Chem.,* **1999**, *48*, 465.

(9) Potvin, P. G.; Lehn, J.-M. *In Synthesis of Macrocycles. The Design of Selective Complexing Agents*; Izatt, R. M., Christensen, J. J ed. New York, **1987**.

(10) Liindoy, L. F. *The Chemistry of Macrocyclic Ligand Complexes*; University Press ed. Cambridge, **1989**.

(11) Dietrich, B.; Viout, P.; Lehn, J.-M. *Aspect de la Chimie des Composés Macrocycliques* Paris, **1991**.

(12) Lehn, J.-M. *Supramolecular Chemistry: Concepts and Perspectives*; VCH ed. Weinheim, **1995**.

(13) Gokel, G. *Crown Ethers and Cryptandts*; Royal Society of Chemistry ed. Cambridges, **1994**.

(14) Beer, P. D.; Gale, P. A.; Smith, D. K. *Supramolecular Chemistry*; Oxford University Press ed. Oxford, **1999**.

(15) Steed, J. W.; Atwood, J. L. *Supramolecular Chemistry: An Introduction*; Wiley ed. Chichester, **2000**.

(16) Buschmann, H. J.; Mutihac, R.-D.; Schollmeyer, E. *J. Solution Chem.,* **2009**, *38*, 209-217.

(17) Lu, T.; Yang, G.; Ji, L.; Inoue, Y.; Ouchi, M.; Yu, K. *Trans. Metal Chem.,* **1999**, *24*, 375-379.

(18) Decken, A.; Jenkins, H. D. B.; Knapp, C.; Nikiforov, G. B.; Passmore, J.; Rautiainen, J. M. *Angew. Chem. Int. Ed.,* **2005**, *44*, 7958.

(19) Aragoni, M. C.; Arca, M.; Bencini, A.; Biagini, S.; Blake, A. J.; Caltagirone, C.; Demartin, F.; De Filippo, G.; Devillanova, F. A.; Garau, A.; Gloe, K.; Isaia, F.; Lippolis, V.; Valtancoli, B.; Wenzel, M. *Inorg. Chem.,* **2008**, *47*, 8391.

(20) Fuangswasdi, S.; Kaveevivitchai, N.; Tuntulani, T.; Savage, P. *J. Solution Chem.,* **2008**, *37*, 45-58.

(21) Li, J.-z.; Xu, B.; Jiang, W.-d.; Zhou, B.; Zeng, W.; Qin, S.-y. *Transition Met. Chem.,* **2008**, *33*, 975-979.

(22) Li, M.-J.; Chu, B. W.-K.; Zhu, N.; Yam, V. W.-W. *Inorg. Chem.,* **2007**, *46*, 720.

(23) Pajerski, A. D.; Parvez, M.; Richey, H. G. *J. Am. Chem. Soc.,* **1988**, *110*, 2660.

(24) Bott, S. G.; Alvanipour, A.; Morley, S. D.; Atwood, D. A.; Means, C. M.; Coleman, A. W.; Atwood, J. L. *Angew. Chem. Int. Ed.,* **1987**, *26*, 485.

(25) Shukla, P. R.; Sattar, A. *Asian J. Chem.,* **1997**, *9*, 598-601.

(26) Tagne Kuate, A. C.; Schürmann, M.; Schollmeyer, D.; Hiller, W.; Jurkschat, K. *Chem. Eur. J.,* **2010**, *16*, 8140.

(27) Reeske, G.; Schürmann, M.; Costisella, B.; Jurkschat, K. *European J. Inorg. Chem.,* **2005**, *2005*, 2881.

(28) Reeske, G.; Schürmann, M.; Costisella, B.; Jurkschat, K. *Organometallics,* **2007**, *26*, 4170.

(29) Reeske, G.; Bradtmöller, G.; Schürmann, M.; Jurkschat, K. *Chem. Eur. J.,* **2007**, *13*, 10239.

(30) Reeske, G.; Schurmann, M.; Jurkschat, K. *Dalton Trans.,* **2008**, 3398.

(31) Tagne Kuate, A. C.; Reeske, G.; Schürmann, M.; Costisella, B.; Jurkschat, K. *Organometallics,* **2008**, *27*, 5577.

(32) Tagne Kuate, A. C.; Iovkova, L.; Hiller, W.; Schürmann, M.; Jurkschat, K. *Organometallics,* **2010**, *29*, 5456.

(33) Holleman, A. F. W., E. *Inorganic Chemistry*; Wiberg N., Ed.; Academic Press ed. London, **2001**.

(34) Jurkschat, K.; Van Dreumel, S.; Dyson, G.; Dakternieks, D.; Bastow, T. J.; Smith, M. E.; Dräger, M. *Polyhedron,* **1992**, *11*, 2747.

(35) Kolb, U.; Draeger, M.; Jousseaume, B. *Organometallics,* **1991**, *10*, 2737.

(36) Schmidt, B. M.; Draeger, M.; Jurkschat, K. *J. Organometal. Chem.,* **1991**, *410*, 43.

(37) Jambor, R.; Dostál, L.; Růžička, A.; Císařová, I.; Brus, B.; Holčapek, M.; Holeček, J. *Organometallics,* **2002**, *21*, 3996.

(38) Varnek, V. A.; Yurchenko, E. N. *Theor. Exp. Chem* **1976**, *11*, 587.

(39) Zöller, T., Jurkschat, K.; unpublished results.

(40) Wagler, J.; Brendler, E.; Langer, T.; Pöttgen, R.; Heine, T.; Zhechkov, L. *Chem. Eur. J.,* **2010**, *16*, 13429.

(41) Jurkschat, K.; Mügge, C.; Tzschach, A.; Zschunke, A.; Engelhardt, G.; Lippmaa, E.; Magi, M.; Larin, M. F.; Pestunovich, V. A.; Voronkov, M. G. *J. Organometal. Chem.,* **1979**, *171*, 301.

(42) Jurkschat, K.; Mügge, C.; Tzschach, A.; Zschunke, A.; Fischer, G. W. *Z. Anorg. Allg. Chem.,* **1980**, *463*, 123.

(43) Swisher, R. G.; Day, R. O.; Holmes, R. R. *Inorg. Chem.,* **1983**, *22*, 3692.

(44) Otera, J.; Hinoishi, T.; Okawara, R. *J. Organometal. Chem.,* **1980**, *202*, C93.

(45) Jung, O.-S.; Hwa Jeong, J.; Soo Sohn, Y. *Polyhedron,* **1989**, *8*, 2557.

(46) Corbridge, D. E. C. *Studies in Inorganic Chemistry 6, Phosphorus*; Elsevier ed. Amsterdam, **1985**.

(47) Prakasha, T. K.; Day, R. O.; Holmes, R. R. *J. Am. Chem. Soc.,* **1993**, *115*, 2690.

(48) Clark, H. C.; O'Brien, R. J.; Trotter, J. *J. Chem. Soc.,* **1964**, *0*, 2332.

(49) Schlemper, E. O.; Hamilton, W. C. *Inorg. Chem.,* **1966**, *5*, 995.

(50) Tudela, D.; Fernandez, R.; Belsky, V. K.; Zavodnik, V. E. *J. Chem. Soc., Dalton Trans.,* **1996**, *0*, 2123.

(51) Tudela, D.; Gutierrez-Puebla, E.; Monge, A. *J. Chem. Soc., Dalton Trans.,* **1992**, *0*, 1069.

(52) Jagirdar, B. R.; Murphy, E. F.; Roesky, H. W. *Prog. Inorg. Chem.* **1998**, *48*, 351.

(53) Al-Juaid, S. S.; Dhaher, S. M.; Eaborn, C.; Hitchcock, P. B.; Smith, J. D. *J. Organometal. Chem.,* **1987**, *325*, 117.

(54) Reuter, H.; Puff, H. *J. Organometal. Chem.,* **1989**, *379*, 223.

(55) Beckmann, J.; Horn, D.; Jurkschat, K.; Rosche, F.; Schürmann, M.; Zachwieja, U.; Dakternieks, D.; Duthie, A.; Lim, A. E. K. *Eur. J. Inorg. Chem.,* **2003**, *2003*, 164.

(56) Kolb, U.; Draeger, M.; Dargatz, M.; Jurkschat, K. *Organometallics,* **1995**, *14*, 2827.

(57) Mehring, M.; Vrasidas, I.; Horn, D.; Schürmann, M.; Jurkschat, K. *Organometallics,* **2001**, *20*, 4647.

(58) Pieper, N.; Klaus-Mrestani, C.; Schürmann, M.; Jurkschat, K.; Biesemans, M.; Verbruggen, I.; Martins, J. C.; Willem, R. *Organometallics,* **1997**, *16*, 1043.

(59) Pieper, N.; Ludwig, R.; Schürmann, M.; Jurkschat, K.; Biesemans, M.; Verbruggen, I.; Willem, R. *Phosphorus Sulfur Silicon Relat. Elem.,* **1999**, *150*, 305.

(60) Svec, P.; Novak, P.; Nadvornik, M.; Padelkova, Z.; Cisarova, I.; Kolarova, L.; Ruzicka, A.; Holecek, J. *J. Fluor. Chem.,* **2007**, *128*, 1390.

(61) Dostal, L.; Jambor, R.; Ruzicka, A.; Jirasko, R.; Cisarova, I.; Holecek, J. *J. Fluor. Chem.,* **2008**, *129*, 167.

(62) Novak, P.; Cisarova, I.; Kolarova, L.; Ruzicka, A.; Holecek, J. *J. Organometal. Chem.,* **2007**, *692*, 4287.

(63) Dostal, S.; Stoudt, S. J.; Fanwick, P.; Sereatan, W. F.; Kahr, B.; Jackson, J. E. *Organometallics,* **1993**, *12*, 2284.

(64) Arens, V. Diplomarbeit, TU-Dortmund, **2008**.

(65) Tagne Kuate, A. C. Ph.D. Thesis, TU- Dortmund, **2009**.

4. On the Reaction of (t-$Bu_2SnO)_3$ with PhX_2SnCH_2R (X = I, Br, Cl; R = 13-crown-4, 16-crown-5). Formation of Novel Asymmetric Tetraorganodistannoxane

4.1. Introduction

Dimeric tetraorganodistannoxannes of the general formula $[R_2(X)SnOSn(Y)R_2]_2$ (R = alkyl, aryl; X, Y= halogen, OH, OR, $OSiMe_3$, OOCR, $OSP(OR)_2$, NO_3, N_3, NCS, SH, $OReO_3$) (Scheme 1, type **A**) represent an interesting class of organotin–oxo clusters that has attracted a growing interest in the last three decades.[1,2] These compounds have been reported to be able to act as homogeneous catalysts in various organic reactions.[3-9] Dimeric tetraorganodistannoxanne derivatives with X, Y = halogen, OH are generally obtained by the controlled hydrolysis of diorganotin dihalides[10,11] or from the reaction of diorganotin dihalides with equimolar amounts of diorganotin oxides.[12,13]The latter method takes advantage of the trimer (t-$Bu_2SnO)_3$ which is a convenient oxide transfer reagent in reactions with organotin halides[14] and of the fact that no by-products are formed that need to be removed.[2] In previous work, *Jurkschat* and coworkers made use of the last synthetic strategy to design the dimeric tetraorganodistannoxane of type **B** (Scheme 1).[13] The latter compound showed that the hydroxide group is bridged between two tin atoms and contains two different organic groups at the *endo*- and *exo*-cyclic tin atoms. Given the ability of crown ethers to interact with Lewis acidic tin center through O→Sn interaction and to be involved in hydrogen bonding interactions, we were interested in the synthesis and structural determination of novel dimeric tetraorganodistannoxanes of type **C** (Scheme 1), with Z = I, Br, Cl; R´´ = 13-crown-4, 16-crown-5.

Scheme 1

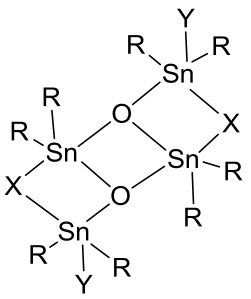

R = alkyl, aryl

X, Y = halogen, OH, OR, $OSiMe_3$ OCOP, $OP(S)(OR)_2$, NO_3, N_3, NCS, $OReO_3$

A

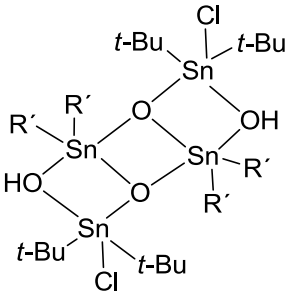

R´ = CH_2SiMe_3

B

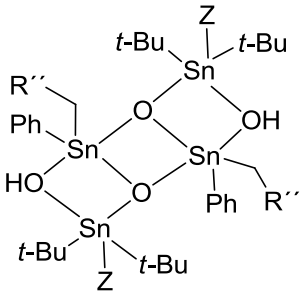

R´´ = 13-crown-4, 16-crown-6

Z = I, Br, Cl

C

4.2. Synthesis of the Tetraorganodistannoxanes.

The reaction of equimolar amounts of di-*tert*-butyltin oxide $(t\text{-}Bu_2SnO)_3$ with dihalogenido diorganotin-substituted crown ethers {(PhX_2SnCH_2-R), R = 13-crown-4, 16-crown-5, X = I, Br, Cl} in dichloromethane provided the dimeric tetraorganodistannoxannes **1**–**5** (eq. 1). All these Compounds are slight yellow (**1** and **3**) or colorless (**2**, **4** and **5**), high-melting crystalline solids, which are soluble in common organic solvents such as dichloromethane, chloroform, and toluene.

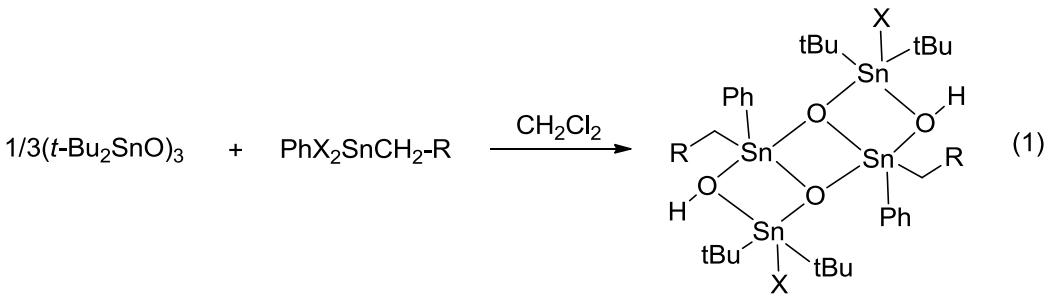

(1)

1, X = I, R = 13-crown-4

2, X = Br, R = 13-crown-4

3, X = I, R = 16-crown-5

4, X = Br, R = 16-crown-5

5, X = Cl, R = 16-crown-5

4.3. Molecular Structures of the Tetraorganodistannoxanes 1–5.

The molecular structures of compounds **1**–**5** are shown in Figures 1–5. Selected bond distances and bond angles are listed in Tables 1 and 2. All five compounds crystallize in the triclinic space group P–1 with one molecule per unit cell. Compounds **4** and **5** crystallize each as dichloromethane solvate.

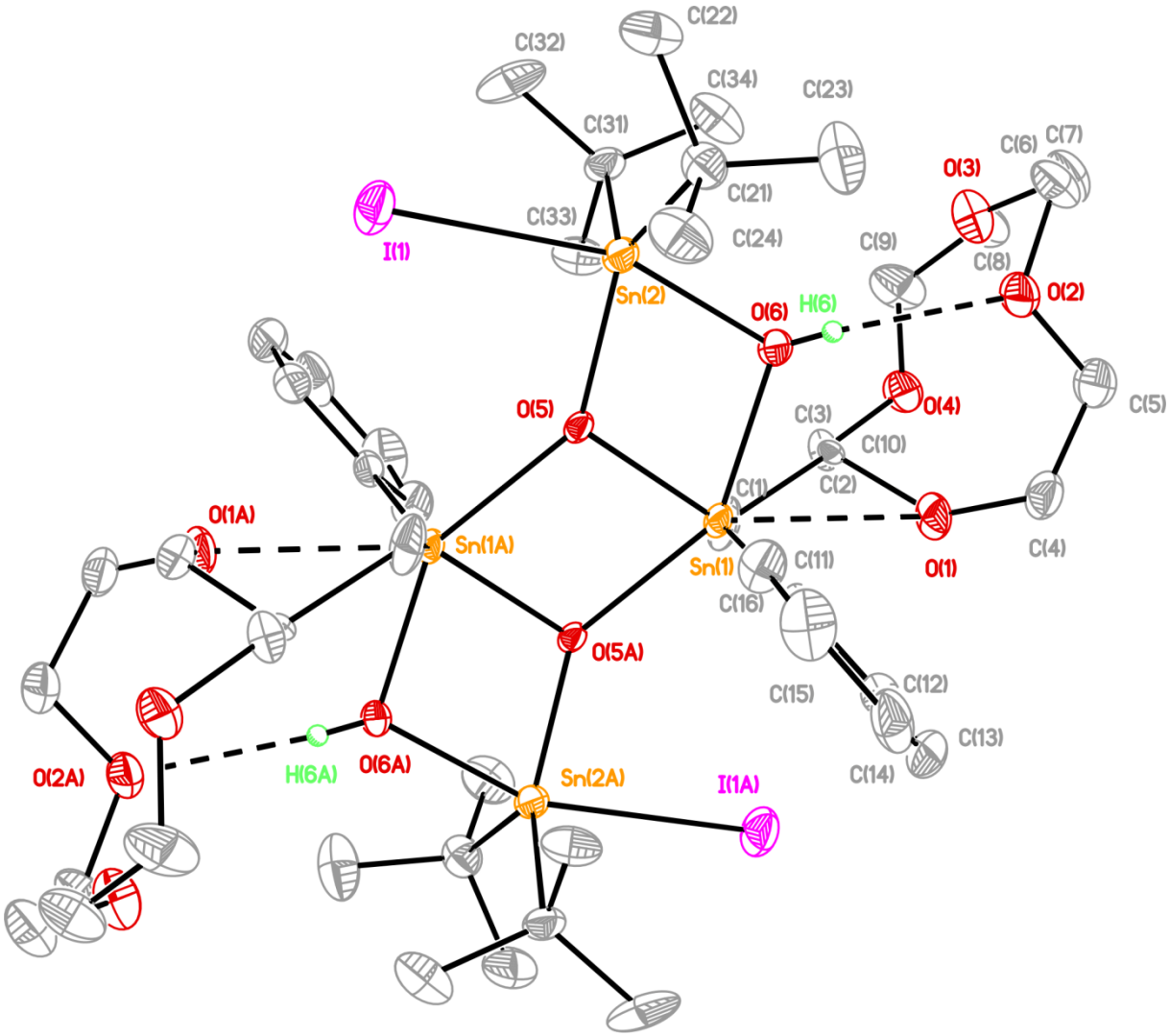

Figure 1. General view (SHELXTL) of a molecule of **1** showing 30% probability displacement ellipsoids and the crystallographic numbering scheme.

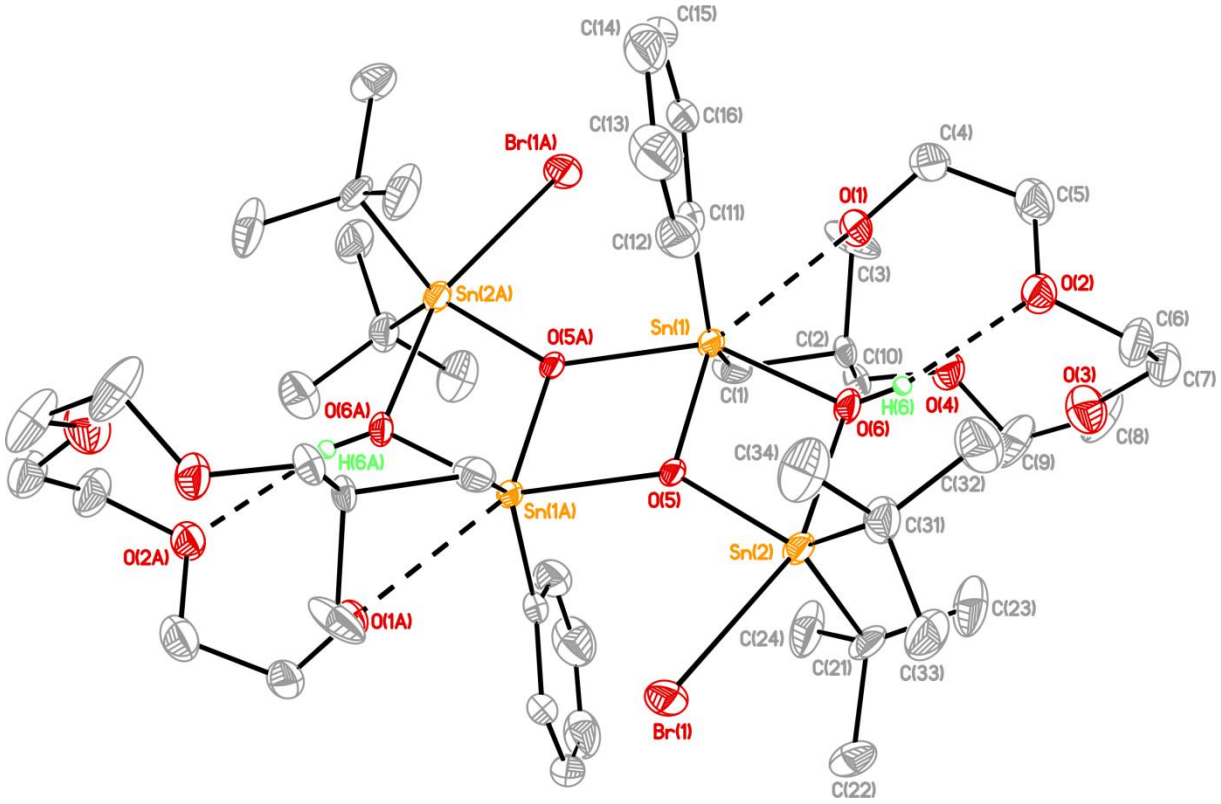

Figure 2. General view (SHELXTL) of a molecule of **2** showing 30% probability displacement ellipsoids and the crystallographic numbering scheme.

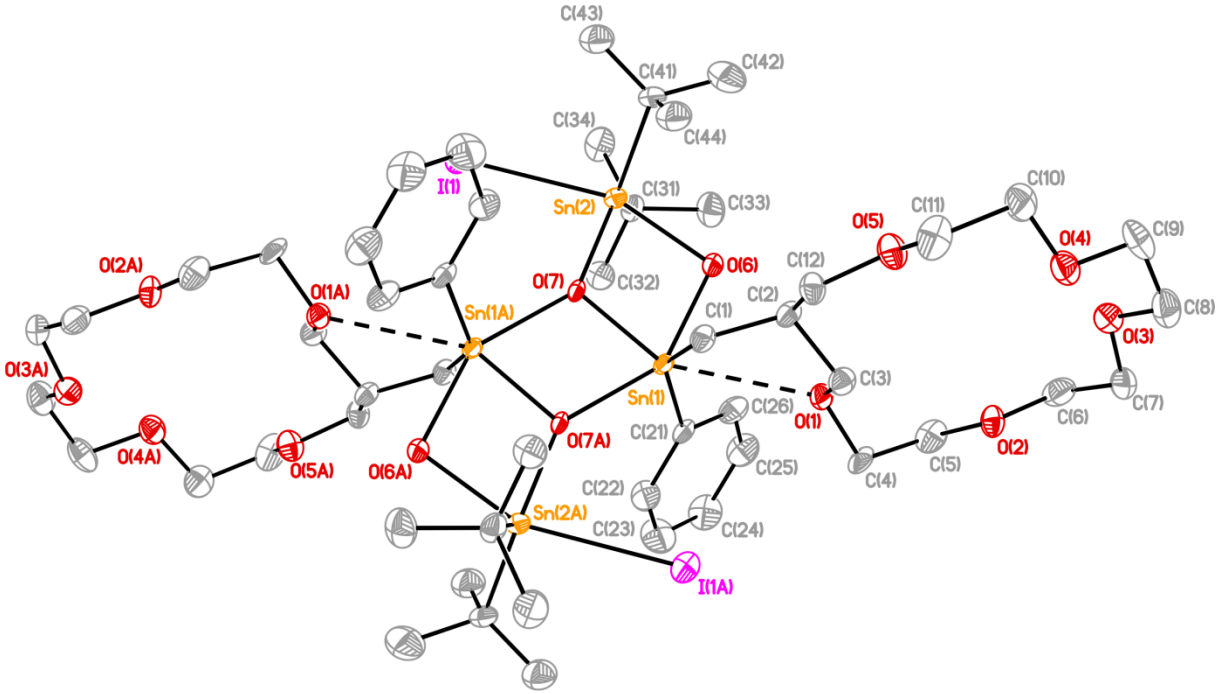

Figure 3. General view (SHELXTL) of a molecule of **3** showing 30% probability displacement ellipsoids and the crystallographic numbering scheme.

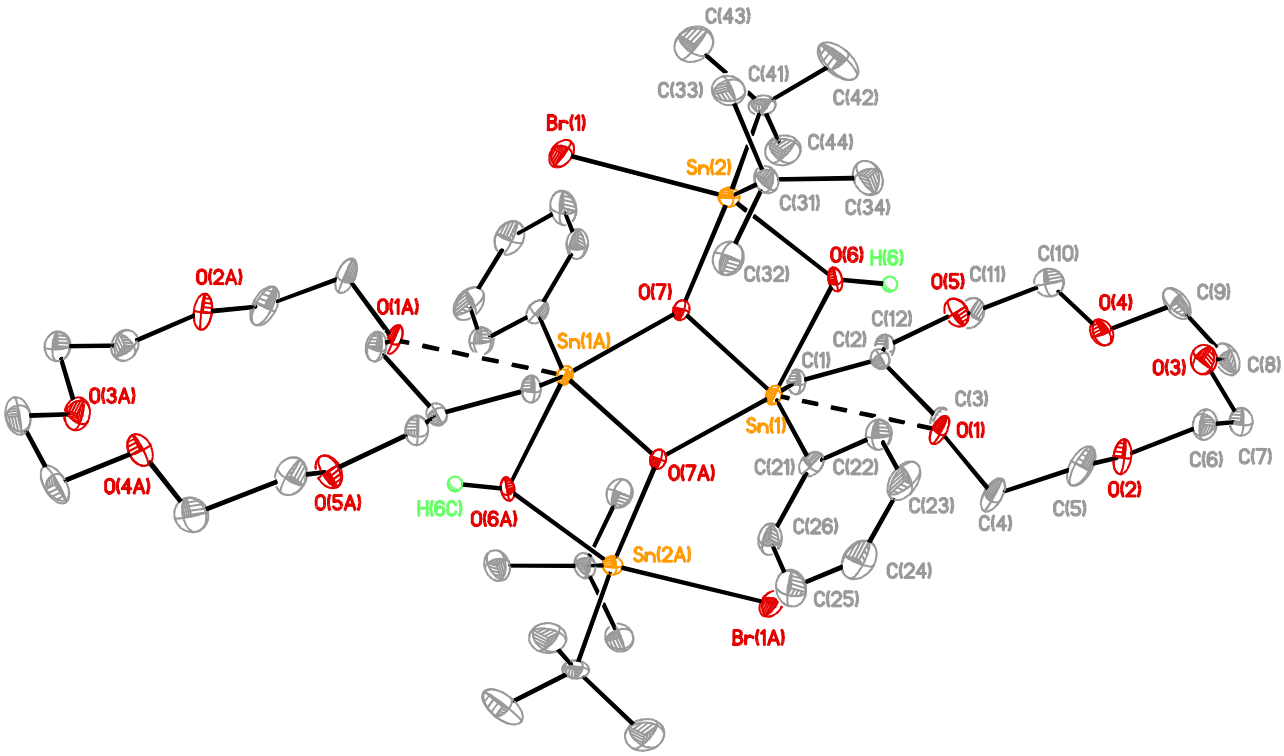

Figure 4. General view (SHELXTL) of a molecule of **4** showing 30% probability displacement ellipsoids and the crystallographic numbering scheme. The dichloromethane molecule is omitted for clarity.

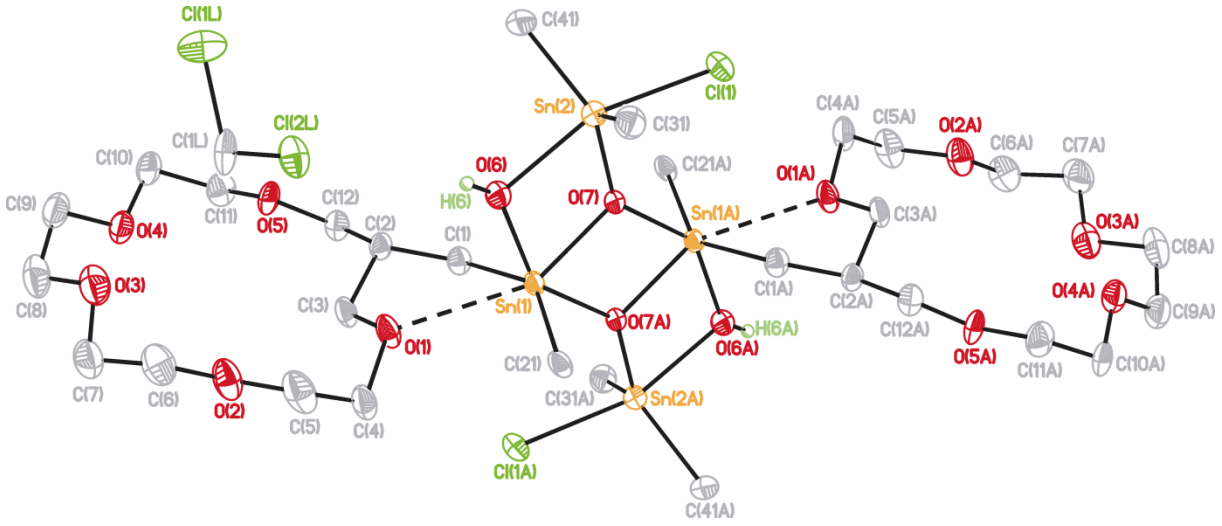

Figure 5. General view (SHELXTL) of a molecule of **5** showing 30% probability displacement ellipsoids and the crystallographic numbering scheme. The *tert*-butyl and phenyl groups are omitted for clarity.

Table1. Selected interatomic distances (Å) for compounds **1–5**.

	1 X = I	**2** X = Br	**3** X = I	**4** X = Br	**5** X = Cl
Sn(1)–O(1)	2.670(3)	2.682(3)	2.819(5)	2.795(3)	2.822(5)
Sn(1)–O(5)	2.062(3)	2.061(3)	–	–	–
Sn(1)–O(7)	–	–	2.070(4)	2.066(3)	2.062(4)
Sn(1)–O(5A)	2.185(3)	2.190(3)	–	–	–
Sn(1)–O(7A)	–	–	2.170(5)	2.155(3)	2.149(4)
Sn(1)–O(6)	2.123(4)	2.169(3)	2.155(5)	2.155(3)	2.145(4)
Sn(1)–C(11)	2.141(5)	2.131(5)	–	–	–
Sn(1)–C(21)	–	–	2.121(7)	2.119(4)	2.126(6)
Sn(1)–C(1)	2.116(6)	2.124(5)	2.124(8)	2.118(4)	2.128(6)
Sn(2)–X(1)	2.9592(5)	2.7114(6)	2.9416(8)	2.7140(7)	2.5367(18)
Sn(2)–O(5)	2.022(3)	2.014(3)	–	–	–
Sn(2)–O(6)	2.158(4)	2.169(3)	2.180(5)	2.172(3)	2.206(4)
Sn(2)–O(7)	–	–	2.017(4)	2.013(2)	2.028(4)
Sn(2)–C(31)	2.189(5)	2.205(5)	2.205(8)	2.196(5)	2.191(8)
Sn(2)–C(21)	2.201(6)	2.191(5)	–	–	–
Sn(2)–C(41)	–	–	2.197(8)	2.190(5)	2.207(7)
H(6)–O(2)	2.23(5)	2.22(2)	–	–	–

Table 2. Selected Bond Angles (deg) for compounds **1**–**5**.

	1 X = I	**2** X = Br	**3** X = I	**4** X = Br	**5** X = Cl
O(5)–Sn(1)–C(1)	113.45(18)	113.95(15)	–	–	–
O(7)–Sn(1)–C(1)	–	–	108.1(2)	108.00(13)	108.4(2)
O(5)–Sn(1)–O(6)	72.69(14)	72.20(11)	–	–	–
O(7)–Sn(1)–O(6)	–	–	72.69(18)	72.18(10)	72.69(16)
C(1)–Sn(1)–O(6)	98.4(2)	100.10(18)	95.0(3)	95.77(14)	97.2(2)
O(7)–Sn(1)–C(21)	–	–	108.4(2)	108.16(14)	109.16(19)
O(5)–Sn(1)–C(11)	104.68(17)	105.28(15)	–	–	–

C(1)–Sn(1)–C(11)	141.2(2)	139.86(18)	–	–	–
C(1)–Sn(1)–C(21)	–	–	143.6(3)	143.84(16)	142.4(2)
O(6)–Sn(1)–C(11)	99.28(19)	99.56(16)	–	–	–
O(6)–Sn(1)–C(21)	–	–	94.5(3)	94.72(14)	95.1(2)
O(5)–Sn(1)–O(5A)	74.04(14)	73.66(11)	–	–	–
O(7)–Sn(1)–O(7A)	–	–	74.78(19)	74.27(10)	73.71(17)
C(1)–Sn(1)–O(5A)	90.00(19)	88.99(16)	–	–	–
C(1)–Sn(1)–O(7A)	–	–	94.4(2)	94.41(13)	93.7(2)
O(6)–Sn(1)–O(5A)	146.32(13)	145.47(10)	–	–	–
O(6)–Sn(1)–O(7A)	–	–	147.46(18)	146.46(10)	146.40(16)
C(11)–Sn(1)–O(5A)	93.96(16)	94.19(13)	–	–	–
C(21)–Sn(1)–O(7A)	–	–	96.1(3)	95.65(14)	95.5(2)
O(5)–Sn(1)–O(1)	146.86(12)	146.44(10)	–	–	–
O(7)–Sn(1)–O(1)	–	–	151.26(16)	150.14(9)	149.46(16)
C(1)–Sn(1)–O(1)	70.93(17)	70.61(15)	69.4(2)	69.49(13)	69.6(2)
O(6)–Sn(1)–O(1)	74.17(14)	74.28(11)	78.97(16)	78.41(10)	77.30(16)
C(11)–Sn(1)–O(1)	81.20(16)	81.64(14)	–	–	–
C(21)–Sn(1)–O(1)	–	–	78.1(2)	78.95(14)	78.73(19)
O(5A)–Sn(1)–O(1)	138.82(12)	139.45(9)	–	–	–
O(7A)–Sn(1)–O(1)	–	–	133.36(16)	134.94(9)	136.13(15)
O(5)–Sn(2)–O(6)	72.70(14)	72.11(11)			
O(7)–Sn(2)–O(6)	–	–	73.17(18)	72.81(10)	72.05(16)
O(5)–Sn(2)–C(31)	113.8(2)	124.16(15)	–	–	–
O(7)–Sn(2)–C(31)	–	–	116.4(3)	116.90(15)	117.9(2)
O(6)–Sn(2)–C(31)	94.68(19)	95.50(17)	94.8(2)	94.68(19)	94.5(2)
O(5)–Sn(2)–C(21)	124.70(18)	114.06(16)	–	–	–
O(7)–Sn(2)–C(41)	–	–	120.7(3)	120.71(15)	118.9(2)
O(6)–Sn(2)–C(21)	95.0(2)	94.21(16)	–	–	–
C(31)–Sn(2)–C(21)	121.0(2)	121.15(19)	–	–	–
C(31)–Sn(2)–C(41)	–	–	122.3(3)	121.70(18)	122.3(3)
O(5)–Sn(2)–X(1)	88.49(9)	87.80(8)	–	–	–
O(7)–Sn(2)–X(1)	–	–	84.48(13)	84.04(8)	84.80(11)
O(6)–Sn(2)–X(1)	160.48(11)	159.45(9)	157.64(13)	156.82(7)	156.77(13)
C(31)–Sn(2)–X(1)	97.76(15)	92.22(13)	94.6(2)	94.72(13)	94.7(2)

C(21)–Sn(2)–X(1)	91.42(15)	98.04(13)	–	–	–
C(41)–Sn(2)–X(1)	–	–	97.7(2)	99.13(13)	99.8(2)

The overall structures of these compounds are similar and differ from each other by the nature of the halogen and the organic groups at the *endo*-cyclic tin atoms. The main feature in the molecular structures of **1**–**5** are the central four-membered Sn_2O_2-rings containing the Sn(1) atoms and the Sn(2) atoms which are linked *exo*-cyclic to these rings. The whole molecule gives rise to the formation of ladder type centrosymmetric dimers. Another aspect of the molecular structures of compounds **1**–**5** is the location of the crown ethers moieties on both sides of the tetraorganodistannoxane ladder core. In other words, compounds **1**–**5** adopt each a *trans*-configuration in the solid state and are comparable to the usual *trans*-configuration found for related compounds in the solid state.[15] Each tin atom exhibits a distorted trigonal bipyramidal configuration [geometrical goodness $\Delta\Sigma(\theta)$[16] 48.06° (Sn1) and 81.83°(Sn2) (**1**), 48.09°(Sn1) and 81.31°(Sn2) (**2**), 43.91° (Sn1) and 82.62°(Sn2)(**3**), 45.36° (Sn1) and 81.42°(Sn2) (**4**), 44.45° (Sn1) and 79.80°(Sn2) (**5**) with {C(1), C(11), O(6) (Sn1) and C(21), C(31), O(5) (Sn2) (**1** and **2**), C(1), C(21), O(6) (Sn1) and C(31), C(41), O(7) (Sn2) (**3**–**5**) occupying the equatorial positions. The axial positions are occupied by O(1) and O(5)(Sn1) (**1** and **2**), O(6), I(1) (**1**), and Br(1)(**2**)(Sn2), O(1) and O(7)(Sn1) (**3**–**5**), O(6), I(1)(**3**) and Br(1) (**4**), Cl(1)(**5**)(Sn2)(**3**–**5**). The distortion is best reflected in the decrease of the O(1)–Sn(1)–O(5) (Sn1, **1**), O(6)–Sn(2)–I(1) (Sn2, **1**), O(1)–Sn(1)–O(5) (Sn1, **2**), O(6)–Sn(2)–Br(1) (Sn2, **2**), O(1)–Sn(1)–O(7) (Sn1, **3**), O(6)–Sn(2)–I(1) (Sn2, **3**), O(1)–Sn(1)–O(7) (Sn1, **4**), O(6)–Sn(2)–Br(1) (Sn2, **4**), O(1)–Sn(1)–O(7) (Sn1, **5**), O(6)–Sn(2)–Cl(1) (Sn2, **5**) axial angles from 180° to 146.86(12)°, 160.48(11)°, 146.44(10)°, 159.45(9)°, 151.26(16)°, 157.64(13)°, 150.14(9)°, 156.82(7)°, 149.46(16)°, 156.77(13)°. Compounds **1**–**5** are characterisized by the intramolecular O(1)→Sn(1) interactions at distances of 2.670(3) Å, 2.682(3) Å, 2.819(5) Å, 2.795(3) Å, and 2.822(5) Å, respectively, which are shorter than the sum of the van der Waals radii[17] of tin (2.17 Å) and oxygen (1.52 Å). In addition, there is formation of an intramolecular H(6)···O(2) coordination (**1** and **2**), when the organic substituent (R) is 13-crown-4. The absence of the intramolecular H(6)···O(2) interactions in compounds **3**–**5** can be explained by the presence of the 16-crown-5 moiety which is more bulky than the 13-

crown-4 analogues. The latter organic group makes the molecule more flexible and promotes intramolecular bonds. This finding was confirmed by the Sn(1)–O(1) distances found in **3**–**5** (2.819(5) (**3**); 2.795(3) (**4**); 2.822(5) (**5**)) which are significantly longer than the corresponding distances obtained for compounds **1** (2.670(3)) and **2** (2.682(3). Both H(6)···O(2) distances (2.23(5)(**1**) Å, 2.22(2)(**2**) Å) are shorter than the sum of the van der Waals radii[17] of H(1.10 Å) and O(1.52 Å). Moreover, the IR spectra of the two latter compounds showed for the SnOH group an absorption band at $\bar{\nu}$ = 3490 and 3499 cm^{-1}, respectively, which are displaced by 47 and 56 cm^{-1}, respectively, in comparison with compound **4** in which no intramolecular O···H bond is present.

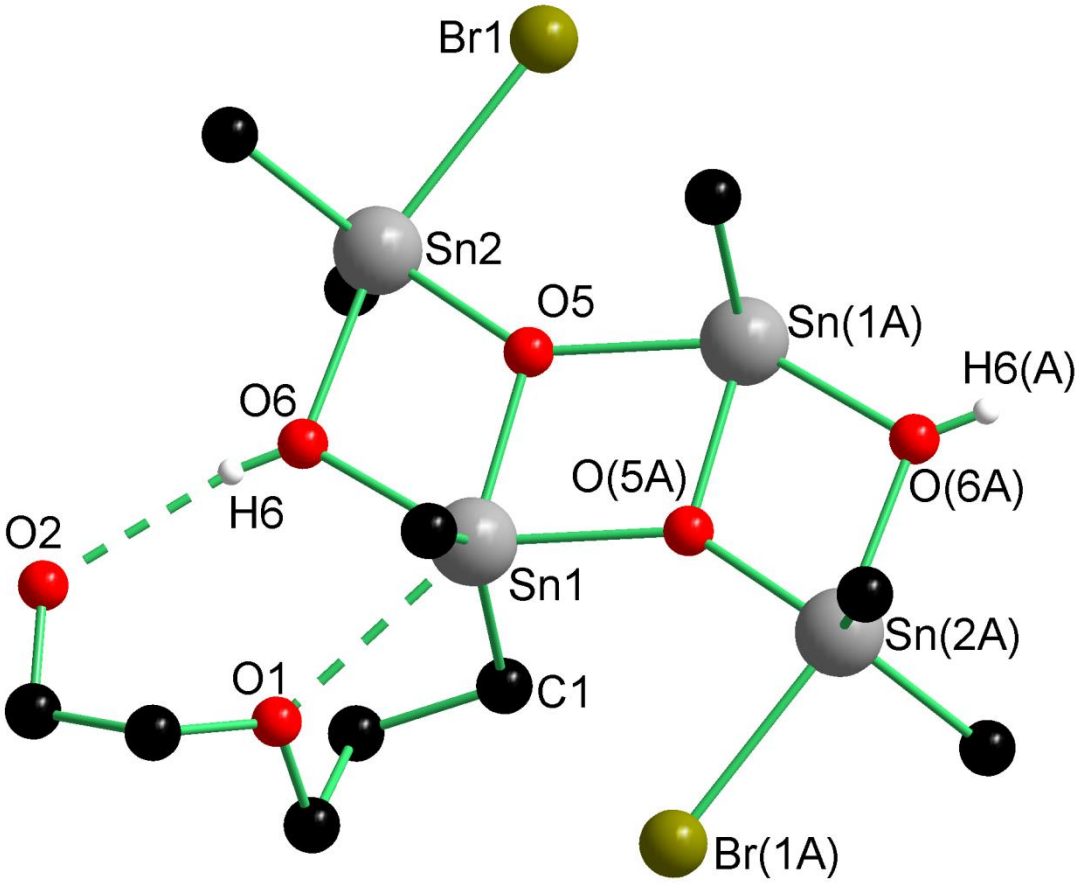

Figure 6. Reduced ball-and-sticks molecular structure of **2** showing the intramolecular O(2)···H(6) and O(1)→Sn(1) interactions. The crown ether ring, the phenyl and the *tert*-butyl groups are omitted.

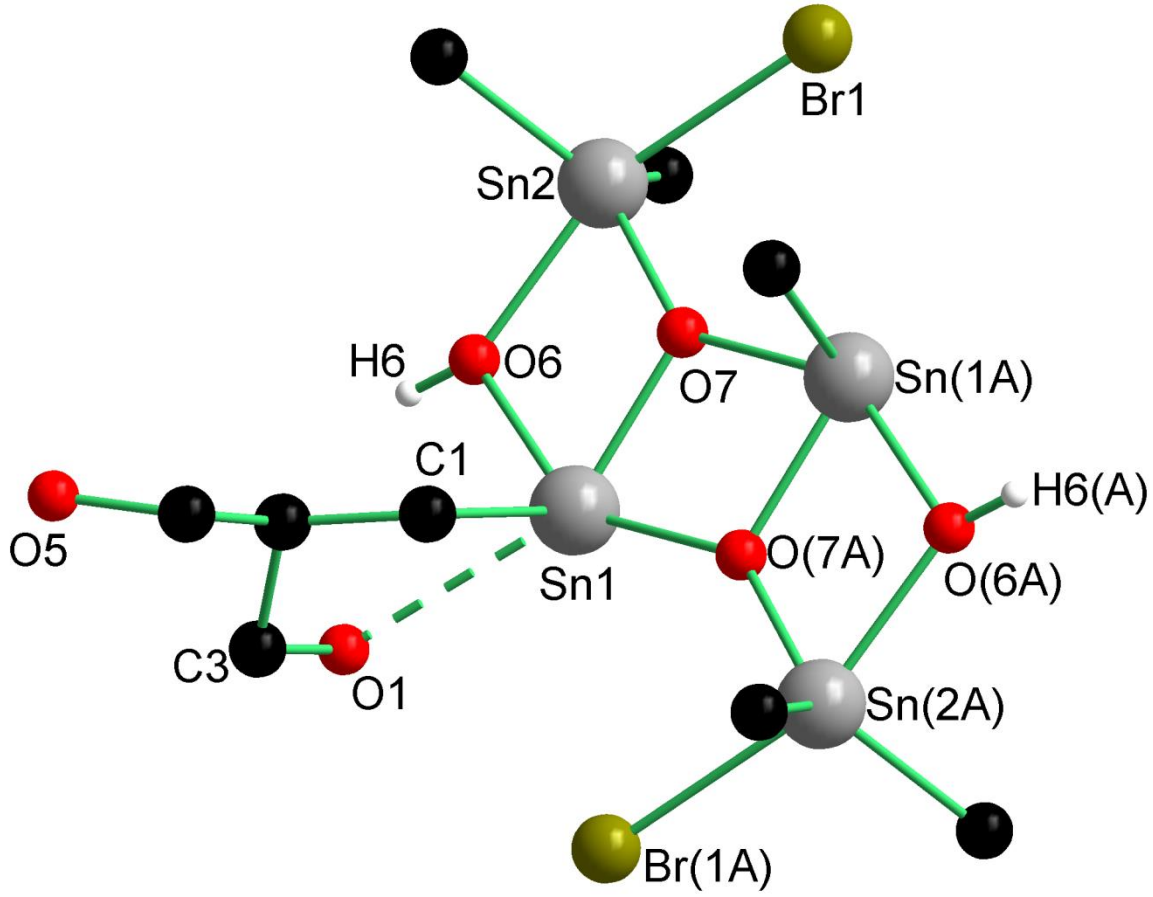

Figure 7. Reduced ball-and-sticks molecular structure of **4** showing the intramolecular O(1)→Sn(1) and no O(5)···H(6) interactions. The crown ether ring, the phenyl and the *tert*-butyl groups are omitted.

4.4. Structures in Solution of the Tetraorganodistannoxanes 1–5.

The ^{119}Sn NMR spectrum of a solution of compound **4** in CD_2Cl_2 shows two major resonances, which account for about 70 % of the total integrated signal intensity of the ^{119}Sn spectrum, at δ –311 ($^{2}J(^{119}Sn–^{117}Sn$ = 254 Hz) and – 208 ($^{2}J(^{119}Sn–^{117}Sn$ = 254 Hz) (Figure 8). Due to the intramolecular Sn(1)–O(1) coordination between the oxygen atom of the crown ether ring and the *endo*-cyclic tin atom, the resonance at δ –311.2 is assigned to the *trans* Sn(1) atom (according to the numbering scheme shown in Scheme 4), whereas the resonance at δ –208 correspond to the *trans* exocyclic (*t*-Bu_2Sn) tin atoms (Scheme 2). In addition, the ^{119}Sn NMR spectrum contains two signals at δ –310.8 and –209, for which the $^{117/119}$Sn satellites could not be detected unambiguously.

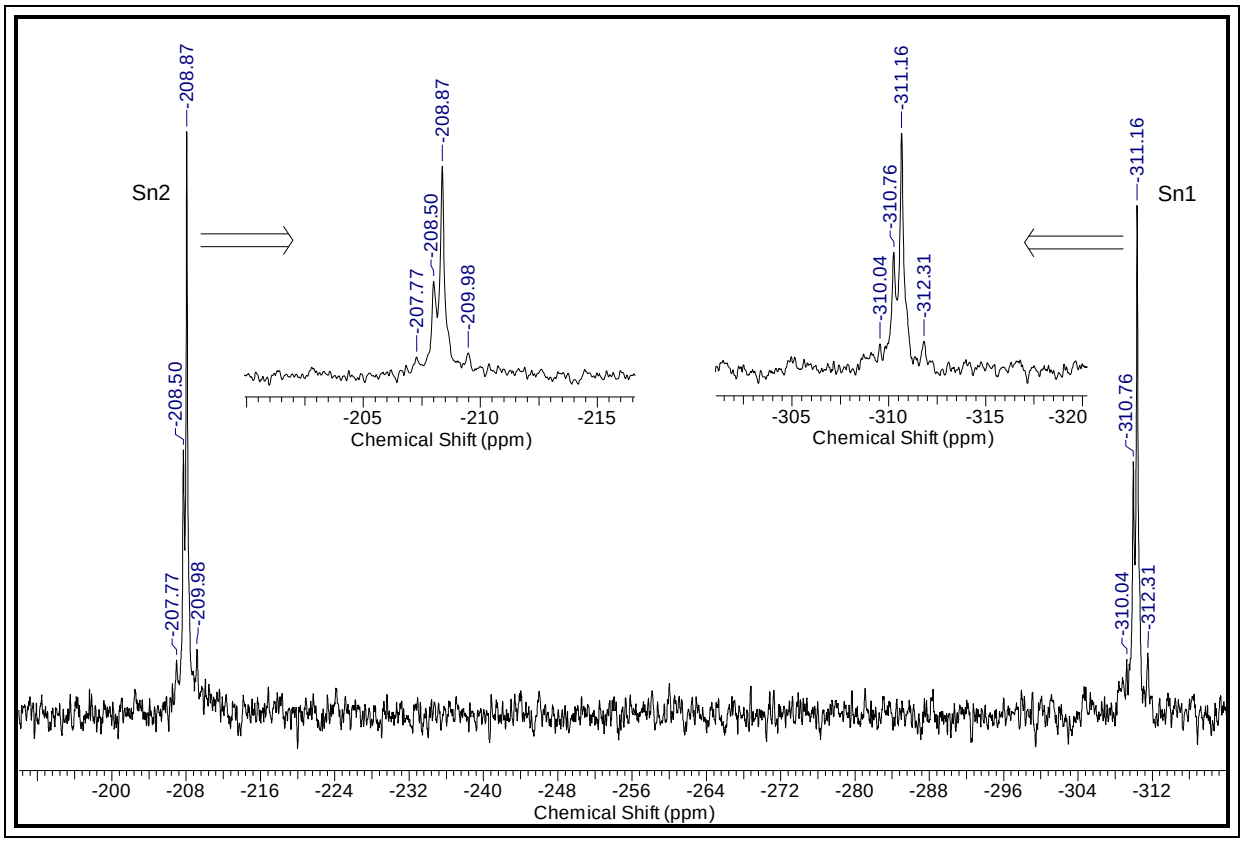

Figure 8. ^{119}Sn NMR spectrum of **4** in CD_2Cl_2 at 23°C.

These resonances contribute approximately 30 % toward the total signal intensity of the spectrum, and were assigned to the *cis* endocyclic (Sn(1)) and the *cis* exocyclic (*t*-Bu_2Sn) tin atoms (Scheme 2).

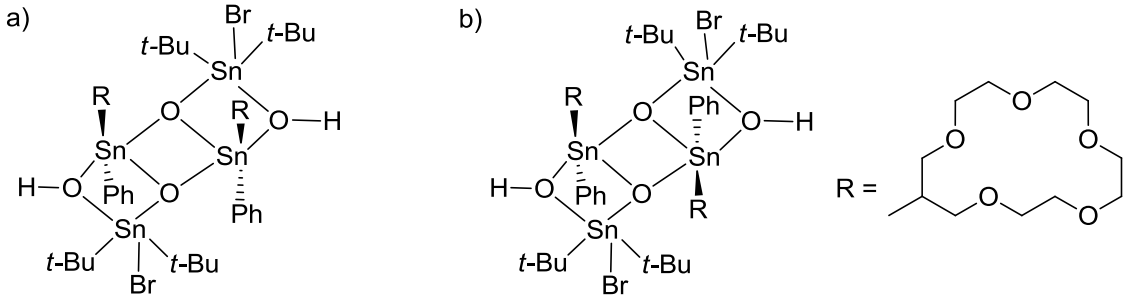

Scheme 2. Configuration adopted by the *endo*-cyclic and *exo*-cyclic tin atoms of compound **4** in solution a) cis and b) trans.

These observations are in contrast to the chemicals shifts of the tin atoms obtained for the tetraorganodistannoxanes containing crown ethers $\{[Bu_2Sn(OCOR)]_2O\}_2$.[18] Indeed, the latter compound showed in the ^{119}Sn NMR spectrum two resonances at δ – 213.0 and – 217.3.

The ^{1}H NMR spectrum of **4** displays three sets of resonances at *δ* 1.3, 3.26–3.58, 7.15-8.01, which are assigned to the *tert*-butyl substituents, the crown ether protons and the phenyl groups, respectively. Additional resonances of low intensity appear at *δ* 1.59 ($^{2}J(^{1}H–^{117/119}Sn)$ = 42 Hz), 2.70, which are attributed to the C1 and C2 protons (according to the numbering scheme shown in Scheme 4), respectively. This assignment is also supported by the ^{13}C NMR spectrum, which displays for the *tert*-butyl substituents, the crown ether carbon atoms and phenyl groups, resonances at *δ* 29.7–30.6, 69.3–70.5 and 127.0–145.3, respectively. There are additional two low-intensity resonances at *δ* 15.1 and 36.1 ($^{2}J(^{13}C–^{117/119}Sn)$ = 21 Hz), which are assigned to the C2 and C1 carbon atoms, respectively. Solution NMR results for compounds **1**–**3** and **5** are similar. The ESI-MS spectra in the positive mode of compounds **1** and **2** are characterized by the observation of mass clusters centered at *m/z* 831.3, 913.3, 1079.3 and 1139.3 that are assigned to the species a, b, c and d (Scheme 3) respectively. For compounds **3**–**5**, the ESI-MS in the positive mode revealed mass clusters centered at m/z 919.2, 959.2 and 1167.2 that correspond to the species a, e and c, respectively (Chart 2). In addition, for compounds **4** and **5**, there are mass clusters centered at m/z 1213.4 and 1227.4 that are assigned to the species f and g (Scheme 3), respectively. Representatives examples of the experimental and simulated mass cluster of compounds **1**–**5** are shown in Figure 9 and 10.

Scheme 3

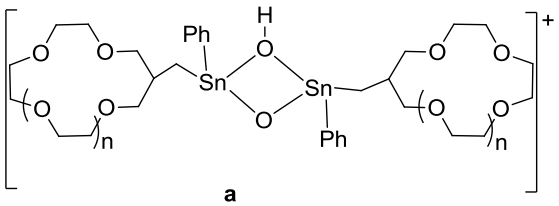

a

$[M\text{-}2(Sn(t\text{-}Bu)XOH)\cdot H]^+$

1a, M = **1**, n = 1, X = **I**, 831.3

2a, M = **2**, n = 1, X = Br, 831.3

3a, M = **3**, n = 2, X = Br, 919.2

4a, M = **4**, n = 2, X = Br, 919.2

5a, M = **5**, n = 2, X = **Cl**, 919.2

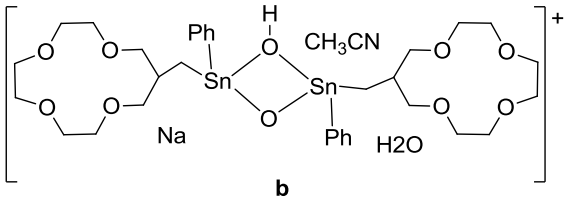

b

$M\text{-}2(Sn(t\text{-}Bu)XOH)\cdot H\cdot Na\cdot H_2O\cdot CH_3CN]^+$

1b, M = **1**, X = **I**, 913.3

2b, M = **2**, X = Br, 913.3

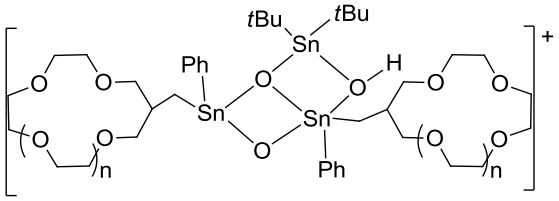

c

[M-2(Sn(*t*-Bu)XOH)·H]+

1c, M = **1**, n = 1, X = **I**,1079.3

2c, M = **2**, n = 1, X = Br, 1079.3

3c, M = **3**, n = 2, X = Br, 1167.2

4c, M = **4**, n = 2, X = Br, 1167.2

5c, M = **5**, n = 2, X = **Cl**, 1167.2

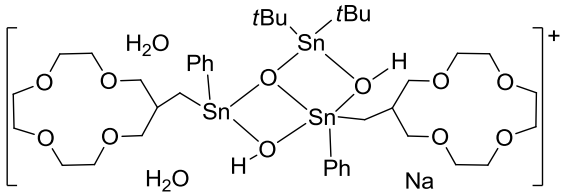

d

$[M\text{-}(Sn(t\text{-}Bu)_2XOH)\cdot 2H_2O\cdot Na]^+$

1d, M = **1**, X = **I**, 1139.3

2d, M = **2**, X = Br, 1139.3

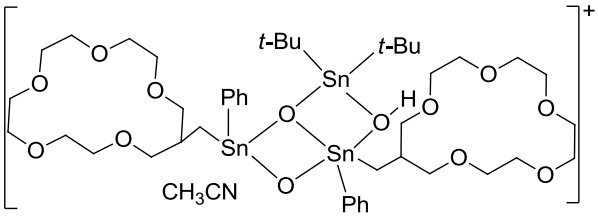

e

$[M\text{-}2(Sn(t\text{-}Bu)XOH)\cdot CH_3CN]^+$

3e, M = **3**, X = **I**, 1167.4

4e, M = **4**, X = Br, 1167.4

5e, M = **5**, X = **Cl**, 1167.4

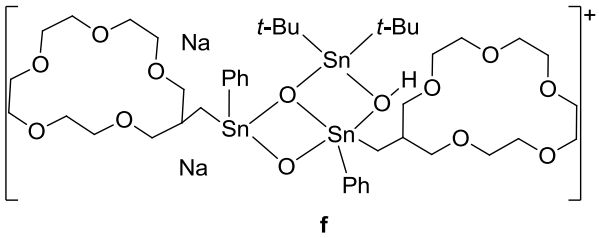

f

$[M\text{-}2(Sn(t\text{-}Bu)XOH)\cdot 2Na]^+$

4f, M = **4**, X = Br, 1213.4

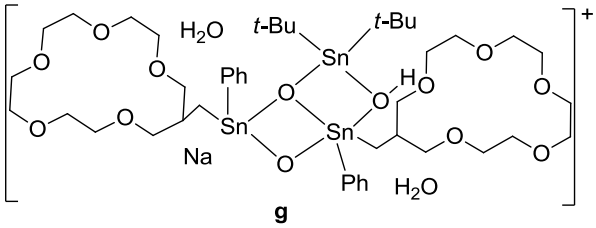

g

$[M\text{-}2(Sn(t\text{-}Bu)XOH)\cdot Na\cdot 2H_2O]^+$

5g, M = **5**, X = **Cl**, 1213.4

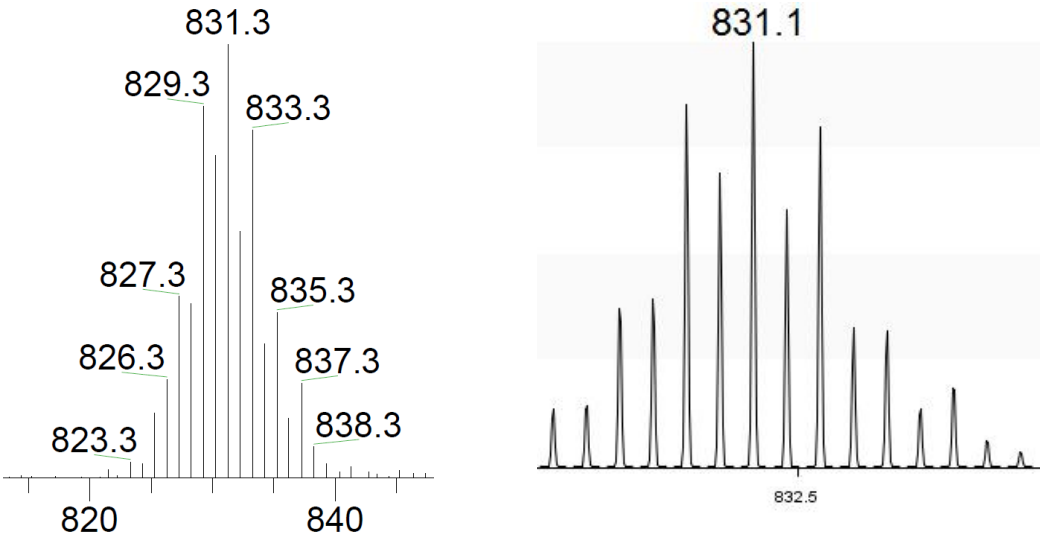

Experimental **Simulation**

Figure 9. Experimental (from ESI-MS) and simulated mass cluster of compounds **1a** and **2a** shown in scheme 3.

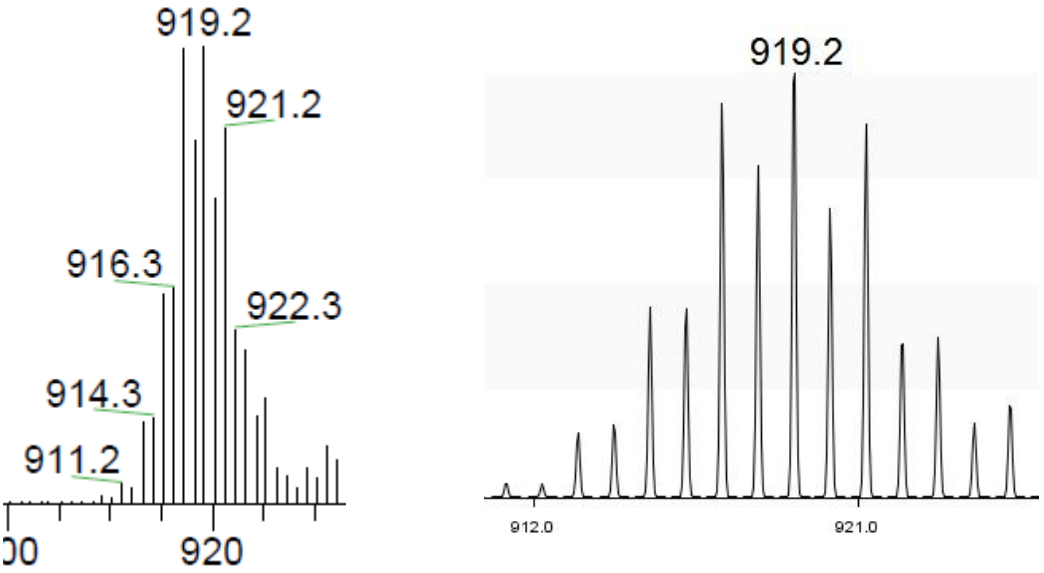

Experimental **Simulation**

Figure 10. Experimental (from ESI-MS) and simulated mass cluster of compounds **3a** –**5a** shown in scheme 3.

4.5. Conclusions

Novel dimeric tetraorganodistannoxanes have been synthesized and characterized. All these compounds exhibit intramolecular O→Sn interactions. It has been shown that depending on the nature of the organic groups at the *endo*-cyclic tin atoms, the intramolecular O→H interactions can take place. In contrast to the trans isomer obtained in the solid state, all these compounds showed cis-trans isomerisation in solution.

4.6. Experimental Section

All solvents were dried according to standart procedures and were freshly distilled prior to use. (*t*-$Bu_2SnO)_3$,[19] PhI_2SnCH_2-13-crown-4,[20] $PhBr_2SnCH_2$-13-crown-4,[20] (PhX_2SnCH_2-16-crown-5, X = I, Cl),[21] and $PhBr_2SnCH_2$-16-crown-5[22] were synthesized according to literature methods. The atom numbering of the crown ether fragment is shown in Scheme 4.

NMR Spectroscopy.The NMR spectra were recorded on Bruker DRX 400 and DRX 300 spectrometers. Chemical shifts *δ* are given in ppm and are referenced to solvent peaks with the usual values calibrated against tetramethysilane (^1H, ^{13}C) and tetramethystannane (^{119}Sn).

Electrospray mass spectra were recorded on a Thermoquest-Finnigan instrument using CH_3CN as the mobile phase. The samples were introduced as solution in CH_3CN via a syringe pump operating at 0.5µL/min. The capillary voltage was 4.5 kV while the cone skimmer voltage varied between 50 and 250 kV. Identification of the expected ions was assisted by comparison of experimental and calculated isotope distribution patterns. The m/*z* values reported correspond to those of the most intense peak in the corresponding isotope pattern. **Elemental analyses** were performed on a LECO-CHNS-932 Analyser. **Melting points** were determined using a Büchi Melting Point M-560.

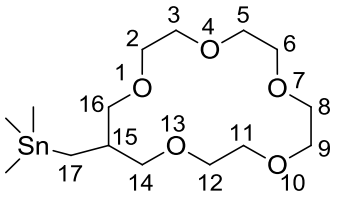

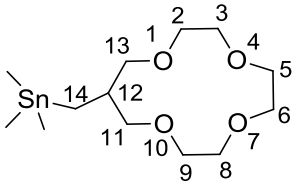

Scheme 4. Atoms numbering of the crown ether moiety.

Synthesis of 1-hydroxy-3-iodo-1-phenyl-1-(1,4,7,10-tetraoxacyclotridec-12-ylmethyl)-3,3-di-*tert*.-butyldistannoxane (1)

(*t*-$Bu_2SnO)_3$ (10 mg, 0.04 mmol) was added to a solution of PhI_2SnCH_2-13-crown-4 (0.08 g, 0.12 mmol) in CH_2Cl_2 (10 mL) at room temperature. The reaction mixture was stirred overnight. The solvent was removed in vacuo. Addition of *n*-hexane (10 mL) to the residue and stirring for two hours, followed by filtration afforded 0.16 g (83

%) of **1** as slight yellow solid of mp 184.1°C. Single crystals of **1** suitable for X-ray diffraction analysis were obtained by slow evaporation of a solution of the compound in CH_2Cl_2/*n*-Hexane.

^{1}H NMR ($CDCl_3$, 400.13 MHz, 300 K) *δ*: 1.2 (complex pattern, 36H, C(Me_3)), 1.56 (bs, $^2J(^1H–^{117}Sn)$ = 40 Hz, $^2J(^1H–^{119}Sn)$ = 56 Hz, 4H, $SnCH_2$), 2.82 (m, 2H, CH), 3.43–3.75 (complex pattern, 32H, CH_2-O-CH_2), 7.18-8.05 (complex pattern, 10H, Ph). **^{13}C{^{1}H} NMR** ($CDCl_3$, 100.63 MHz, 300 K) *δ*: 15.7 ($SnCH_2$), 29.7–32.0 (C(Me_3)), 37.1 ($^2J(^{13}C–^{117/119}Sn)$ = 26 Hz, C15), 70.0–72.6 (C2–C16), 127.9 ($^3J(^{13}C–^{117/119}Sn)$ = 31 Hz, C_m), 129.3 (C_p), 136.7 ($^2J(^{13}C–^{117}Sn)$ = 14 Hz, $^2J(^{13}C–^{117}Sn)$ = 23 Hz, C_o), 147.5 (C_i). **^{119}Sn{^{1}H} NMR** ($CDCl_3$, 111.92 MHz, 294.16 K) *δ*: –307 ($^2J(^{119}Sn–^{117}Sn)$ = 245 Hz, Sn1 (trans)), *δ*: –300 ($^2J(^{119}Sn–^{117}Sn)$ = 293 Hz, Sn1 (cis)), –184 ($^2J(^{119}Sn–^{117}Sn)$ = 226 Hz, Sn2 (cis)), –183 ($^2J(^{119}Sn–^{117}Sn)$ = 291 Hz, Sn2 (trans)),. Anal. Calcd for $C_{48}H_{82}I_2O_{12}Sn_4$ (1579.70): C 36.5; H 5.2. Found: C 37.5; H 5.4.

Synthesis of 1-hydroxy-3-bromo-1-phenyl-1-(1,4,7,10-tetraoxacyclotridec-12-ylmethyl)-3,3-di-*tert*.-butyldistannoxane (2)

(*t*-$Bu_2SnO)_3$ (16 mg, 0.07 mmol) was added to a solution of $PhBr_2SnCH_2$-13-crown-4 (0.11 g, 0.20 mmol) in CH_2Cl_2 (10 mL) at room temperature. The reaction mixture was stirred overnight. The solvent was removed in vacuo. Addition of *n*-hexane (10 mL) to the residue and stirring for two hours, followed by filtration afforded 0.25 g (85 %) of **2** as a white solid. Recrystallization from ethanol at ambient temperature afforded **2** as white crystals, mp 188.9°C.

^{1}H NMR ($CDCl_3$, 400.13 MHz, 300 K) *δ*: 1.2 (complex pattern, 36H, C(Me_3)), 1.57 (d, $^3J(^1H–^1H)$ = 4.0 Hz, $^2J(^1H–^{117}Sn)$ = 96 Hz, $^2J(^1H–^{119}Sn)$ = 120 Hz, 4H, $SnCH_2$), 2.70 (m, $^3J(^1H–^{117/119}Sn)$ = 40 Hz, 2H, CH), 3.29–3.65 (complex pattern, 32H, CH_2-O-CH_2), 7.18-8.05 (complex pattern, 10H, Ph). **^{13}C{^{1}H} NMR** ($CDCl_3$, 100.63 MHz, 300 K) *δ*: 15.7 ($SnCH_2$), 27.6–31.2 (C(Me_3)), 37.1 ($^2J(^{13}C–^{117/119}Sn)$ = 29 Hz, C15), 68.8–73.5 (C2–C16), 127.9 ($^3J(^{13}C–^{117}Sn)$ = 13 Hz, $^3J(^{13}C–^{119}Sn)$ = 23 Hz, C_m), 129.1 (C_p), 136.5 ($^2J(^{13}C–^{117/119}Sn)$ = 54 Hz, C_o), 147.5 (C_i). **^{119}Sn{^{1}H} NMR** ($CDCl_3$, 111.92 MHz, 294.16 K) *δ*: –308 ($^1J(^{119}Sn–^{117}Sn)$ = 249 Hz, Sn1(trans)), –299 ($^2J(^{119}Sn–^{117}Sn)$ = 252 Hz, Sn1 (cis)), –209 ($^2J(^{119}Sn–^{117}Sn)$ = 56 Hz, Sn2 (cis)) –208 ($^1J(^{119}Sn–^{117}Sn)$ = 316 Hz, Sn2 (trans)). Anal. Calcd for $C_{48}H_{86}Br_2O_{12}Sn_4$ (1489.75): C 38.7; H 5.8. Found: C 38.6; H 5.8.

Synthesis of 1-hydroxy-3-iodo-1-phenyl-1-(1,4,7,10,13-pentaoxacyclohexadec-15-yl-methyl)-3,3-di-*tert*.-butyldistannoxane (3)

(*t*-$Bu_2SnO)_3$ (10 mg, 0.05 mmol) was added to a solution of PhI_2SnCH_2-16-crown-5 (0.10 g, 0.14 mmol) in CH_2Cl_2 (10 mL) at room temperature. The reaction mixture was stirred overnight. The solvent were removed in vacuo. Addition of *n*-hexane (10 mL) to the residue and stirring for two hours, followed by filtration afforded 0.20 g (80 %) of **3** as slight yellow solid of mp 170°C. Single crystals of **3** suitable for X-ray diffraction analysis were obtained by slow evaporation of a solution of the compound in CH_2Cl_2/*n*-Hexane.

^{1}H NMR ($CDCl_3$, 400.13 MHz, 300 K) *δ*: 1.3 (complex pattern, 36H, $C(Me_3)$), 1.56 (bs, $^2J(^1H–^{117/119}Sn)$ = 40 Hz, 4H, $SnCH_2$), 2.87 (m, 2H, CH), 3.29–3.65 (complex pattern, 40H, CH_2-O-CH_2), 7.11-7.76 (complex pattern, 10H, Ph). **^{13}C{^{1}H} NMR** ($CDCl_3$, 100.63 MHz, 300 K) *δ*: 14.0 ($SnCH_2$), 30.1–31.3 ($C(Me_3)$), 35.9 ($^2J(^{13}C–^{117/119}Sn)$ = 24 Hz, C15), 69.5–70.6 (C2–C16), 127.4 (C_m), 127.7 (C_p), 137.7 (C_o), 144.5 (C_i). **^{119}Sn{^{1}H} NMR** ($CDCl_3$, 111.92 MHz, 294.16 K) *δ*: –315 ($^2J(^{119}Sn–^{117}Sn)$ = 298 Hz, Sn1 (trans)), –313 (Sn1 (cis)), –185 ($^2J(^{119}Sn–^{117}Sn)$ = 287 Hz, Sn2 (trans)), –184.0 (Sn2 (cis)). Anal. Calcd for $C_{52}H_{102}I_2O_{18}Sn_4$ (1743.90): C 35.8; H 5.9. Found: C 36.0; H 5.7.

Synthesis of 1-Hydroxy-3-Bromo-1-Phenyl-1-(1,4,7,10,13-pentaoxacyclohexadec-15-yl-methyl)-3,3-di-*tert*.-butyldistannoxane (4)

(*t*-$Bu_2SnO)_3$ (17 mg, 0.07 mmol) was added to a solution of $PhBr_2SnCH_2$-16-crown-5 (0.12 g, 0.20 mmol) in CH_2Cl_2 (10 mL) at room temperature. The reaction mixture was stirred overnight. The solvent was removed in vacuo. Addition of *n*-hexane (10 mL) to the residue and stirring for two hours, followed by filtration afforded 0.28 g (86 %) of **4** as slight yellow solid of mp 186.3°C. Single crystals of **4** suitable for X-ray diffraction analysis were obtained by slow evaporation of the compound in CH_2Cl_2/*n*-Hexane.

^{1}H NMR (CD_2Cl_2, 300.13 MHz, 294.16 K) *δ*: 1.3 (complex pattern, 36H, $C(Me_3)$), 1.59 (bs, $^2J(^1H–^{117/119}Sn)$ = 42 Hz, $SnCH_2$), 2.70 (m, 2H, CH), 3.26–3.58 (complex pattern, 40H, CH_2-O-CH_2), 7.15-8.01 (complex pattern, 10H, Ph). **^{13}C{^{1}H} NMR** (CD_2Cl_2, 75.47 MHz, 296.16 K) *δ*: 15.1 ($SnCH_2$), 29.7–30.6 ($C(Me_3)$), 36.1 ($^2J(^{13}C–^{117/119}Sn)$ = 21 Hz, C15), 69.3–70.5 (C2–C16), 127.0 ($^3J(^{13}C–^{117/119}Sn)$ = 15 Hz, C_m), 128.7

($^4J(^{13}C–^{117/119}Sn)$ = 23 Hz, C_p), 136.7 ($^2J(^{13}C–^{117/119}Sn)$ = 24 Hz, C_o), 145.3 ($^1J(^{13}C–^{117/119}Sn)$ = 12 Hz, C_i). **$^{119}Sn\{^1H\}$ NMR** (CD_2Cl_2, 111.92 MHz, 296.16 K) *δ*: –311 ($^2J(^{119}Sn–^{117}Sn)$ = 254 Hz, Sn1 (*trans*)), –311 (Sn1 (*cis*)), –209 ($^2J(^{119}Sn–^{117}Sn)$ = 247 Hz, Sn2 (*trans*)), –208.5 (Sn2 (*cis*)). Anal. Calcd for $C_{53}H_{96}Br_2Cl_2O_{14}Sn_4$ (1662.78): C 38.3; H 5.8. Found: C 38.7; H 6.0.

Synthesis of 1-hydroxy-3-chloro-1-phenyl-1-(1,4,7,10,13-pentaoxacyclohexadec-15-yl-methyl)-3,3-di-*tert*.-butyldistannoxane (5)

(*t*-$Bu_2SnO)_3$ (26 mg, 0.10 mmol) was added to a solution of $PhCl_2SnCH_2$-16-crown-5 (0.16 g, 0.31 mmol) in CH_2Cl_2 (12 mL) at room temperature. The reaction mixture was stirred overnight. The solvent was removed in vacuo. Addition of *n*-hexane (10 mL) to the residue and stirring for two hours, followed by filtration afforded 0.38 g (82 %) of **5** as slight yellow solid of mp 188.2 °C. Single crystals of **5** suitable for X-ray diffraction analysis were obtained by slow evaporation of a solution of the compound in CH_2Cl_2/*n*-Hexane.

^1H NMR ($CDCl_3$, 300.13 MHz, 293.16 K) *δ*: 1.25 (complex pattern, 36H, $C(Me_3)$), 1.55 (bs, $^2J(^1H–^{117}Sn)$ = 18 Hz, $^2J(^1H–^{119}Sn)$ = 30 Hz, 4H, $SnCH_2$), 2.70 (m, 2H, CH), 3.25–3.58 (complex pattern, 40H, CH_2-O-CH_2), 7.10-7.80 (complex pattern, 10H, Ph). **$^{13}C\{^1H\}$ NMR** (CD_2Cl_2, 100.63 MHz, 300 K) *δ*: 14.3 ($SnCH_2$), 30.3–31.0 ($C(Me_3)$), 36.5 ($^2J(^{13}C–^{117/119}Sn)$ = 28 Hz, C15), 69.7–70.8 (C2–C12), 74.13 (C14/C16), 127.5 ($^3J(^{13}C–^{117}Sn)$ = 20 Hz, $^3J(^{13}C–^{119}Sn)$ = 29 Hz, Cm), 127.8 ($^3J(^{13}C–^{117/119}Sn)$ = 13 Hz, C_p), 129.1 ($^3J(^{13}C–^{117/119}Sn)$ = 13 Hz, Co), 137.1(C_i). **$^{119}Sn\{^1H\}$ NMR** (CD_2Cl_2, 111.92 MHz, 296.16 K) δ: –304.1 (Sn1 (*cis*)), –303.5 ($^2J(^{119}Sn–^{117}Sn)$ = 237 Hz, Sn1 (*trans*)), –223.1 ($^2J(^{119}Sn–^{117}Sn)$ = 241 Hz, Sn2 (*trans*)), –222.7 (Sn2 (*cis*)). Anal. Calcd for $C_{52}H_{94}Cl_2O_{14}Sn_4$ (1489): C 41.9; H 6.4. Found: C 41.5; H 6.8.

4.7. References

(1) Chandrasekhar, V.; Nagendran, S.; Baskar, V. *Coord. Chem. Rev.,* **2002**, *235*, 1.

(2) Jurkschat., K. *Tetraorganodistannoxanes: Simple Chemistry From a Personal Perspective. Tin Chemistry Fundamentals, Frontiers, and Applications*; A. G. Davies, M. Gielen, K. H. Pannell, E. R. T. Tiekink ed., **2008**; Vol. Chapter 2.10.

(3) Otera, J.; Danoh, N.; Nozaki, H. *J. Org. Chem.,* **1991**, *56*, 5307.

(4) Orita, A.; Mitsutome, A.; Otera, J. *J. Org. Chem.,* **1998**, *63*, 2420.

(5) Houghton, R. P.; Mulvaney, A. W. *J. Organometal. Chem.,* **1996**, *517*, 107.

(6) Suciu, E. N.; Kuhlmann, B.; A. Knudsen, G.; Michaelson, R. C. *J. Organometal. Chem.,* **1998**, *556*, 41.

(7) Beckmann, J.; Jurkschat, K.; Kaltenbrunner, U.; Rabe, S.; Schürmann, M.; Dakternieks, D.; Duthie, A.; Müller, D. *Organometallics,* **2000**, *19*, 4887.

(8) Beckmann, J.; Jurkschat, K.; Rabe, S.; Schürmann, M.; Dakternieks, D. *Z: Anorg. Allg. Chem.,* **2001**, *627*, 458.

(9) Beckmann, J.; Dakternieks, D.; Duthie, A.; Sheen Kuan, F.; Jurkschat, K.; Schürmann, M.; Tiekink, E. R. T. *New J. Chem.,* **2004**, *28*, 1268.

(10) Chu, C. K.; Murray, J. D. *J. Chem. Soc. A,* **1971**, *0*, 360.

(11) Vollano, J. F.; Day, R. O.; Holmes, R. R. *Organometallics,* **1984**, *3*, 745.

(12) Davies, A. G.; Harrison, P. G.; Palan, P. R. *J. Chem. Soc. C,* **1970**, *0*, 2030.

(13) Dakternieks, D.; Jurkschat, K.; van Dreumel, S.; Tiekink, E. R. T. *Inorg. Chem,* **1997**, *36*, 2023.

(14) Dakternieks, D.; Jurkschat, K.; Schollmeyer, D.; Wu, H. *Organometallics,* **1994**, *13*, 4121.

(15) Zobel, B.; Schürmann, M.; Jurkschat, K.; Dakternieks, D.; Duthie, A. *Organometallics,* **1998**, *17*, 4096.

(16) Kolb, U.; Draeger, M.; Jousseaume, B. *Organometallics,* **1991**, *10*, 2737.

(17) Mantina, M.; Chamberlin, A. C.; Valero, R.; Cramer, C. J.; Truhlar, D. G. *J. Phys. Chem. A,* **2009**, *113*, 5806.

(18) Kemmer, M.; Ghys, L.; Gielen, M.; Biesemans, M.; Tiekink, E. R. T.; Willem, R. *J. Organometal. Chem.,* **1999**, *582*, 195.

(19) Puff, H.; Schuh, W.; Sievers, R.; Wald, W.; Zimmer, R. *J. Organometal. Chem.,* **1984**, *260*, 271.

(20) Tagne Kuate, A. C.; Iovkova, L.; Hiller, W.; Schürmann, M.; Jurkschat, K. *Organometallics,* **2010**, *29*, 5456.

(21) Reeske, G.; Schürmann, M.; Costisella, B.; Jurkschat, K. *Organometallics,* **2007**, *26*, 4170.

(22) Siakam Wendji, A.; Jurkschat, K. unpublished results.

5. Summary

The main purpose of this work were the syntheses, structures of new ditopic receptors based on tin-containing crown ether-substituted ferrocene and ferrocenophanes, respectively, and the study of their complexation behaviour toward metal salts as well as their electrochemical properties.

The synthesis of the host molecules was achieved by the combination of a suitable Grignard reagent with an organotin halide (Scheme 1). Thus, the tetraorganotin-substituted crown ethers **1** and **19** and the bis(tetraorganotin)-substituted crown ether **2** were synthesized and characterized.

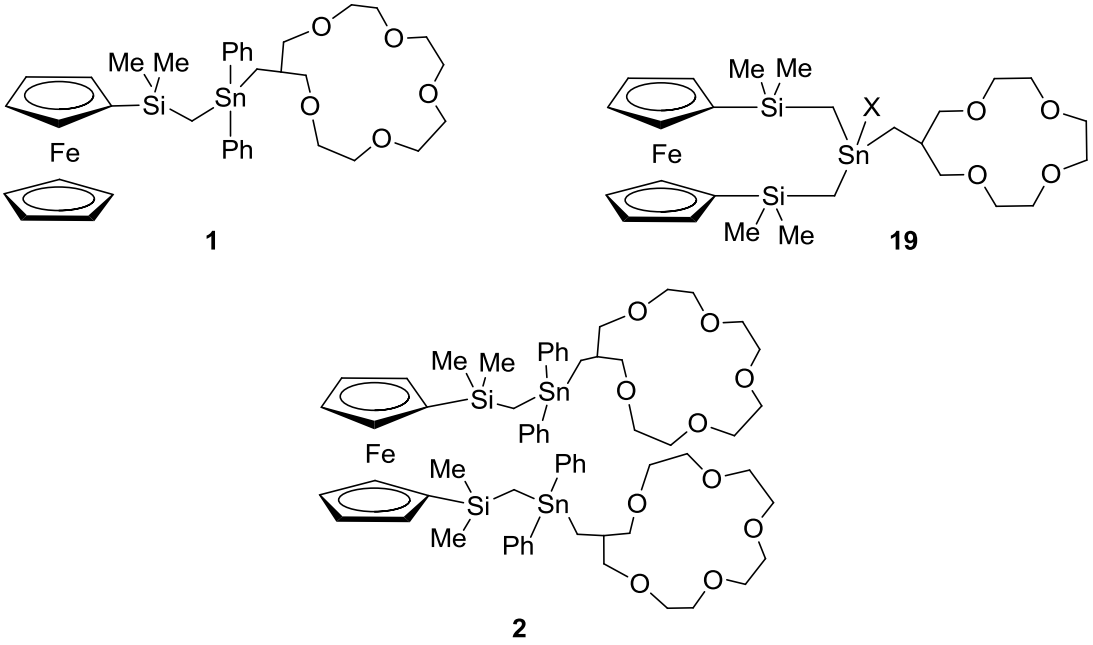

Scheme 1. Tetraorganotin- and bis(tetraorganotin)-substituted crown ethers.

The functionalization of the tin atoms of the tetraorganostannane compounds **1**, **2** and **19** with suitable amounts of electron-withdrawing substituents such as halogen atoms provided the monohalogenidotriorganotin- and the dihalogenidodiorganotin-substituted crown ethers **3**, **5**, **7**, **20**, **21**, **22** and **11**, **13**, and the bis(monohalogenidotriorganotin)- and the bis(dihalogenidodiorganotin)-substituted crown ethers **4**, **6**, **8**, and **12** and **14** (Scheme 2). A common characteristic of all these compounds, except compound **20** are the intramolecular O→Sn interactions. Compound **20** can formally be interpreted as a Frustrated Lewis Pair in which the Lewis base (oxygen atom) does not coordinate to the Lewis acidic Sn atom.

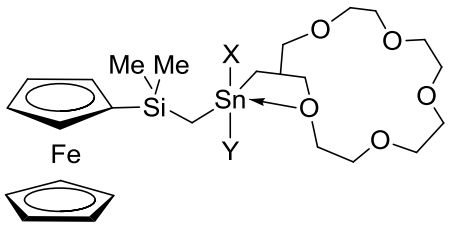

3, X = I, Y = Ph

5, X = Cl, Y = Ph

7, X = F, Y = Ph

11, X = I, Y = I

13, X = Cl, Y = Cl

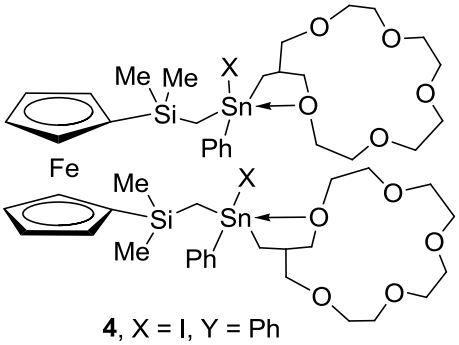

4, X = I, Y = Ph

6, X = I, Y = Ph

8, X = I, Y = Ph

12, X = I, Y = I

14, X = Cl, Y = Cl

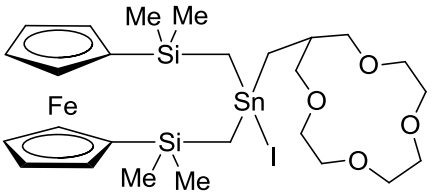

20

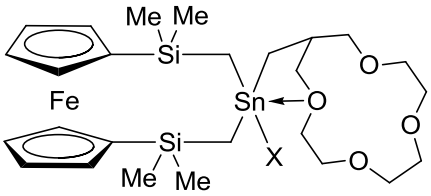

21, X = Cl

22, X = F

Scheme 2. Di- and triorganotin- and bis(di- and triorganotin)-substituted crown ethers.

The ability of these receptors to complex ditopically salts was investigated. Thus compounds **4**, **6**, **13**, **14** and **21** showed a high affinity for lithium chloride, whereas compound **8** can bind cesium fluoride.

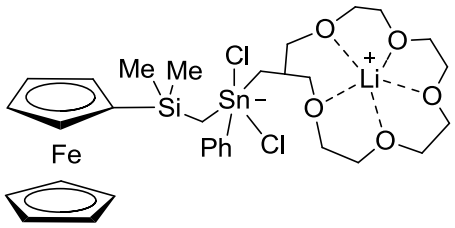

5·LiCl

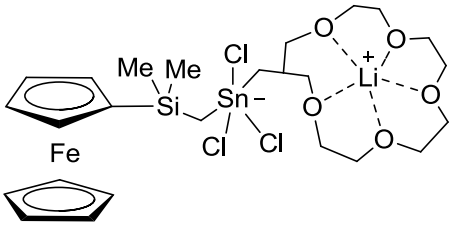

13·LiCl

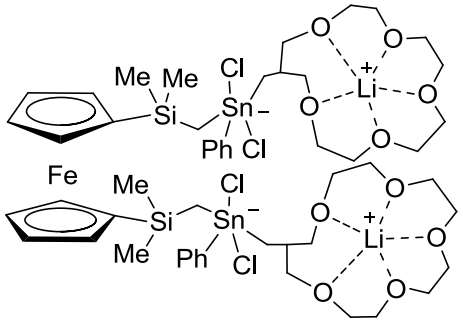

6·2LiCl

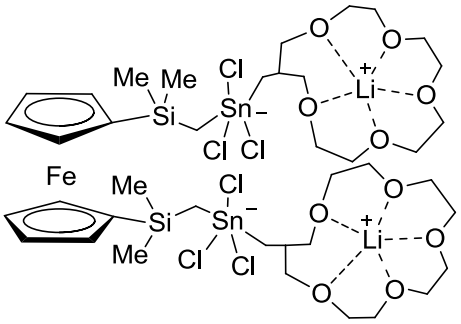

14·2LiCl

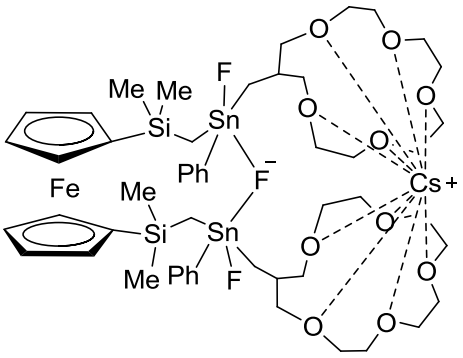

[**8**·CsF]

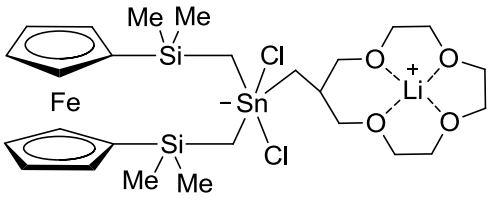

[**21**·LiCl]

Scheme 3. Ditopic complexes [**5**·LiCl], [**6**·LiCl], [**8**·CsF], [**13**·LiCl], [**14**·2LiCl], and [**21**·LiCl].

The formation of these complexes was confirmed by multinuclear NMR spectroscopy and in the case of [**21**·LiCl] also by X-ray diffraction analysis. The molecular structure of [**21**·LiCl] shows that the lithium cation is bound inside the cavity of the crown ether and the chloride anion is bound to the tin atom.

Cyclic voltammetry was also employed to prove that compounds **4**, **6**, **13**, **14** and **21** can concurrently complex lithium chloride.

DFT calculations of compounds **20**–**22** revealed important two-electron stabilization in **21** and **22** due to O→Sn coordination that is absent in **20**.

Moreover, it has been also shown that compounds **3–8, 11**–**14** may be involve in surface modification. Indeed, it has been demonstrated that covalent grafting of these molecules, via the formation of C-Sn bond, occurs allowing one to immobilize Fc moiety at such surfaces.

In the second chapter, novel cationic monoorganotin(IV) complexes of crown ethers (**4** and **5**), as well as the neutral dimeric monoorganotin sulfide derivative (**6**) have been synthesized and characterized (Scheme 4). The molecular structure of compound **4** shows that the tin atom is intramolecularly encapsulated by the five crown ether oxygen atoms. Most remarkably, the molecular structure of the complex **4** showed a complete replacement of the OH substituent by the *p*-MeC_6H_4S group, whereas in **6**, the more hindered $Ph_2P(S)S$ fragment induced an eviction of the tin atom from the crown ether cavity leading to a neutral compound in the solid state. Interestingly, a rare example of the monomeric monoorganotin(IV) trifluoride, the trifluoridomonoorganotin(IV)-substituted-crown-5 ether compound (**10**), has been synthesized and structurally characterized (Scheme 4).

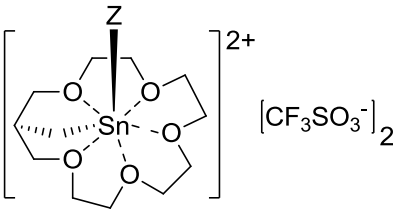

4, Z = SPhMe
5, Z = SC_8H_{10}

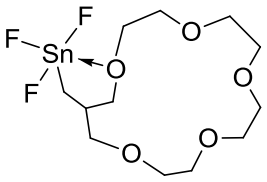

10

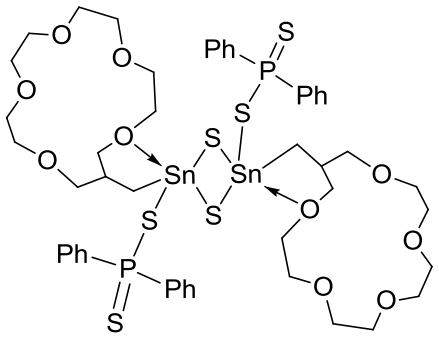

6

Scheme 4. Cationic organotin(IV) complexes of crown ether (**4** and **5**), dimeric monoorganotin sulfide derivative (**6**) and moorganotin(IV) trifluoride (**10**).

In the third chapter, novel dimeric tetraorganodistannoxanes have been synthesized and characterized (Scheme 5). The molecular structures of these compounds show that each compound exhibits intramolecular O→Sn interactions and depending on the nature of organic groups at the *endo*-cyclic tin atoms, an intramolecular O→H interactions can take place. In contrast to the trans isomer obtained in the solid state, all these compounds displayed cis-trans isomerisation in solution.

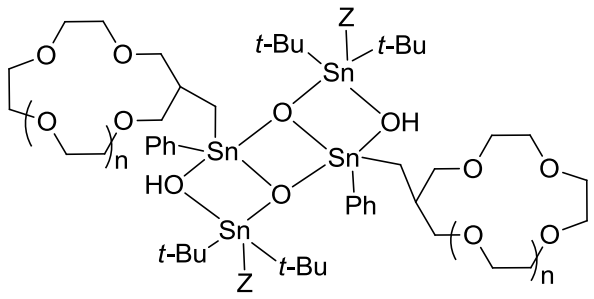

1, Z = I, n = 1

2, Z = Br, n = 1

3, Z = I, n = 2

4, Z = Br, n = 2

5, Z = Cl, n = 2

Scheme 5. Tetraorganodistannoxanes.

6. Zusammenfassung

Das Ziel dieser Arbeit waren die Synthese und strukturelle Charakterisierung von neuen Organozinn-substituierten Kronenethern. Diese werden im Folgenden in drei Klasse unterteilt, (1) in Ferrocen- bzw. Ferrocenophan-substituierte zinnhaltige Kronenether, die als ditope Rezeptoren dienen, (2) kationische Monoorganozinn(IV)-Komplexe und neutrale dimere Monoorganozinn(IV)-Trithio-Komplexe von Kronenethern, sowie (3) dimere Tetraorganodistannoxane.

Ein weiteres Ziel war es, die unter (1) genannten ditopen Rezeptoren auf ihr Komplexierungsverhalten gegenüber Metallsalzen zu untersuchen, und sie auf ihre elektrochemischen Eigenschaften zu prüfen.

(1) Die Synthese der Wirtmoleküle wurde durch die geeignete Kombination aus einem Grignard-Reagens mit einem Organozinnhalogenid (Schema 1) erreicht. Mit diesem Konzept wurden die Tetraorganozinn-substituierten Kronenether **1**, **19** und der Bis (tetraorganozinn)-substituierte Kronenether **2** synthetisiert und anschließend charakterisiert.

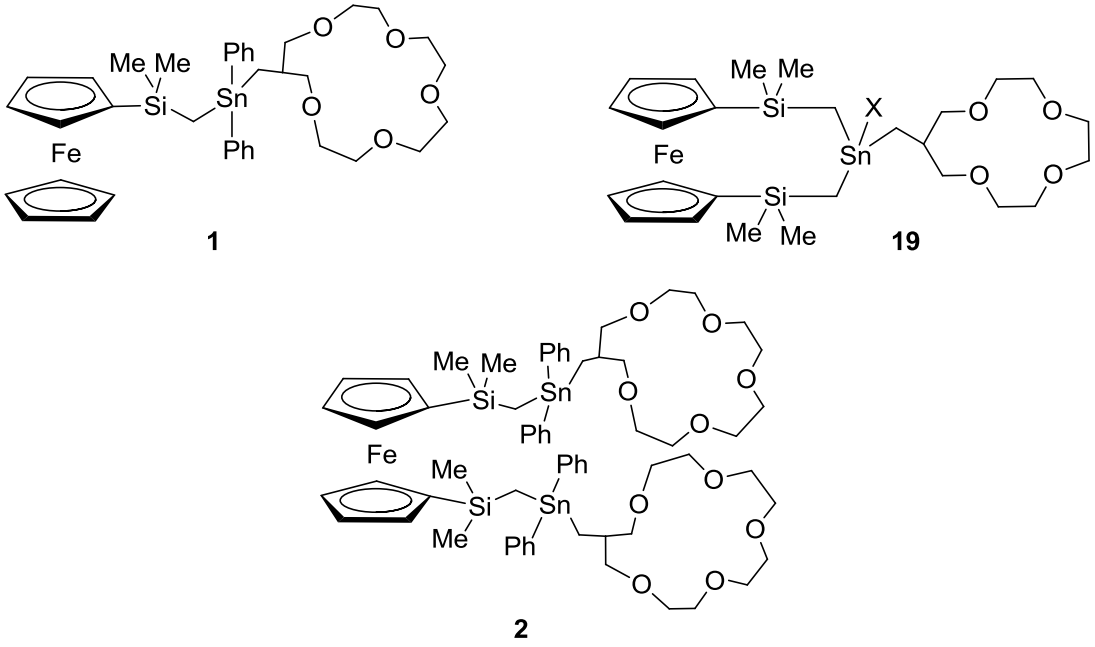

Schema 1. Tetraorganozinn-und Bis(tetraorganozinn)-substituierten Kronenether.

Die Funktionalisierung des Tetraorganozinnfragments erfolgt durch die Reaktion mit elementaren Iod und anschließende Umsetzung mit AgCl bzw. KF. Die Halogenidotriorganostannyl- und die Dihalogenidodiorganostannyl-substituierten

Kronenether **3**, **5**, **7**, **20**, **21**, **22** und **11**, **13** und die Bis(halogenidotriorganostannyl)- and Bis(dihalogenidodiorganostannyl)-substituierten Kronenether **4**, **6**, **8**, **12** und **14** wurden synthesiert (Schema 2). Ein wesentliches Merkmal dieser Verbindungen(ausgenommen **20**) ist die intramolekulare O→Sn Wechselwirkung. Verbindung **20** kann als ein frustriertes Lewis-Paar interpretiert werden, in dem die Lewis-Base (das Sauerstoffatom) mit dem Lewis-sauren Sn-Atom nicht koordinieren kann.

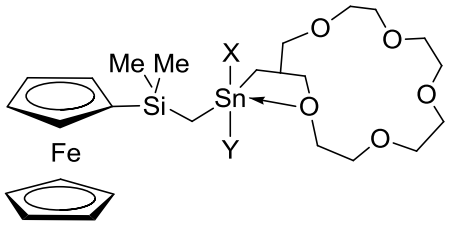

3, X = I, Y = Ph
5, X = Cl, Y = Ph
7, X = F, Y = Ph
11, X = I, Y = I
13, X = Cl, Y = Cl

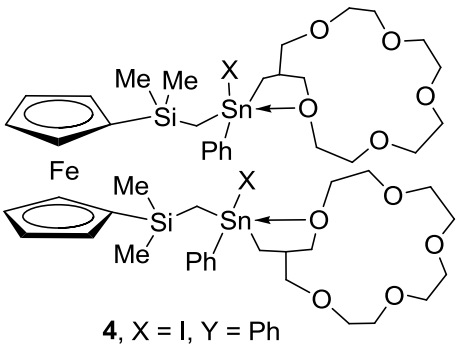

4, X = I, Y = Ph
6, X = I, Y = Ph
8, X = I, Y = Ph
12, X = I, Y = I
14, X = Cl, Y = Cl

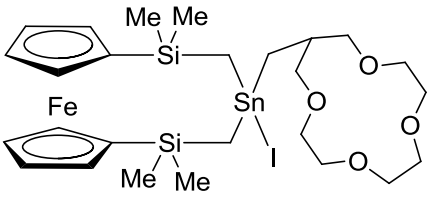

20

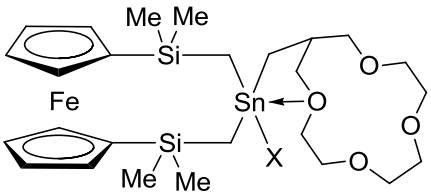

21, X = Cl
22, X = F

Schema 2. Di- und Triorganozinn- und Bis(di-und triorganozinn) substituierte Kronenether.

Die Fähigkeit dieser Rezeptoren zur ditopen Komplexierung von Salzen wurde untersucht. Die Verbindungen **4**, **6**, **13**, **14** und **21** zeigen eine hohe Affinität gegenüber Lithiumchlorid, während Verbindung **8** Cäsiumfluorid binden kann.

Schema 3

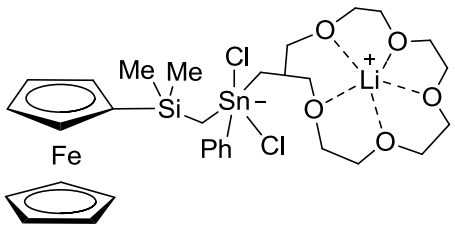

5·LiCl

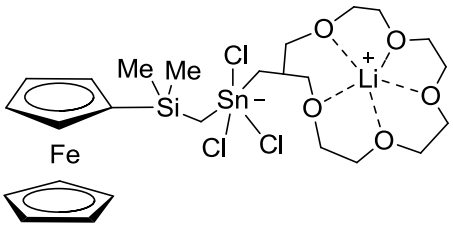

13·LiCl

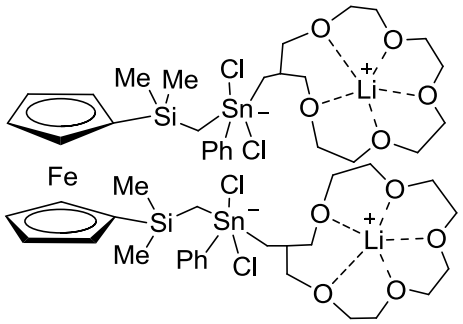

6·2LiCl

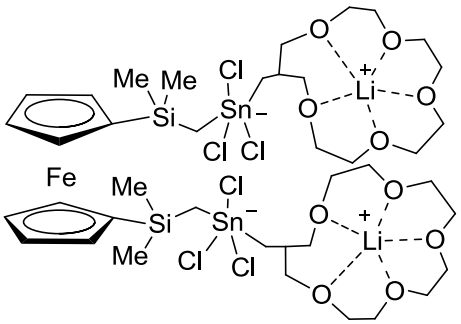

14·2LiCl

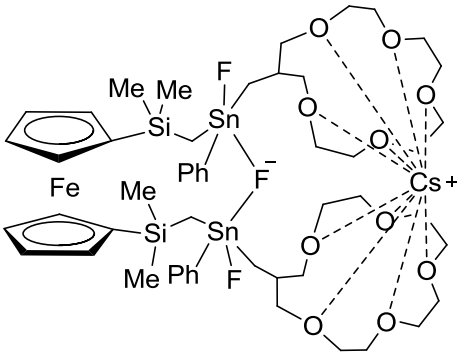

[**8**·CsF]

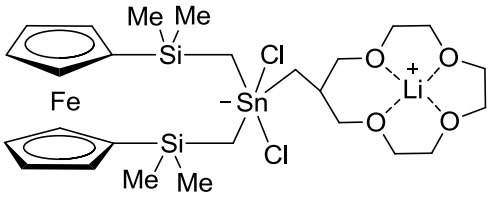

[**21**·LiCl]

Die Bildung dieser Komplexe wurde durch NMR-Spektroskopie und ESI-Massen spektrometrie nachgewiesen. Der Komplex [**21**·LiCl] wurde auch durch eine Einkristalleröntgenstrukturanalyse charakterisiert. Die molekulare Struktur von [**21**·LiCl] zeigt, dass das Lithium-Kation im Inneren des Kronenetherhohlraumes und das Chlorid-Anion am Zinnatom gebunden ist.

Cyclovoltammetrie wurde ebenfalls verwendet, um zu beweisen, dass die Verbindungen **4**, **6**, **13**, **14** und **21** gleichzeitig Lithium und Chlorid komplexieren können.

DFT-Rechnungen zu den Verbindungen **20–22** zeigen eine Zwei-Elektronen-Stabilisierung in **21** und **22** aufgrund der O→Sn Koordination, die in **20** nicht vorhanden ist.

Mit den Verbindungen **3**–**8**, und **11**–**14** wurden darüber hinaus Untersuchungen zur Oberflächenmodifizierung durchgeführt. Hier hat sich gezeigt, dass die “cathodic grafting“ Methode diese Verbindungen kovalent an eine glasartige Kohlenstoff-Oberfläche aufbringen kann und somit die Immobilisierung der Ferroceneinheiten auf der Elecktrodenoberfläche ermöglicht.

(2) Im zweiten Kapitel wurden neue kationische Monoorganozinn(IV)-Komplexe von Kronenethern (**4** und **5**), sowie die neutralen dimeren Monoorganozinn Trithio Komplexe (**6**) synthetisiert und charakterisiert (Schema 4). Die molekulare Struktur der Verbindung **4** zeigt, dass das Zinnatom intramolekular durch fünf Kronenether-Sauerstoffatome eingekapselt ist. Bemerkenswerterweise zeigte die molekulare Struktur des Komplexes **4** einen kompletten Austausch des OH-substituenten durch die *p*-SC_6H_4Me Gruppe, während in **6** die zwei sterisch anspruchsvollen $Ph_2P(S)S$-substituenten eine Verdrängung des Zinnatoms aus dem Kronenether-Hohlraum induzieren. Weiterhin wurde mit Verbindung **10** ein seltenes Beispiel eines monomeren Monoorganozinn(IV)-fluorids, strukturell charakterisiert (Schema 4).

Schema 4

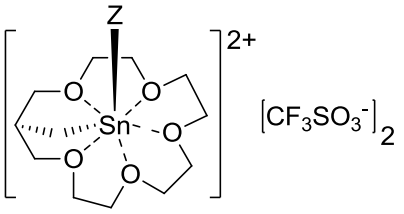

4, Z = *p*-SC_6H_4Me
5, Z = SC_8H_{10}

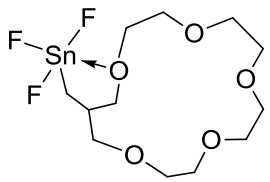

10

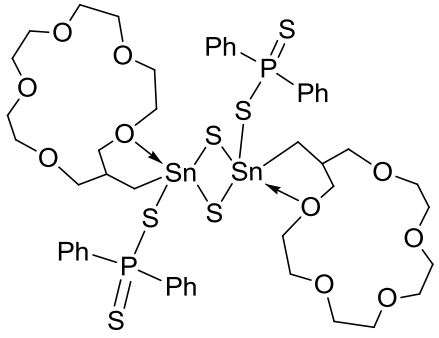

6

(3) Im dritten Kapitel wurden neue dimere Tetraorganodistannoxane dargestellt, die sich durch eine intramolekulare O→Sn Koordination auszeichnen (Schema 5). Die

molekularen Strukturen dieser Verbindungen zeigten, dass in Abhängigkeit von der Natur der organischen Gruppen an den endo-cyclisch Zinnatomen, eine intramolekulare O→H Wechselwirkungen stattfinden kann. Im Gegensatz zu dem trans-Isomer im festen Zustand liegt in Lösung eine cis-trans-Isomerisierung dieser Verbindungen vor.

Schema 5

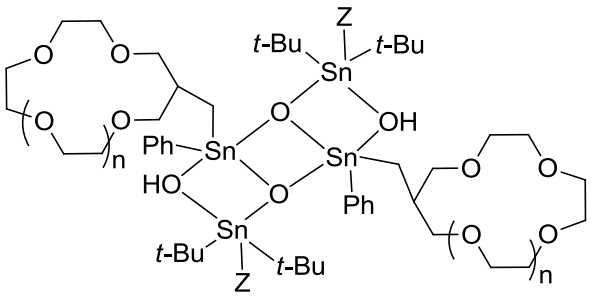

1, Z = I, n = 1

2, Z = Br, n = 1

3, Z = I, n = 2

4, Z = Br, n = 2

5, Z = Cl, n = 2

7. Appendix

7.1. Crystallographic Data and Structure Refinements

Intensity data for all crystals were collected on an XcaliburS CCD diffractometer (Oxford Diffraction) with graphite-monochromated MoKα radiation at 173 K, except those of crystal **23**, which are collected on STOE IPDS2T CCD diffractometer. The structure was solved by direct methods using SHELXS-97.[1] Refinements were carried out against F^2 by using SHELXL-97.[1] For decimal rounding of numerical parameters and su values the rules of the IUCr have been employed.[2] The C–H hydrogen atoms were positioned with idealized geometry and refined using a riding model. The crystallographic data of compounds **12**, **13**, **14**, [**13**·Cl]$^-$[Bu_4P]$^+$, **14**·2H_2O, **20**, **21**, [**21**·LiCl], **22**, **23**, **24** and **25** from chapter 1 are given in Table A1–A4. Those of compounds **4**, **6**, **9**, **10** and 11 from chapter 2 are given in table A5 and A6. The crystallographic data of compounds **1**–**5** from chapter 3 are given in table A7 and A8.

Table A1. Crystallographic data and structure refinements for compounds 12–14 (Chapter 2).

	12	**13**	**14**
formula	$C_{40}H_{70}FeI_4O_{10}Si_2Sn_2$	$C_{25}H_{40}Cl_2FeO_5SiSn$	$C_{40}H_{70}Cl_4FeO_{10}Si_2Sn_2$
fw	1567.97	694.10	1202.17
cryst syst	Monoclinic	Triclinic	Triclinic
cryst size, mm	0.47 x 0.21 x 0.10	0.22 x 0.18 x 0.05	0.17 x 0.15 x 0.07
space group	P2(1)/n	P-1	P-1
a, Å	13.1321(8)	9.2069(7)	9.1460(4)
b, Å	14.6977(7)	11.9182(9)	10.4192(4)
c, Å	15.1354(10)	14.7860(11)	14.0765(6)
α, deg	90	88.164(6)	90.747(3)
β, deg	110.509(7)	72.788(7)	108.474(4)
γ, deg	90	70.766(7)	101.357(3)
V, Å^3	2736.1(3)	1459.4(2)	1243.26(9)
Z	2	2	1
ρ_{calcd}, Mg/m^3	1.903	1.579	1.606
μ, mm^{-1}	3.514	1.609	1.598

F(000)	1512	708	612
θ range, deg	2.25 to 25.50	2.40 to 25.50	2.00 to 25.49
index ranges	-15≤h≤12 –17≤k≤17 -18≤l≤16	-11≤h≤11 –14≤k≤14 –17≤l≤17	–11≤h≤11 –12≤k≤12 –17≤l≤16
no. of reflns collcd	18730	12689	13100
completeness to θ_{max}	99.9	99.9	99.9
no. of indep reflns/R_{int}	5091/ 0.0391	5418/0.0686	4629/0.0443
no. of reflns obsd with ($I > 2\sigma(I)$)	3571	2739	3509
no. of refined Params	268	316	268
GooF (F^2)	0.917	0.640	0.867
$R1$ (F) ($I > 2\sigma(I)$)	0.0341	0.0409	0.0279
$wR2$ (F^2) (all data)	0.0685	0.0544	0.0506
$(\Delta/\sigma)_{max}$	0.001	0.000	0.001
largest diff. peak/hole, e/Å^3	1.092 and -0.830	0.701 and -0.744	0.549 and -0.354
Absorpn corr	multiscan	multiscan	multiscan

Table A2. Crystallographic data and structure refinements for compounds [13·Cl]$^-$[Bu$_4$P]$^+$ and [14·2H$_2$O] (Chapter 2).

	[**13**·Cl]$^-$[Bu$_4$P]$^+$	[**14**·2H$_2$O]
formula	$C_{41}H_{76}Cl_3FeO_5PSiSn$	$C_{80}H_{148}Cl_8Fe_2O_{24}Si_4Sn_4$
fw	988.97	2476.40
cryst syst	Triclinic	Monoclinic
cryst size, mm	0.50 x 0.19 x 0.17	0.25 x 0.18 x 0.04
space group	P-1	P2/c
a, Å	11.1357(4)	29.2506(14)
b, Å	13.1604(5)	8.3814(6)
c, Å	18.5056(6)	21.8557(12)
α, deg	81.705(3)	90
β, deg	74.328(3)	94.257(5)
γ, deg	66.346(3)	90
V, Å^3	2389.82(15)	5343.4(5)
Z	2	2
ρ_{calcd}, Mg/m^3	1.374	1.539
μ, mm^{-1}	1.091	1.493
F(000)	1036	2528
θ range, deg	2.00 to 25.50	2.25 to 25.50
index ranges	–13≤h≤13 –15≤k≤15 –22≤l≤22	–34≤h≤35 –10≤k≤9 –26≤l≤26
no. of reflns collcd	32424	26206
completeness to θ_{max}	99.9	99.7
no. of indep reflns/R_{int}	8887/ 0.0370	9926/0.0682
no. of reflns obsd with ($I > 2\sigma(I)$)	6534	4717

no. of refined Params	455	586
GooF (F^2)	1.110	0.445
$R1$ (F) ($I > 2\sigma(I)$)	0.0555	0.0361
$wR2$ (F^2) (all data)	0.1629	0.0985
$(\Delta/\sigma)_{max}$	0.000	0.001
largest diff. peak/hole, e/Å^3	1.432 and -1.455	0.648 and -0.457
Absorpn corr	multiscan	multiscan

Table A3. Crystallographic data for compounds 20 and 21 (Chapter 2).

	20	**21**
formula	$C_{26}H_{43}FeIO_4Si_2Sn$	$C_{26}H_{43}ClFeO_4Si_2Sn$
fw	777.22	685.77
cryst syst	Triclinic	Monoclinic
cryst size, mm	0.40 x 0.06 x 0.02	0.21 x 0.20 x 0.03
space group	$P\bar{1}$	$P2_1/c$
a, Å	8.4753(5)	32.4255(14)
b, Å	11.1021(5)	10.5826(5)
c, Å	16.6772(8)	17.6993(7)
α, deg	87.349(4)	90
β, deg	88.247(4)	95.689(4)
γ, deg	77.650(4)	90
V, Å^3	1530.92(14)	6043.5(5)
Z	2	8
ρ_{calcd}, Mg/m^3	1.686	1.507
μ, mm^{-1}	2.405	1.503

$F(000)$	776	2816
θ range, deg	2.20 to 25.50	2.25 to 25.50
index ranges	$-10 \le h \le 10$ $-13 \le k \le 13$ $-19 \le l \le 20$	$-39 \le h \le 39$ $-12 \le k \le 12$ $-21 \le l \le 21$
no. of reflns collcd	16310	53652
completeness to θ_{max}	100.0	100.0
no. of indep reflns/R_{int}	5694/ 0.0578	11239/0.0876
no. of reflns obsd with ($I > 2\sigma(I)$)	3416	5966
no. of refined Params	328	639
GooF (F^2)	0.741	0.634
$R1$ (F) ($I > 2\sigma(I)$)	0.0321	0.0298
$wR2$ (F^2) (all data)	0.0472	0.0426
$(\Delta/\sigma)_{max}$	0.001	0.002
largest diff. peak/hole, e/Å^3	0.594/–0.523	0.458/–0.427
Absorpn corr	multiscan	multiscan

Table A3. Crystallographic data for compounds 22 and [21·LiCl] (Chapter 2).

	22	[**21**·LiCl]
formula	$C_{26}H_{43}FFeO_4Si_2Sn$	$C_{26}H_{43}Cl_2FeLiO_4Si_2Sn$
fw	669.32	728.16
cryst syst	Orthorhombic	Monoclinic
cryst size, mm	0.39 x 0.27 x 0.21	0.46 x 0.23 x 0.21
space group	$P2_12_12_1$	$P2_1$
a, Å	11.4441(5)	9.7753(4)
b, Å	14.9310(10)	12.5265(6)
c, Å	17.1827(8)	12.9160(7)
α, deg	90	90
β, deg	90	96.522(4)
γ, deg	90	90
V, Å^3	2936.0(3)	1571.33(13)
Z	4	2
ρ_{calcd}, Mg/m^3	1.514	1.539
μ, mm^{-1}	1.461	1.532
F(000)	1376	744
θ range, deg	2.14 to 25.50	2.10 to 25.50
index ranges	–13≤h≤13 –15≤k≤18 –20≤l≤18	–11≤h≤11 –15≤k≤15 –15≤l≤15
no. of reflns collcd	12998	18426
completeness to θ_{max}	99.9	100.0
no. of indep reflns/R_{int}	5281/0. 0418	5848/0.0509
no. of reflns obsd with ($I > 2\sigma(I)$)	4198	5202
no. of refined	320	338

Params		
GooF (F^2)	0.905	0.937
$R1$ (F) ($I > 2\sigma(I)$)	0.0359	0.0306
$wR2$ (F^2) (all data)	0.0640	0.0517
$(\Delta/\sigma)_{max}$	0.001	0.001
largest diff. peak/hole, e/Å^3	0.706/–0.743	0.438/–0.412
Absorpn corr	multiscan	multiscan

Table A4. Crystallographic data and structure refinements for compounds 23–25 (Chapter 2) .

	23	**24**	**25**
formula	$C_{18}H_{28}Br_2O_5Sn$	$C_{17.50}H_{27}Cl_5O_4Sn_2$	$C_{32}H_{48}Cl_4O_8Sn_2$
fw	602.91	716.02	939.88
cryst syst	Monoclinic	Monoclinic	Monoclinic
cryst size, mm	0.20 x 0.20 x 0.10	0.07 x 0.05 x 0.04	0.22 x 0.05 x 0.03
space group	P 21/c	P2(1)/n	P2(1)/c
a, Å	8.9498(5)	10.2930(6)	8.3624(9)
b, Å	13.0285(4)	16.0603(9)	14.3979(15)
c, Å	18.9267(11)	15.6300(12)	15.9579(16)
α, deg	90	90	90
β, deg	101.839(4)	100.393(7)	90.379(10)
γ, deg	90	90	90
V, Å^3	2159.95(19)	2541.4(3)	1921.3(3)
Z	4	4	2
ρ_{calcd}, Mg/m^3	1.854	1.871	1.625
μ, mm^{-1}	4.907	2.512	1.623
F(000)	1184	1396	944
θ range, deg	2.70 to 28.00	2.20 to 25.50	2.44 to 25.50

index ranges	-11≤h≤11 -17≤k≤16 -24≤l≤24	-12≤h≤12 -19≤k≤19 -18≤l≤18	-10≤h≤10 –17≤k≤17 –19≤l≤19
no. of reflns collcd	19396	12247	15309
completeness to θ_{max}	99.7	100.0	99.9
no. of indep reflns/R_{int}	5201/0.0664	4733/0.0480	3563/ 0.0855
no. of reflns obsd with ($I > 2\sigma(I)$)	3783	2978	1810
no. of refined Params	235	271	196
GooF (F^2)	1.052	0.715	0.823
$R1$ (F) ($I > 2\sigma(I)$)	0.0373	0.0284	0.0396
$wR2$ (F^2) (all data)	0.0982	0.0453	0.0438
$(\Delta/\sigma)_{max}$	0.001	0.001	0.001
largest diff. peak/hole, e/Å^3	1.575 and -1.411	0.595 and -0.510	1.305 and -1.018
Absorpn corr	multiscan	multiscan	multiscan

Table A5. Crystallographic data and structure refinements for compounds 4 and 6 (Chapter 3).

	4	**6**
formula	$C_{21}H_{30}F_6O_{11}S_3Sn$	$C_{52}H_{72}N_2O_{10}P_2S_6Sn_2$
fw	787.32	1376.80
cryst syst	Orthorhombic	Triclinic

cryst size, mm	0.40 x 0.06 x 0.02	0.21 x 0.20 x 0.03
space group	Cmc21	P2(1)/c
a, Å	16.3525(19)	7.5738(3)
b, Å	22.897(2)	11.7774(4)
c, Å	7.8002(6)	17.4502(7)
α, deg	90	81.239(3)
β, deg	90	81.076(3)
γ, deg	90	77.526(3)
V, Å^3	2920.6(5)	1489.98(10)
Z	4	1
ρ_{calcd}, Mg/m^3	1.791	1.534
μ, mm^{-1}	1.182	1.157
F(000)	1584	704
θ range, deg	2.49 to 25.49	2.26 to 25.50
index ranges	–19≤h≤18 –27≤k≤27 –9≤l≤9	–9≤h≤9 –14≤k≤14 –21≤l≤21
no. of reflns collcd	9195	17495
completeness to θ_{max}	99.8	99.9
no. of indep reflns/R_{int}	2791/ 0.0528	5542/0.0393
no. of reflns obsd with ($I > 2\sigma(I)$)	2056	4245
no. of refined Params	203	335
GooF (F^2)	0.791	0.825
*R*1 (*F*) ($I > 2\sigma(I)$)	0.0299	0.0233
*wR*2 (F^2) (all	0.0328	0.0427

data)		
$(\Delta/\sigma)_{max}$	0.000	0.015
largest diff. peak/hole, e/Å^3	1.002/-0.547	0.441/-0.353
Absorpn corr	multiscan	multiscan

Table A6. Crystallographic data and structure refinements for compounds 9–10 (Chapter 3).

	9	**10**	**10**
formula	$C_6H_6S_2$	$C_{24}H_{20}OP_2S_2$	$C_{52}H_{72}N_2O_{10}P_2S_6Sn_2$
fw	142.23	450.46	1376.80
cryst syst	Monoclinic	Monoclinic	Triclinic
cryst size, mm	0.29 x 0.12 x 0.05	0.50 x 0.20 x 0.19	0.20 x 0.12 x 0.08
space group	P2(1)/c	C 1 2/c 1	P-1
a, Å	7.7316(8)	15.2637(15)	7.5738(3)
b, Å	7.1861(12)	9.0462(6)	11.7774(4)
c, Å	5.8713(7)	17.0707(17)	17.4502(7)
α, deg	90	90	81.239(3)
β, deg	92.070(10)	113.608(12)	81.076(3)
γ, deg	90	90	77.526(3)
V, Å^3	326.00(7)	2159.8(3)	1489.98(10)
Z	2	4	1
ρ_{calcd}, Mg/m^3	1.449	1.385	1.534
μ, mm^{-1}	0.697	0.408	1.157
F(000)	148	936	704
θ range, deg	2.64 to 25.46	2.60 to 25.49	2.26 to 25.50
index ranges	–9≤h≤9 –6≤k≤8 –7≤l≤7	-18≤h≤18 -10≤k≤10 -20≤l≤20	-9≤h≤9 -14≤k≤14 -21≤l≤21
no. of reflns collcd	1479	7834	17495

completeness to θ_{max}	100.0	100.0	99.9
no. of indep reflns/R_{int}	606/0.0355	2013/0.0341	5542/0.0393
no. of reflns obsd with ($I > 2\sigma(I)$)	405	1607	4245
no. of refined Params	41	132	335
GooF (F^2)	0.870	1.018	0.825
$R1$ (F) ($I > 2\sigma(I)$)	0.0311	0.0320	0.0233
$wR2$ (F^2) (all data)	0.0535	0.0760	0.0427
$(\Delta/\sigma)_{max}$	0.001	0.001	0.015
largest diff. peak/hole, e/Å^3	0.246 and -0.285	0.334 and -0.227	0.441 and -0.353
Absorpn corr	multiscan	multiscan	multiscan

Table A7. Crystallographic data and structure refinements for compounds 1–3 (Chapter 4).

	1	**2**	**3**
formula	$C_{48}H_{82}I_2O_{12}Sn_4$	$C_{48}H_{86}Br_2O_{12}Sn_4$	$C_{52}H_{102}I_2O_{18}Sn_4$
fw	1579.70	1489.75	1743.90
cryst syst	Triclinic	Triclinic	Triclinic
cryst size, mm	0.36 x 0.28 x 0.16	0.14 x 0.13 x 0.03	0.41 x 0.12 x 0.04
space group	P-1	P-1	P-1
a, Å	10.6472(5)	10.6755(6)	10.7486(4)
b, Å	12.3834(5)	12.3191(7)	13.2113(6)
c, Å	13.3100(7)	13.2499(9)	14.8078(7)
α, deg	65.219(5)	65.725(6)	114.114(4)

β, deg	68.078(5)	68.669(6)	100.338(4)
γ, deg	88.824(3)	89.774(4)	100.818(4)
V, Å^3	1458.71(12)	1457.73(18)	1806.57(16)
Z	1	1	1
ρ_{calcd}, Mg/m^3	1.798	1.697	1.603
μ, mm^{-1}	2.803	3.117	2.278
F(000)	772	740	864
θ range, deg	2.50 to 29.13	2.08 to 25.50	2.26 to 25.50
index ranges	–13≤h≤14 –16≤k≤15 –17≤l≤17	–12≤h≤12 –14≤k≤14 –16≤l≤16	–13≤h≤13 –15≤k≤15 –17≤l≤17
no. of reflns collcd	26381	13472	15485
completeness to θ_{max}	99.9	99.1	98.9
no. of indep reflns/R_{int}	6984/0.0578	5377/0.0454	6632/0.0465
no. of reflns obsd with ($I > 2\sigma(I)$)	3962	2928	4012
no. of refined Params	339	329	337
GooF (F^2)	0.845	0.515	0.835
$R1$ (F) ($I > 2\sigma(I)$)	0.0387	0.0284	0.0430
$wR2$ (F^2) (all data)	0.0875	0.0630	0.1255
$(\Delta/\sigma)_{max}$	0.001	0.005	0.001
largest diff. peak/hole, e/Å^3	1.633 and –1.371	0.571 and –0.509	1.353 and –1.335
Absorpn corr	multiscan	multiscan	multiscan

Table A8. Crystallographic data and structure refinements for compounds 4 and 5 (Chapter 4).

	4	**5**
formula	$C_{53}H_{96}Br_2Cl_2O_{14}Sn_4$	$C_{53}H_{96}Cl_4O_{14}Sn_4$
fw	1662.78	1573.86
cryst syst	Triclinic	Triclinic
cryst size, mm	0.40 x 0.36 x 0.27	0.15 x 0.06 x 0.05
space group	P-1	P-1
a, Å	10.7255(8)	10.6910(5)
b, Å	13.0905(11)	13.1423(7)
c, Å	14.7342(12)	14.8318(7)
α, deg	114.611(8)	114.979(5)
β, deg	100.450(7)	100.155(4)
γ, deg	99.884(7)	100.008(4)
V, Å^3	1777.5(2)	1786.00(18)
Z	1	1
ρ_{calcd}, Mg/m^3	1.553	1.463
μ, mm^{-1}	2.640	1.583
F(000)	1236	794
θ range, deg	2.29 to 29.25	2.18 to 25.50
index ranges	–12≤h≤13 –17≤k≤15 –20≤l≤19	–12≤h≤12 –15≤k≤15, –17≤l≤17
no. of reflns collcd	13755	21012
completeness to θ_{max}	99.9	99.9
no. of indep reflns/R_{int}	8143/0.0341	6635/0.0376
no. of reflns obsd with ($I > 2\sigma(I)$)	5100	5314

no. of refined Params	328	361
GooF (F^2)	0.853	1.381
$R1$ (F) ($I > 2\sigma(I)$)	0.0362	0.0484
$wR2$ (F^2) (all data)	0.0707	0.1604
$(\Delta/\sigma)_{max}$	0.001	0.002
largest diff. peak/hole, e/Å^3	0.651 and –0.712	1.489 and –0.794
Absorpn corr	multiscan	multiscan

7.2. Reference

(1) Sheldrick, G. M. *Acta Cryst. A,* **2008**, *64*, 112.

(2) Clegg, W. Acta Cryst. E, **2003**, 59, e2–e5.

7.3. Structure parameters for the ferrocenophanes 20-22 from DFT B3LYP/(LANL2DZ + Def2-TZVP) optimization

Ferrocenophane **20**:

Standard orientation:

Center Number	Atomic Number	Atomic Type	Coordinates (Angstroms) X	Y	Z
1	50	0	0.050866	0.574592	-0.724619
2	26	0	-4.404004	-0.795131	0.360000
3	14	0	-2.156865	-1.535793	-2.456317
4	14	0	-1.626829	0.069024	2.432155
5	8	0	5.568658	1.301404	-0.527892
6	8	0	3.004208	-0.470642	1.229595
7	6	0	2.089602	0.188866	-1.347465

8	1	0	2.249212	-0.865450	-1.143032
9	1	0	2.149035	0.333910	-2.421986
10	6	0	3.209772	0.992152	-0.656099
11	1	0	3.169727	2.033445	-0.949597
12	6	0	4.563384	0.422658	-1.079133
13	1	0	4.679263	-0.568895	-0.680730
14	1	0	4.651929	0.392859	-2.160282
15	6	0	6.932991	0.946796	-0.790379
16	1	0	7.518941	1.791300	-0.455745
17	1	0	7.100326	0.795492	-1.850637
18	6	0	3.609124	-0.919493	2.453705
19	1	0	2.865747	-0.971327	3.239852
20	1	0	4.406063	-0.255569	2.760214
21	6	0	3.122852	0.924991	0.868424
22	1	0	4.026510	1.346850	1.282599
23	1	0	2.267387	1.472149	1.245963
24	6	0	-1.352371	0.199085	-2.320986
25	1	0	-2.134157	0.952222	-2.272887
26	1	0	-0.806078	0.386960	-3.245394
27	6	0	-0.351868	-0.468235	1.116028
28	1	0	-0.628592	-1.473237	0.795393
29	1	0	0.632955	-0.563457	1.566644
30	6	0	-2.935696	-1.706245	-4.196945
31	1	0	-3.683918	-0.937686	-4.370203
32	1	0	-3.414845	-2.674208	-4.308367
33	1	0	-2.177723	-1.609975	-4.969260
34	6	0	-0.797834	-2.874295	-2.246655
35	1	0	-0.304190	-2.820576	-1.279746
36	1	0	-0.035484	-2.766147	-3.014088
37	1	0	-1.229190	-3.866182	-2.340536
38	6	0	-1.045702	1.639030	3.353350

39	1	0	-1.765085	1.903513	4.123167
40	1	0	-0.947718	2.484996	2.682920
41	1	0	-0.084615	1.472887	3.833620
42	6	0	-1.793848	-1.354298	3.709187
43	1	0	-2.168290	-2.263234	3.246777
44	1	0	-2.472867	-1.080699	4.512392
45	1	0	-0.828578	-1.578332	4.155020
46	6	0	-3.521039	-1.867726	-1.187447
47	6	0	-4.933917	-1.687944	-1.398582
48	1	0	-5.318667	-1.262039	-2.130283
49	6	0	-5.643441	-2.258398	-0.314189
50	1	0	-6.568303	-2.268681	-0.210330
51	6	0	-4.704390	-2.806624	0.582982
52	1	0	-4.898383	-3.248000	1.378559
53	6	0	-3.422505	-2.568179	0.060251
54	1	0	-2.626032	-2.826469	0.464943
55	6	0	-3.324222	0.351785	1.655044
56	6	0	-4.579793	-0.011954	2.223041
57	1	0	-4.696579	-0.483321	3.015642
58	6	0	-5.623442	0.461302	1.385946
59	1	0	-6.535839	0.343087	1.524874
60	6	0	-5.032740	1.135447	0.313272
61	1	0	-5.485382	1.541956	-0.389602
62	6	0	-3.651921	1.097567	0.479241
63	1	0	-3.033480	1.496525	-0.090665
64	8	0	6.951119	-1.454941	-0.826086
65	8	0	5.405192	-2.099124	1.427965
66	6	0	7.369786	-0.307684	-0.049952
67	1	0	8.450909	-0.317989	0.048455
68	1	0	6.914460	-0.331106	0.925426
69	6	0	7.065159	-2.720678	-0.159362

70	1	0	7.347408	-3.454265	-0.902317
71	1	0	7.829947	-2.687522	0.607988
72	6	0	4.193251	-2.292598	2.179250
73	1	0	3.469757	-2.863173	1.610851
74	1	0	4.412367	-2.813866	3.103644
75	6	0	5.740955	-3.116314	0.471370
76	1	0	4.974536	-3.175615	-0.291311
77	1	0	5.839290	-4.086055	0.949692
78	53	0	-0.126520	3.419543	-0.404537

Ferrocenophane **21**:

Standard orientation:

Center Number	Atomic Number	Atomic Type	Coordinates (Angstroms) X	Y	Z
1	50	0	0.193605	-0.879247	-0.809297
2	26	0	-3.861852	0.860098	0.671755
3	14	0	-0.942231	2.473751	-0.702510
4	14	0	-2.677011	-2.544956	0.508401
5	6	0	1.846078	-1.676946	-2.006773
6	1	0	1.588718	-2.732064	-2.157973
7	1	0	1.788536	-1.203636	-2.992686
8	6	0	3.259421	-1.567110	-1.410876
9	1	0	3.849350	-2.442766	-1.718491
10	6	0	3.246967	-1.589146	0.119508
11	1	0	2.847987	-2.546836	0.486750
12	1	0	4.253753	-1.444861	0.515945
13	6	0	2.409026	-0.272089	1.988977
14	1	0	2.392559	-1.217862	2.547562

15	1	0	1.480259	0.267259	2.203861
16	8	0	2.394460	-0.615443	0.767105
17	6	0	3.575441	0.590649	2.456573
18	1	0	3.725387	1.416065	1.747546
19	1	0	3.312950	1.018764	3.438774
20	6	0	5.934132	0.536498	2.908160
21	1	0	6.364778	0.091109	3.814494
22	1	0	5.691260	1.583857	3.126706
23	8	0	4.755759	-0.198327	2.571591
24	6	0	6.957962	0.468678	1.848236
25	1	0	7.879661	0.728325	2.396745
26	1	0	7.080699	-0.539627	1.427712
27	6	0	7.108199	0.985406	-0.566645
28	1	0	7.809042	0.143744	-0.489162
29	1	0	7.674213	1.873152	-0.886344
30	8	0	6.475575	1.236523	0.686751
31	6	0	6.040890	0.651222	-1.595282
32	1	0	5.252460	1.416821	-1.555808
33	1	0	6.476148	0.661086	-2.608059
34	8	0	5.323954	-0.332505	-1.441515
35	6	0	3.997198	-0.338423	-1.955735
36	1	0	3.479903	0.586224	-1.661257
37	1	0	4.012181	-0.378717	-3.056645
38	6	0	0.215724	1.144619	-0.007918
39	1	0	0.050753	1.048917	1.071762
40	1	0	1.246637	1.503537	-0.122229
41	6	0	-0.793113	-2.408293	0.389761
42	1	0	-0.421117	-3.362370	-0.010103
43	1	0	-0.379666	-2.334022	1.404193
44	6	0	-0.456884	2.824348	-2.494299
45	1	0	-1.056088	3.640991	-2.913755

46	1	0	-0.618088	1.937215	-3.116364
47	1	0	0.599489	3.111712	-2.575894
48	6	0	-0.693781	4.037586	0.339828
49	1	0	-1.288778	4.874352	-0.045235
50	1	0	0.356904	4.351081	0.333593
51	1	0	-0.982580	3.875991	1.385430
52	6	0	-3.460504	-2.849634	-1.179576
53	1	0	-3.109418	-2.127698	-1.922963
54	1	0	-4.553689	-2.784741	-1.122993
55	1	0	-3.210729	-3.853438	-1.545286
56	6	0	-3.061477	-4.038213	1.617630
57	1	0	-2.640878	-3.910105	2.621927
58	1	0	-2.647650	-4.962947	1.196236
59	1	0	-4.143035	-4.182614	1.730895
60	6	0	-2.762471	2.034376	-0.641993
61	6	0	-3.437278	0.977380	-1.333000
62	1	0	-3.014395	0.306900	-1.857972
63	6	0	-4.830548	1.085146	-1.111901
64	1	0	-5.497543	0.504493	-1.463209
65	6	0	-5.064096	2.204159	-0.277266
66	1	0	-5.909373	2.510045	0.031859
67	6	0	-3.804672	2.785745	0.013660
68	1	0	-3.668565	3.553856	0.556079
69	6	0	-3.375332	-1.033392	1.369795
70	6	0	-4.745011	-0.719721	1.604354
71	1	0	-5.483153	-1.217283	1.270155
72	6	0	-4.849155	0.443975	2.409858
73	1	0	-5.655018	0.855911	2.702560
74	6	0	-3.542452	0.876657	2.696316
75	1	0	-3.305923	1.634868	3.217597
76	6	0	-2.636615	-0.021679	2.065772

77	1	0	-1.688952	0.040595	2.101155
78	17	0	-1.329742	-0.659494	-2.702634

Ferrocenophane **22**:

Standard orientation:

Center Number	Atomic Number	Atomic Type	Coordinates (Angstroms) X	Y	Z
1	50	0	0.183013	-0.163738	-1.222831
2	9	0	-1.216293	0.479667	-2.547664
3	26	0	-3.908147	0.266727	0.940473
4	14	0	-1.303551	2.670571	0.264155
5	14	0	-2.382630	-2.582390	-0.652109
6	6	0	1.834873	-0.108576	-2.663371
7	1	0	1.638791	-0.942653	-3.347334
8	1	0	1.708667	0.804347	-3.255753
9	6	0	3.261384	-0.216842	-2.091522
10	1	0	3.948658	-0.535962	-2.887646
11	6	0	3.363814	-1.281042	-0.996959
12	1	0	3.079251	-2.268735	-1.390697
13	1	0	4.378902	-1.334918	-0.603994
14	6	0	2.592494	-1.654350	1.283305
15	1	0	2.615922	-2.734141	1.081207
16	1	0	1.686751	-1.431178	1.855468
17	8	0	2.452764	-0.918291	0.062510
18	6	0	3.803652	-1.261373	2.122482
19	1	0	3.954812	-0.177113	2.073931
20	1	0	3.604003	-1.540436	3.170504
21	6	0	6.187710	-1.573479	2.268926

22	1	0	6.799755	-2.480200	2.342321
23	1	0	6.017103	-1.197896	3.287272
24	8	0	4.958499	-1.963448	1.657013
25	6	0	6.959965	-0.544966	1.454113
26	1	0	7.986227	-0.475236	1.854146
27	1	0	7.019865	-0.888915	0.412753
28	6	0	6.710271	1.672627	0.541797
29	1	0	7.478077	1.252932	-0.119839
30	1	0	7.140234	2.547098	1.048824
31	8	0	6.308234	0.718956	1.526424
32	6	0	5.511735	2.109136	-0.285325
33	1	0	4.711579	2.447997	0.389734
34	1	0	5.794178	2.957456	-0.931262
35	8	0	5.070973	1.003982	-1.060744
36	6	0	3.754976	1.144978	-1.587771
37	1	0	3.083443	1.522836	-0.803788
38	1	0	3.750740	1.872368	-2.414798
39	6	0	0.040077	1.336449	0.346668
40	1	0	-0.043228	0.793125	1.294879
41	1	0	1.015020	1.840317	0.371555
42	6	0	-0.538249	-2.169905	-0.763724
43	1	0	-0.104492	-2.811812	-1.543211
44	1	0	-0.051922	-2.472828	0.172078
45	6	0	-0.997631	3.756497	-1.251227
46	1	0	-1.713491	4.586025	-1.288238
47	1	0	-1.109961	3.176550	-2.173726
48	1	0	0.010614	4.189883	-1.240234
49	6	0	-1.149773	3.724626	1.831935
50	1	0	-1.864517	4.556245	1.827239
51	1	0	-0.145394	4.156355	1.918770
52	1	0	-1.332632	3.134351	2.737709

53	6	0	-3.262004	-2.256104	-2.287978
54	1	0	-3.046926	-1.254416	-2.670454
55	1	0	-4.348619	-2.362390	-2.185461
56	1	0	-2.935148	-2.978356	-3.046628
57	6	0	-2.526686	-4.435487	-0.264607
58	1	0	-2.046106	-4.683850	0.688918
59	1	0	-2.058120	-5.047087	-1.045626
60	1	0	-3.577025	-4.743242	-0.191250
61	6	0	-3.053904	2.005998	0.193008
62	6	0	-3.661447	1.237426	-0.851157
63	1	0	-3.210801	0.898299	-1.616586
64	6	0	-5.035826	1.060093	-0.565966
65	1	0	-5.660832	0.586969	-1.105389
66	6	0	-5.323455	1.705798	0.660283
67	1	0	-6.169717	1.745459	1.091428
68	6	0	-4.116504	2.283109	1.128268
69	1	0	-4.022735	2.778150	1.933799
70	6	0	-3.161503	-1.664128	0.786885
71	6	0	-4.534115	-1.657304	1.168088
72	1	0	-5.237385	-2.071578	0.680338
73	6	0	-4.700811	-0.942144	2.382431
74	1	0	-5.521030	-0.794587	2.840962
75	6	0	-3.430975	-0.491552	2.783964
76	1	0	-3.238329	0.016438	3.563322
77	6	0	-2.485259	-0.930036	1.815211
78	1	0	-1.550464	-0.761528	1.846166

---

8. List of New Compounds

Chapter 2	
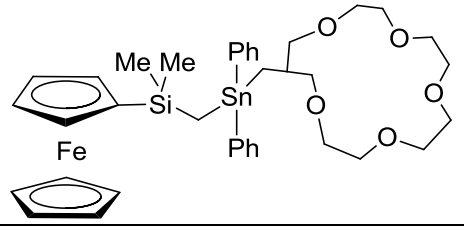	**1**
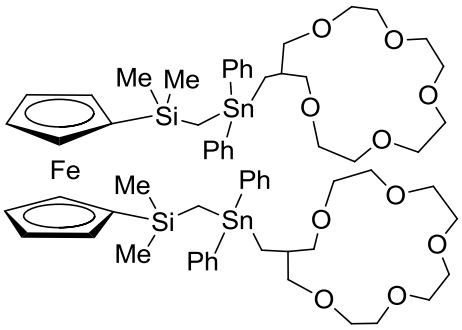	**2**
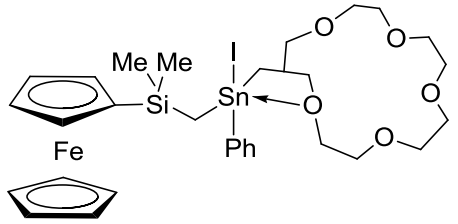	**3**
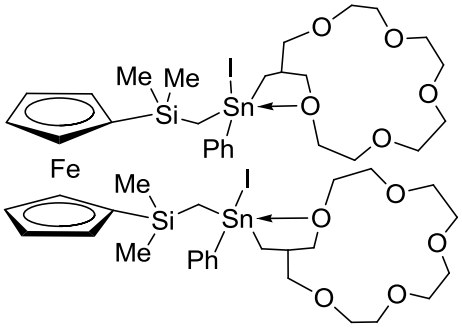	**4**
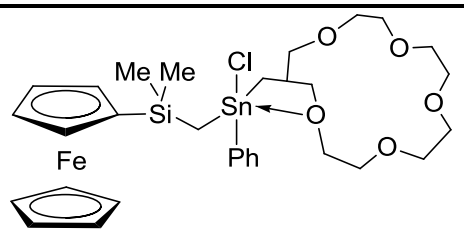	**5**
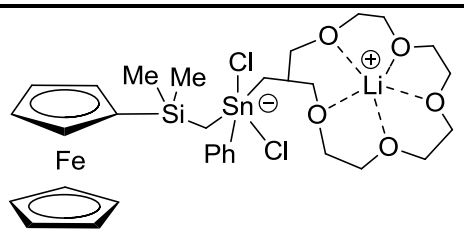	**5**·LiCl

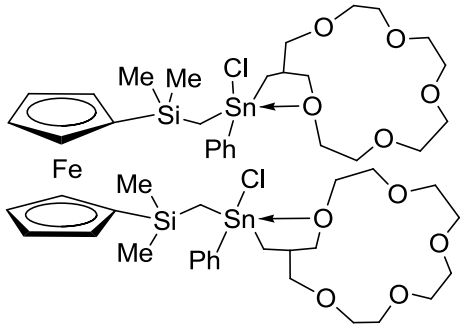	**6**
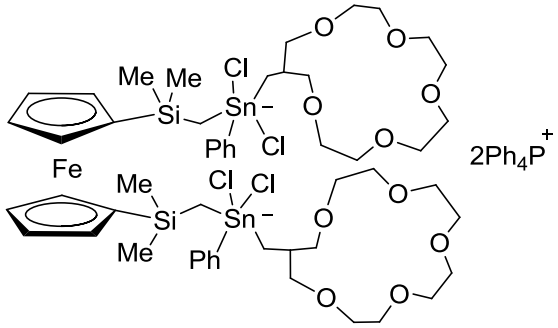	[**6**·2Cl]$^{-}$[2Ph$_4$P]$^{+}$
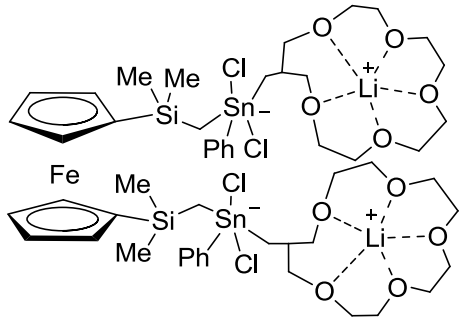	[**6**·2LiCl]
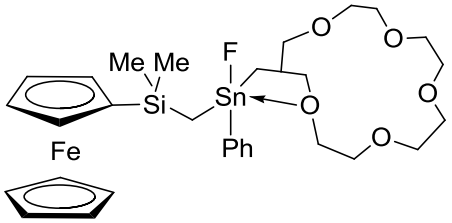	**7**
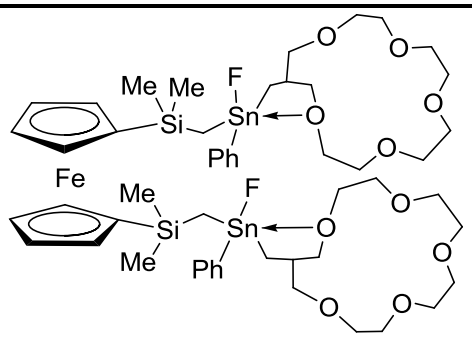	**8**

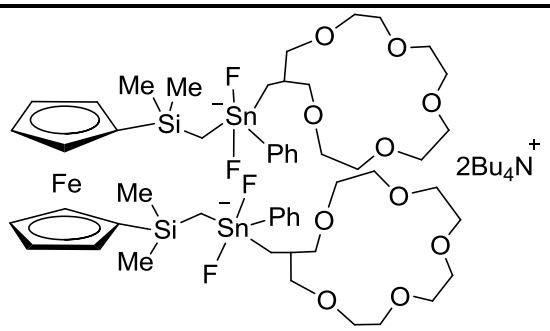	[**8**·2F]$^{-}$[2Bu$_4$N]$^{+}$
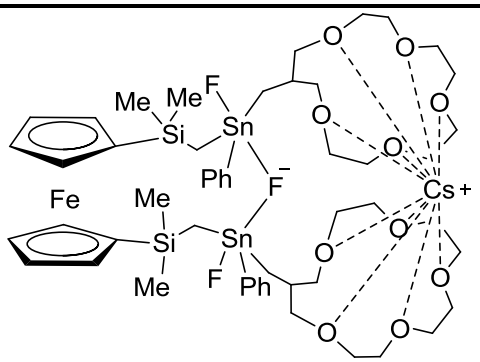	[**8**·CsF]
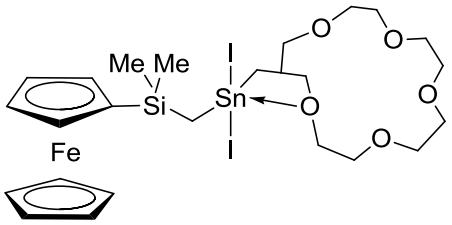	**11**
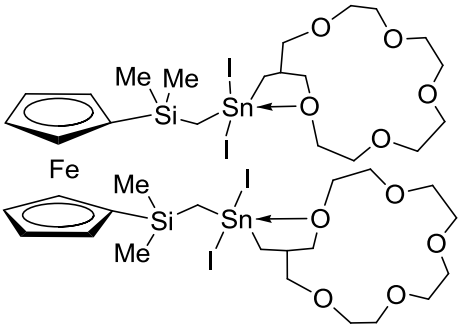	**12**
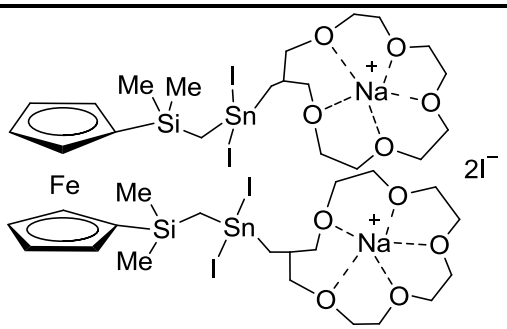	[**12**·2NaI]
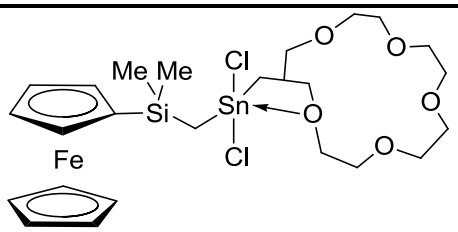	**13**

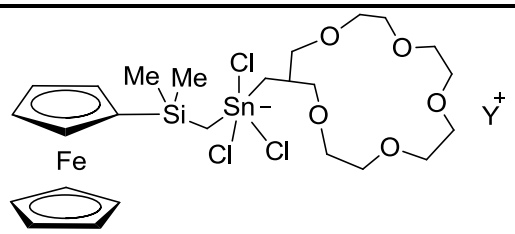	[**13**·Cl]$^-$[Y]$^+$ Y = Ph_4P, $(Ph_3P)_2N$, Bu_4P
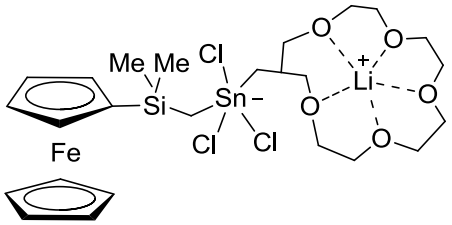	[**13**·LiCl]
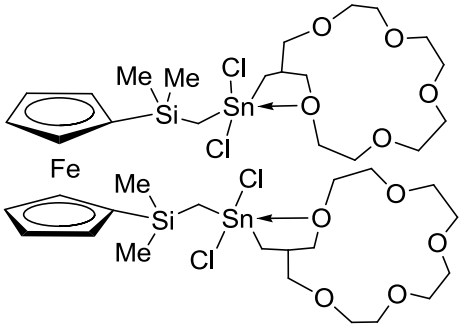	**14**
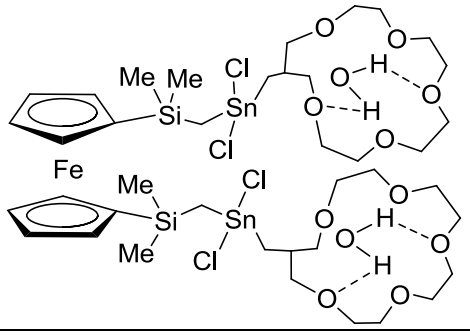	[**14**·2H_2O]
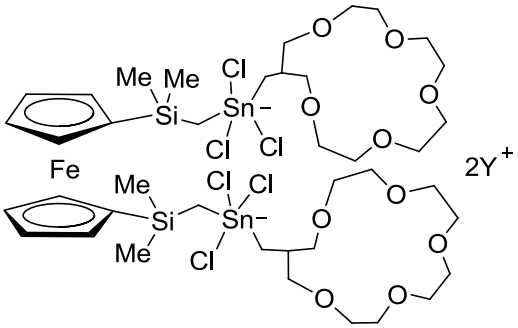	[**14**·2Cl]$^-$[2Y]$^+$ Y = Ph_4P, $(Ph_3P)_2N$, Bu_4P
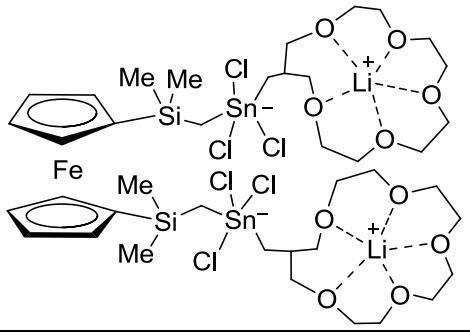	[**14**·2LiCl]

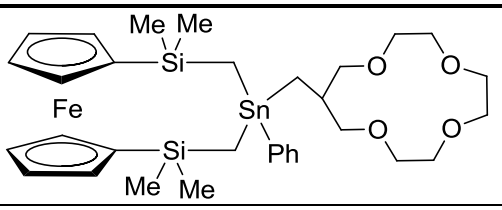	**19**
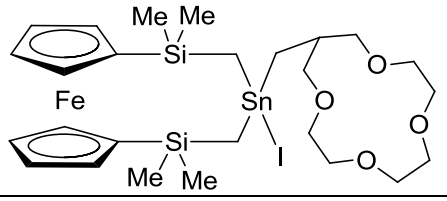	**20**
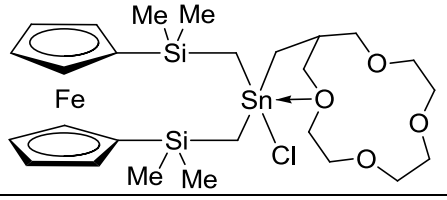	**21**
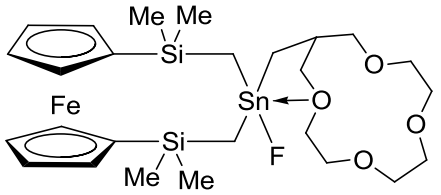	**22**
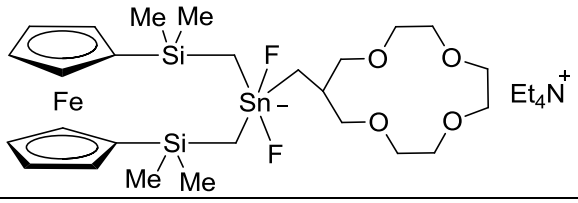	[**22**·F]$^-$[Et_4N]$^+$
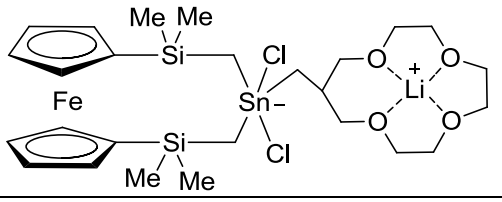	[**21**·LiCl]
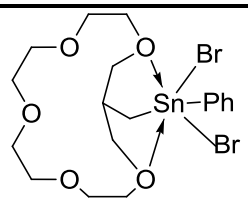	**23**
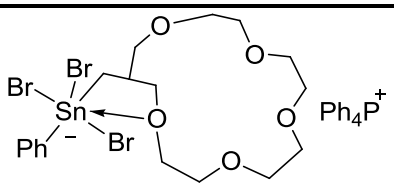	[**23**·Br]$^-$[Ph_4P]$^+$

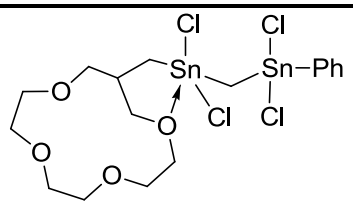	**24**
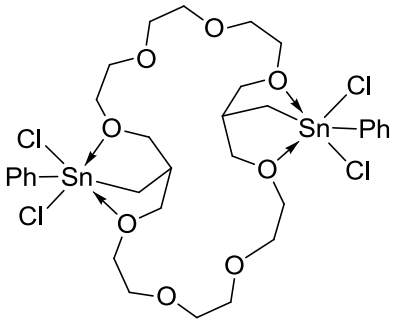	**25**
Chapter 3	
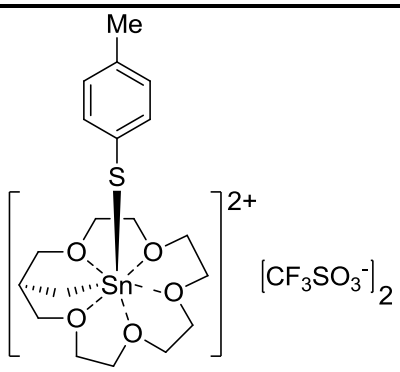	**4**
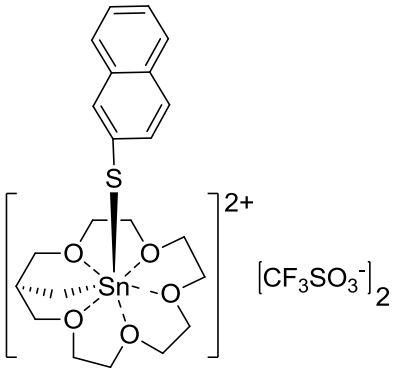	**5**
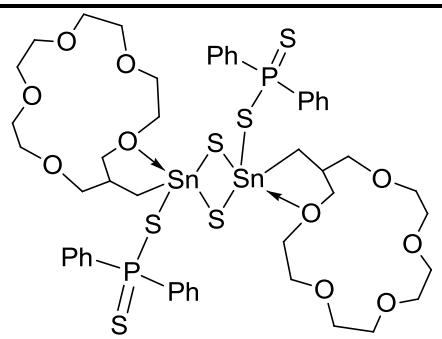	**6**

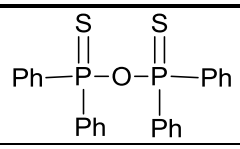	**7**
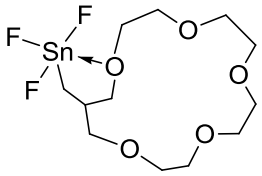	**10**
Chapter 4	
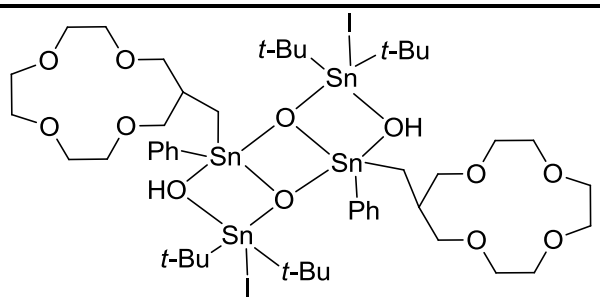	**1**
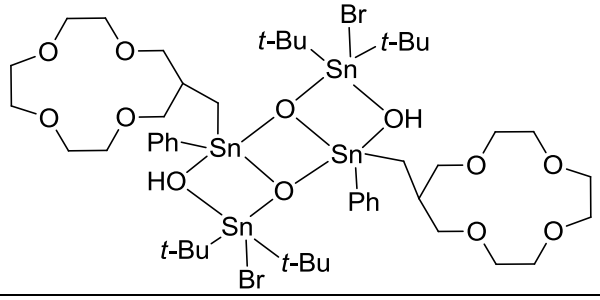	**2**
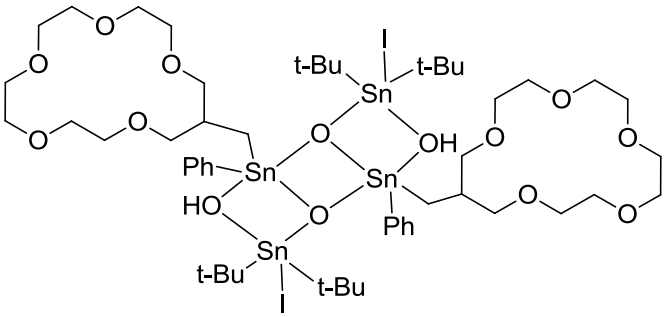	**3**
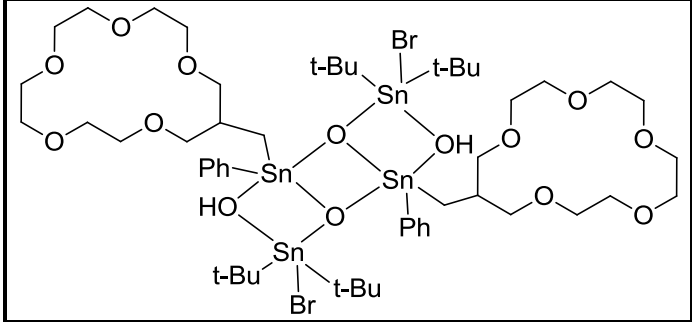	**4**

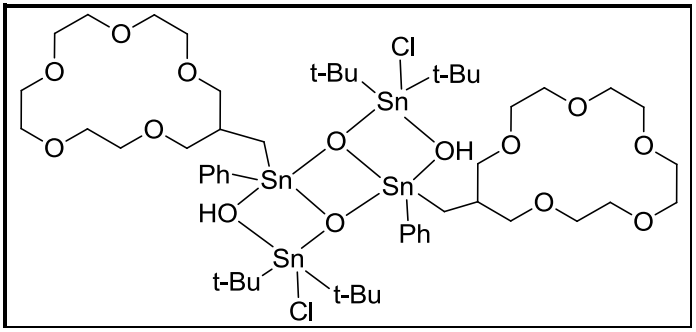	**5**

9. Curriculum Vitae

Personal data

Name	Siakam Wendji, Anicet
Adress	Schulte-Heuthaus-Str.49, 44379 Dortmund
Birthdate	15 august 1979
Birthplace	Bangoua-Cameroon
Marital status	Married
Citizenship	Cameroonian
Confession	Christian

Education

1984 –1990	Primary School, Yaoundé and Nkongsamba-Cameroon
1990 – 1997	Secondary School, Nkongsamba-Cameroon
Oct. 1997	Registration at the University of Yaoundé I, Cameroon, Department of Chemistry
Feb. 2001	Bachelor, Chemistry
Juli 2002	Master I, Chemistry
Sept. 2003	Master II, Inorganic Chemistry
Juli 2004	DIPES II (Secondary High School Teacher´s Diploma Grade II)
Oct. 2004 – May 2009	Teacher of Physic and Chemistry, Cameroon
Oct. 2009 – May 2013	Ph.D at the Institute of Inorganic Chemistry II at the Universität Dortmund as DAAD Fellow, under the supervision of Prof. Dr. K. Jurkschat
April 2012– Aug. 2013	Scientific Assistant at the Department of Chemistry of the Universität Dortmund Dortmund-Germany

10. Tabellarischer Lebenslauf

Persönliche Daten

Name	Siakam Wendji, Anicet
Adresse	Schulte Heuthaus-Str.49, 44379 Dortmund
Geboren	am 15 August 1979 in Bangoua-Cameroon
Familienstand	verheiratet
Staatsangehörigkeit	Kamerun
Konfession	katholisch

Ausbildungsdaten

1984 –1990	Grundschule, Yaoundé und Nkongsamba-Kamerun
1990 – 1997	Gymnasium, Nkongsamba-Kamerun
Okt. 1997	Immatrikulation an der Universität Yaoundé I, Kamerun, Fachrichtung Chemie
Feb. 2001	Bachelor Chemie
Juli 2002	Master I, Chemie
Sept. 2003	Master II, Anorganische Chemistry
Juli 2004	DIPES II (Diplom Lehrer in Physik und Chemie)
Oct. 2004 – May 2009	Lehrer für Physik and Chemie, Kamerun
Oct. 2009 – May 2013	Promotion am Lehrstuhl für Anorganische Chemie II der Technische Universität Dortmund unter der Leitung von Prof. Dr. K. Jurkschat als DAAD Stipendiat
April 2012– Okt. 2013	Wissenschaftlicher Hilfskraft im Fachbereich Chemie der Technische Universität Dortmund

Erklärung

Hiermit erkläre ich, dass ich die vorliegende Arbeit selbstständig und nur unter Verwendung der angegebenen Hilfsmittel angefertigt habe.

Dortmund, den 16. Mai 2013